pharmaceuticals

Special Issue Reprint

Pharmacological Activities of Flavonoids and Their Analogues 2024

Edited by
Fernando Calzada and Miguel Valdes

mdpi.com/journal/pharmaceuticals

MDPI

Pharmacological Activities of Flavonoids and Their Analogues 2024

Pharmacological Activities of Flavonoids and Their Analogues 2024

Guest Editors

Fernando Calzada
Miguel Valdes

MDPI

Basel • Beijing • Wuhan • Barcelona • Belgrade • Novi Sad • Cluj • Manchester

Guest Editors

Fernando Calzada
Medical Research Unit in Pharmacology
National Medical Center Siglo XXI
México City
Mexico

Miguel Valdes
Medical Research Unit in Pharmacology
National Medical Center Siglo XXI
Mexico City
Mexico

Editorial Office

MDPI AG
Grosspeteranlage 5
4052 Basel, Switzerland

This is a reprint of the Special Issue, published open access by the journal *Pharmaceuticals* (ISSN 1424-8247), freely accessible at: https://www.mdpi.com/journal/pharmaceuticals/special_issues/93293XO38H.

For citation purposes, cite each article independently as indicated on the article page online and as indicated below:

Lastname, A.A.; Lastname, B.B. Article Title. *Journal Name* **Year**, *Volume Number*, Page Range.

ISBN 978-3-7258-8191-8 (Hbk)
ISBN 978-3-7258-8192-5 (PDF)
https://doi.org/10.3390/books978-3-7258-8192-5

© 2026 by the authors. Articles in this reprint are Open Access and distributed under the Creative Commons Attribution (CC BY) license. The reprint as a whole is distributed by MDPI under the terms and conditions of the Creative Commons Attribution-NonCommercial-NoDerivs (CC BY-NC-ND) license (https://creativecommons.org/licenses/by-nc-nd/4.0/).

Contents

About the Editors . . . . . **vii**

Preface . . . . . **ix**

Aline B. Hora, Laiza S. Biano, Ana Carla S. Nascimento, Zaine T. Camargo, Greice I. Heiden, Ricardo L. C. Albulquerque-Júnior, et al.
Correction: Hora et al. Isoorientin Improves Excisional Skin Wound Healing in Mice. *Pharmaceuticals* 2024, *17*, 1368
Reprinted from: *Pharmaceuticals* **2025**, *18*, 1343, https://doi.org/10.3390/ph18091343 . . . . . **1**

Huiming Xue, Zhen Feng, Chang Jin, Yue Zhang, Yongxing Ai, Jing Wang, et al.
Soy Isoflavones Protects Against Stroke by Inhibiting Keap1/NQO1/Nrf2/HO-1 Signaling Pathway: Network Pharmacology Analysis Combined with the Experimental Validation
Reprinted from: *Pharmaceuticals* **2025**, *18*, 548, https://doi.org/10.3390/ph18040548 . . . . . **3**

Eun-Ji Go, Byeong Ryeol Ryu, Gyeong Ju Gim, Ye Rim Shin, Min Ji Kang, Min Jun Kim, et al.
Regulation of Intestinal Barrier Function and Gut Microbiota by Hot Melt Extrusion-Drug Delivery System-Prepared Mulberry Anthocyanin in an Inflammatory Bowel Disease Model
Reprinted from: *Pharmaceuticals* **2025**, *18*, 475, https://doi.org/10.3390/ph18040475 . . . . . **28**

Juan Salazar, Ángel Ortega, José Luis Pérez, Bermary Garrido, Raquel Santeliz, Néstor Galbán, et al.
Role of Polyphenols in Dermatological Diseases: Exploring Pharmacotherapeutic Mechanisms and Clinical Implications
Reprinted from: *Pharmaceuticals* **2025**, *18*, 247, https://doi.org/10.3390/ph18020247 . . . . . **58**

Yeon Kim, Hyun-Joo Park, Mi-Kyoung Kim, Hyung Joon Kim, Yong-Il Kim, Soo-Kyung Bae, et al.
Effects of Hispidulin on the Osteo/Odontogenic and Endothelial Differentiation of Dental Pulp Stem Cells
Reprinted from: *Pharmaceuticals* **2024**, *17*, 1740, https://doi.org/10.3390/ph17121740 . . . . . **83**

Aline B. Hora, Laiza S. Biano, Ana Carla S. Nascimento, Zaine T. Camargo, Greice I. Heiden, Ricardo L. C. Albulquerque-Júnior, et al.
Isoorientin Improves Excisional Skin Wound Healing in Mice
Reprinted from: *Pharmaceuticals* **2024**, *17*, 1368, https://doi.org/10.3390/ph17101368 . . . . . **94**

Mahmoud Emam, Samah A. El-Newary, Hanan Y. Aati, Bin Wei, Mohamed Seif and Abeer Y. Ibrahim
Anti-Alzheimer's Potency of Rich Phenylethanoid Glycosides Extract from *Marrubium vulgare* L.: In Vitro and In Silico Studies
Reprinted from: *Pharmaceuticals* **2024**, *17*, 1282, https://doi.org/10.3390/ph17101282 . . . . . **105**

Yu Yan, Xuexue Xia, Aiman Fatima, Li Zhang, Ganjun Yuan, Fengxian Lian, et al.
Antibacterial Activity and Mechanisms of Plant Flavonoids against Gram-Negative Bacteria Based on the Antibacterial Statistical Model
Reprinted from: *Pharmaceuticals* **2024**, *17*, 292, https://doi.org/10.3390/ph17030292 . . . . . **126**

About the Editors

Fernando Calzada

Fernando Calzada is a Senior Researcher and Principal Investigator at the Medical Research Unit in Pharmacology of the Speciality Hospital, National Medical Center Siglo XXI, within the Mexican Institute of Social Security, and is recognized as a level 3 scientist in the National System of researchers. His primary research interests bridge the fields of parasitology, cell biology, and neuroscience, with a specific focus on the pharmacology and phytochemistry of medicinal plants. He actively leads multidisciplinary projects dedicated to investigating the antidiabetic, anticancer, diuretic, antiprotozoal, and antidiarrheal properties of Mexican flora, aiming to address critical global health challenges. His major scientific achievements include over 130 high-impact peer-reviewed publications, significant contributions to the structural optimization of plant-derived compounds, and advanced computational in silico molecular docking models for targeted drug discovery.

Miguel Valdes

Miguel Valdes is a researcher and professor affiliated with Escuela Superior de Medicina of the Instituto Politécnico Nacional, where he also serves as a core faculty member for the Master of Science in Pharmacology program. His primary research interests focus on the pharmacological evaluation of medicinal plants, synthetic organic chemistry, and advanced in silico molecular docking studies for targeted drug discovery. He actively leads frontier science projects dedicated to developing novel molecular analogues and optimizing bioactive compounds to target metabolic pathways. His recent scientific achievements include publishing high-impact peer-reviewed research on the antidiabetic activity of natural product derivatives, successfully mentoring bachelor students and graduate students in pharmacology, and medical specialties.

Preface

This Reprint explores the chemistry and pharmacology of flavonoids and their analogues. It showcases chemical modification, synthetic optimization, and in silico docking models to enhance bioavailability. It is addressed to pharmacologists and medicinal chemists, focusing on novel drug discovery.

Fernando Calzada and Miguel Valdes
Guest Editors

pharmaceuticals

MDPI

Correction

Correction: Hora et al. Isoorientin Improves Excisional Skin Wound Healing in Mice. *Pharmaceuticals* 2024, *17*, 1368

Aline B. Hora [1], Laiza S. Biano [2], Ana Carla S. Nascimento [2], Zaine T. Camargo [3], Greice I. Heiden [4], Ricardo L. C. Albulquerque-Júnior [4], Renata Grespan [2], Jessica M. D. A. Aragão [2] and Enilton A. Camargo [1,2,*]

[1] Graduate Program in Health Sciences, Federal University of Sergipe, São Cristóvão 49060-676, Brazil
[2] Graduate Program in Physiological Sciences, Federal University of Sergipe, São Cristóvão 49107-230, Brazil
[3] Graduate Program in Chemistry, Federal University of Sergipe, São Cristóvão 49107-230, Brazil
[4] Graduate Program in Dentistry, Federal University of Santa Catarina, Florianópolis 88040-900, Brazil
* Correspondence: eniltoncamargo@academico.ufs.br; Tel.: +55-79-3198-6644

In the original publication [1], there were mistakes in affiliation for author Renata Grespan and Figure 2 as published.

The correct affiliation for Renata Grespan is 2.

An error was made during the assembly of the figure, resulting in the inadvertent duplication of the same image for two different treatment conditions. The written description of the results in the manuscript is accurate, correctly reflecting the distinct morphological features observed in each treatment group. The error is restricted to the photomicrographic panel, where an incorrect image was mistakenly included, which does not correspond to the text. The corrected Figure 2 appears below. The authors state that the scientific conclusions are unaffected. This correction was approved by the Academic Editor. The original publication has also been updated.

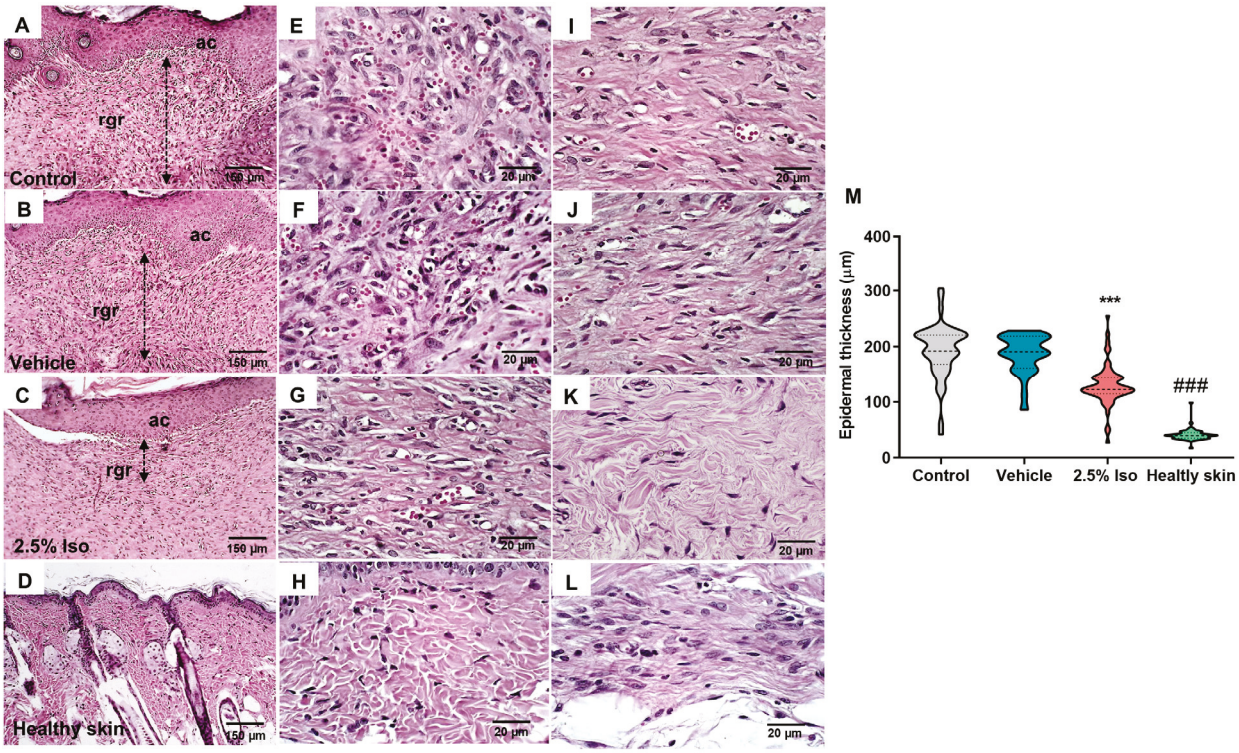

Figure 2. Representative images of the wound tissues 14 days after induction and quantification of the epidermal thickness. Histological sections stained with hematoxylin and eosin represent each experimental group's epidermis and papillary/reticular dermis. Panoramic views of the groups—control (**A**), vehicle (**B**), 2.5% Iso (**C**), and healthy skin (**D**)—show the measurement of the granulation reaction depth (dotted lines with double arrows), epidermal acanthosis (ac), and residual granulation reaction (rgr) in the lamina propria (100×). Details of the granulation reaction and the deeper dermal portion in the control (**E**,**I**), vehicle (**F**,**J**), 2.5% Iso (**G**,**K**), and healthy skin (**H**,**L**) groups (400×) are shown. A violin plot shows the measurement of the mean epidermal thickness in the experimental groups (**M**), n = 6 animals with 6–8 measurements each. The Kruskal–Wallis and Dunn's post hoc tests were used. *** $p < 0.001$ and ### $p < 0.001$ compared to the control or vehicle groups.

Reference

1. Hora, A.B.; Biano, L.S.; Nascimento, A.C.S.; Camargo, Z.T.; Heiden, G.I.; Albulquerque-Júnior, R.L.C.; Grespan, R.; Aragão, J.M.D.A.; Camargo, E.A. Isoorientin Improves Excisional Skin Wound Healing in Mice. *Pharmaceuticals* **2024**, *17*, 1368. [CrossRef] [PubMed]

Disclaimer/Publisher's Note: The statements, opinions and data contained in all publications are solely those of the individual author(s) and contributor(s) and not of MDPI and/or the editor(s). MDPI and/or the editor(s) disclaim responsibility for any injury to people or property resulting from any ideas, methods, instructions or products referred to in the content.

pharmaceuticals

MDPI

Article

Soy Isoflavones Protects Against Stroke by Inhibiting Keap1/NQO1/Nrf2/HO-1 Signaling Pathway: Network Pharmacology Analysis Combined with the Experimental Validation

Huiming Xue [1], Zhen Feng [1], Chang Jin [1], Yue Zhang [1], Yongxing Ai [2], Jing Wang [3], Meizhu Zheng [3,*] and Dongfang Shi [3,*]

[1] College of Life Sciences, Changchun Normal University, Changchun 130032, China; qx202310010@stu.ccsfu.edu.cn (H.X.); fengzhen0915@163.com (Z.F.); j1504408478@163.com (C.J.); 15942907284@163.com (Y.Z.)
[2] College of Animal Science, Jilin University, Changchun 130062, China; aiyx@jlu.edu.cn
[3] Central Laboratory, Changchun Normal University, Changchun 130032, China; ccsfxy888@163.com
* Correspondence: zhengmz605@mail.cncnc.edu.cn (M.Z.); shidongfang3@ccsfu.edu.cn (D.S.); Tel./Fax: +0431-86168708 (M.Z.); +0431-86168378 (D.S.)

Abstract: Objectives: Ischemic stroke is a severe neurological disorder with high morbidity, mortality, and disability rates, posing a substantial burden on patients, families, and healthcare systems. Soy isoflavone (SI), a naturally occurring phytoestrogen, has demonstrated promising neuroprotective effects. This study aimed to evaluate the anti-stroke efficacy of SI and elucidate its underlying mechanisms through integrated phytochemical profiling, network pharmacology, and both in vitro and in vivo experimental validation. **Methods**: Active constituents of SI were extracted via reflux and identified using liquid chromatography–mass spectrometry (LC-MS). Network pharmacology was employed to predict therapeutic targets and signaling pathways. The neuroprotective effects of SI were first assessed in PC12 cells subjected to oxygen–glucose deprivation/reoxygenation (OGD/R) injury in vitro. For in vivo evaluation, transient cerebral ischemia–reperfusion injury was induced using the bilateral common carotid artery occlusion (BCCAO) model in adult male ICR rats (27.3 ± 1.8 g; 6–8 weeks old), obtained from the Shanghai Experimental Animal Center, Chinese Academy of Sciences. Forty-eight rats were randomly assigned into four groups (n = 12): sham, model (BCCAO), SI-treated (100 mg/kg, oral gavage for 5 days), and edaravone (EDA)-treated (10 mg/kg, i.p., positive control). All procedures were approved by the Institutional Animal Care and Use Committee of Changchun Normal University (Approval No. 2024003, 13 March 2024) and conducted in accordance with the NIH guidelines and ARRIVE 2.0 reporting standards. **Results**: In vitro, SI significantly enhanced PC12 cell viability from 57.23 ± 2.88% to 80.76 ± 4.43% following OGD/R. It also reduced intracellular Ca^{2+} by 58.42%, lactate dehydrogenase (LDH) release by 37.67%, caspase-3 activity by 55.05%, and reactive oxygen species (ROS) levels by 74.13% ($p < 0.05$). A flow cytometry analysis revealed that OGD/R increased the apoptosis rate from 5.34% (control) to 30.85% (model group), which was significantly attenuated by SI treatment, especially in the 560 μg/mL group (20.00%), followed by the 140 and 280 μg/mL groups. In vivo, SI improved neurological scores from 8.3 ± 1.09 to 6.8 ± 1.68, reduced cerebral infarction volume by 18.49%, and alleviated brain edema by 10.42% ($p < 0.05$). SI also decreased malondialdehyde (MDA) and LDH levels by 31.15% and 39.46%, respectively, while increasing the activity of antioxidant enzymes: superoxide dismutase (SOD) by 11.70%, catalase (CAT) by 26.09%, and glutathione peroxidase (GSH-px) by 27.55% ($p < 0.01$). Scratch assay results showed that SI restored the impaired migratory ability of

the OGD/R-treated PC12 cells, further supporting its role in cellular repair. A Western blot analysis demonstrated the upregulation of nuclear factor erythroid 2–related factor 2 (Nrf2), heme oxygenase-1 (HO-1), and NAD(P)H:quinone oxidoreductase 1 (NQO1) and the downregulation of Kelch-like, ECH-associated protein 1 (Keap1) in the cerebral ischemia–reperfusion model. **Conclusions**: These findings indicate that soy isoflavone confers significant neuroprotective effects against cerebral ischemia–reperfusion injury by enhancing endogenous antioxidant defense mechanisms, reducing oxidative stress, inhibiting apoptosis, and promoting cell migration. The protective effects are likely mediated through the activation of the Nrf2/Keap1 signaling pathway, supporting the therapeutic potential of SI in ischemic stroke treatment.

Keywords: stroke; soybean isoflavones; Nrf2; Keap1; rat

1. Introduction

Stroke is identified as a spectrum of disorders characterized by the interruption of blood circulation within the brain, leading to compromised neurological functions. These disorders are generally categorized into two principal types: hemorrhagic strokes and ischemic strokes (ISs). The latter, ischemic stroke, arises from the occlusion or constriction of arteries that are responsible for the cerebral blood supply, accounting for over seventy percent of all stroke instances [1,2]. Ischemic stroke is associated with a significant incidence of death, disability, and morbidity, posing a severe risk to patients' lives and markedly affecting their quality of life [3]. Globally, stroke remains a leading cause of mortality and long-term disability, imposing substantial public health and economic burdens. Therefore, effective therapeutic strategies are urgently needed to mitigate its impact.

In the realm of physicochemical analysis, the development of ischemic stroke is predominantly attributed to mechanisms such as glutamate excitotoxicity, calcium accumulation, oxidative stress, apoptosis, and inflammation, among others [4–7]. The Keap1/Nrf2 signaling pathway is a key mechanism for maintaining the redox balance in the body [8]. Under normal physiological conditions, when cells are exposed to harmful external stimuli, such as environmental toxins or oxidative stress, reactive oxygen species (ROS) and electrophilic compounds can cause structural changes in Kelch-like, ECH-associated protein 1 (Keap1). This modification leads to the activation and nuclear translocation of a protein called nuclear factor erythroid 2–related factor 2 (Nrf2). Once inside the nucleus, Nrf2 functions as a transcription factor, turning on the expression of several protective genes that help the body defend itself against oxidative damage. These genes produce antioxidant and detoxifying enzymes, which play essential roles in neutralizing harmful molecules. Among these are enzymes like heme oxygenase-1 (HO-1) and NAD(P)H quinone dehydrogenase 1 (NQO1), which together help reduce oxidative stress and restore the cellular balance [9–11]. This signaling cascade is not only crucial for protection during acute injuries such as ischemic stroke but has also been implicated in the development and progression of a wide range of both cancerous and non-cancerous diseases [11]. Given its pivotal role in cellular defense, the Keap1/Nrf2 pathway has emerged as a promising therapeutic target for neuroprotection in ischemic stroke. However, effective modulators of this pathway remain limited, particularly among natural compounds.

Currently, the interest in natural medicinal research has surged globally. Evidence from numerous studies indicates a clear beneficial impact of botanicals and their bioactive constituents against ischemic stroke [12]. Soybeans, belonging to the legume family, have been identified as a significant source of isoflavones. Notably, soy isoflavones (SI), recognized

as bioactive compounds, exhibit a range of biological activities. These include mimicking estrogen, combating aging and cancer, offering antioxidant and anti-inflammatory benefits, lowering lipid levels, preventing cardiovascular diseases, and improving memory functions [13,14]. Despite these diverse bioactivities, the neuroprotective potential of soy isoflavones in ischemic stroke is still underexplored. Their ability to modulate oxidative stress-related pathways, particularly Keap1/Nrf2, may provide a novel avenue for therapeutic development.

Network pharmacology integrates the principles of systems biology, omics technologies, and computational biology. This integration facilitates a comprehensive and synergistic exploration of the modes of action of pharmaceuticals, offering insights into their pharmacological effects [15]. Molecular docking techniques enable the prediction of protein–ligand interactions, including binding conformations and associated binding free energies, thereby supporting the functional validation of candidate compounds and clarifying their mechanisms of action [16]. The combined application of network pharmacology and molecular docking thus provides a powerful platform for investigating the multi-target and multi-pathway actions of complex natural products, such as soy isoflavones (SI), in ischemic stroke models.

Building on this integrated approach, the present study explored the potential role of SI in the prevention and treatment of ischemic stroke (IS), with a specific focus on redox regulation and oxidative stress modulation via the Nrf2 signaling pathway. An in vitro model of ischemic injury was established using $Na_2S_2O_4$-induced hypoxic damage in PC12 cells, and a rat model of cerebral ischemia–reperfusion injury was induced via the embolization of the common carotid artery.

The primary objective of this study is to elucidate the neuroprotective mechanisms of soy isoflavones (SIs) in ischemic stroke (IS) by integrating in silico, in vitro, and in vivo approaches. First, network pharmacology and molecular docking were employed to systematically predict the putative targets and signaling pathways through which SI may exert therapeutic effects against IS. Next, a hypoxia-induced injury model in PC12 cells was established using sodium dithionite ($Na_2S_2O_4$) to assess the in vitro protective effects of SI. Additionally, a rat model of cerebral ischemia–reperfusion injury was induced via common carotid artery embolization to evaluate the in vivo efficacy of SI. Particular attention was given to the Keap1/Nrf2/HO-1/NQO1 signaling axis to determine whether SI modulates oxidative stress through this pathway. By combining computational prediction with experimental validation, this study aims to provide mechanistic insights and preclinical evidence supporting the therapeutic potential of SI in ischemic stroke.

2. Results

2.1. Extraction and Identification of Soybean Isoflavone Cells: Experimental Results

The analysis and separation process for soybean isoflavones revealed a total of seven distinct isoflavone compounds, as demonstrated in Figure 1a. The mass spectral analysis and detailed data for each compound were systematically examined, with the findings presented in Figure 1b and Table 1. The identified isoflavone components included daidzin, glycitin, genistin, acetyldaidzin, acetylcitin, malonylgenistin, and acetylgenistin. The molecular structures of these seven isoflavones are depicted in Figure 1b.

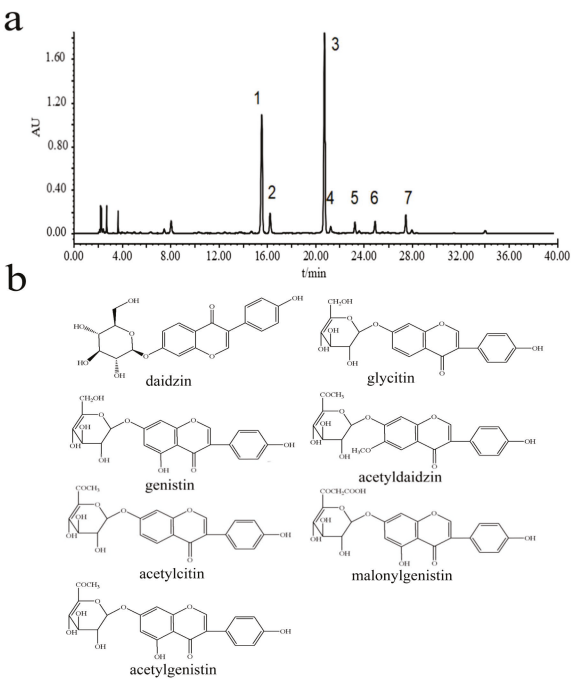

Figure 1. Analysis of crude soybean extract. (**a**) HPLC chromatogram. (**b**) Seven isoflavone structural formulas.

Table 1. LC-MS analysis data of soybean's active ingredients Comprehensive LC-MS data for identifying active compounds in soybeans.

NO.	Retention Time (min)	MS (m/z)	MS2 (m/z)	Compound
1	15.4	417, $[M + H]^+$	255, 137	Daidzin
2	16.2	447, $[M + H]^+$	285, 270	Glycitin
3	20.7	433, $[M + H]^+$	271, 153	Genistin
4	21.4	459, $[M + H]^+$	255	Acetyldaidzin
5	23.3	489, $[M + H]^+$	285	Acetylcitin
6	25.2	519, $[M + H]^+$	271, 215, 197, 153	Malonylgenistin
7	27.5	475, $[M + H]^+$	271	Acetylgenistin

2.2. Network Pharmacological Target Prediction

A review of the literature in the CNKI database revealed twelve components of soy isoflavone, comprising both three free glycosides and nine conjugated glycosides (refer to Table 2). Through the analysis of pharmacokinetic parameters using the SwissADME database, three free glycosides were identified as potent active ingredients: daidzein, genistein, and glycitein. In total, 111 targets for soy isoflavone were derived from two pharmacological databases (Figure 2a), while 4598 disease-related targets for IS were collated from four disease-specific databases (Figure 2b), leading to the identification of 84 common targets (Figure 2c). Utilizing String11.5, a PPI network was constructed, comprising 84 nodes and 524 connections (Figure 2d). Visualization using Cytoscape 3.8.0 indicated that nodes with a larger size and darker color within the figure represent a greater impact on IS. The top five pivotal genes, identified through the MCC algorithm in the cytoHubba plugin, were MMP9, EGFR, PPARG, PTGS2, and ESR1(Figure 2e). Afterwards, an "drug-component-disease-target" network diagram was constructed (Figure 2f).

Table 2. Existing forms and structural formulas of 12 soy isoflavones.

Type	Types of Isoflavones	R1	R2	R3
Free type	Daidzein	H	H	
	Glycitein	H	OCH_3	
	Genistein	OH	H	
Glucoside type	Daidzin	H	H	H
	Genistein	H	OCH_3	H
	Glycitin	OH	H	H
Acetyl glucoside type	Acetyldaidzin	H	H	$COCH_3$
	Acetylglycitin	H	OCH_3	$COCH_3$
	Acetylgenistin	OH	H	$COCH_3$
Malonylglucoside type	Malonyldaidzin	H	H	$COCH_2COOH$
	Malonylglycitin	H	OCH_3	$COCH_2COOH$
	Malonylgenistin	OH	H	$COCH_2COOH$

The GO analysis forecast that the principal biological processes involve reactions to xenobiotic stimuli, the cyclooxygenase pathway, the positive regulation of the apoptotic process, the cellular response to reactive oxygen species, signal transduction, the inflammatory response, and antifolate resistance, among others. Regarding molecular functions, the key activities identified include enzyme binding, protein binding, iron ion binding, interaction with proteins and phosphatases, kinase activity, and ATP binding (Figure 2g).

The investigation into soy isoflavone's role in mitigating IS via the KEGG pathway analysis unveiled its involvement across a spectrum of signaling pathways. These pathways encompass IL-17 associated with IS, along with the FoxO, cAMP, TNF, and ErbB signaling pathways and the regulation of TRP channels through inflammatory mediators. Additional pathways implicated include the Ras, neurotrophin, VEGF, and Relaxin signaling mechanisms (Figure 2h). Combined with a literature review, we hypothesized that soy isoflavone may delay the translation of brain tissue damage after a stroke by affecting redox-related signaling pathways. For the in vitro and in vivo experimental verification, we chose the classical keap1/NQO1/Nrf2/HO-1 signaling pathway.

Figure 2i,j categorized the top 50 pathways enriched by KEGG, and these pathways could be classified into four categories, including metabolism (amino acid metabolism, lipid metabolism, global and overview maps, and energy metabolism), cellular processes (transport and catabolism, cell growth and death), organismal systems (immune system, endocrine system, sensory and regeneration, nervous system, development, and regeneration), human diseases (neurodegenerative diseases, cardiovascular diseases), signal transduction (Sphingolipid signaling pathway, FoxO signaling pathway, MAPK signaling pathway, ErbB signaling pathway, VEGF signaling pathway, PI3K Akt signaling pathway, Ras signaling pathway, and so on).

Based on this, soy isoflavones' active ingredients (daidzein, genistein, and glycitein) were molecularly docked with the pathway protein Nrf2/keap1/NQO1/HO-1 (Figure 3a). An affinity of less than -4.25 kcal·mol^{-1} indicates binding activity between the ligand and the target; an affinity of less than -5.0 kcal·mol^{-1} indicates good binding activity; and an affinity of less than -7.0 kcal·mol^{-1} indicates strong docking activity. Their affinities are shown in Figure 3b.

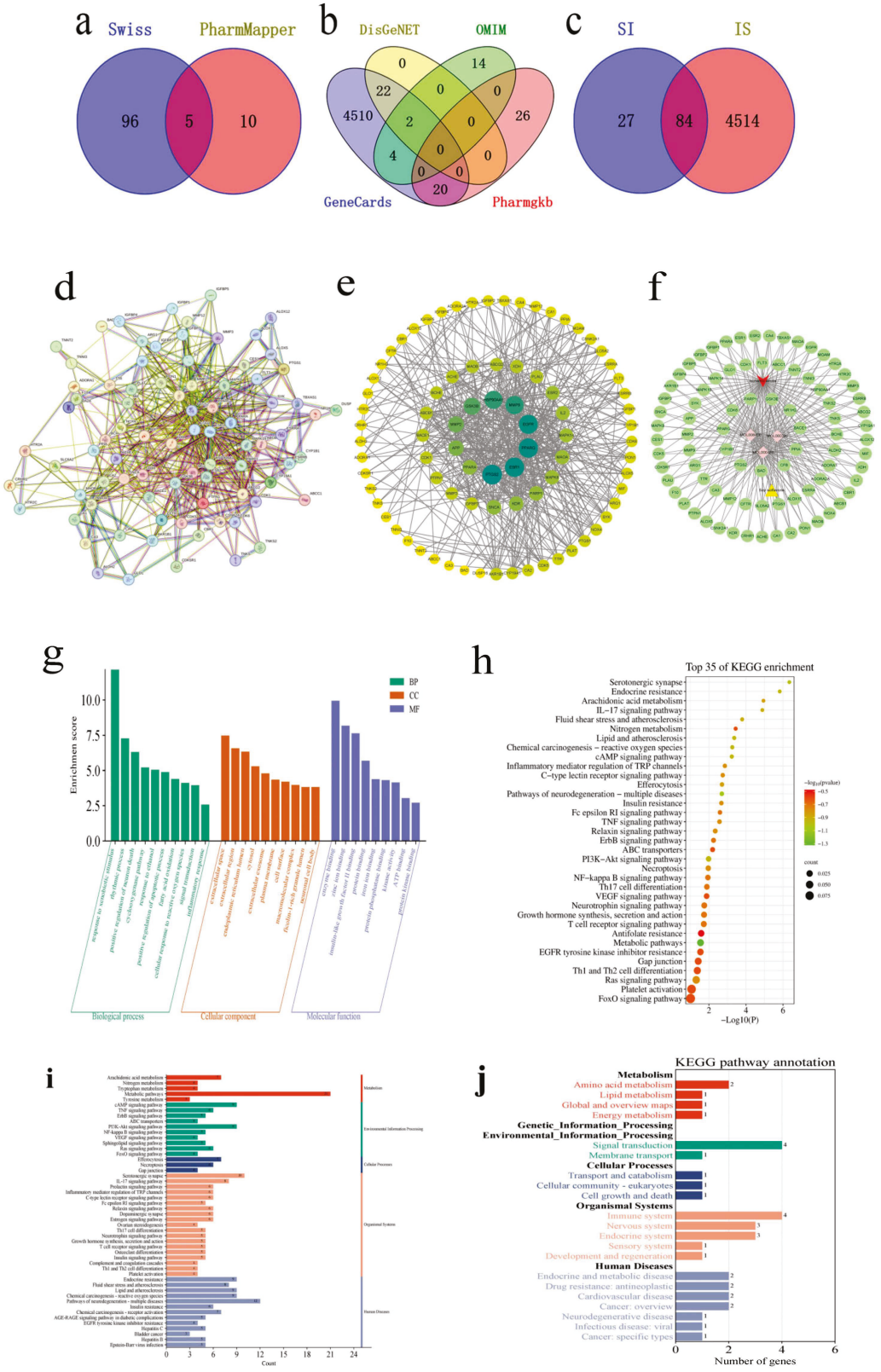

Figure 2. The exploration of the soy isoflavone (IS) network through a pharmacological analysis. (**a**) Drug Venn diagram. (**b**) Disease Venn diagram. (**c**) Drug–Disease Venn Diagram. (**d**) PPI network. (**e**) Beautified PPI network. (**f**) Drug–component–disease–target network. (**g**) GO enrichment analysis results. (**h**) KEGG pathway enrichment analysis findings. (**i**) A first-level taxonomic analysis of the KEGG enrichment pathway. (**j**) Secondary classification analysis of KEGG enrichment pathways.

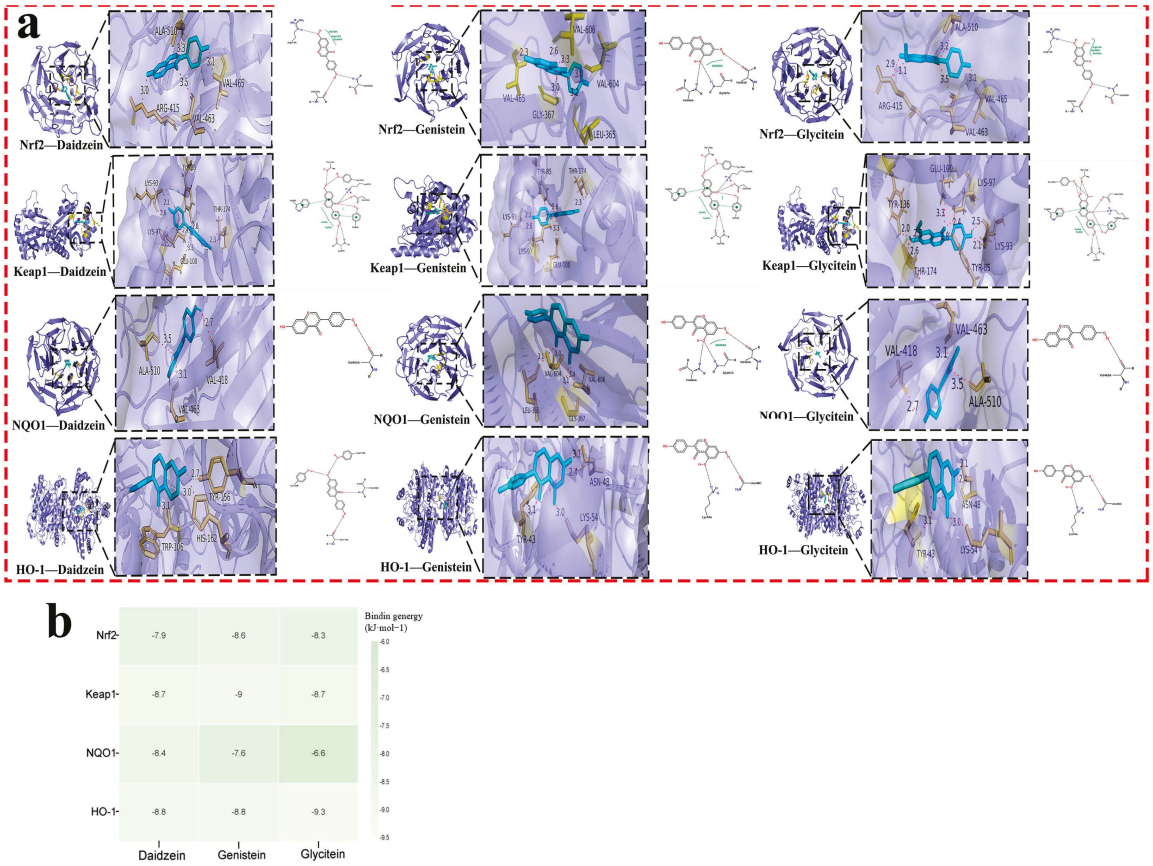

Figure 3. The molecular docking of the main active ingredients of soy isoflavones with key target proteins. (**a**) Visualization diagram of molecular docking. Ligands are shown in cyan, protein surfaces are shown in blue/purple, and yellow residues indicate key binding interactions. (**b**) Heat map. Darker green indicates stronger binding affinity (more negative binding energy, in kJ·mol^{-1}).

2.3. Cell Experimental

2.3.1. Establishment of Soy Isoflavone Concentration

The MTT assay was used to assess the cytotoxicity of soy isoflavones and determine their concentration. The results indicated that as the concentration of soy isoflavones increased, their cytotoxicity was enhanced, particularly when concentrations exceeded 2240 μg/mL, which significantly reduced cell viability ($p < 0.05$). Therefore, concentrations below 2240 μg/mL were considered within the biosafe range. Based on this, concentrations of 140 μg/mL, 280 μg/mL, and 560 μg/mL were selected for subsequent experiments. In further experiments, the concentration range of soy isoflavones was expanded up to 40 g/L, and the EC_{50} value was calculated. The EC_{50} of soy isoflavones was determined to be 37.01 g/L (Figure 4).

2.3.2. Morphological Changes in PC12 Cells

A microscopic examination revealed that the normal control group exhibited a higher quantity of PC12 cells and superior cell proliferation. In contrast, the model group showed a reduction in both the PC12 cell count and synaptic connections. The groups treated with soy isoflavone and the positive control showed an increased number of viable cells, a decrease in cellular damage, and a partial restoration of cells to their normal morphology (Figure 5a).

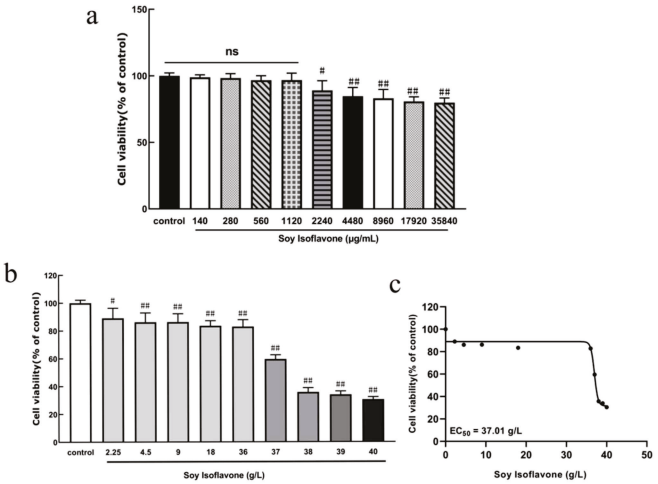

Figure 4. (**a**,**b**) Effects of different concentrations of soy isoflavones on cytotoxicity of PC12 vs. normal cell group. (Values are indicated as mean ± SD; statistical analysis was performed using one-way ANOVA followed by Tukey's post hoc test; ns: no significant difference. $n = 4$, # $p < 0.05$, ## $p < 0.01$.) (**c**) Dose-response curve of soy isoflavone's effect on PC12 cell viability. The normalized inhibition rate was calculated based on the control's response. (EC_{50} value was estimated using Kaplan-Meier model. $n = 4$).

2.3.3. The Effect of the Treatment on the PC12 Cells with Increasing Concentrations of Soy Isoflavone

Figure 5b presents a comparative study showing that PC12 cells in the model group displayed a significantly lower survival rate compared to the control group. However, treating these cells with soy isoflavones at a dose of 560 μg/mL markedly improved their survival rates. The data presented in Figure 5c–f elucidate that the levels of Ca^{2+}, ROS, LDH, and Caspase-3 were considerably elevated in the model group when juxtaposed with the control group. Remarkably, the administration of soy isoflavone at a 560 μg/mL dosage markedly diminished these levels, indicating a protective effect against cellular stress and apoptosis. The flow cytometry analysis, as shown in Figure 5g,h, revealed an apoptosis rate of 5.34% in the control group, which surged to 30.85% in the model group, underscoring the detrimental impact of the OGD/R treatment. Conversely, the soy isoflavone-treated groups displayed a significant reduction in apoptosis rates, with the 560 μg/mL dosage group showing the most pronounced decrease to 20.00%, followed by the 140 μg/mL and 280 μg/mL dosage groups. The edaravone-positive control also showed a decrease in apoptosis, validating the protective efficacy of both treatments against cellular apoptosis induced by OGD/R. Furthermore, Figure 5i,j highlight the detrimental effect of OGD/R treatment on the migratory capacity of PC12 cells. The scratch assay results indicate a substantial recovery in the scratch area for the groups treated with soy isoflavone and the positive control, evidencing the compound's role in facilitating cellular repair and migration post-injury.

2.3.4. Effect of Soybean Isoflavones on Nrf2 Pathway in Sodium Metabisulfite-Treated PC12 Cells

To explore the protective mechanisms of soy isoflavones, the study utilized Western blotting to assess the nuclear Nrf2 expression levels and the expressions of Keap1, HO-1, and NQO1. As depicted in Figure 6, the soy isoflavone and edaravone treatments significantly elevated the nuclear expression of Nrf2 when compared to the model group ($p < 0.01$). Furthermore, soy isoflavones distinctly reduced the expression of Keap1 while simultaneously increasing the expressions of HO-1 and NQO1 ($p < 0.01$ for each). These

findings suggest that the protective effects of soy isoflavones may be intricately linked to the modulation of the Nrf2 and Keap1 pathways (Figure 6).

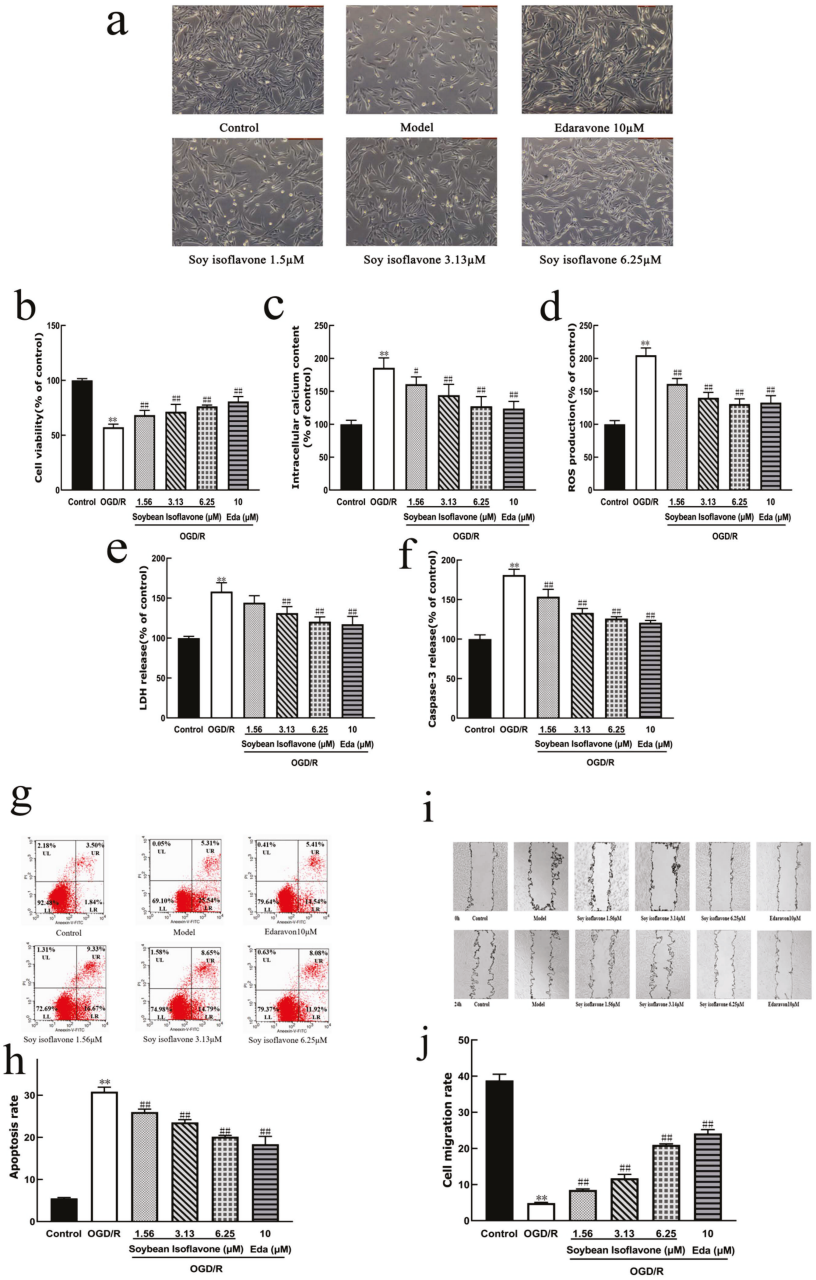

Figure 5. Effects of soybean isoflavones (SI) on PC12 cells under OGD/R conditions. (**a**) Representative morphological images of PC12 cells in each treatment group. Cells were exposed to different concentrations of soybean isoflavones (1.56, 3.13, and 6.25 μM) or edaravone (10 μM) following OGD/R induction. (**b**) Cell viability was assessed using the MTT assay. (**c**) Intracellular calcium levels were measured to evaluate calcium overload. (**d**) Reactive oxygen species (ROS) production was determined as an indicator of oxidative stress. (**e**) Lactate dehydrogenase (LDH) release was measured as a marker of membrane damage. (**f**) Caspase-3 release was detected to assess apoptosis activation. (**g**) Flow cytometric analysis of apoptosis using Annexin V-FITC/PI staining. (**h**) Quantification of apoptosis rate based on flow cytometry results. (**i**) Representative images of the wound healing assay to evaluate PC12 cell migration. (**j**) Quantification of cell migration rate. All values are expressed as mean ± SD. Statistical significance was determined by one-way ANOVA followed by Tukey's post hoc test. (Values are indicated as mean ± SD; statistical analysis was performed using one-way ANOVA followed by Tukey's test. $n = 6$ for (**b**)–(**f**), $n = 3$ for (**h**)–(**j**). ** $p < 0.01$, compared to control, # $p < 0.05$, ## $p < 0.01$ versus model cohort).

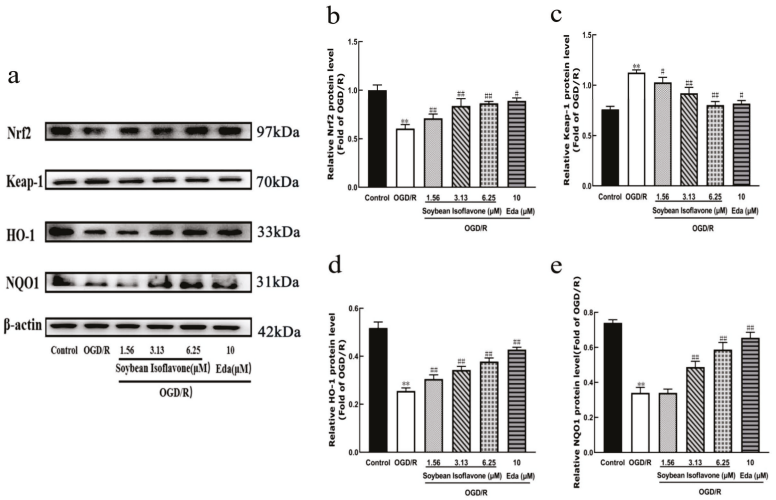

Figure 6. Examination of soy isoflavone (SI)'s influence on oxygen–glucose deprivation/reoxygenation (OGD/R) protein expression in PC12 cells. (**a**) Western blotting analysis. (**b**) Comparative expression of nuclear factor erythroid 2-related factor 2 (Nrf2) protein. (**c**) Kelch-like, ECH-associated protein 1 (Keap1) protein expression levels. (**d**) Heme oxygenase-1 (HO-1) protein expression. (**e**) NAD(P)H quinone dehydrogenase 1 (NQO1) protein expression levels. (Values are indicated as mean ± SD; statistical analysis was performed using one-way ANOVA followed by Tukey's post hoc test. $n = 3$, ** $p < 0.01$, compared to control, # $p < 0.05$, ## $p < 0.01$ versus model cohort).

2.4. Animal Experimentation

2.4.1. Soybean Isoflavones Improved the Neurological Function Score, Brain Tissue Water Content, and Cerebral Infarct Volume of Rats in Each Group

In order to evaluate the therapeutic impact of soy isoflavones on cerebral ischemic injury, this study conducted an analysis focusing on the neurological function score, the moisture content of brain tissue, and the extent of cerebral infarction following ischemic damage. The investigation revealed that, in comparison to the sham-operated control group, the model group exhibited significantly elevated scores for behavioral dysfunction, increased moisture levels in brain tissue, and expanded cerebral infarction volumes, highlighting extensive neuronal injury. In contrast, pretreatment with soy isoflavones (100 mg/kg) administered via intraperitoneal injection notably reduced the scores for neurological dysfunction, decreased the water content within the brain, and minimized the volume of cerebral infarction (Figure 7). Compared to the model group, the application of soy isoflavones and edaravone markedly enhanced recovery from neurological dysfunction, with statistical significance ($p < 0.01$ for both treatments). These significant findings are systematically presented in Table 3.

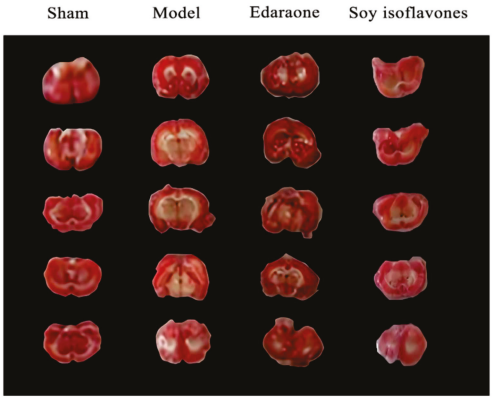

Figure 7. The impact of Tectoridin on neurological deficits.

Table 3. Comparative assessment of neurological function, brain water content, and cerebral infarct volume in rat groups, indicating statistical significance. (Values are indicated as mean ± SD; statistical analysis was performed using one-way ANOVA followed by Tukey's post hoc test. $n = 10$, ** $p < 0.01$, compared to control, # $p < 0.05$, ## $p < 0.01$ versus model cohort).

Group	Neurological Function Score	Brain Tissue Water Content	Cerebral Infarct Volume
Sham operation group	0 ± 0	78.5 ± 3.6	0 ± 0
Model group	8.3 ± 1.09 **	85.4 ± 2.6 **	27.6 ± 1.6 **
Edaravone	5.4 ± 2.11 ##	77.5 ± 2.4 ##	23.9 ± 1.4 ##
Soybean isoflavone	6.8 ± 1.68 ##	76.5 ± 3.2 ##	22.5 ± 2.1 #

2.4.2. Soybean Isoflavones Improved the Brain Histopathology of the Rats in Each Group

Following HE staining and microscopic examination, the sham-operated group exhibited no signs of ischemic alterations. Observations revealed that the architecture and cytoplasm of neuronal cells remained intact, with nucleoli distinctly visible, and no cellular abnormalities were observed near or within the vasculature. Contrastingly, in the model group, focal ischemia–reperfusion injuries were predominantly localized to the brain's central region, characterized by loosened brain tissue, edema, and neuronal tract ischemic changes, including pyknosis within the affected lesions. Soy isoflavone pretreatment markedly mitigated the neuronal damage within the ischemic zone, as evidenced in Figure 8.

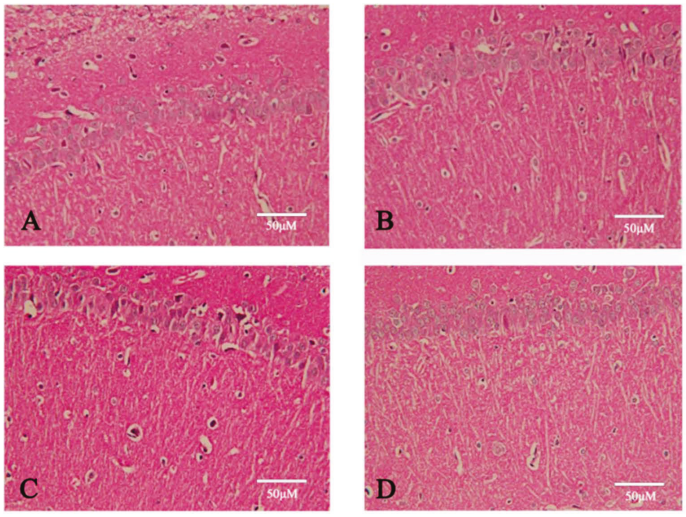

Figure 8. Pathological alterations in brain tissue across different experimental groups. (**A**) Sham-operated group. (**B**) Model. (**C**) Treated with soybean isoflavones (100 mg/kg). (**D**) Treated with edaravone (10 mg/kg).

2.4.3. Effects of Soybean Isoflavones on Activities of SOD, GSH-px, CAT, and Contents of MDA and LDH in Rat Brains

Compared with the control group subjected to a sham procedure, the model group displayed diminished activity levels of SOD, GSH-px, and CAT within the cerebral tissue. This group also showed elevated levels of MDA and LDH, with all the differences being statistically significant ($p < 0.01$). Following treatment with soybean isoflavones and edaravone, a significant reduction in MDA concentrations and LDH release was observed. Concurrently, there was a significant enhancement of the activities of SOD, GSH-px, and CAT ($p < 0.01$), as detailed in Table 4.

Table 4. Evaluation of antioxidant activities (SOD, GSH-Px, CAT) and levels of oxidative stress markers (MDA, LDH) in the brain tissue of rat groups, with significance denoted. (Values are indicated as mean ± SD; statistical analysis was performed using one-way ANOVA followed by Tukey's post hoc test. $n = 4$, ** $p < 0.01$, compared to control, ## $p < 0.01$ versus model cohort).

Group	SOD (U/mg prot)	GSH-px (U/mg prot)	CAT (U/mg prot)	MDA (nmol/mg)	LDH (U/L)
Sham operation group	18.5 ± 1.6	26.7 ± 2.6	5.6 ± 1.2	3.8 ± 0.6	180.8 ± 15.3
Model group	9.4 ± 1.6 **	9.8 ± 1.6 **	2.3 ± 1.1 **	6.1 ± 1.1 **	319.3 ± 25.1 **
Edaravone	12.5 ± 1.4 ##	13.9 ± 1.4 ##	3.3 ± 1.3 ##	4.4 ± 1.2 ##	216.4 ± 22.21 ##
Soybean isoflavone	10.5 ± 1.2 ##	12.5 ± 2.1 ##	2.9 ± 1.4 ##	4.2 ± 1.6 ##	193.3 ± 11.7 ##

2.4.4. Soybean Isoflavones Reduce Oxidative Stress Injury by Increasing Nrf2 Signaling Pathway

Figure 9 illustrates that, in comparison to the model group, treatment with soybean isoflavones and edaravone significantly augmented the nuclear expression of Nrf2 ($p < 0.01$). Additionally, soybean isoflavones markedly reduced the expression of Keap1 while simultaneously enhancing the expression levels of HO-1 and NQO1 ($p < 0.01$ for all). These findings suggest a strong correlation between the protective effects of soybean isoflavones and the regulatory activities on the Nrf2 and Keap1 pathways.

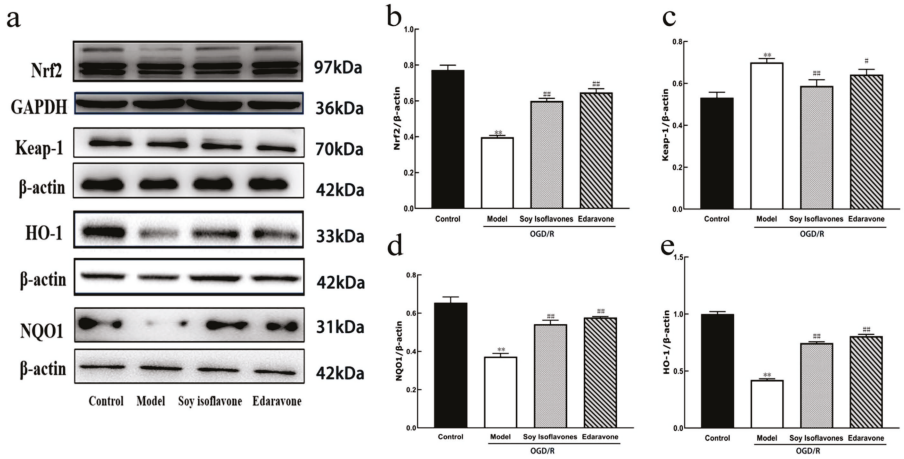

Figure 9. Soy isoflavones (SI) reduce oxidative stress injury by increasing nuclear factor erythroid 2-related factor 2 (Nrf2) signaling pathway. (**a**) Western blot representation of nuclear Nrf2 levels and expression of Kelch-like, ECH-associated protein 1 (Keap1), heme oxygenase-1 (HO-1), and NAD(P)H quinone dehydrogenase 1 (NQO1). (**b**) Comparative expression of Nrf2 protein. (**c**) Keap1 protein expression levels. (**d**) NQO1 protein expression. (**e**) HO-1 protein expression levels. (Values are indicated as mean ± SD; statistical analysis was performed using one-way ANOVA followed by Tukey's post hoc test. $n = 4$, ** $p < 0.01$, compared to control, # $p < 0.05$, ## $p < 0.01$ versus model cohort).

3. Discussion

Ischemic stroke has emerged as a critical health issue worldwide. The primary treatment options available are thrombolytic drugs, which, despite their efficacy, pose significant risks to health. These drugs are only effective within a narrow therapeutic window of 3 to 6 h following a stroke; administration beyond this period risks causing ischemia–reperfusion injury [17]. Studies have elucidated that the cessation of blood flow results in ischemia, and the subsequent restoration of circulation, or reperfusion, leads to an influx of oxygen, generating excessive oxygen free radicals [18]. Concurrently, this process suppresses the activity of antioxidant enzymes, precipitating oxidative stress that exacerbates

brain damage. Although thrombolytic agents offer crucial benefits for acute ischemic stroke, potentially saving lives, their long-term application is hindered by their chemical composition, which can interfere with patient metabolism. On the other hand, natural biological agents present a more favorable profile, characterized by gentler effects and reduced toxicity and side effects, making them more suitable for extended use [19].

Soybean isoflavones possess multiple pharmacological effects, significantly contributing to antioxidation, mitigating inflammation following cerebral ischemia, cholesterol reduction, and the prevention of cardiovascular diseases [20,21]. This study utilized the reflux method to extract isoflavones from soybean, with the constituents of the soybean extract subsequently identified through HPLC-DAD-MS. The primary components identified were daidzin, glycitin, genistin, acetyldaidzin, acetylcitin, malonylgenistin, and acetylgenistin. The network pharmacology analysis suggested that soy isoflavones may modulate the oxidative stress in brain tissues induced by stroke through their influence on redox signaling pathways, thereby offering potential prevention and treatment for ischemic stroke. In vivo experiments entailed establishing a rat model of transient global cerebral ischemia–reperfusion by occluding the bilateral common carotid arteries. Preliminary findings revealed that soybean isoflavone pretreatment markedly ameliorated neurological damages in cerebral ischemia–reperfusion rats, significantly diminishing the brain water content and the infarct volume. Additionally, there was a significant elevation in the activities of SOD, GSH, and CAT within the brain tissues, alongside a marked reduction in MDA and LDH levels. Morphological observations further confirmed the significant mitigation of cerebral lesions by soybean isoflavones in rats subjected to cerebral ischemia–reperfusion injury.

An imbalance between the generation of ROS and the capacity of the organism to counteract their negative effects with antioxidants leads to oxidative stress [22]. The body possesses an elaborate defense system against free radicals, comprising antioxidant enzymes such as SOD, CAT, and GSH-px [23]. SOD, a metalloproteinase found across various tissues, cells, and organelles, plays a crucial role in scavenging excess free radicals, thus maintaining the cellular peroxidation balance. Its activity is often used as an indicator of the body's antioxidant capability [24]. Furthermore, GSH-px and CAT effectively catalyze the breakdown of hydrogen peroxide, eliminating harmful superoxide metabolites to reduce peroxidative damage [25]. Therefore, the body's antioxidant capacity can be gauged by the activities of SOD, GSH-px, and CAT and the levels of ROS. Ischemia/reperfusion injury induces a surge in ROS, leading to an increase in lipid peroxides, which are then converted into MDA (malondialdehyde) [26]. Simultaneously, the activity of Ca^{2+} pumps declines, causing an elevation in cellular Ca^{2+} concentration and accumulation, which interferes with Ca^{2+} signal transduction [27]. An increase in Ca^{2+} concentration triggers the production of free fatty acids, leading to a surge in free radicals [28], which disturbs both the energy and the intracellular environmental equilibrium. This process activates Caspase-3, fostering neuronal apoptosis, exacerbating cellular damage, and heightening the risk of myocardial infarction. Concurrently, oxidative stress can escalate serum LDH (lactate dehydrogenase) levels, causing further cellular and tissue damage. Thus, serum concentrations of MDA, Ca^{2+}, Caspase-3, and LDH serve as indicators of oxidative harm. It was discovered that SI significantly mitigates the damage to PC12 cells induced by oxygen–glucose deprivation/reoxygenation, reduces apoptosis, boosts cell viability, and diminishes levels of Ca^{2+}, LDH, and ROS. Hence, SI exerts a notable protective effect against Na2S2O4-induced injury in PC12 cells, likely through mitigating oxidative stress. Additionally, this investigation reveals that pretreatment with soybean isoflavones markedly lowers MDA and LDH levels in the brain tissue of rats suffering from cerebral ischemia–reperfusion injury while notably enhancing the activities of SOD, GSH-px, and CAT. Consequently,

soybean isoflavones effectively elevate antioxidant enzyme activity in rats subjected to cerebral ischemia–reperfusion injury, thereby alleviating oxidative stress-induced damage.

Nrf2 is recognized as a key defender against oxidative stress in ischemic stroke [29,30]. Research indicates that Nrf2 not only indirectly modulates the expression of various transcription factors but also contributes to neuroprotection by dampening inflammatory responses, combating oxidative stress, diminishing apoptosis and necrosis, and fostering cell growth and differentiation [31]. Moreover, the Nrf2 signaling pathway plays a crucial role in neuroprotection, as evidenced by studies on numerous traditional Chinese medicinal compounds [32]. Normally, Nrf2 forms an inactive complex with Keap1 [33]. Upon activation, Nrf2 separates from Keap1, migrates from the cytoplasm to the nucleus, and binds to the ARE, thereby activating antioxidant enzymes like HO-1 and NQO1 [34]. This investigation highlighted that soy isoflavones notably increase the concentrations of Nrf2, HO-1, and NQO1, while significantly reducing Keap1 levels (Figure 10). It suggests that the neuroprotective mechanisms of soy isoflavones could be linked to stimulating the Nrf2 signaling pathway. Through this pathway, the regulation of antioxidant responses to oxidative stress from cerebral ischemia–reperfusion is achieved, potentially facilitating cellular growth, differentiation, and angiogenesis, thus contributing to neuroprotection.

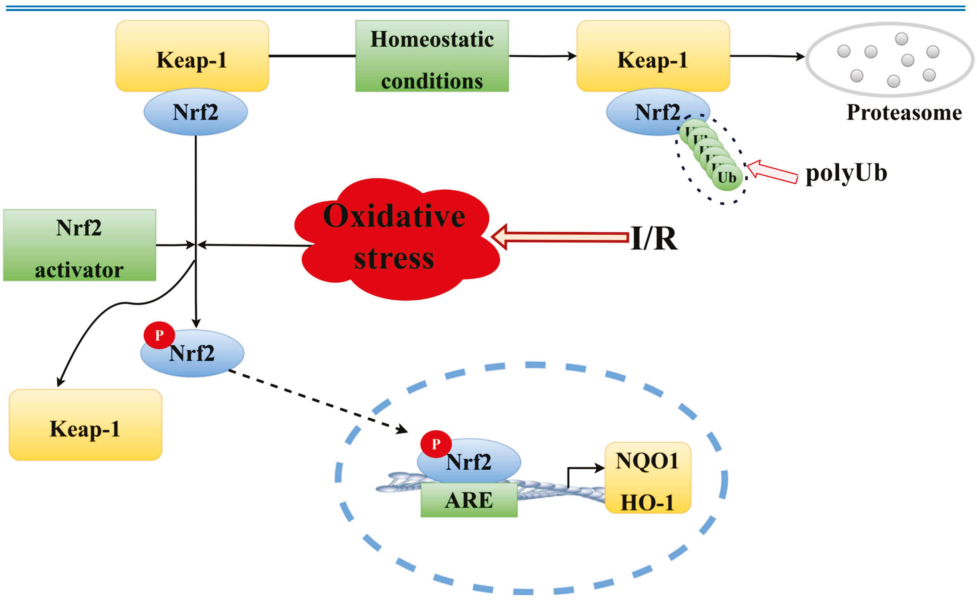

Figure 10. The molecular mechanism of the Keap1/NQO1/Nrf2/HO-1 pathway. Solid black arrows indicate biological processes; dashed black arrows represent translocation.

Research indicates that soy isoflavones exhibit a protective capacity in the context of cerebral ischemia–reperfusion injuries. This protective effect is attributed to the enhancement of antioxidant enzyme activities and the suppression of oxidative stress. Furthermore, soy isoflavones' defense against ischemic stroke is linked to the stimulation of Nrf2 and the reduction of Keap1 activity. These findings are consistent with previous in vivo and in vitro studies, further supporting the multi-target neuroprotective potential of SI.

In vitro, Zhang et al. (2022) reported that SI protected PC12 cells from $CoCl_2$-induced hypoxic injury by activating Nrf2 and suppressing the p38 MAPK and AKT–mTOR pathways, thereby reducing ROS levels, enhancing cell viability, and inhibiting apoptosis [35]. These mechanisms align with our observations in the OGD/R model, where SI demonstrated antioxidant and anti-apoptotic effects. In vivo, Schreihofer et al. (2005) found that a high-soy diet significantly reduced the infarct size in female rats subjected to permanent middle cerebral artery occlusion (MCAO), indicating notable neuroprotective effects under

physiological conditions [36]. Similarly, Huang et al. (2009) showed that SI alleviated brain tissue damage and improved neurological function in ischemic rats by modulating the Notch signaling pathway [37]. Moreover, Li et al. (2025) demonstrated that genistein, a major component of SI, mitigated cerebral ischemia–reperfusion injury in rats by inhibiting the Wnt/Ca^{2+} signaling pathway, emphasizing its role in calcium homeostasis [38]. These studies reinforce our findings that SI exerts neuroprotective effects through multiple signaling pathways, particularly those related to oxidative stress and apoptosis regulation.

In conclusion, our findings are in strong agreement with existing in vivo and in vitro research, underscoring the multifaceted mechanisms by which soy isoflavones alleviate ischemic brain injury. These results support the therapeutic potential of SI and provide a solid foundation for its future clinical application. Although this study provides evidence supporting the neuroprotective role of soy isoflavones through the activation of the Nrf2 signaling pathway, several limitations should be noted. First, the study was conducted using a single animal model (BCCAO) and PC12 cells, which may not fully reflect the complexity of human ischemic stroke pathology. Second, the exact active monomer(s) within the soy isoflavone extract responsible for the observed effects remain to be identified. Third, the long-term safety and efficacy of soy isoflavones were not assessed. Future studies should explore the effects of individual isoflavone components, investigate additional models of stroke (e.g., MCAO), and assess chronic outcomes such as cognitive function and neuroregeneration.

4. Materials and Methods

4.1. Chemical, Reagents, and Software

Soy isoflavones standards, including Daidzin, Glycitin, Genistein, Acetyldaidzin, Acetylglycitin, Malonylgenistein, and Acetylgenistein, were purchased from Aladdin Industrial Corporation (Cat# various; Shanghai, China). Acetonitrile (HPLC grade) was obtained from Thermo Fisher Scientific (Cat# A955-4; Waltham, MA, USA). Ultrapure water was prepared using a Milli-Q system (Millipore, Billerica, MA, USA). Analytical-grade reagents were provided by Beijing Chemical Works (Beijing, China). Kits for superoxide dismutase (SOD), glutathione peroxidase (GSH-px), malondialdehyde (MDA), and total protein were from the Nanjing Jiancheng Bioengineering Institute (Cat# A001-3, A005, A003-1, A045-2-2; Nanjing, Jiangsu, China). Kits for catalase (CAT), 3-(4,5-dimethylthiazol-2-yl)-2,5-diphenyltetrazolium bromide (MTT), lactate dehydrogenase (LDH), reactive oxygen species (ROS), Fluo-3 acetoxymethyl ester (Fluo-3AM), and caspase-3 were obtained from Beyotime Biotechnology (Shanghai, China). Other chemicals, including internal standard, Earle's Balanced Salt Solution (EBSS), phosphate-buffered saline (PBS), sodium dithionite ($Na_2S_2O_4$), and edaravone, were purchased from Sigma-Aldrich (St. Louis, MO, USA).

Primary antibodies: Anti-Nrf2 (Cat# 12721, Cell Signaling Technology, Danvers, MA, USA); Anti-Keap1 (Cat# ab227828), Anti-HO-1 (Cat# ab68477), Anti-NQO1 (Cat# ab34173), and Anti-β-actin (Cat# ab8227) (all from Abcam, Cambridge, UK). The GraphPad Prism version 9.5.1 (GraphPad Software, San Diego, CA, USA) was used for the statistical analysis. ImageJ version 1.53 (National Institutes of Health, Bethesda, MD, USA) was used for the densitometric analysis. FlowJo version 10.8.1 (BD Biosciences, Ashland, OR, USA) was used for the flow cytometry data analysis. Cytoscape version 3.9.1 (The Cytoscape Consortium, San Diego, CA, USA), AutoDockTools version 1.5.7, AutoDock Vina version 1.2.3, and PyMOL version 2.5.4 (Schrödinger, LLC, New York, NY, USA) were used for molecular docking and visualization.

4.2. Extraction and Identification of Soybean Isoflavones

A precise 10 g sample of soybean was measured and subjected to a reflux extraction process using 100 mL of 65% ethanol, conducted twice for a duration of 2 h each. The resultant filtrate was then concentrated and pooled together, followed by dilution to a fixed volume of 10 mL with methanol. Subsequent to comprehensive homogenization, the filtration of the solution through a membrane with a pore size of 0.45 μm was performed in preparation for the analytical procedures. The identification of chemical components within the soybean extracts was carried out utilizing HPLC-DAD-MS [39].

The procedure for high-performance liquid chromatography (HPLC) involved using a binary linear gradient elution technique [40]. Here, acetonitrile served as mobile phase A, while mobile phase B consisted of water containing 0.05% phosphoric acid. The gradient schedule for the mobile phases was meticulously programmed: starting with mobile phase B at 90%, it was gradually reduced to 82% over the first 10 min, then further decreased to 80% between 10 and 13 min, followed by a drop to 60% from 13 to 30 min, and was ultimately adjusted to 50% for the final 10 min, from 30 to 40 min. The flow rate was consistently held at 1.0 mL/min, with a sample injection volume of 10 μL, and the detection was conducted at a wavelength of 254 nm, all while maintaining the column at a stable temperature of 30 °C.

For the mass spectrometry, the diode array detector (DAD) was linked to the mass spectrometer via a three-way valve, employing an electrospray ionization (ESI) source in positive ion mode. The scan range was set between M/Z 50 and 1000. The ion source spray voltage was established at 4.5 kV, with a sheath gas flow rate of nitrogen set at 20 L/min and an ion trap pressure at 3.1×10^7 Pa. The temperature for the metal capillary was 250 °C with a voltage of 20 V. The resolution for ESI-MSˆn was maintained at 1.0 Da, and the collision-induced dissociation (CID) collision energy ranged from 20 to 30%.

4.3. Network Pharmacology Research

The research on soy isoflavone was initiated by exploring the CNKI database using "soy isoflavone" as the search term to compile a list of soy isoflavone components. The SwissADME online server was utilized to screen soy isoflavone's active ingredients, evaluating each component's pharmacokinetic parameters and adherence to the Lipinski Rule of Five [15]. The potential targets of these active ingredients were then predicted through the Swiss Target Prediction and PharmMapper databases. To identify relevant targets for ischemic stroke, searches were conducted in the GeneCards, OMIM, PharmGkb, and DisGeNET databases. The identified soy isoflavone targets were aligned with those related to drug actions to pinpoint common targets, and a Venn diagram was created to visualize these intersections. Subsequently, these intersecting targets were analyzed for Protein–Protein Interactions (PPIs) using the String database (version 12.0), with the findings visualized in Cytoscape 3.8.0. The intersection targets underwent further analysis of the GO and KEGG pathways using the DAVID website. The top 50 KEGG pathways were classified and summarized according to the first 6 classifications in the KEGG pathway database. Molecular docking between the core components and the core targets was performed based on the above analysis. The 3D crystal structures of the target proteins were obtained from the Protein Data Bank (PDB). Their pdb format files were downloaded, de-watered, and hydrogenated in AutoDockTools (version: 1.5.7) and then selected as receptors and saved as pdbqt files. The mol2 files of the active components were obtained through the TCMSP database, hydrogenated in AutoDockTools, selected as ligands, and exported as pdbqt files. Molecular docking was carried out through AutoDock Vina (version: 1.2.3) and the affinity of each component for the target was obtained and visualized by PyMOL (version: 2.7.0) and the ZBH-Center for Bioinformatics. The results were illustrated

through histograms and bubble maps representing the pathway information, which were crafted by the bioinformatics.com.cn platform, accessed last on 28 December 2023 [41].

4.4. In Vitro Studies

4.4.1. PC12 Cell Culture

PC12 cells, acquired from the Chinese Academy of Sciences in Shanghai, were cultivated in a nutrient-rich Dulbecco's Modified Eagle Medium (DMEM), a high-glucose medium, which was further supplemented with 10% fetal bovine serum and a 1% mixture of penicillin and streptomycin antibiotics. These cells were then incubated at a constant temperature of 37 °C in an environment enriched with 5% CO_2 for a duration spanning between three and four d, until they reached a confluence of 70–80%. Following this phase of growth, a solution containing 0.25% trypsin was employed to gently detach the cells, facilitating their transfer to new culture containers for continued propagation. In preparation for a range of experimental activities, the cells were subsequently allocated into 96-well plates, with 100 μL of the cell culture introduced into each well. Post-seeding, an additional period of incubation was undertaken in a 5% CO_2 atmosphere at 37 °C, extending from one to two d, to allow the cells to achieve a confluence between 80 and 90%, thereby rendering them suitable for further experimental investigations [42].

4.4.2. Establishment of Soy Isoflavone Concentrations

PC12 cells were inoculated into 96-well culture plates at a density of 9×10^4/mL, 100 μL per well, and incubated at 37 °C with 5% CO_2 for 24 h. Afterwards, the original culture medium was discarded, and different concentrations of soy isoflavones (140, 280, 560, 1120, 2240, 4480, 8960, 17,920, and 35,840 μg/mL) were added to incubate the cells for 24 h. At the end of the incubation period, the cytotoxicity of the PC12 cells was detected by MTT.

4.4.3. The Establishment and Experimental Grouping of a Glucose–Oxygen Deprivation/Reoxygenation (OGD/R) Ex Vivo Stroke Model

To evaluate the protective impact of a natural isoflavone, SI, on PC12 cells subjected to OGD/R-induced injury, the cells, prepared as previously mentioned, were allocated to various groups: the control group received no OGD/R injury treatment. In the model group, the cells were treated with 100 μL of glucose-free EBSS solution enriched with 10 mmol/L $Na_2S_2O_4$ for 2 h. Subsequently, the medium was replaced with a standard culture medium to allow reoxygenation, and the cells were further incubated for 24 h, establishing an OGD/R injury model to mimic ischemic brain damage. For the treatment groups, OGD/R conditions were amended with a standard culture medium containing different concentrations of SI (1.56 μM, 3.13 μM, and 6.25 μM) for 24 h. Additionally, a positive control group was treated with 10 μM edaravone under OGD/R conditions (n = 6), to compare the efficacy of SI against a known neuroprotective agent [43].

4.4.4. Morphological Observation

Following the incorporation of various treatment agents, the PC12 cells were maintained at 37 °C for a 24 h period. Post-treatment, the cells underwent examination under an inverted microscope to assess any morphological alterations across the specified groups (n = 6).

4.4.5. MTT Method to Measure Cellular Activity

Following treatment, each well in a 96-well cell culture plate was treated with 10 μL of 3-(4,5-dimethylthiazol-2-yl)-2,5-diphenyltetrazolium bromide (MTT) solution (5 g/L concentration) in a light-protected environment. After incubating for 4 h at 37 °C in a 5% CO_2 atmosphere, the supernatant was discarded. Subsequently, to dissolve the resultant

formazan crystals, 100 μL of dimethyl sulfoxide (DMSO) was added to each well. The optical density of the solutions in each well was measured at 490 nm wavelength using an enzyme-linked immunosorbent assay, with measurements taken within 10 to 15 min. All the data are presented as the mean ± SD (n = 6 per group), and statistical comparisons were performed using a one-way ANOVA followed by Tukey's post hoc test.

4.4.6. Detection of Ca^{2+} Content in PC12 Cells

After applying the treatment, the cells were incubated for one hour at 37 °C in a 5% CO_2 atmosphere with the culture medium that included the Fluo-3AM fluorescent probe at a concentration of 2.5 μmol/L. Following this incubation period, any residual probe was meticulously washed away, and the fluorescence indicative of intracellular Ca^{2+} levels was detected using a fluorescence microscope [44]. The intensity of this fluorescence, with the excitation and emission wavelengths set at 488 nm and 530 nm, respectively, was quantitatively measured through enzyme-linked assay techniques. To account for differences in cell density, an MTT assay was utilized to standardize the cell density before calculating the concentrations of intracellular Ca^{2+} in PC12 cells.

$$H = \frac{A}{O} \div B \times 100\% \quad (1)$$

In this methodology, H represents the content of Ca^{2+} within the sample, A denotes the value obtained from the calcium ion assay for each individual well, and O signifies the absorbance measured for each specific well. Additionally, MTT B refers to the average value derived from the MTT assay across all the wells within a given treatment group, with each group comprising six replicates. All the data are presented as the mean ± SD (n = 6 per group), and statistical comparisons were performed using a one-way ANOVA followed by Tukey's post hoc test.

4.4.7. LDH Release Assay in PC12 Cells

Following the completion of the drug treatment, the release of lactate dehydrogenase (LDH) from the PC12 cells was quantitatively assessed as per the protocol provided by the LDH assay kit, with the experiment being replicated six times [45]. All the data are presented as the mean ± SD (n = 6 per group), and statistical comparisons were performed using a one-way ANOVA followed by Tukey's post hoc test.

4.4.8. Detection of ROS Levels in PC12 Cells

Following the treatment, the PC12 cells were exposed to a serum-free culture medium containing a 10 μmol/L DCFH-DA probe for 20 min in an environment of 5% CO_2 at 37 °C. Subsequently, the cells were washed to remove any residual serum-free medium. The levels of ROS within the PC12 cells were then quantified utilizing an enzyme marker, employing the same calculation method as previously described for Ca^{2+} levels, with the process repeated in six samples [46]. All the data are presented as the mean ± SD (n = 6 per group), and statistical comparisons were performed using a one-way ANOVA followed by Tukey's post hoc test.

4.4.9. Caspase-3 Release Assay in PC12 Cells

Following the completion of the drug treatment, the release of Caspase-3 from the PC12 cells was quantified in accordance with the guidelines provided by the Caspase-3 assay kit, with the analysis conducted on six replicates [47]. All the data are presented as the mean ± SD (n = 6 per group), and statistical comparisons were performed using a one-way ANOVA followed by Tukey's post hoc test.

4.4.10. Apoptosis Assay

Following the administration of the drug, PC12 cell apoptosis was evaluated using flow cytometry with the assistance of the Annexin V-FITC Apoptosis Assay Kit (Beyotime Biotechnology, Shanghai, China). This kit employs fluorescein isothiocyanate-labeled Annexin V, a phospholipid-binding protein, in conjunction with propidium iodide (PI) for staining. The apoptotic rates were determined using the FACSCanto II flow cytometry system(BD Biosciences, San Jose, CA, USA), and the proportion of apoptotic cells was analyzed and calculated using FlowJo software version 10.6.2, across three experimental replicates. All the data are presented as the mean ± SD (n = 3 per group), and statistical comparisons were performed using a one-way ANOVA followed by Tukey's post hoc test.

4.4.11. Wound Healing Assay

For the cell scratch assay, a 6-well plate was prepared. Parallel lines spaced 0.5 cm apart were marked on the underside of the plate using a marker, with three lines per well to delineate the observation area. The cells were plated at a concentration of 5×10^5 cells per milliliter in each well. Following this, a pipette tip was utilized to generate a straight scratch through the cell monolayer. Any detached cells resulting from the scratch were removed by washing with PBS. Images of the scratch were captured at 0 and 24 h post-scratch using a microscope to evaluate cell migration. The assessment was based on measuring the changes in the width of the scratch, indicating the cells' migratory capacity. All the data are presented as the mean ± SD (n = 3 per group), and statistical comparisons were performed using a one-way ANOVA followed by Tukey's post hoc test.

4.4.12. Western Blot Analysis

For protein sample preparation, the cells underwent lysis on ice for approximately 20 min. This was followed by centrifugation at 4 °C at 13,000× g for 5 min. The protein concentrations in the resulting supernatants were accurately measured using the bicinchoninic acid (BCA) protein assay method. Post-separation, the proteins were subjected to a 5–15% sodium dodecyl sulfate–polyacrylamide gel electrophoresis (SDS-PAGE) electrophoresis process, subsequently being transferred to polyvinylidene fluoride (PVDF) membranes. To inhibit non-specific binding, these membranes underwent incubation with 5% skimmed milk at room temperature for an hour. Overnight incubation at 4 °C was carried out with primary antibodies specifically targeting Nrf2, Keap1, HO-1, β-actin, and NQO1, with dilutions prepared at 1:1000 for all but NQO1, which was diluted to 1:4000. Following thorough washes, the membranes were treated with secondary antibodies diluted to 1:1000 for an hour at room temperature. After additional washing steps, the protein bands were detected with an ECL detection system and captured for analysis. A semi-quantitative assessment of these bands was performed using ImageJ (version 1.53) software, providing an analytical basis for evaluating protein expression levels. All the data are presented as the mean ± SD (n = 3 per group), and statistical comparisons were performed using a one-way ANOVA followed by Tukey's post hoc test.

4.5. In Vivo Studies

4.5.1. Animals and Treatment

Forty-eight adult male ICR rats (average body weight 27.3 ± 1.8 g, age 6–8 weeks) were obtained from the Shanghai Experimental Animal Center, Chinese Academy of Sciences (Shanghai, China). The animal procedures were approved by the Institutional Animal Care and Use Committee (IACUC) of Changchun Normal University (Approval No. 2024003, approved on 13 March 2024). All animal handling followed the guidelines set by the National Institutes of Health (NIHs) and complied with the ARRIVE 2.0 reporting standards.

4.5.2. Housing Conditions and Welfare Measures

Rats were housed in ventilated cages under a controlled environment (temperature: 18–22 °C; relative humidity: 50–60%; 12/12 h light/dark cycle), with ad libitum access to standard chow and water. Daily monitoring was performed for food intake, weight, and clinical symptoms. All efforts were made to minimize animal suffering, and the minimum number of animals required for statistical validity was used.

4.5.3. Experimental Design and Surgical Procedure

A total of 48 rats (body weight 25–30 g) were randomly assigned into four groups (n = 12 per group) using a random number generator: The sham group underwent identical surgical procedures without carotid occlusion. The model group received bilateral common carotid artery occlusion (BCCAO) to induce cerebral ischemia–reperfusion injury. The SI treatment group was treated with soy isoflavones (100 mg/kg, dissolved in saline) via intragastric administration for 5 consecutive d prior to ischemia [48,49]. The edaravone group received edaravone (10 mg/kg, i.p.), a standard neuroprotective agent, once daily for 5 d as a positive control.

Transient cerebral ischemia–reperfusion injury was induced using the bilateral common carotid artery occlusion (BCCAO) model [50]. The rats were anesthetized with pentobarbital sodium (45 mg/kg, i.p.). A midline neck incision (~3 cm) was made to isolate and occlude the bilateral common carotid arteries with vascular clips for 60 min, followed by reperfusion for 24 h. For the sham group, the arteries were exposed but not occluded. Intraoperatively, the rectal temperature of the rats was maintained at 37.0 ± 0.5 °C using an automated thermostatic heating pad. Postoperatively, the animals were housed in a climate-controlled environment (ambient temperature: 23 ± 1 °C; relative humidity: 55 ± 5%) with sterile bedding and ad libitum access to food/water. Subsequently, behavioral tests were performed on the animals. After the completion of the behavioral tests, the animals were euthanized under deep anesthesia by cervical dislocation, in accordance with the AVMA guidelines. Brain tissues were immediately harvested and processed as follows: 5 rats per group for histopathological examination, 3 rats per group for Western blot analysis, and 4 rats per group for HE staining. All the relevant pairwise comparisons among the four experimental groups (control, model, SI, and edaravone) were pre-defined and included in the statistical analysis to comprehensively assess the treatment effects and control efficacy.

4.5.4. Neurological Function Score

Neurological function was assessed according to the method described by Bederson et al. The assessment was conducted in a blinded manner to exclude an observer bias. Briefly, each rat was initially placed on a flat surface to observe its spontaneous movements. Circling behavior toward the side opposite the ischemic region was scored as 1 point. When the rats were gently lifted by the tail, a flexion of the elbow was scored as 2 points, an internal rotation of the shoulder as 3 points, and a wrist flexion of the forelimb as 1 point. Additionally, pushing resistance tests were performed, with scores from 1 to 3 assigned based on the degree of motor deficit (greater distances corresponded to higher scores). The rats were placed on a metal mesh and were further assessed for contralateral muscle tension reduction, with the severity scored from 1 to 3 points according to the degree of impairment [16]. Subsequently, the rats were euthanized under deep anesthesia, and their brains were harvested and maintained in cold saline (4 °C). The olfactory bulb, cerebellum, and brainstem were removed, and the remaining brain tissue was briefly frozen at −20 °C for 10 min. Coronal brain slices were made (four cuts, yielding five slices in total), quickly immersed in 2% 2,3,5-triphenyltetrazolium chloride (TTC) solution, and incubated at 37 °C for 20 min in the dark. Viable brain tissues were stained a rose-red color, while

ischemic tissues remained unstained. Each brain slice was digitally photographed, and the cerebral infarct area was quantitatively analyzed using the BI-2000 image analysis software,version 3.0 (Taimeng Medical Imaging, Chengdu, China). All the data are presented as the mean ± SD (n = 10 per group), and statistical comparisons were performed using a one-way ANOVA followed by Tukey's post hoc test.

4.5.5. The Water Content of Brain Tissue Was Measured

Following the ischemia–reperfusion process, the cerebellum, olfactory bulb, and lower brainstem were meticulously removed from the rats. The mass of the brain tissue left, referred to as the wet weight (W), was then accurately determined. This tissue was subsequently placed in an oven set at a constant temperature of 110 °C and dried for a duration of 48 h. Upon the completion of the drying period, the dry weight (D) of the tissue was recorded. The percentage of the water content in the brain tissue was calculated using the formula water content = $[(W - D)/W] \times 100\%$. All the data are presented as the mean ± SD (n = 10 per group), and statistical comparisons were performed using a one-way ANOVA followed by Tukey's post hoc test.

4.5.6. The Pathological Morphology of the Brain Tissue Was Observed

Following euthanasia, the brains of the rats were rapidly dissected and rinsed in cold saline at 4 °C. The olfactory bulb, cerebellum, and brainstem were removed. The brains were then fixed in 4% paraformaldehyde (Solarbio, Beijing, China) for 24–48 h, followed by dehydration in graded ethanol, clearing in xylene, embedding in paraffin, and coronal sectioning into 5 μm thick slices using a microtome (Leica RM2235, Leica Biosystems, Wetzlar, Germany). The sections were stained using standard hematoxylin and eosin (H&E) protocols. Hematoxylin stained cell nuclei dark blue, while eosin stained the cytoplasm and extracellular matrix pink. A microscopic examination was performed under a light microscope (Leica DM3000, Germany) to evaluate the degree of cellular damage, tissue disorganization, and neuronal loss in the ischemic regions. Representative images were captured, and pathological scoring or area quantification was performed using BI-2000 image analysis software,version 3.0 (Taimeng Medical Imaging, Chengdu, China). From each rat (n = 5 per group), three coronal sections were analyzed. For each section, three non-overlapping fields from the cortex and hippocampus were randomly selected and imaged at 200× magnification, yielding a total of nine images per animal for the statistical analysis. (n = 5; histological scores compared using a one-way ANOVA).

Histopathological evaluation focused on key morphological features indicative of ischemic injury, including neuronal cell loss, nuclear condensation and pyknosis, cytoplasmic eosinophilia, edema in the neuropil, vascular congestion or hemorrhage, and inflammatory cell infiltration. A semi-quantitative scoring system was used to assess tissue damage based on the extent and severity of histological alterations in the cortex and hippocampus. Each parameter was scored on a scale from 0 to 3 (0 = normal, 1 = mild, 2 = moderate, 3 = severe). All the sections were assessed blindly by two independent observers.

4.5.7. The Activities of SOD, GSH-px, CAT, MDA, and LDH in the Brain Tissue Were Detected

Following the ischemia–reperfusion procedure in the rats, the olfactory bulb, cerebellum, and brainstem were removed. The remaining brain tissues were then finely chopped on ice. These tissues were mixed with physiological saline in a centrifuge tube at a specified ratio and homogenized using a tissue homogenizer until no visible solid particles remained. The mixture underwent centrifugation at 3000 rpm for 10 min, facilitating the separation of the supernatant, which was then carefully transferred into a fresh centrifuge tube. The concentrations of SOD, GSH-px, CAT, MDA, and LDH within the rat brain tissue were

accurately measured using a multifunctional microplate reader [51]. All the data are presented as the mean ± SD (n = 10 per group), and statistical comparisons were performed using a one-way ANOVA followed by Tukey's post hoc test.

4.5.8. Detection of Nrf2, Keap1, HO-1, and NQO1 Protein Expression by Western Blot

The brain tissues were processed in a cell lysis buffer that included complete inhibitors for proteases and phosphatases. The nucleoproteins and total proteins were extracted, and their concentrations were determined using the BCA technique. Identical quantities of proteins from each group underwent separation via 10% SDS-PAGE and were subsequently transferred onto a PVDF membrane. The next complete steps follow the method in Section 4.4.12. All the data are presented as the mean ± SD (n = 3 per group), and statistical comparisons were performed using a one-way ANOVA followed by Tukey's post hoc test.

4.5.9. Statistical Analysis

The data from the experiments were processed and analyzed using the GraphPad Prism 9 software, which meant that all the results were presented as the mean ± SD. A one-way ANOVA was used for multiple group comparisons, followed by Tukey's post hoc test to determine the statistical significance between all the group pairs (sham vs. model, SI vs. model, edaravone vs. model, and SI vs. edaravone). This approach ensured that every possible comparison between the study groups was systematically considered and appropriately tested. A p-value below 0.01 was interpreted as denoting a more substantial level of significance.

5. Conclusions

This study demonstrates that soy isoflavones exert a significant neuroprotective effect on PC12 cells damaged by $Na_2S_2O_4$, enhancing neurological functions and reducing cerebral infarction in rats. These isoflavones notably enhance the activity of antioxidant enzymes, thereby mitigating oxidative stress resulting from ischemia–reperfusion. The underlying mechanisms of these protective effects are likely mediated through the activation of the Nrf2 signaling pathway.

Author Contributions: Conceptualization, H.X.; methodology, H.X.; software, H.X.; validation, Z.F and C.J.; formal analysis, H.X; investigation, H.X.; resources, M.Z.; data curation, H.X., Z.F., C.J. and Y.Z.; writing—original draft preparation, H.X.; writing—review and editing, H.X. and M.Z.; visualization, H.X. and J.W.; supervision, M.Z.; project administration, M.Z. and D.S.; funding acquisition, M.Z., Y.A. and J.W. All authors have read and agreed to the published version of the manuscript.

Funding: This work was supported by the Natural Science Foundation of Jilin Province, China (20210101031JC and 20240402045GH).

Institutional Review Board Statement: The animal procedures were approved by the Institutional Animal Care and Use Committee (IACUC) of Changchun Normal University (Approval No. 2024003, approved on 13 March 2024).

Informed Consent Statement: Not applicable.

Data Availability Statement: The data that support the findings of this study are available within the article.

Conflicts of Interest: The authors declare no conflicts of interest.

References

1. Feske, S.K. Ischemic Stroke. *Am. J. Med.* **2021**, *134*, 1457–1464. [CrossRef] [PubMed]
2. Powers, W.J. Acute Ischemic Stroke. *N. Engl. J. Med.* **2020**, *383*, 252–260. [CrossRef]

3. Pu, L.; Wang, L.; Zhang, R.; Zhao, T.; Jiang, Y.; Han, L. Projected Global Trends in Ischemic Stroke Incidence, Deaths and Disability-Adjusted Life Years From 2020 to 2030. *Stroke* **2023**, *54*, 1330–1339. [CrossRef] [PubMed]
4. Maida, C.D.; Norrito, R.L.; Daidone, M.; Tuttolomondo, A.; Pinto, A. Neuroinflammatory Mechanisms in Ischemic Stroke: Focus on Cardioembolic Stroke, Background, and Therapeutic Approaches. *Int. J. Mol. Sci.* **2020**, *21*, 6454. [CrossRef] [PubMed]
5. Fu, K.; Chen, L.; Hu, S.; Guo, Y.; Zhang, W.; Bai, Y. Grape seed proanthocyanidins attenuate apoptosis in ischemic stroke. *Acta Neurol. Belg.* **2021**, *121*, 357–364. [CrossRef]
6. Salaudeen, M.A.; Bello, N.; Danraka, R.N.; Ammani, M.L. Understanding the Pathophysiology of Ischemic Stroke: The Basis of Current Therapies and Opportunity for New Ones. *Biomolecules* **2024**, *14*, 305. [CrossRef]
7. Wang, Q.; Yang, F.; Duo, K.; Liu, Y.; Yu, J.; Wu, Q.; Cai, Z. The Role of Necroptosis in Cerebral Ischemic Stroke. *Mol. Neurobiol.* **2023**, *61*, 3882–3898, *Advance online publication*. [CrossRef]
8. Tang, H.; He, K.; Zhao, K.; Zheng, C.; Wu, W.; Jin, W.; Yang, L.; Xie, B. Protective Effects of Hinokitiol on Neuronal Ferroptosis by Activating the Keap1/Nrf2/HO-1 Pathway in Traumatic Brain Injury. *J. Neurotrauma* **2024**, *41*, 734–750. [CrossRef]
9. Zhang, R.; Xu, M.; Wang, Y.; Xie, F.; Zhang, G.; Qin, X. Nrf2-a Promising Therapeutic Target for Defensing Against Oxidative Stress in Stroke. *Mol. Neurobiol.* **2017**, *54*, 6006–6017. [CrossRef]
10. Jiang, Y.; Nguyen, T.V.; Jin, J.; Yu, Z.N.; Song, C.H.; Chai, O.H. Tectorigenin inhibits oxidative stress by activating the Keap1/Nrf2/HO-1 signaling pathway in Th2-mediated allergic asthmatic mice. *Free Radic. Biol. Med.* **2024**, *212*, 207–219. [CrossRef]
11. Schiavoni, V.; Emanuelli, M.; Milanese, G.; Galosi, A.B.; Pompei, V.; Salvolini, E.; Campagna, R. Nrf2 Signaling in Renal Cell Carcinoma: A Potential Candidate for the Development of Novel Therapeutic Strategies. *Int. J. Mol. Sci.* **2024**, *25*, 13239. [CrossRef] [PubMed]
12. Li, P.; Yao, L.Y.; Jiang, Y.J.; Wang, D.D.; Wang, T.; Wu, Y.P.; Li, B.X.; Li, X.T. Soybean isoflavones protect SH-SY5Y neurons from atrazine-induced toxicity by activating mitophagy through stimulation of the BEX2/BNIP3/NIX pathway. *Ecotoxicol. Environ. Saf.* **2021**, *227*, 112886. [CrossRef]
13. Sathyapalan, T.; Aye, M.; Rigby, A.S.; Thatcher, N.J.; Dargham, S.R.; Kilpatrick, E.S.; Atkin, S.L. Soy isoflavones improve cardiovascular disease risk markers in women during the early menopause. *NMCD* **2018**, *28*, 691–697. [CrossRef] [PubMed]
14. Lu, C.; Wang, Y.; Wang, D.; Zhang, L.; Lv, J.; Jiang, N.; Fan, B.; Liu, X.; Wang, F. Neuroprotective Effects of Soy Isoflavones on Scopolamine-Induced Amnesia in Mice. *Nutrients* **2018**, *10*, 853. [CrossRef] [PubMed]
15. Wu, Z.; Li, W.; Liu, G.; Tang, Y. Network-Based Methods for Prediction of Drug-Target Interactions. *Front. Pharmacol.* **2018**, *9*, 1134. [CrossRef]
16. Crampon, K.; Giorkallos, A.; Deldossi, M.; Baud, S.; Steffenel, L.A. Machine-learning methods for ligand-protein molecular docking. *Drug Discov. Today* **2022**, *27*, 151–164. [CrossRef]
17. Daina, A.; Michielin, O.; Zoete, V. SwissADME: A free web tool to evaluate pharmacokinetics, drug-likeness and medicinal chemistry friendliness of small molecules. *Sci. Rep.* **2017**, *7*, 42717. [CrossRef]
18. Bederson, J.B.; Pitts, L.H.; Tsuji, M.; Nishimura, M.C.; Davis, R.L.; Bartkowski, H. Rat middle cerebral artery occlusion: Evaluation of the model and development of a neurologic examination. *Stroke* **1986**, *17*, 472–476. [CrossRef]
19. Herpich, F.; Rincon, F. Management of Acute Ischemic Stroke. *Crit. Care Med.* **2020**, *48*, 1654–1663. [CrossRef]
20. Yang, J.L.; Mukda, S.; Chen, S.D. Diverse roles of mitochondria in ischemic stroke. *Redox Biol.* **2018**, *16*, 263–275. [CrossRef]
21. Zhang, B.; Saatman, K.E.; Chen, L. Therapeutic Potential of Natural Compounds from Chinese Medicine in Acute and Subacute Phases of Ischemic Stroke. *Neural Regen. Res.* **2020**, *15*, 416–424. [CrossRef] [PubMed]
22. Vitolins, M.Z.; Anthony, M.; Burke, G.L. Soy protein isoflavones, lipids and arterial disease. *Curr. Opin. Lipidol.* **2001**, *12*, 433–437. [CrossRef] [PubMed]
23. Grisley, E.D.; Huber, K.N.; Knapp, A.N.; Butteiger, D.N.; Banz, W.J.; MacLean, J.A.; Wallace, D.G.; Cheatwood, J.L. Effects of Dietary Soy Protein Isolate Versus Isoflavones Alone on Poststroke Skilled Ladder Rung Walking and Cortical mRNA Expression Differ in Adult Male Rats. *J. Med. Food* **2022**, *25*, 158–165. [CrossRef]
24. Yao, H.; Yuan, Z.; Wei, G.; Chen, C.; Duan, J.; Li, Y.; Wang, Y.; Zhang, C.; Liu, Y. Thevetiaflavone from Wikstroemia indica ameliorates PC12 cells injury induced by OGD/R via improving ROS-mediated mitochondrial dysfunction. *Mol. Med. Rep.* **2017**, *16*, 9197–9202. [CrossRef]
25. Menshchikova, E.B.; Chechushkov, A.V.; Kozhin, P.M.; Romakh, L.P.; Serykh, A.E.; Khrapova, M.V.; Petrova, E.S.; Kandalintseva, N.V. Effect of Inducers and Inhibitors of the Keap1/Nrf2/ARE System on the Viability and Functional Activity of Model Neuronal-Like and Glial Cells. *Bull. Exp. Biol. Med.* **2024**, *176*, 332–337. [CrossRef]
26. Lin, S.P.; Tu, C.; Huang, W.; Wu, Y.; Lin, P.Y.; Ye, S.; Long, Y.; Xu, W.; Chen, S.; Wen, Y.S.; et al. Acute-phase serum superoxide dismutase level as a predictive biomarker for stroke-associated infection. *Int. J. Neurosci.* **2020**, *130*, 186–192. [CrossRef]
27. Liu, M.; Li, H.; Zhang, L.; Xu, Z.; Song, Y.; Wang, X.; Chu, R.; Xiao, Y.; Sun, M.; Ma, Y.; et al. Cottonseed Oil Alleviates Ischemic Stroke-Induced Oxidative Stress Injury Via Activating the Nrf2 Signaling Pathway. *Mol. Neurobiol.* **2021**, *58*, 2494–2507. [CrossRef]

28. Liu, H.; Zhang, X.; Du, Y.; Ji, H.; Li, S.; Li, L.; Xing, Y.; Zhang, X.; Dong, L.; Wang, C.; et al. Leonurine protects brain injury by increased activities of UCP4, SOD, CAT and Bcl-2, decreased levels of MDA and Bax, and ameliorated ultrastructure of mitochondria in experimental stroke. *Brain Res.* **2012**, *1474*, 73–81. [CrossRef]
29. Ludhiadch, A.; Sharma, R.; Muriki, A.; Munshi, A. Role of Calcium Homeostasis in Ischemic Stroke: A Review. *CNS Neurol. Disord. Drug Targets* **2022**, *21*, 52–61. [CrossRef]
30. Jo-Watanabe, A.; Inaba, T.; Osada, T.; Hashimoto, R.; Nishizawa, T.; Okuno, T.; Ihara, S.; Touhara, K.; Hattori, N.; Oh-Hora, M.; et al. Bicarbonate signalling via G protein-coupled receptor regulates ischaemia-reperfusion injury. *Nat. Commun.* **2024**, *15*, 1530. [CrossRef]
31. Liu, L.; Locascio, L.M.; Doré, S. Critical Role of Nrf2 in Experimental Ischemic Stroke. *Front. Pharmacol.* **2019**, *10*, 153. [CrossRef] [PubMed]
32. Wang, J.; Zhang, W.; Lv, C.; Wang, Y.; Li, X. Corrigendum to "A novel biscoumarin compound ameliorates cerebral ischemia reperfusion induced mitochondrial oxidative injury via Nrf2/Keap-1/ARE signaling". *Neuropharmacology* **2019**, *203*, 108894. [CrossRef]
33. Yin, H.; Wu, M.; Jia, Y. Knockdown of IL-32 protects PC12 cells against oxygen-glucose deprivation/reoxygenation-induced injury via activation of Nrf2/NF-κB pathway. *Metab. Brain Dis.* **2020**, *35*, 363–371. [CrossRef] [PubMed]
34. Kaspar, J.W.; Niture, S.K.; Jaiswal, A.K. Nrf2:INrf2 (Keap1) signaling in oxidative stress. *Free. Radic. Biol. Med.* **2009**, *47*, 1304–1309. [CrossRef]
35. Zhang, Y.; Yin, L.; Dong, J.; Xia, X. Soy Isoflavones Protect Neuronal PC12 Cells against Hypoxic Damage through Nrf2 Activation and Suppression of p38 MAPK and AKT–mTOR Pathways. *Antioxidants* **2022**, *11*, 2037. [CrossRef]
36. Schreihofer, D.A.; Do, K.D.; Schreihofer, A.M. High-soy Diet Decreases Infarct Size after Permanent Middle Cerebral Artery Occlusion in Female Rats. *Am. J. Physiol. Regul. Integr. Comp. Physiol.* **2005**, *289*, R103–R108. [CrossRef]
37. Huang, G.; Cao, X.; Zhang, X.; Chang, H.; Yang, Y.; Du, W.; Wilson, J.X. Effects of Soybean Isoflavone on the Notch Signal Pathway of the Brain in Rats with Cerebral Ischemia. *J. Nutr. Sci. Vitaminol.* **2009**, *55*, 326–331. [CrossRef]
38. Li, L.; Liu, S.; Wang, M.; Li, M.; Liu, Y.; Chen, H.; Chen, J.; Tao, W.; Huang, L.; Zhao, S. Gen Inhibiting the Wnt/Ca2+ Signaling Pathway Alleviates Cerebral Ischemia/Reperfusion Injury. *Sci. Rep.* **2025**, *15*, 4661. [CrossRef]
39. Yi, T.; Zhu, L.; Peng, W.L.; Zhao, T.; Jiang, Y.; Han, L. Comparison of ten major constituents in seven types of processed tea using HPLC-DAD-MS followed by principal component and hierarchical cluster analysis. *LWT Food Sci. Technol.* **2015**, *54*, 194–201. [CrossRef]
40. Wilson, I.D.; Plumb, R.; Granger, J.; Major, H.; Williams, R.; Lenz, E.M. HPLC-MS-Based Methods for the Study of Metabonomics. *J. Chromatogr. B* **2005**, *817*, 67–76. [CrossRef]
41. Wilson, I.D.; Plumb, R.; Granger, J.; Major, H.; Williams, R.; Lenz, E.M. Network Pharmacology, a Promising Approach to Reveal the Pharmacology Mechanism of Chinese Medicine Formula. *Stroke* **2023**, *309*, 116306. [CrossRef]
42. Westerink, R.H.S.; Ewing, A.G. The PC12 Cell as Model for Neurosecretion. *Acta Physiol.* **2008**, *192*, 273–285. [CrossRef]
43. Qin, J.; Zhou, L.; Yu, L.; Ye, J.; Wang, F.; Zhou, J.; Gu, Y.; Chen, G.; Chen, X. Exosomes Derived from HUVECs Alleviate Ischemia-Reperfusion Induced Inflammation in Neural Cells by Upregulating KLF14 Expression. *Front. Pharmacol.* **2024**, *15*, 1365928. [CrossRef] [PubMed]
44. Li, Z.Y.; Guo, Z.; Liu, Y.M.; Liu, X.M.; Chang, Q.; Liao, Y.H.; Pan, R.L. Neuroprotective Effects of Total Saikosaponins of Bupleurum yinchowense on Corticosterone-Induced Apoptosis in PC12 Cells. *J. Ethnopharmacol.* **2013**, *148*, 794–803. [CrossRef] [PubMed]
45. Korzeniewski, C.; Callewaert, D.M. An Enzyme-Release Assay for Natural Cytotoxicity. *J. Immunol. Methods* **1983**, *64*, 313–320. [CrossRef]
46. Wu, D.; Yotnda, P. Production and Detection of Reactive Oxygen Species (ROS) in Cancers. *J. Vis. Exp. JoVE* **2011**, *57*, 3357. [CrossRef]
47. Stennicke, H.R.; Salvesen, G.S. Caspase Assays. In *Methods in Enzymology*; Academic Press: Cambridge, MA, USA, 2000; pp. 91–100. [CrossRef]
48. Zhang, D.; Li, X.; He, X.; Xing, Y.; Jiang, B.; Xiu, Z.; Bao, Y.; Dong, Y. Protective Effect of Flavonoids against Methylglyoxal-Induced Oxidative Stress in PC-12 Neuroblastoma Cells and Its Structure–Activity Relationships. *Molecules* **2022**, *27*, 7804. [CrossRef]
49. Ariyani, W.; Koibuchi, N. The Effect of Soy Isoflavones in Brain Development: The Emerging Role of Multiple Signaling Pathways and Future Perspectives. *Endocr. J.* **2024**, *71*, 317–333. [CrossRef]

50. Handayani, E.S.; Nurmasitoh, T.; Akhmad, S.A.; Fauziah, A.N.; Rizani, R.; Rahmawati, R.Y.; Afriandi, A. Effect of BCCAO Duration and Animal Model Sex on Brain Ischemic Volume after 24 Hours Reperfusion. *Bangladesh J. Med. Sci.* **2018**, *17*, 129–137. [CrossRef]
51. Crack, P.J.; Wong, C.H.Y. Modulation of Neuro-Inflammation and Vascular Response by Oxidative Stress following Cerebral Ischemia-Reperfusion Injury. *Curr. Med. Chem.* **2008**, *15*, 1–14. [CrossRef]

Disclaimer/Publisher's Note: The statements, opinions and data contained in all publications are solely those of the individual author(s) and contributor(s) and not of MDPI and/or the editor(s). MDPI and/or the editor(s) disclaim responsibility for any injury to people or property resulting from any ideas, methods, instructions or products referred to in the content.

pharmaceuticals

MDPI

Article

Regulation of Intestinal Barrier Function and Gut Microbiota by Hot Melt Extrusion-Drug Delivery System-Prepared Mulberry Anthocyanin in an Inflammatory Bowel Disease Model

Eun-Ji Go [1], Byeong Ryeol Ryu [1,2], Gyeong Ju Gim [3], Ye Rim Shin [1], Min Ji Kang [1], Min Jun Kim [1], Jong-Suep Baek [1,4] and Jung Dae Lim [1,4,*]

[1] Department of Bio-Health Convergence, Kangwon National University, Chuncheon 24341, Republic of Korea; a01040363654@kangwon.ac.kr (E.-J.G.); byeongryeol.ryu@csupueblo.edu (B.R.R.); tlsdpfladldi@kangwon.ac.kr (Y.R.S.); mzk1227@kangwon.ac.kr (M.J.K.); alswns1172@kangwon.ac.kr (M.J.K.); jsbaek@kangwon.ac.kr (J.-S.B.)
[2] Institute of Cannabis Research, Colorado State University-Pueblo, 2200 Bonforte Blvd, Pueblo, CO 81001-4901, USA
[3] National Agrobiodiversity Center, National Academy of Agricultural Science, Rural Development Administration, Jeonju 54874, Republic of Korea; gyeongju159@korea.kr
[4] Department of Bio-Functional Material, Kangwon National University, Samcheok 25949, Republic of Korea
* Correspondence: ijdae@kangwon.ac.kr; Tel.: +82-33-540-3323

Abstract: Background/Objectives: Anthocyanins (ACNs) derived from mulberry (*Morus alba* L.) exhibit potent antioxidant and anti-inflammatory activities. However, their low stability and bioavailability in physiological environments limit their therapeutic potential. This study aimed to enhance the stability and controlled release ACNs using a hot-melt extrusion drug delivery system (HME-DDS) formulation, HME-MUL-F2, and evaluate its effects on gut barrier function and microbiota composition in a DSS-induced colitis model. **Methods:** The anthocyanin content of HME-MUL-F2 was quantified and compared with that of raw mulberry extract. The formulation's protective effects were assessed in Caco-2 and RAW 264.7 cells, confirming its biocompatibility and anti-inflammatory properties. The therapeutic efficacy was further evaluated in a dextran sulfate sodium (DSS)-induced inflammatory bowel disease (IBD) model, focusing on gut barrier integrity, inflammatory cytokine modulation, and gut microbiota composition. **Results:** HME-MUL-F2 significantly improved gut barrier function by upregulating tight junction proteins and reducing inflammatory cytokine levels in the colitis model. Moreover, the formulation modulated gut microbiota composition, promoting beneficial bacteria while suppressing pathogenic strains. HME-MUL-F2 administration led to a significant increase in the Bacteroidetes-to-Firmicutes ratio, which is associated with improved gut health. These results indicate that HME-MUL-F2 significantly enhances anthocyanin bioavailability, leading to improved gut health and potential therapeutic applications for inflammatory conditions. **Conclusions:** This study highlights the potential of HME technology for improving the stability, bioavailability, and therapeutic efficacy of anthocyanins. HME-MUL-F2 is a sustained-release formulation that enhances gut barrier function and modulates intestinal microbial balance in a DSS-induced inflammatory bowel disease model. These findings strongly suggest that the observed therapeutic effects of HME-MUL-F2 are primarily due to enhanced anthocyanin bioavailability and targeted delivery to the colon, although further clinical studies will provide more definitive confirmation.

Keywords: mulberry; anthocyanin; hot-melt extrusion; drug release; gut microbiota; intestinal microbial flora; intestinal barrier; bioavailability; inflammatory disease

1. Introduction

The gastrointestinal tract serves as a primary defense mechanism, where epithelial cells create a physical barrier to minimize direct contact with external substances [1]. These cells regulate the entry and exit of substances, as well as absorption and secretion [2]. The intestinal wall provides the first line of defense for the mucosa, protecting it from stomach and pancreatic secretions and bacterial antigens [3].

Intestinal barrier homeostasis depends on the relationship between the microbiome and the epithelium. The innate immune system, especially pattern recognition receptors in enterocytes, is essential for maintaining this homeostasis [4]. The intestinal barrier, including the microbiota, epithelial cells, and mucosal immunity, forms a defense unit interconnected through cytokines, antimicrobial peptides (AMPs), and metabolites [5]. Maintaining this barrier is crucial for the body's anti-infective defense [6]. A damaged epithelium allows for the movement of various bacteria and toxins, leading to severe complications like sepsis and spontaneous bacterial peritonitis [7].

The intestinal epithelium recognizes microbe-associated molecular patterns (MAMPs) from microbial species, triggering inflammatory signals [8]. MAMPs, including lipopolysaccharides (LPS) in Gram-negative bacteria, lipoteichoic acid (LTA) in Gram-positive bacteria, and peptidoglycan, activate the NF-κB signaling pathway, induce pro-inflammatory interleukins, and maintain a controlled inflammatory state [9].

Enteric pathogens contribute to inflammatory bowel disease (IBD) by altering the intestinal barrier and microbiota, increasing inflammation, and releasing toxins [10]. The microbiota, consisting of millions of microorganisms, support metabolic, immune, and anti-infective processes [11]. Dysbiosis, a disruption in microbial balance, weakens the intestinal barrier, leading to infections and IBD [12].

Inflammatory bowel disease (IBD), encompassing Crohn's disease and ulcerative colitis, is a chronic inflammatory condition of the gastrointestinal tract. Recent studies have highlighted a significant association between gut microbiota dysbiosis and the pathogenesis of IBD. Specifically, IBD patients exhibit reduced microbial diversity, with a decrease in beneficial bacteria such as Lachnospiraceae and Bifidobacterium species, and an increase in harmful bacteria like Proteobacteria and Fusobacterium species [13].

There is no permanent cure for IBD, and lifelong medication is often required. Maintaining remission and preventing inflammation recurrence are the main treatment goals [14]. Amino salicylates like 5-amino salicylic acid (5-ASA) are the preferred initial treatment for mild to moderate IBD symptoms, exerting anti-inflammatory effects through antioxidant activity [15]. However, rapid absorption from the small intestine reduces its availability in the inflamed colon, leading to side effects [16].

Mulberry (*Morus alba*), commonly known as white mulberry, is a fruit-bearing tree widely cultivated for its leaves, which are the primary food source for silkworms. The fruit, known as mulberry, is rich in various nutrients and bioactive compounds, including vitamins, minerals, dietary fibers, and phenolic compounds, particularly anthocyanins (ACNs) [17]. These compounds are responsible for the fruit's vibrant color and have significant health benefits, such as antioxidant, anti-inflammatory, and anti-cancer properties [18]. Mulberry supports cardiovascular health, helps regulate blood sugar levels, enhances immune function, and shows potential for protecting against neurodegenerative diseases and improving digestive health due to its high fiber content and beneficial effects on gut microbiota [19].

Anthocyanins (ACNs) possess antioxidant, anti-inflammatory, and anticancer properties but display low bioavailability due to their instability [20]. In vivo studies show that ACN is absorbed most efficiently in the jejunum, with much less absorption in the duodenum [21]. Consequently, ACN's impact on maintaining the balance of intestinal

microbial flora in the colon is limited [22]. The antioxidant properties of anthocyanins are crucial in maintaining the balance of the gut microbiota and supporting the integrity of the intestinal barrier by reducing oxidative stress and inflammation [23].

Hot-melt extrusion (HME) technology enhances the bioavailability of poorly soluble substances [24]. HME is used in the pharmaceutical and food industries to increase the water solubility, particle stability, and antioxidant effects of compounds. The HME-MUL-F2 formulation, developed in the study "Hot-Melt Extrusion Enhances Antioxidant Effects of Mulberry on Probiotics and Pathogenic Microorganisms", demonstrated the increased solubility and stability of ACNs. This formulation helps maintain the mucosal barrier by preserving the balance of intestinal microbiota and preventing the proliferation of harmful bacteria [25]. By using HME-DDS, ACN is safely delivered to the colon, without decomposing in stomach acid, improving ulcerative colitis caused by dextran sulfate sodium (DSS) by enhancing intestinal barrier function and controlling microorganisms.

Mulberry was chosen for this study due to its high content of bioactive compounds, particularly anthocyanins, which have been shown to have significant health benefits. The use of mulberry in combination with HME technology aims to overcome the bioavailability issues associated with anthocyanins and to enhance their therapeutic effects on intestinal health and inflammation. Compared to conventional anthocyanin formulations, HME-MUL-F2 enhances stability, scalability, and targeted colonic delivery, making it a promising alternative to existing delivery systems.

2. Results and Discussion

2.1. Toxicity of HME-MUL-F2 to Caco-2 and RAW 264.7 Cells

To assess the toxicity of MUL and HME-MUL-F2 to Caco-2 and RAW 264.7 cells, an MTT assay was conducted. When the cells reached 80% confluence, they were pretreated with MUL and HME-MUL-F2 at concentrations of 1, 2, and 4 mg/mL for 24 h. Studies have been conducted to evaluate the cytotoxicity of extracts containing anthocyanins such as C3G (cyanidin-3-glucoside) and C3R (cyanidin-3-rutinoside) in Caco-2 and RAW 264.7 cells. However, no studies have been identified that assess the toxicity of these compounds at high concentrations exceeding 0.1 mg/mL [26]. Cell viability was measured and found to reach 100% across all treatment groups, with no significant difference compared to the results for the untreated group. This indicates that MUL and HME-MUL-F2 did not exhibit toxicity, even at high doses. Therefore, a concentration of 2 mg/mL, which showed efficacy in previous intestinal microbiome improvement experiments, was used for further studies. There was no statistically significant difference in cell viability (Figure 1, $p < 0.05$).

Additionally, the anthocyanin contents of the mulberry extracts used in this study are presented in Table 1. Table 1 shows the contents of C3G and C3R of mulberry extracts, comparing raw materials (MUL) and the HME-MUL-F2 formulation, and the anthocyanin content of MUL was determined to be 43.13 $\pm$ 2.63 mg/g DW, which is comparable to previously reported values for mulberry (*Morus alba*) fruit ranging from 4.11 to 52.88 mg/g DW of C3G mL [27]. On the other hand, HME-MUL-F2 exhibited an anthocyanin content of 325.02 $\pm$ 11.12 mg/g DW, which is significantly higher than that of raw mulberry extract. HME-MUL-F2 exhibited significantly higher concentrations of anthocyanins compared to raw mulberry ($p < 0.05$), indicating enhanced stability and bioavailability through the hot-melt extrusion (HME) process.

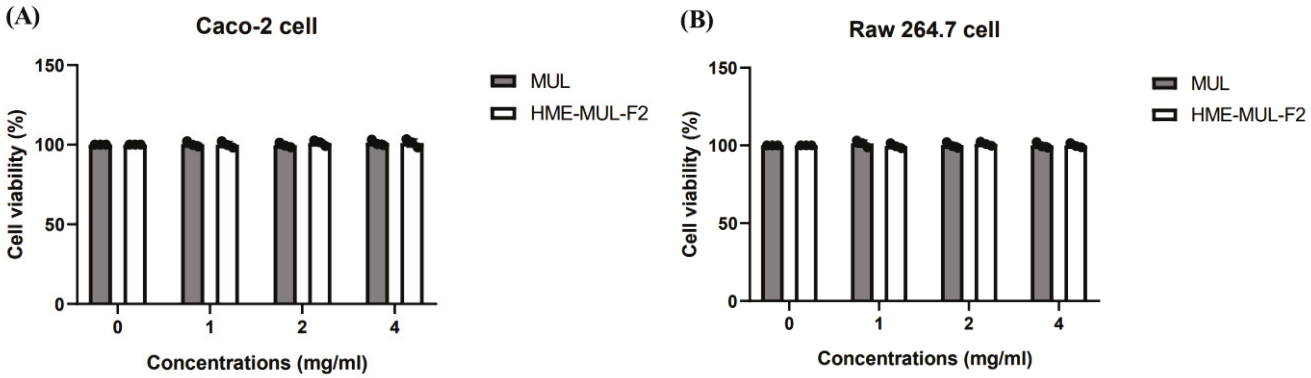

Figure 1. Effects of HME-DDS formulate (HME-MUL-F2) on cell viability in Caco-2 and RAW 264.7 cells. Increasing concentrations of mulberry raw materials (MUL) and HME-DDS formulate (HME-MUL-F2) in amounts of 1, 2, 4 mg/mL were applied to (**A**) Caco-2 cells and (**B**) RAW 264.7 cells. The cytotoxicity of RAW 264.7 cells and HME-MUL-F2 cells after 24 h was evaluated using the MTT assay. One-way ANOVA was conducted, followed by Duncan's multiple range test, to analyze statistical differences at a 5% significance level ($p < 0.05$, $n = 3$).

Table 1. Anthocyanin contents of mulberry extract [28].

		Anthocyanin Content (mg/g DW)	
		C3G	**C3R**
Raw materials	MUL	43.13 ± 2.63^{e}	2.99 ± 1.25^{f}
Extrusion materials	HME-MUL	117.44 ± 1.44^{d}	68.91 ± 1.35^{e}
	HME-MUL-F2	325.02 ± 11.12^{b}	154.73 ± 11.30^{bc}

MUL—mulberry; MUL-HME—only solid formulations of the extrudate of MUL; HME-MUL-F2—treatment with mulberry HME-DDS formulation. Values having different letters (b–f) indicate significant differences obtained via Duncan's multiple range test (DMRT, $p < 0.05$).

2.2. Effect of HME-MUL-F2 on Tight Junction Integrity of Caco-2 Cells

Cellular models are more accessible than in vivo models and offer a method to investigate substance effects without risking animal welfare [29]. Caco-2 cells, derived from human colorectal adenocarcinoma, are widely used as an intestinal barrier model due to their strong correlation with passive permeability [30]. These cells form a polarized monolayer characteristic of human enterocytes [31]. However, they cannot produce mucus, so RAW 264.7 cells are used to better mimic the internal environment [32]. An in vitro model was developed using Caco-2 cells on the apical side and RAW 264.7 cells on the basolateral side of a Transwell insert [33]. This setup allows for the investigation of transport, metabolism, and cell–cell interactions relevant to gut inflammation [33]. LPS stimulation of RAW 264.7 cells increased cytokine secretion and reduced TEER value [34], indicating immune stress and damage to tight junctions [35].

LPS treatment in the basolateral compartment caused pro-inflammatory cytokine secretion, affecting Caco-2 cells and leading to barrier function failure. TEER decreased from 840 $\Omega \times cm^2$ to 696 $\Omega \times cm^2$ over 48 h. The effect of HME-MUL-F2 and MUL on Caco-2 cell tight junctions was evaluated. After pretreatment with MUL-F2 at 2 mg/mL for 24 h, the TEER value was measured, while treating the basolateral compartment with LPS at 2 μg/mL for 48 h [36].

LPS treatment alone decreased TEER to 696 $\Omega \times cm^2$, 0.92 times lower than that for the untreated group (754 $\Omega \times cm^2$). However, with 24 h pretreatment of MUL and HME-MUL-F2, followed by LPS treatment, TEER values were 783 $\Omega \times cm^2$ and 817 $\Omega \times cm^2$, respectively (Figure 2A, $p < 0.05$). Through their intrinsic self-repair mechanisms, Caco-2 cells possess inherent self-repair capabilities that can restore tight junction integrity over

time [37]. TEER measurements demonstrated that HME-MUL-F2 effectively mitigated LPS-induced increases in permeability in Caco-2 monolayers, suggesting its protective role in regards to intestinal barrier integrity. The recovery of TEER values within 24 h and their further elevation beyond control levels at 48 h indicate accelerated barrier repair, potentially due to the sustained release of anthocyanins (Figure 2B). Previous studies have reported that anthocyanins from aronia berries similarly prevent LPS-induced disruption of Caco-2 barrier function. Additionally, Jiang et al. have shown that barrier function restoration is a time-dependent process, supporting our observation that HME-MUL-F2 promotes faster TEER recovery [38].

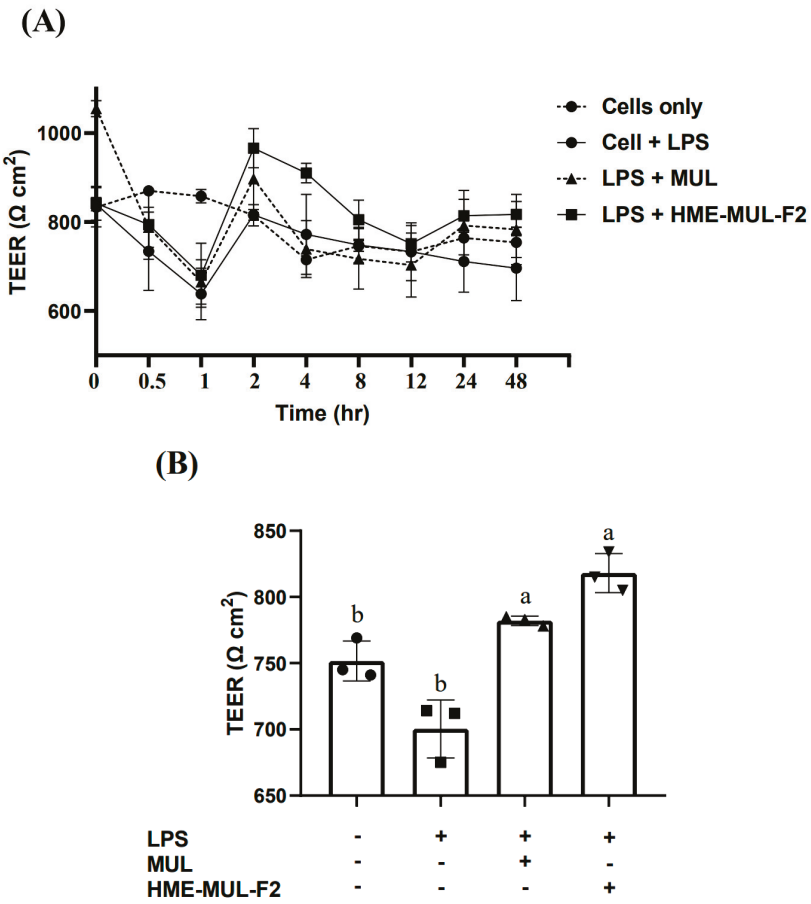

Figure 2. Preventive effects of HME-DDS formulate (HME-MUL-F2) on reduced tight junction integrity by treatment with LPS in an in vitro gut inflammation model. Tight junction integrity of Caco-2 cells (apical compartment) in the absence or presence of mulberry raw materials (MUL) and HME-DDS formulate (HME-MUL-F2) by treatment with 2 μg/mL LPS in RAW 264.7 cells (basolateral compartment) was determined by (**A**) time course and (**B**) final (treatment with LPS after 48 h) TEER values. Different letters (a,b) of error bars within each column indicate significant differences among treatments. One-way ANOVA was conducted, followed by Duncan's multiple range test, to analyze the statistical differences at a 5% significance level ($p < 0.05$, $n = 3$).

The higher TEER value for HME-MUL-F2 compared to MUL is likely due to the structure of sugar molecules and macromolecules in HME-MUL-F2, which may enhance ACN uptake in Caco-2 cells. However, final TEER values at 48 h were not significantly different between MUL and HME-MUL-F2. These results align with reports that mulberry anthocyanins (ACN) reduce tight junction permeability to LPS [39], helping to maintain the intestinal barrier.

The hot-melt extrusion (HME) process has been shown to improve the stability and solubility of anthocyanins, leading to a sustained release profile [28]. This enhancement

ensures a more consistent and prolonged interaction with the intestinal epithelium, thereby supporting tight junction integrity. Moreover, the enhanced performance of HME-MUL-F2 may be attributed to the HME process, which improves anthocyanin solubility and stability, leading to sustained release and prolonged retention in the intestinal environment [28]. Unlike non-extruded formulations, which exhibit rapid anthocyanin degradation within 180 min, HME-MUL-F2 maintained significant anthocyanin levels for extended durations [28]. These findings indicate that the optimized formulation facilitates gradual release, resulting in superior intestinal barrier protection compared to that of raw mulberry materials (MUL).

2.3. Effect of HME-MUL-F2 on Inhibition of Cytokine Production

LPS treatment in the Caco-2 monolayer reduced TEER levels, indicating compromised tight junctions. Treatment with MUL and HME-MUL-F2 prevented this reduction and decreased inflammatory cytokine expression in the apical compartment. PGE_2 levels increased significantly with LPS treatment (262.00 ± 25.94 pg/mL to 2879.33 ± 102.10 pg/mL). MUL and HME-MUL-F2 pretreatment reduced PGE_2 levels to 1902.67 ± 20.50 pg/mL, although not to untreated levels (Figure 3A, $p < 0.05$). IL-1β increased from 271.33 ± 21.78 pg/mL to 530.33 ± 42.15 pg/mL with LPS. MUL and HME-MUL-F2 reduced IL-1β to 350.00 ± 7.21 pg/mL and 287.00 ± 13.00 pg/mL, respectively, with HME-MUL-F2 showing a statistically significant reduction to near untreated levels (Figure 3B, $p < 0.05$). TNF-α levels increased to 437.67 ± 19.50 pg/mL with LPS. MUL and HME-MUL-F2 reduced TNF-α to 330.67 ± 20.82 pg/mL and 278.67 ± 17.47 pg/mL, respectively, although not to untreated levels (205.00 ± 7.00 pg/mL, $p < 0.05$). IL-6 increased from 23.00 ± 3.61 pg/mL to 78.00 ± 3.00 pg/mL with LPS but was reduced to 51.33 ± 3.51 pg/mL with MUL and 41.00 ± 2.00 pg/mL with HME-MUL-F2 treatment (Figure 3C,D, $p < 0.05$).

Gene expression and production of inflammatory cytokines like IFN-α, TNF-α, IL-1β, IL-6, IL-17, and IL-22 form a complex network that can lead to chronic inflammation and autoimmune diseases when imbalanced [40]. LPS can cause chronic inflammation of the intestinal mucosal barrier, but MUL and HME-MUL-F2 can inhibit this by reducing inflammatory cytokines. HME-MUL-F2 significantly reduced the levels of pro-inflammatory cytokines (PGE_2, TNF-α, IL-1β, and IL-6) in LPS-stimulated Caco-2/RAW264.7 co-culture, demonstrating its anti-inflammatory potential. Previous studies have shown that anthocyanins from natural sources inhibit the nuclear translocation of NF-κB p65 and prevent IκB-α degradation, leading to reduced cytokine production [41]. In our study, the downregulation of PGE_2, TNF-α, IL-1β, and IL-6 further supports the hypothesis that HME-MUL-F2 modulates NF-κB signaling, leading to a suppressed inflammatory response. Additionally, alginate—an excipient in the HME-MUL-F2 formulation—has been reported to exhibit independent anti-inflammatory effects by modulating macrophage activation and cytokine secretion [42].

The potential synergistic interaction between anthocyanins and alginate may further contribute to the anti-inflammatory effects observed in our study. HME-MUL-F2, which includes alginate and ascorbyl palmitate and is derived using extrusion technology, improves intestinal barrier function more effectively than does the raw material alone. It can be used as a preventive and therapeutic agent to maintain intestinal mucosal integrity.

Following LPS treatment, a decrease in TEER values was observed, followed by a gradual recovery. This phenomenon is consistent with findings from other studies, such as the work of Jiang et al. [38]. Despite cellular damage induced by LPS, the cells can recover relatively quickly due to their intrinsic self-repair mechanisms. Therefore, the initial

decrease and subsequent increase in TEER values after LPS treatment can be interpreted as a reflection of the processes of cellular damage and recovery.

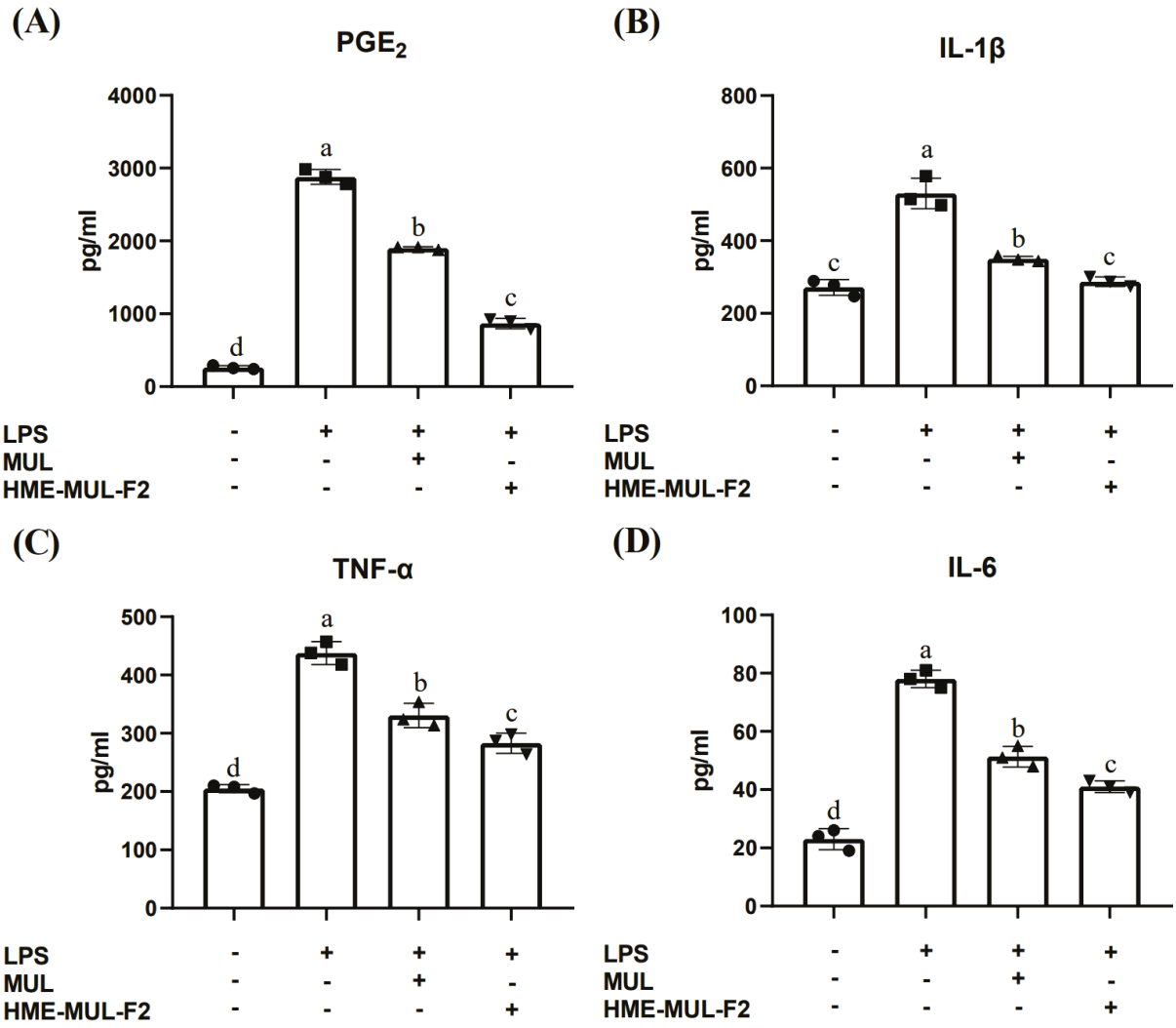

Figure 3. Impact of HME-DDS formulation (HME-MUL-F2) on proinflammatory cytokine production in Caco-2 cells. Caco-2 monolayers were pre-treated apically with 2 mg/mL of mulberry raw materials (MUL) and HME-DDS formulation (HME-MUL-F2) for 24 h. This was followed by incubation, with RAW 264.7 cells exposed to lipopolysaccharide (LPS) in the basolateral compartment for an additional 24 h. ELISA kit analysis for cytokine production of (**A**) prostaglandin E_2 (PGE_2), (**B**) interleukin-beta (IL-1β), (**C**) tumor necrosis factor-α (TNF-α), and (**D**) IL-6 was performed. Different letters (a–d) of error bars within each column indicate significant differences among treatments. One-way ANOVA was conducted, followed by Duncan's multiple range test, to analyze statistical differences at a 5% significance level ($p < 0.05$, $n = 3$).

These results suggest that HME-MUL-F2 may exert its anti-inflammatory effects by suppressing pro-inflammatory cytokine expression.

2.4. Effects of HME-MUL-F2 on Gene Expression Related to Tight Junction

LPS was used in the basolateral compartment to induce an inflammatory reaction in RAW 264.7 cells. Tight junction protein gene expression in Caco-2 cells was measured to evaluate the protective effects of HME-MUL-F2 on intestinal barrier function (Figure 4). LPS treatment reduced mRNA levels of the tight junction (TJ)-related genes ZO-1 (0.39), occludin (0.61), JAM-1 (0.60), claudin-1 (0.35), claudin-3 (0.24), and claudin-4 (0.57) compared to

the results for the control (A relative value, assuming the control group is set as 1 for comparison, $p < 0.05$).

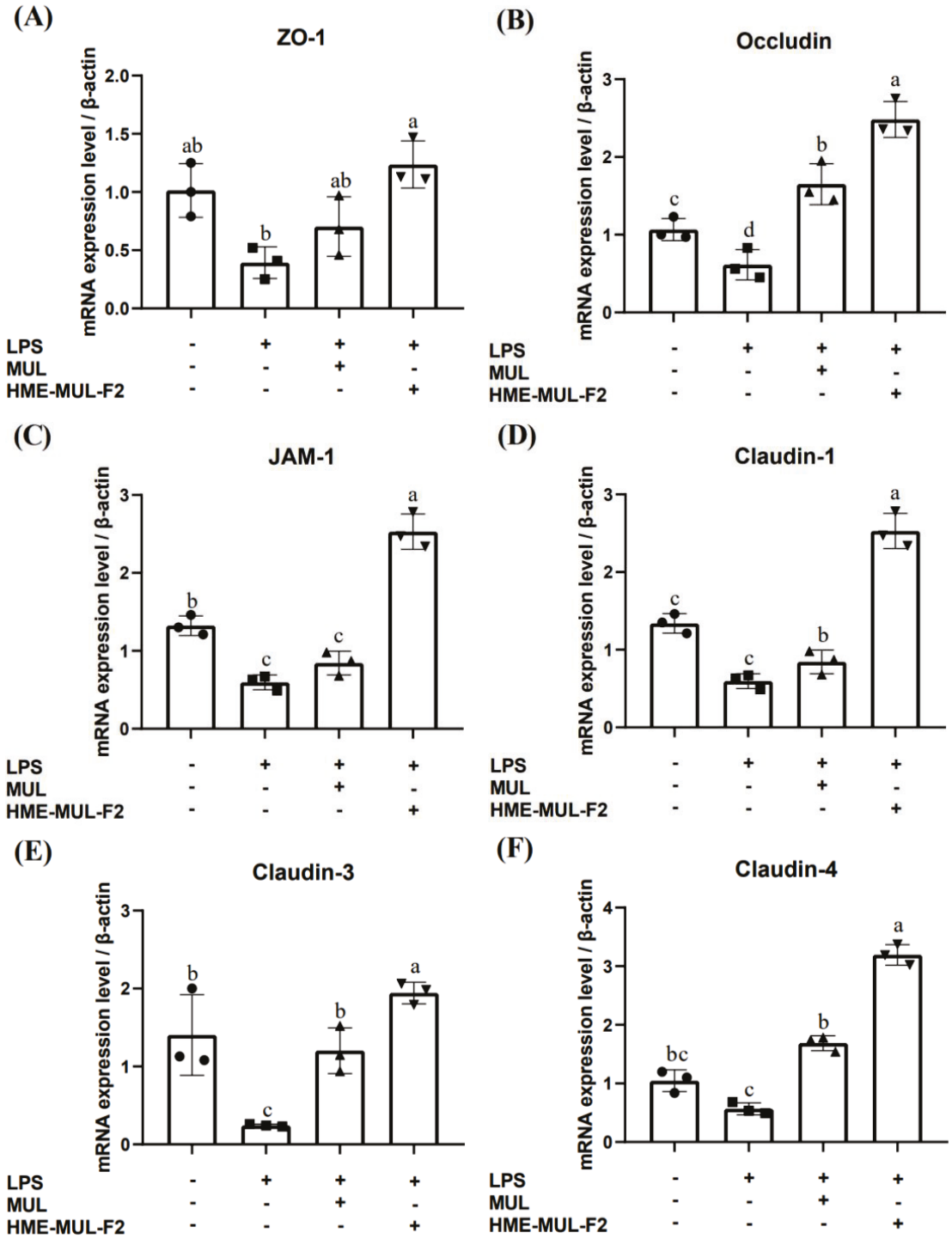

Figure 4. The comparison of mRNA gene expressions of the tight junction obtained from HME-DDS formulate (HME-MUL-F2) in Caco-2 cells. Quantitative RT-PCR analysis was conducted to examine the gene expression levels of tight junction proteins, including (**A**) ZO-1, (**B**) occludin, (**C**) JAM-1, (**D**) claudin-1, (**E**) claudin-3, and (**F**) claudin-4. LPS: lipopolysaccharide, MUL: mulberry raw materials, HME-MUL-F2: HME-DDS formulation using mulberry. Different letters (a–d) of error bars within each column indicate significant differences among treatments. One-way ANOVA was conducted, followed by Duncan's multiple range test, to analyze statistical differences at a 5% significance level ($p < 0.05$, $n = 3$).

These results align with reports that LPS-induced inflammation disrupts the small intestine epithelial barrier by altering TJ proteins [43]. MUL treatment increased occludin, claudin-1, and claudin-4 mRNA levels above control levels, while HME-MUL-F2 increased all TJ proteins above control levels, even after LPS treatment.

HME-MUL-F2 significantly boosted the expression of genes reduced by LPS, demonstrating twice the effectiveness of MUL. Tight junctions are crucial barriers against harmful substances like bacteria and toxins [44]. Endothelial TJs regulate vascular permeability and leukocyte leakage [45], and their dysfunction can lead to continuous inflammation and tissue damage [46]. Inflammation rearranges and modifies transcription in epithelial and endothelial cells, increasing permeability [47]. Natural substances can mitigate TJ rearrangement and help control inflammation-induced permeability [48]. ACN supplementation reduces intestinal permeability and endotoxemia [49].

HME-DDS promotes TJ-related gene expression more effectively than that of the untreated groups, likely due to excipients in HME-MUL-F2. Sodium alginate enhances the immune response and strengthens intestinal cell membranes [50]; poloxamer 188 regulates cytokines and increases occludin and ZO-1 proteins [51].

2.5. HME-MUL-F2 Ameliorates DSS-Induced Colitis

To confirm the preventive effects of MUL and HME-MUL-F2 on DSS-induced colitis in mice, treatments included 5-ASA (150 mg/kg), MUL (250 mg/kg), and HME-MUL-F2 (125 mg/kg, 250 mg/kg), alongside DSS (250 mg/kg) for 7 days. Colon length, a marker of inflammation, was significantly reduced in the DSS group (9.55 ± 0.47 cm to 7.75 ± 0.48 cm). MUL and HME-MUL-F2 treatments resulted in longer colon lengths, i.e., MUL + DSS (8.10 ± 0.27 cm), HME-MUL-F2 + DSS (125 mg/kg: 8.53 ± 0.41 cm, 250 mg/kg: 8.85 ± 0.72 cm), indicating protection against colon shortening (Figure 5A,B, $p < 0.05$).

Weight change, an indicator of disease severity, and the disease activity index (DAI) were evaluated. MUL and HME-MUL-F2 treatments resulted in weight and DAI scores similar to those of the untreated group, except for the 5-ASA positive control. Although not highly significant, weight gain and reduced DAI scores were observed compared to the results for the DSS group, showing protective potential (Figure 5C–F).

HME-MUL-F2 treatment significantly mitigated weight loss and improved disease activity index (DAI) in DSS-induced colitis mice. These effects align with previous findings on mulberry anthocyanins, where supplementation restored tight junction protein expression (ZO-1, occludin, claudin-3) and alleviated DSS-induced colitis symptoms [52].

Notably, our study demonstrated that HME-MUL-F2 achieved comparable or superior protective effects at half the dosage of the raw mulberry extract (MUL), suggesting that the optimized formulation enhances therapeutic efficacy. This is consistent with studies on sustained-release formulations of 5-ASA, where improved drug delivery resulted in enhanced anti-inflammatory outcomes [53]. Thus, HME-MUL-F2 can improve DSS-induced colitis.

2.6. The Effects of HME-MUL-F2 on Serum Inflammatory Cytokines in DSS-Induced Colitis

IL-1β is a key cytokine in immune and inflammatory responses, secreted by monocytes, mast cells, smooth muscle cells, and endothelial cells. It activates lymphocytes and promotes immune cell infiltration at injury sites, with higher expression in UC patients than in healthy individuals [54]. TNF-α enhances phagocytosis and cytokine secretion and influences the NF-κB pathway, critical in both inflammation and IBD [55]. Both TNF-α and IL-1 upregulate MCP-1, impacting various immune cells, and are elevated in the mucosal tissues of CD and UC patients and in experimental colitis models [56].

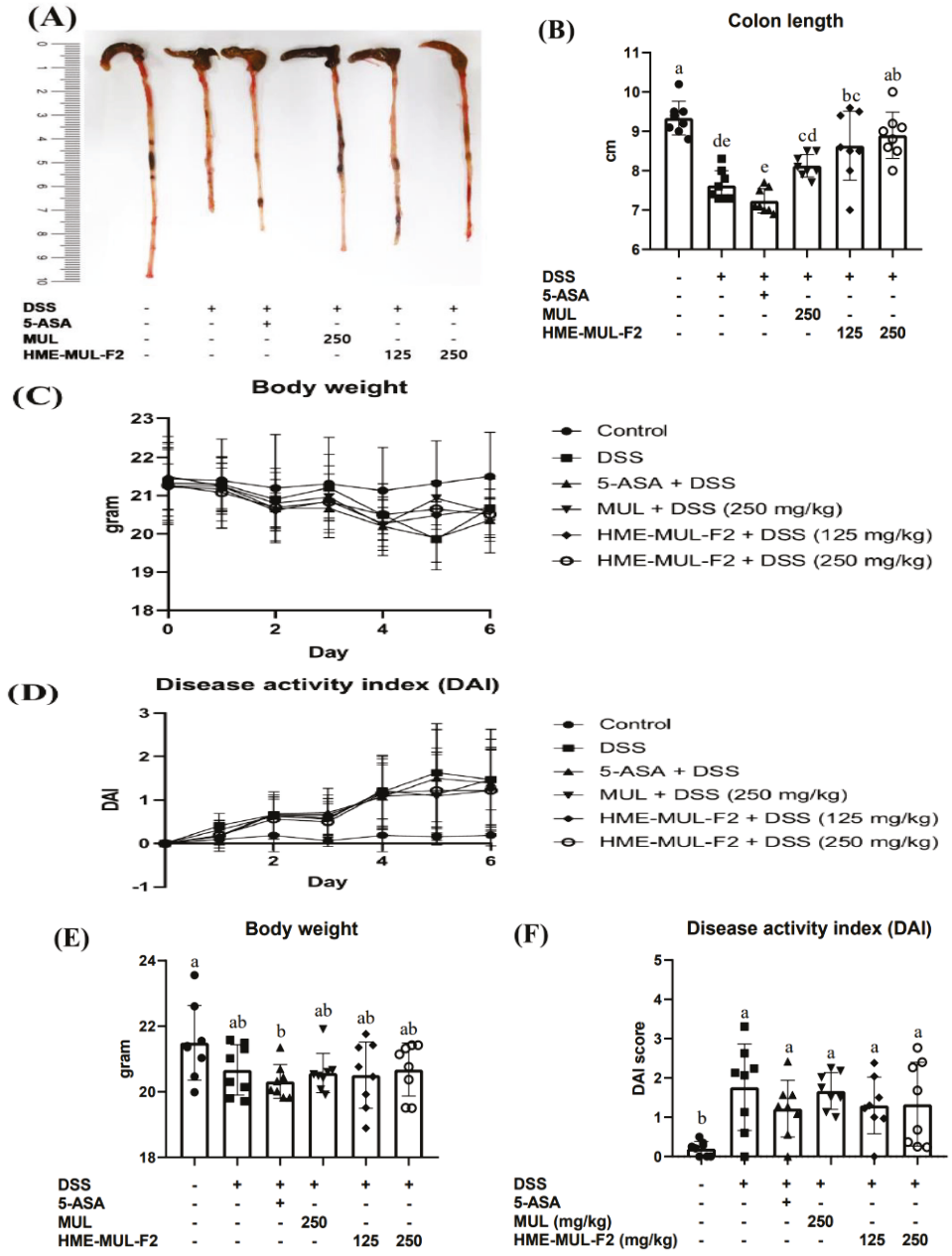

Figure 5. Effects of HME-MUL-F2 and MUL on histopathological parameters. (**A**) Picture of colon; (**B**) colon length; (**C**,**E**) body weight; (**D**,**F**) disease activity index. DSS: dextran sulfate sodium; 5-ASA: 5-aminosalicylic acid; MUL: mulberry raw materials; HME-MUL-F2: HME-DDS formulation using mulberry. Different letters (a–e) of error bars within each column indicate significant differences among treatments. One-way ANOVA was conducted, followed by Duncan's multiple range test to analyze statistical differences at a 5% significance level ($p < 0.05$, $n = 8$).

IBD diagnosis and management are often invasive and costly. Biomarkers like MPO offer a reliable method to monitor IBD activity, indicating disease onset and severity [57]. MPO, found in the neutrophils, indicates neutrophil infiltration and inflammation, with studies showing increased MPO in DSS-induced colitis, suggesting MCP-1's role in colitis pathogenesis [58].

MUL and HME-MUL-F2 reduced the DSS-induced expression of IL-1β, TNF-α, IL-6, and MCP-1, while increasing IL-10 expression (Figure 6, $p < 0.05$). HME-MUL-F2, containing alginate and ascorbyl palmitate and utilizing HME technology, improves intestinal inflammation, even in small amounts [59].

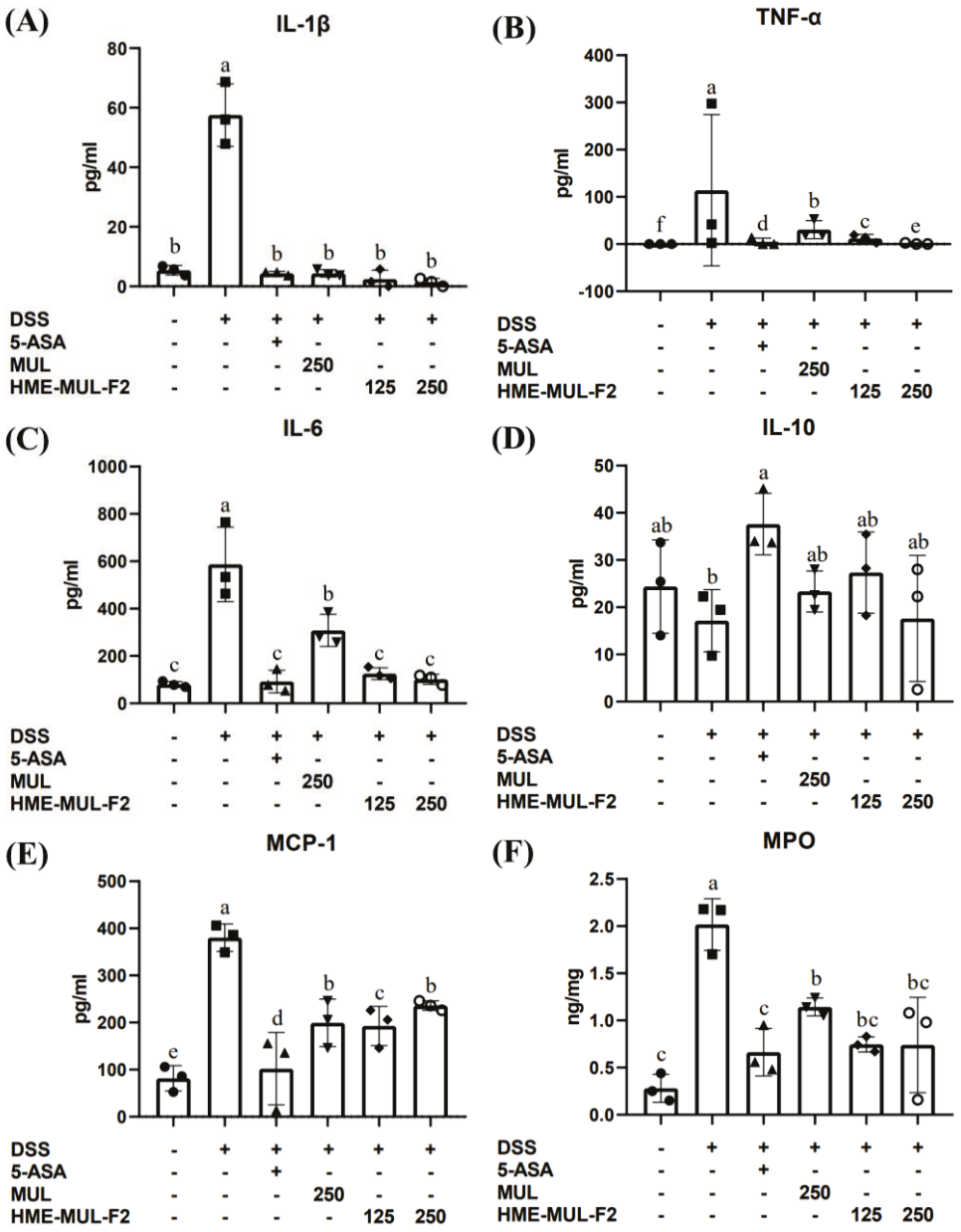

Figure 6. The effect of MUL and HME-MUL-F2 on inflammatory cytokines and MPO. (**A**) IL-1β; (**B**) TNF-α; (**C**) IL-6; (**D**) IL-10; (**E**) MCP-1; (**F**) MPO. DSS: dextran sulfate sodium; 5-ASA: 5-aminosalicylic acid; MUL: mulberry raw materials; HME-MUL-F2: HME-DDS formulation using mulberry. Different letters (a–f) of error bars within each column indicate significant differences among treatments. One-way ANOVA was conducted, followed by Duncan's multiple range test to analyze statistical differences at a 5% significance level ($p < 0.05$, $n = 3$).

2.7. Histopathology of DSS Induced Colitis

A hematoxylin and eosin stain assay (H&E staining) was performed to determine whether morphological changes appeared in the epithelium of the mouse small intestine. Hematoxylin stains the portion corresponding to the nucleus of the tissue in purple, and eosin stains the part corresponding to the cytoplasm of the tissue in red. When inflammation occurs in the intestine, inflammatory cells corresponding to macrophages and T cells infiltrate the lower part of the villus, which is called immune cell infiltration. As a result of H&E staining, it was confirmed that inflammatory cell infiltration appeared clearly in the small intestine of DSS group mice compared to the results for the control group

(Figures 7 and 8). This result is consistent with the report that inflammatory cell infiltration occurs in the large intestine of mice administered with DSS [60].

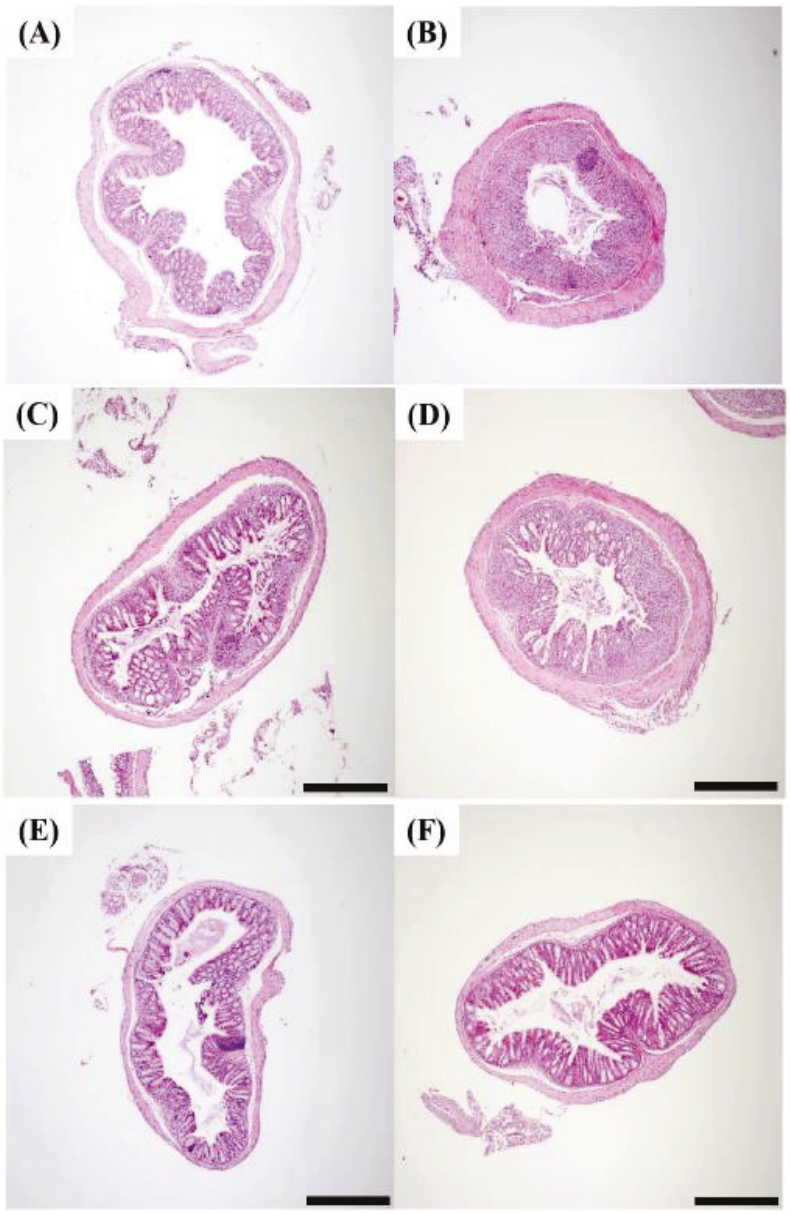

Figure 7. Hematoxylin and eosin (H&E) staining of colon tissues (arrows, ×40; scale bar, 500 μm). (**A**) Control; (**B**) dextran sulfate sodium (DSS); (**C**) DSS + 5-aminosalicylic acid (5-ASA); (**D**) DSS + mulberry raw material (MUL), 250 mg/kg; (**E**) DSS + HME-DDS formulation using mulberry (HME-MUL-F2), 125 mg/kg; (**F**) DSS + HME-MUL-F2, 250 mg/kg.

These results show that DSS induces an inflammatory response in both the large and small intestines of mice. Colonic sections from control mice showed intact mucosa, with no signs of mucosal inflammation. It was confirmed that the epithelium was not damaged, there was no edema in the mucosa, and neutrophils and macrophages did not infiltrate into the mucosa and submucosa. In contrast, colonic sections from mice with colitis showed severe histologic signs. Observation revealed epithelial damage, mucosal edema, and the infiltration of neutrophils and macrophages into both the mucosal and submucosal layers [61].

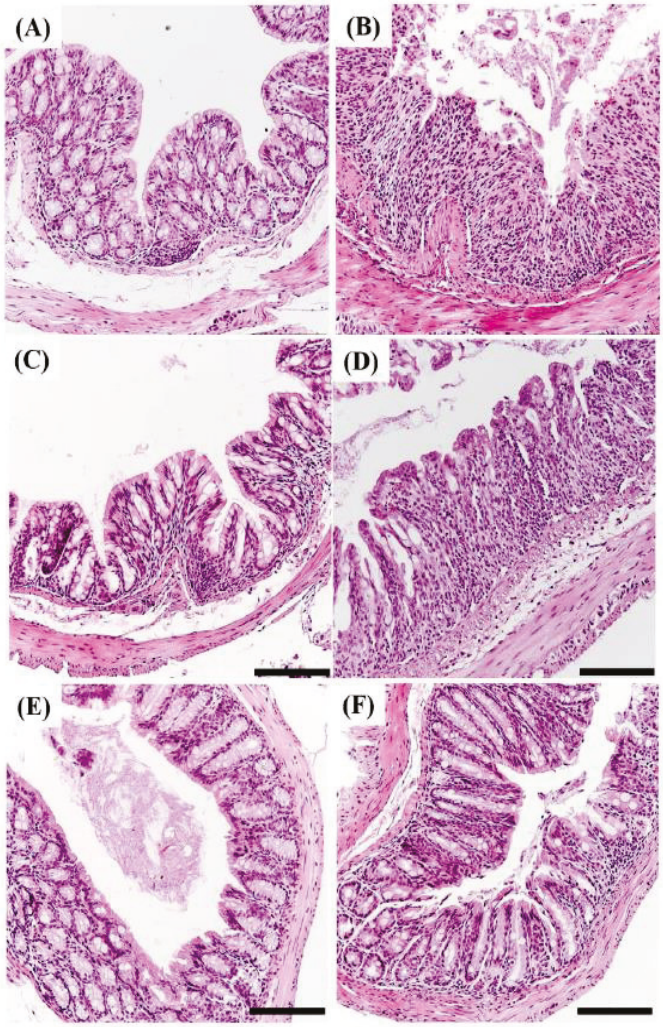

Figure 8. Hematoxylin and eosin (H&E) staining of colon tissues (arrows, ×200; scale bar, 100 μm). (**A**) Control; (**B**) dextran sulfate sodium (DSS); (**C**) DSS + 5-aminosalicylic acid (5-ASA); (**D**) DSS + mulberry raw material (MUL), 250 mg/kg; (**E**) DSS + HME-DDS formulation using mulberry (HME-MUL-F2), 125 mg/kg; (**F**) DSS + HME-MUL-F2, 250 mg/kg.

In the HME-MUL-F2-treated group, no mucosal edema was observed, and the infiltration of neutrophils and macrophages was significantly reduced, leading to an inflammatory cell infiltration rate comparable to that of the healthy control group. The extent of epithelial reconstitution and tissue recovery in the HME-MUL-F2-treated group was comparable to that observed in the healthy control mice, indicating effective mucosal healing. These results indicate that HME-MUL-F2 treatment was associated with improved histological outcomes compared to the results for MUL. This suggests a potential role of enhanced anthocyanin bioavailability; further studies are needed to directly establish whether this effect is due to increased anthocyanin delivery to the colon.

2.8. HME-MUL-F2 Alleviated DSS-Induced Colonic Barrier Dysfunction

One common symptom of IBD is the loss of tight junctions (TJs), leading to epithelial breakdown and altered TJ protein composition. These changes contribute to diarrhea and increase the permeability of the intestinal barrier, allowing for pathogen penetration and inflammation [62]. TJs are essential for maintaining intestinal barrier integrity and selective permeability. In IBD, TJ loss is a predictor for diagnosing Crohn's disease and preventing disease recurrence [63]. Tight junctions consist of proteins such as zonula occludens (ZO), occludin, claudins, and junctional adhesion molecules (JAMs) [64].

Patients with IBD exhibit heightened intestinal permeability due to defective TJs. Claudin-1 and claudin-4 enhance the epithelial barrier, while occludin regulates paracellular permeability [65]. ZO-1 interacts with β-actin and myosin II to construct the cytoskeleton [66]. In Crohn's disease (CD), there is a decrease in occludin, claudin-3, claudin-5, claudin-8, and JAM-A, but an increase in claudin-2 [67]. In ulcerative colitis (UC), occludin, claudin-1, claudin-4, and JAM-A are decreased, while claudin-2 is increased [68].

The effect of MUL and HME-MUL-F2 on mRNA expression of TJ-related proteins (ZO-1, occludin, JAM-1, claudin-3, claudin-4) in DSS-induced colitis was evaluated using RT-qPCR. After DSS treatment, mRNA levels of TJ-related genes were significantly reduced, i.e., ZO-1 (0.02), occludin (0.12), JAM-1 (0.11), claudin-3 (0.01), and claudin-4 (0.10) compared to the results for the control group (Figure 9, $p < 0.05$). These results are consistent with reports that cytokines in DSS-induced inflammation loosen the epithelial barriers by altering protein expression and movement [69].

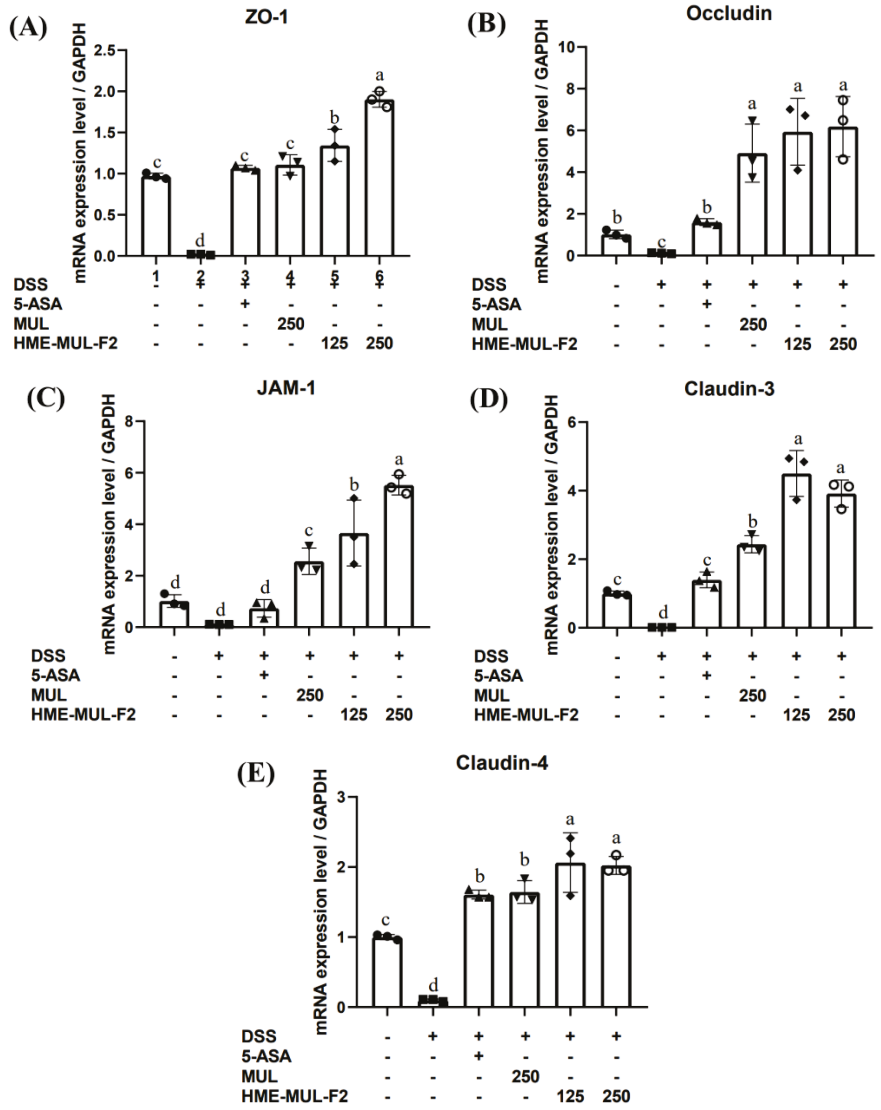

Figure 9. Effect of MUL and HME-MUL-F2 on intestinal barrier protection. (**A**) ZO-1; (**B**) occludin; (**C**) JAM-1; (**D**) claudin-3; (**E**) claudin-4. DSS: dextran sulfate sodium; 5-ASA: 5-aminosalicylic acid; MUL: mulberry raw material; HME-MUL-F2: HME-DDS formulation using mulberry. Different letters (a–d) of error bars within each column indicate significant differences among treatments. One-way ANOVA was conducted, followed by Duncan's multiple range test to analyze statistical differences at a 5% significance level ($p < 0.05$, $n = 3$).

After 5-ASA treatment, the expression of TJ proteins returned to control levels. MUL and HME-MUL-F2 treatment resulted in statistically higher TJ-related gene expression levels than those of the control. HME-MUL-F2 (125 mg/kg) showed higher gene expression than did MUL (250 mg/kg), indicating that HME-DDS has a significant effect on intestinal inflammatory modulators in DSS-induced colitis and can improve intestinal damage.

2.9. HME-MUL-F2 Suppressed the Expression of p-NF-κB p65 and IκB in DSS-Induced Colitis

Inflammatory responses are mediated by pro-inflammatory cytokines like TNF, IL-1β, and IL-6 through the activation of NF-κB, a key inflammatory transcription factor. NF-κB consists of five proteins: p50, p52, c-Rel, RelA (p65), and RelB [70]. Normally, NF-κB proteins are maintained in the cytosol by binding with IκB proteins. Upon stimulation, the p65-p50 dimer of NF-κB is released from IκB through phosphorylation, leading to ubiquitylation and the proteasomal degradation of IκB [71]. The liberated p65-p50 dimer translocates to the nucleus and induces gene expression involved in the inflammatory response [72].

The inhibition of NF-κB activation by HME-MUL-F2 may be attributed to the stabilization of anthocyanins, which have been reported to block the phosphorylation of IκBα and reduce the nuclear translocation of NF-κB p65.

Clinical studies suggest that NF-κB p65 oligonucleotides significantly reduce NF-κB p65 and cytokine expression in the mucosa, improving clinical symptoms [73] NF-κB, a heterodimer of p50 and p65, is regulated by IκB and IKK. Inactive IKK is bound to IκB in the cytoplasm. Noxious stimuli activate IKK, leading to the phosphorylation of IκBα, which activates NF-κB, causing it to move to the nucleus and bind to DNA, encoding inflammatory mediators [74].

When bound to IκB, NF-κB does not function as a transcription factor. However, when IκB is phosphorylated by stimulants like DSS, it degrades, allowing NF-κB to enter the nucleus and promote the synthesis of inflammatory mediators [75]. In assessing the anti-inflammatory effect of HME-MUL-F2 on NF-κB expression (Figure 10, $p < 0.05$), it was found that DSS-induced NF-κB expression in the nucleus was reduced in a concentration-dependent manner by HME-MUL-F2 treatment. Additionally, the phosphorylated NF-κB p65 (p-p65) and phosphorylated IκB (p-IκB) levels increased with DSS treatment but were suppressed by HME-MUL-F2, indicating that its anti-inflammatory effect may be related to blocking cytokine-mediated NF-κB activation. These results suggest that HME-MUL-F2 may exert its anti-inflammatory effects by inhibiting the NF-κB signaling pathway, preventing the degradation of IκBα and thereby suppressing pro-inflammatory cytokine expression.

2.10. Effects of HME-MUL-F2 on Gut Microbiota

Recent studies have highlighted the role of gut microbiota in IBD. The human gut microbiome, consisting of over 1000 bacterial species, includes key phyla like Bacteroidetes, Firmicutes, Actinobacteria, and Proteobacteria [76]. This microbiome supports digestion, nutrient metabolism, and energy supply. Disruption of the microbial balance promotes inflammation and disrupts homeostasis [77]. Increased intestinal permeability in IBD can lead to bacterial translocation, exacerbating inflammation [78]. Microbial metabolites like short-chain fatty acids and bile acids help control inflammation [79]. Reduced microbial diversity is linked to IBD severity [80].

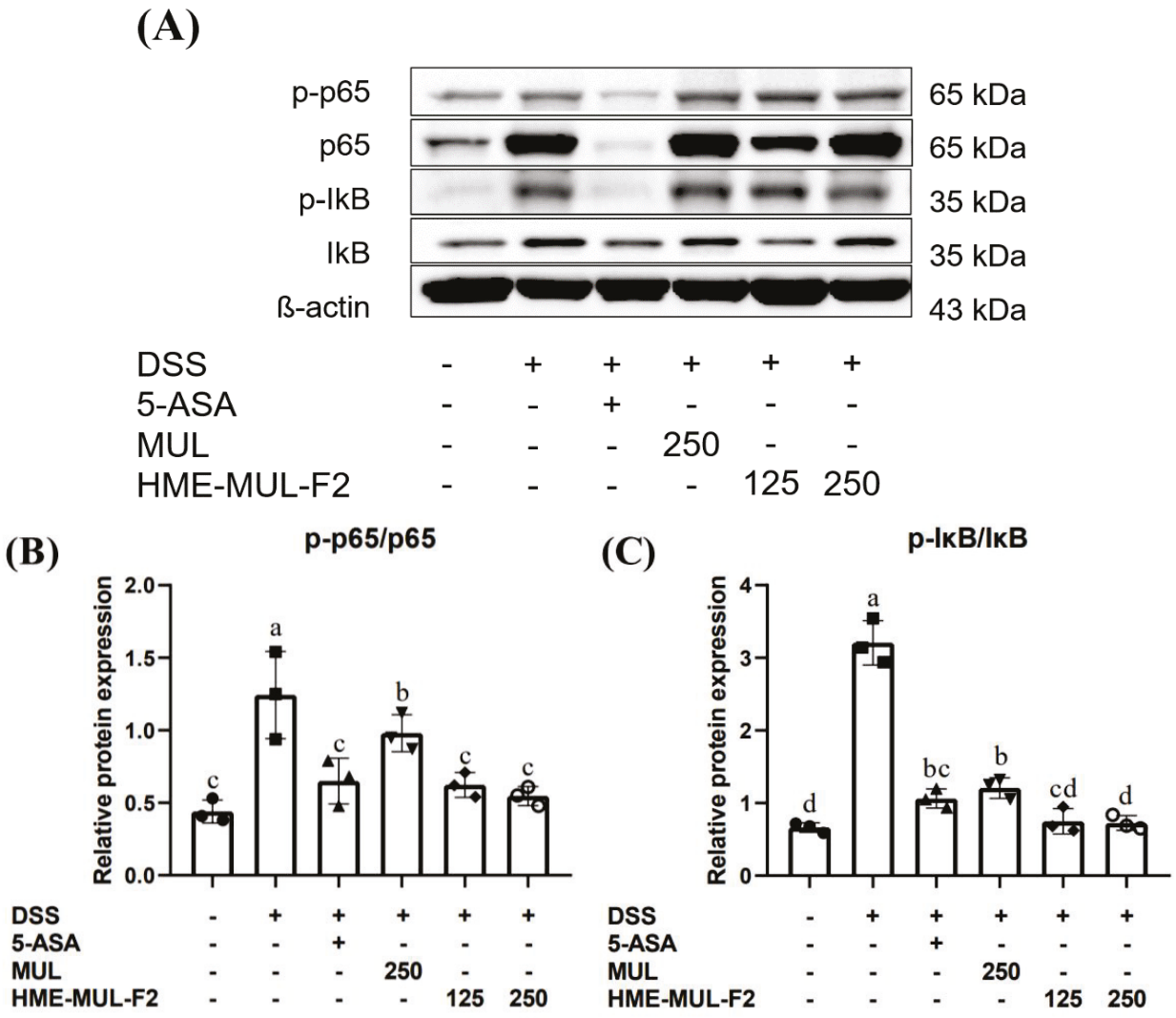

Figure 10. Effect of MUL and HME-MUL-F2 on the activation of NF-κB in the colon of DSS-induced colitis mice. Protein samples underwent Western blot analysis with specific antibodies; β-actin was used as an internal control. The results were consistent across three independent experiments, with one representative experiment shown. The expression levels of p-p65, p65, p-IκB, and IκB in colon tissue were assessed by Western blotting (**A**). Relative quantification of p-p65 and p65 protein expression was performed (**B**). The relative quantification of p-IκB and IκB protein expression (**C**). Different letters (a–d) of error bars within each column indicate significant differences among treatments. One-way ANOVA was conducted, followed by Duncan's multiple range test to analyze statistical differences at a 5% significance level ($p < 0.05$, $n = 3$).

The Shannon diversity index and principal coordinates analysis (PCoA) were used to assess microbial diversity. Higher Shannon index values indicate greater diversity [81]. PCoA visualizes data similarity, showing that microbial imbalances are crucial in UC progression [82]. Alpha diversity decreased in DSS-induced colitis compared to the results for the controls (Figures 11A and 12A). MUL (250 mg/kg) did not maintain alpha diversity, but HME-MUL-F2 did. Beta diversity showed a clustering of the control, HME-MUL-F2, and MUL groups, while the DSS group was distinct (Figures 11B and 12B). HME-MUL-F2 maintains microbial composition and diversity in DSS treatment.

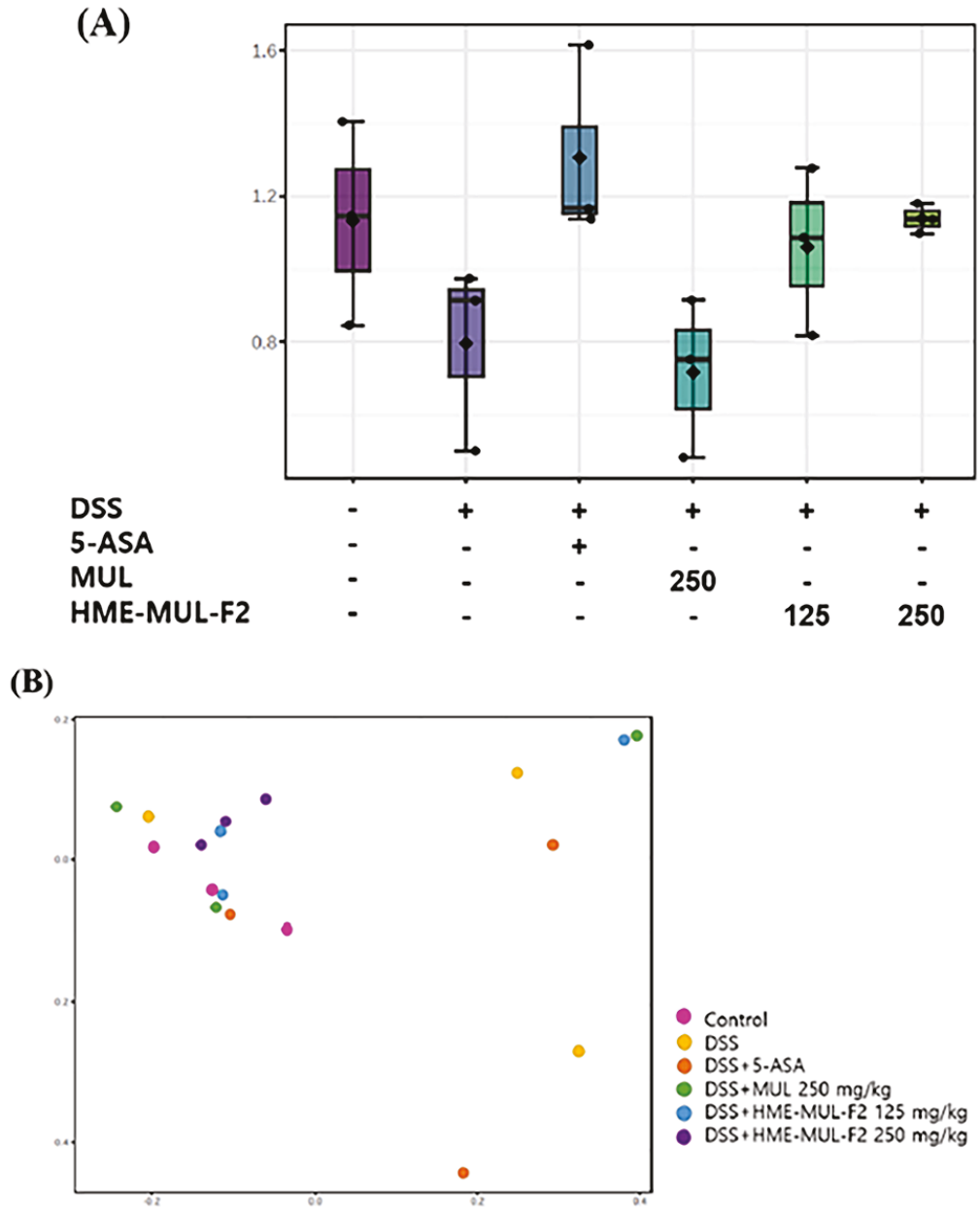

Figure 11. Metagenomic analysis of intestinal flora following dextran sulfate sodium (DSS), 5-aminosalicylic acid (5-ASA), mulberry raw material (MUL), and HME-DDS formulation using mulberry (HME-DDS-F2) treatments at the phylum level. (**A**) Shannon index; (**B**) PCoA plot.

Several natural compounds and probiotic formulations have been investigated for their protective effects against DSS-induced colitis, including *Bacteroides ovatus* V975 (engineered to express TGF-β1), *Clostridium butyricum* MIYAIRI 588, and *Faecalibacterium prausnitzii* [83]. These formulations primarily exert their effects by modulating gut microbiota composition, promoting anti-inflammatory cytokines, or enhancing mucosal healing. In comparison, While the mechanisms differ, HME-MUL-F2 shows comparable or superior efficacy to those of other natural formulations by providing both anti-inflammatory and gut-protective benefits.

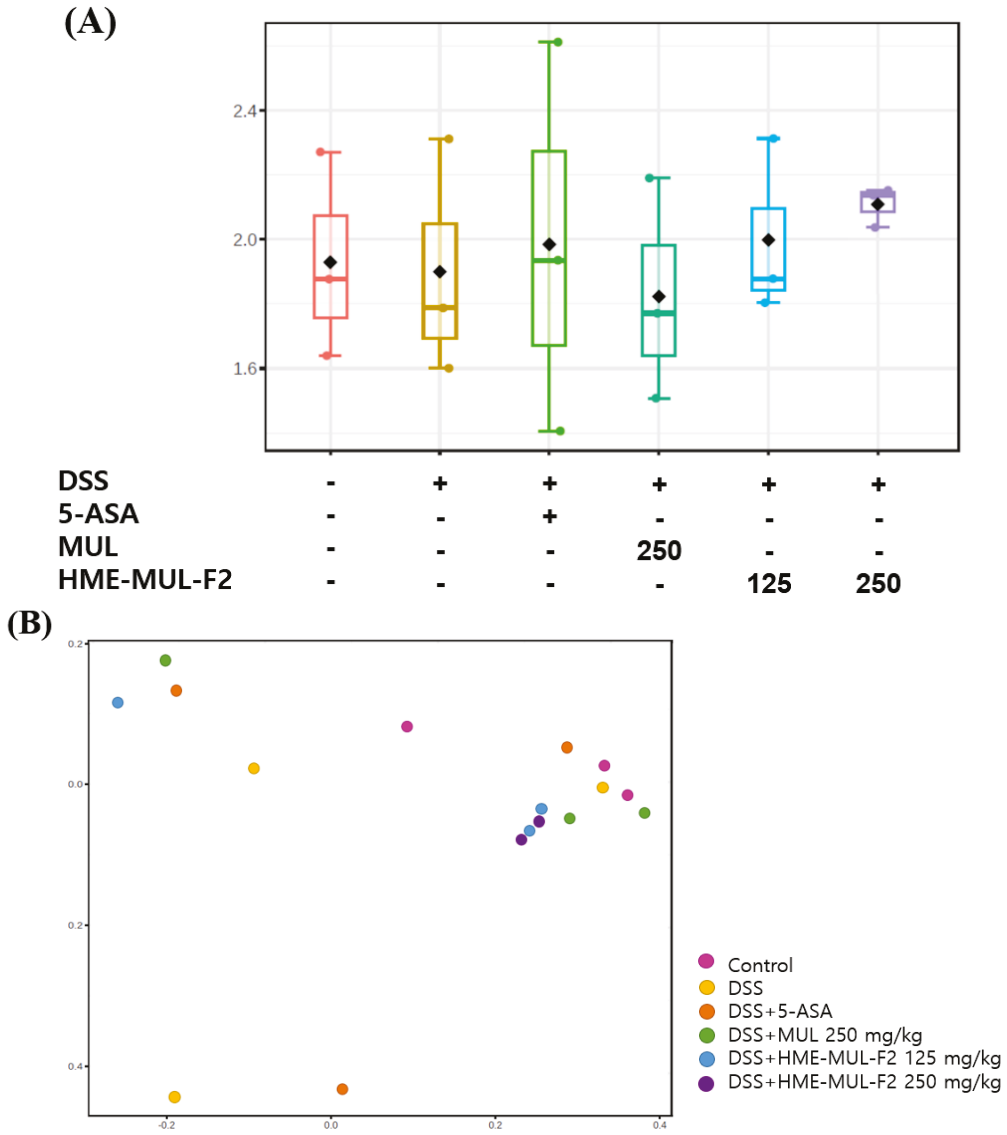

Figure 12. Metagenomic analysis of intestinal flora following dextran sulfate sodium (DSS), 5-aminosalicylic acid (5-ASA), mulberry raw material (MUL), and HME-DDS formulation using mulberry (HME-DDS-F2) treatments at the genus level. (**A**) Shannon index; (**B**) PCoA plot.

The enhanced effectiveness of HME-MUL-F2 compared to MUL may be attributed to the use of appropriate excipients in the hot-melt extrusion (HME) process, which facilitates the formation of a colloidal dispersion system. The enhanced gut microbiota modulation observed with HME-MUL-F2 may be partially due to the improved bioavailability of anthocyanins, allowing for greater interaction with intestinal microbiota and a subsequent reduction in inflammation. Unlike pH-sensitive coatings, which are highly depend on gastric transit variations, HME-MUL-F2 ensures consistent and prolonged release, allowing for more effective colonic targeting.

Colitis patients often exhibit a decreased Firmicutes/Bacteroides ratio, reduced biodiversity, and an imbalance in intestinal bacteria [84]. After DSS administration, Firmicutes, Bacteroidota, and Proteobacteria increased, indicating epithelial dysfunction [84]. DSS treatment increased Firmicutes and decreased Bacteroidota (Figure 13A). Following the 5-ASA treatment, both Firmicutes and Bacteroidota decreased. MUL and HME-MUL-F2 treatments increased Firmicutes and Bacteroidota.

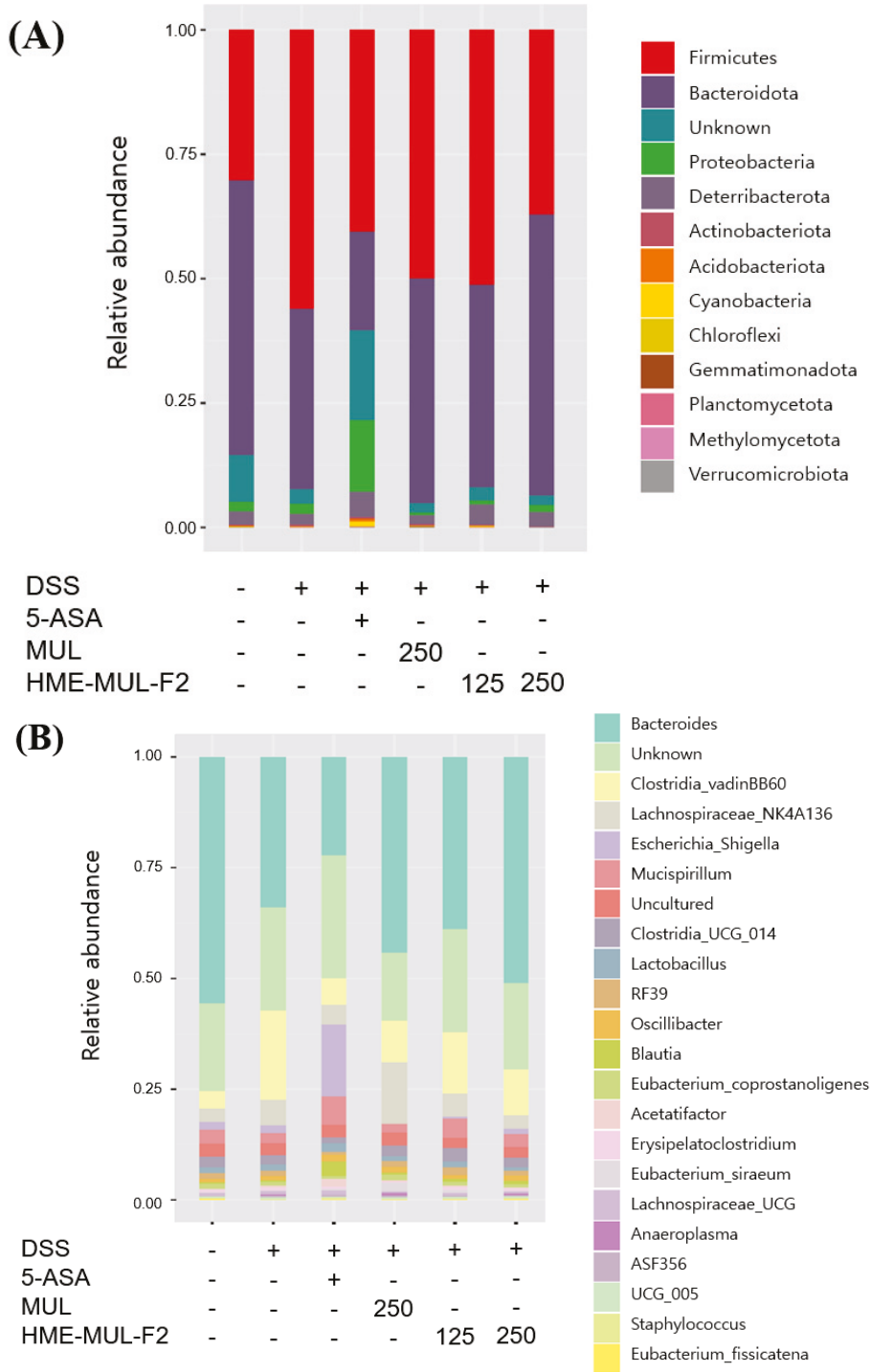

Figure 13. Metagenomic analysis of intestinal flora following dextran sulfate sodium (DSS), 5-aminosalicylic acid (5-ASA), mulberry raw material (MUL), and HME-DDS formulation using mulberry (HME-DDS-F2) treatments. (**A**) Phylum level; (**B**) genus level.

At the genus level, colitis mice showed decreased Bacteroides and increased Lachnospiraceae_NK4A136 and Escherichia-Shigella [85]. MUL and HME-MUL-F2 treatments reversed this imbalance by increasing beneficial bacteria. Escherichia-Shigella is a pathogenic bacterium that promotes physiological changes and tissue infiltration in the intestinal epithelium [86]. Lachnospiraceae_NK4A136 correlates positively with colitis pathology [87]. MUL treatment showed high levels of Lachnospiraceae_NK4A136, but HME-MUL-F2 treatment reduced it, overcoming colitis.

HME-MUL-F2 treatment strengthened the barrier function by reducing harmful bacteria (Lachnospiraceae_NK4A136 and Escherichia-Shigella) and increasing beneficial bacteria (Bacteroides). These results align with reports that polymer nanoparticles relieve mucosal inflammation by protecting the mucosal layer and regulating macrophage function [88]. Therefore, HME-MUL-F2 can be used as a dietary component for preventing and treating colitis, suggesting its anti-ulcerative colitis effect by improving intestinal bacterial balance.

Recent advances in natural polymer-based drug delivery systems have significantly improved the bioavailability and therapeutic efficacy of bioactive compounds, particularly polyphenols such as anthocyanins. These natural biopolymer matrices offer enhanced stability, controlled release, and targeted delivery, making them promising candidates for gastrointestinal drug administration [89].

Dietary fibers and polysaccharides, including alginate, pectin, and chitosan, have been utilized as sustained-release carriers for polyphenols, allowing for prolonged retention and gradual absorption in the intestinal tract [90].

Traditional anthocyanin formulations, such as simple aqueous extracts or freeze-dried powders, often suffer from low stability and poor bioavailability due to rapid degradation in physiological conditions. In contrast, HME-MUL-F2 improves anthocyanin stability by incorporating polymeric excipients, which protect the bioactive compounds from oxidative and enzymatic degradation.

Various nano- and microencapsulation techniques have been developed to enhance the stability and intestinal absorption of polyphenols, including anthocyanins [91]. For instance, chitosan–pectin composite nanoparticles have been utilized as mucoadhesive carriers for anti-inflammatory compounds, improving their retention time in the gastrointestinal tract and enabling targeted release in the colon [92]. Similarly, liposomal and exosome-like nanoparticle formulations derived from plant sources have been shown to enhance polyphenol delivery and bioactivity [93].

Liposomal and nanoparticle-based delivery systems have been explored to enhance anthocyanin bioavailability; however, these systems often face challenges related to high production costs, limited scalability, and stability issues during storage. In comparison, HME-MUL-F2 offers a cost-effective and scalable alternative, utilizing hot-melt extrusion (HME) technology to create a solid dispersion system that facilitates sustained release and targeted delivery to the colon.

pH-sensitive or enteric-coated formulations are designed to bypass gastric degradation and enhance colonic delivery, but their efficiency is highly dependent on variations in individual gastric transit times and intestinal pH levels. In contrast, HME-MUL-F2 achieves sustained release through matrix-controlled dissolution, ensuring a more consistent and prolonged release profile, thereby enhancing local bioavailability at the site of action in the colon.

While conventional sustained-release systems often rely on hydrophilic polymers for controlled drug release, they may not effectively prevent early degradation in the upper gastrointestinal tract. HME-MUL-F2, by contrast, combines hydrophobic and mucoadhesive polymers, creating a protective matrix that enhances both stability and retention time, leading to improved therapeutic efficacy.

These findings indicate that natural polymer-based carriers not only enhance bioavailability but may also deliver additional biological benefits, such as gut microbiome modulation and immune regulation. Future studies could explore whether HME-MUL-F2 could be further optimized through its incorporation into such nanoformulations. The findings of this study suggest that HME-MUL-F2 could serve as a novel bioactive formulation with potential applications in inflammatory bowel disease (IBD) management. Compared to con-

ventional anti-inflammatory agents such as 5-ASA, natural anthocyanin-based formulations offer the advantage of lower toxicity and enhanced gut microbiota compatibility [94].

Given the increasing interest in functional foods and nutraceuticals, HME-MUL-F2 could also be explored as a dietary supplement for gut health maintenance or as an adjunct therapy for patients with chronic inflammatory conditions. Moreover, incorporating biopolymer-based or nanoencapsulated formulations may further optimize its bioavailability and targeted release, paving the way for potential clinical trials.

Future research should focus on pharmacokinetic studies to confirm the absorption dynamics and sustained-release properties of HME-MUL-F2, along with gut microbiota analyses to determine its potential role in microbiome modulation. These advancements could provide a deeper understanding of how HME-MUL-F2 can be integrated into next-generation natural compound-based therapeutics.

3. Materials and Methods

3.1. Materials

The preparation of HME-MUL-F2 followed previously established methodologies. A detailed description of the formulation process, including the composition and extrusion parameters, is included in Ref. [28]. HME-MUL-F2 was prepared using a twin-screw extruder (STS-25HS, co-rotating intermeshing type, Pyeongtaek, Republic of Korea). The raw mulberry powder was mixed with excipients including ascorbyl palmitate (5%), mannitol (35%), sodium alginate (5%), and poloxamer 188 (5%) to enhance the stability and controlled release properties. The extrusion parameters were set as follows: feeding rate, 40 g/min; screw speed, 150 rpm; temperature, 70–100 °C. This process was adapted from our previous work [28] to improve the stability and bioavailability of anthocyanins.

In this study, the mulberry raw material (MUL) and HME-MUL-F2, which involves the use of excipients and the HME process on MUL, were utilized. The mulberries were collected from the Rural Development Administration in 2020, identified as *Morus alba* L., immediately washed, frozen, and stored at −20 °C until use. The HME-MUL-F2 formulation was able to delay the drug release rate in vitro, increase lactic acid bacteria, reduce harmful bacteria, and enhance antioxidant effects.

3.2. Cell Culture Conditions

To examine the effect of HME-MAL-F2 on tight junctions in the human small intestine, Caco-2 cells (30,037.1, Korean Cell Line Bank, Seoul, Republic of Korea) were placed in the apical compartment with a semi-permeable membrane, while RAW264.7 macrophages (40,071, Korean Cell Line Bank, Seoul, Republic of Korea) were co-cultured in the basolateral compartment. This in vitro gut inflammation model was used to study the transport, metabolism, and cell–cell interactions of the pharmacological components. The cell culture used penicillin–streptomycin solution, PBS, DMEM, 0.05% trypsin-EDTA solution, and FBS from Gibco, Grand Island, NY, USA, as well as 30 mm cell culture dishes from SPL Life Sciences [95]. Caco-2 cells were cultured in DMEM medium with 10% FBS, 1% antibiotics, and 5% CO_2 at 37 °C [96].

3.3. Toxicity Evaluation

The impact of MUL and HME-MUL-F2 samples on cell stimulation and viability was assessed using the MTT test. RAW 264.7 cells (passage: 28), at 4×10^4 cells/well, and Caco-2 cells (passage: 36), at 5×10^4 cells/well, were incubated in a 96-well plate until 80% confluence was reached. The samples were diluted in culture medium to concentrations of 1, 2, and 4 mg/mL, pre-treated for one hour, and then treated for 24 h. After treatment, 10 µL of MTT solution (5 mg/mL) was added to each well and incubated for 4 h at 37 °C.

The reaction was stopped by adding 200 µL of DMSO after removing the supernatant. The purple formazan was dissolved by gently shaking the plate in the dark. Subsequently, 50 µL from each well was transferred to a 96-well plate, and absorbance was measured at 570 nm using a microplate reader. Cell viability (%) was calculated using the following formula:

$$\text{Cell viability (\%)} = [(A_{\text{tretment}} - A_{\text{blank}})/A_{\text{control}} - A_{\text{blank}}] \times 100$$

A: absorbance

3.4. In Vitro Inflammation Model

To study the effects of HME-MAL-F2 on tight junctions in the human small intestine, Caco-2 cells (passage: 36) were cultured in the apical compartment of a 6-well Transwell insert plate at a density of 1×10^5 cells/well with 2 mL of medium [97]. The medium was changed every 2–3 days for 21 days. Care was taken during medium exchanges to avoid disturbing the membrane. In a 6-well plate, 1×10^5 RAW 264.7 cells (passage: 28) were planted per well, with 3 mL of medium in the basolateral compartment, for 48 h.

After the culture period, the Transwell insert plate with Caco-2 cells was transferred to a 6-well plate containing RAW 264.7 cells. All media were replaced with serum-free DMEM [98].

3.5. TEER Measurement

Once Caco-2 cells formed an intact monolayer with tight junctions (TEER > 800 $\Omega \times cm^2$); MAL and HME-MAL-F2 samples (2 mg/mL) were added to the apical wells and cultured for 24 h [99]. The basolateral wells were washed with PBS, and then 2 µg/mL of LPS in serum-free DMEM was added and cultured for another 24 h.

The integrity of tight junctions was verified by measuring TEER (transepithelial electrical resistance) using a Millicell ERS-2 resistance meter. The probe was positioned with the long side perpendicular to the bottom of the basolateral well and the short side slightly immersed in the medium of the apical well. Before measuring the next well, the probe was washed with PBS. TEER values were measured in triplicate and calculated using the following formula:

$$\text{TEER (transepithelial electrical resistance)} = \text{resistance } (\Omega) \times \text{membrane area } (cm^2).$$

3.6. Cytokine and RNA Analysis

To assess the permeability increase and the resulting transfer of inflammatory cytokines from RAW 264.7 cells to the apical compartment, levels of NO, IL-1β, PGE2, and TNF-α were measured using Invitrogen ELISA kits. The cytokine content was analyzed in the apical compartment with Caco-2 cells to determine the effect of HME-MAL-F2 on maintaining tight junction integrity. If tight junctions were disrupted, cytokines from the basolateral RAW 264.7 cells would appear in the apical compartment.

For RNA analysis, Caco-2 cells treated with LPS were analyzed 24 h after treatment with MUL and HME-MUL-F2 samples. The cells were washed with 2 mL of PBS at 4 °C and collected. Total RNA was extracted using the Hybrid-R kit and dissolved in DEPC-H2O [100]. The RNA concentration was measured at 260/280 nm using a NanoDrop Spectrophotometer. Only RNA samples with an A260/A280 ratio of 1.8–2.1 were used. The isolated total RNA was stored at −70 °C.

3.7. Quantitative RT-PCR (qRT-PCR) Analysis

Total RNA was converted into cDNA using the Hyperscript 2X RT Master Mix. A 20 µL reaction mixture included the master mix, oligo dT, total RNA, and RNase-free water. cDNA synthesis was performed using a SimpliAmp Thermal Cycler with priming at 42 °C

for 5 min, reverse transcription at 55 °C for 60 min, and inactivation at 95 °C for 5 min. Synthesized cDNA was stored at 4 °C for qRT-PCR.

Gene expression levels were measured using the Light Cycler 96 system, with specific primers. The 20 μL reaction mixture contained SYBR Green PCR master mix, forward and reverse primers, cDNA, and distilled water. PCR cycling involved 10 min at 95 °C for initial denaturation, followed by 40 cycles of 15 s at 95 °C, 30 s at 55 °C, and 30 s at 72 °C. The ΔCt value was calculated by subtracting β-actin's Ct value from the target gene's Ct value, and ΔΔCt was obtained by subtracting the control group's average ΔCt from the experimental group's ΔCt. Data were analyzed using the $2^{-\Delta\Delta Ct}$ method to analyze the relative changes in gene expression from real-time quantitative PCR experiments. Primer sequences for tight junction-related genes and β-actin were produced in a manner similar to that used by Kim et al. (2020) [101].

3.8. Animal Preparation

Animal studies were carried out with permission from Gyeongsang National University's Animal Ethics Committee (approval number: GNU-230303-M0040, 3 March 2023). Male Balb/c mice (20 ± 2 g, 6 weeks old) were purchased from Orient Bio (Seongnam, Republic of Korea) and were specific pathogen-free (SPF). The mice were kept at a temperature of 23 ± 2 °C, 55–60% relative humidity, and a regular 12/12-h light/dark cycle. Following a week of acclimatization, each mouse was randomly assigned to one of six groups, with eight mice per group (n = 8). Oral administration was performed in each of the following six groups: the untreated group, the DSS group (250 mg/kg), the 5-aminosalicylic acid (5-ASA) group (150 mg/kg), the MUL group (250 mg/kg), and the two HME-MUL-F2 groups (125 mg/kg and 250 mg/kg). To induce colitis, the experimental groups were treated with a 2.5% DSS (MFCD00081551, MP Biomedical, Santa Ana, CA, USA) solution for 7 days.

3.9. Clinical Indicators and Pathological Evaluation

Clinical indicators, including body weight loss, stool consistency, and fecal blood, were monitored daily to assess disease activity. These parameters were used to calculate the disease activity index (DAI), following the methodology described by Khater et al. (2022) [102]. Weight loss was measured on a scale from 0 to 4 (0: no change, 1: 1–5% loss, 2: 5–10% loss, 3: 10–20% loss, 4: >20% loss). Stool viscosity, occult blood, and clinical scores were each rated from 0 to 4 (0: no change, 1: +, 2: ++, 3: +++, 4: ++++).

After euthanasia, colonic tissues were harvested for histopathological examination. Tissues were fixed in 10% neutral-buffered formalin, embedded in paraffin, sectioned at 5 μm, and stained with hematoxylin and eosin (H&E) for microscopic evaluation, as previously detailed by Khater et al. (2022) [102].

3.10. Cytokine, Chemokine, and Protein Analysis

Colon tissue was crushed using the BioMasher II device, and the supernatant was centrifuged at 4 °C and 12,000 rpm for 10 min. The enzyme solution was measured using the MPO expression ELISA kit (Thermo Fisher Scientific, Waltham, MA, USA). For serum cytokine measurement, blood was drawn from the mouse's abdominal vena cava, centrifuged for 20 min at 4 °C at 3500 rpm, and the serum was separated. Cytokines IL-1β, IL-6, IL-10, MCP-1, and TNF-α were measured using kits from Thermo Fisher.

For protein analysis, colon tissue was lysed using RIPA buffer and BioMasher II, then centrifuged at 4 °C and 12,000 rpm for 30 min. Protein concentration was quantified using the Bradford method. Thirty micrograms of protein were electrophoresed on a 10% SDS-PAGE gel and transferred onto a PVDF membrane using an iBlot2 device. The membrane was blocked with 5% non-fat dried milk, incubated overnight at 4 °C with primary

antibodies (for IκB, p65, p-IκB, β-actin; Cell Signaling, Danvers, MA, USA), washed with TBST, and then incubated for one hour with secondary antibodies at room temperature [92]. After washing, the membrane was treated with ECL solution (Intron, Seongnam, Republic of Korea). Protein bands were quantified using ChemiDoc XRS+ software Image Lab 6.1 (Bio-Rad, Hercules, CA, USA), and the results were analyzed as the ratio of relative expression to β-actin.

3.11. cDNA Synthesis and qPCR from Colon Tissue

A 1 cm section above the upper rectum was collected from the colon and stored at −80 °C immediately after collection. RNA was isolated using the RNeasy Mini Kit (Qiagen, Hilden, Germany), and its concentration and purity was assessed by measuring the absorbance at 260 and 280 nm. Only RNA samples with an OD260/280 ratio of 1.8 or higher were used for cDNA synthesis and qPCR.

cDNA was synthesized from total RNA using the TOP script cDNA synthesis kit (Enzynomics, Daejeon, Republic of Korea). qPCR was performed using MIC equipment (BMS, New York, NY, USA) with TOP real SYBR Green qPCR premix and specific primers. The qPCR protocol included initial denaturation at 95 °C for 10 min, followed by 50 cycles of 95 °C for 10 s, 60 °C for 15 s, and 72 °C for 15 s. GAPDH was used as the reference gene, and relative gene expression was calculated using the $2^{-\Delta\Delta Ct}$ method (Table 2).

Table 2. Sequences of sense and antisense primers used for reverse transcription-quantitative PCR (RT-qPCR) of colon tissue.

Gene	Orientation	Primers Sequence (5′→3′)
ZO-1 (*NM_175610*)	Forward	AAGGTTAGCTTACTGTCACACGCTT
	Reverse	ACCTAGAAGACATTGAAGGCATC
Occludin (*NM_002538*)	Forward	GTACCCACCAGTGACCAACA
	Reverse	GTTGCTGGAGCTTAGCCTGT
JAM-1 (*NM_016946*)	Forward	ACAGCCATGAGGTCAGAGGCT
	Reverse	CGACTCTAGAAACACAAGAGCAAGA
claudin-3 (*NM_001306*)	Forward	CACCACTACCAGCAGTCGATGAAC
	Reverse	AGACTGTGTGTCGTCTGTCACCATC
claudin-4 (*NM_001305*)	Forward	GGTAGCTCAGCTGTGACTTTGGACTC
	Reverse	CTGGAGTAACGTGTAGGCTGAGTGAG
GAPDH (*NM_002046*)	Forward	TCCCACTCTTCCACCTTCGA
	Reverse	CAGGAAATGAGCTTGACAAAGTTG

3.12. Intestinal Microbial Community Metagenomic Analysis

Intestinal contents were collected from excised colon tissue, stored at a low temperature, and kept at −80 °C until DNA extraction. Feces from the colon were scraped and used for analysis. DNA was isolated using the FastDNA spin kit (MPBio, Santa Ana, CA, USA). After amplicon PCR with primers 518F (5′-CCAGCAGCCGCGGTAATACG-3′) and 805R (5′-GACTACCAGGGTATCTAATCC-3′), the PCR products were purified using Ampure XP. Indexing PCR was then performed with the Illumina Nextera XT index kit, followed by secondary purification. Sequencing was conducted via the iSeq 100 platform using a paired-end (151 bp × 2) method. The paired-end reads were merged and trimmed, based on quality criteria. The VSEARCH technique was used to identify operational taxonomic units (OTUs) at a 97% sequence identity threshold, and the RDP classifier was employed for taxonomic assignment. Alpha diversity and heatmap clustering analyses were performed using MicrobiomeAnalyst.

3.13. Statistical Analysis

The findings are shown as averages. The statistical analysis was conducted using SPSS software (version 16.0, IBM, Armonk, NY, USA). One-way ANOVA was performed, followed by Duncan's multiple range test, to analyze statistical differences at a 5% significance level ($p < 0.05$, $n = 3$). Due to the small sample size, the results should be interpreted with caution.

4. Conclusions and Prospectives

This study developed HME-MUL-F2 using hot-melt extrusion (HME) technology to enhance the bioavailability and sustained release of C3G and C3R in mulberry. The optimized formulation was designed to protect active compounds, improve absorption, and enable controlled release, thereby potentially improving the stability and bioavailability of anthocyanins in the gastrointestinal environment.

Previous studies have demonstrated that HME-MUL-F2 exhibits antibacterial activity against pathogenic microorganisms such as *E. coli*, *S. aureus*, and *E. faecalis*, and promotes the proliferation of probiotics such as *L. rhamnosus* and *P. pentosaceus*. These findings were established in our previous study and were referenced in this study to provide context for the formulation's potential effects on gut microbiota [28]. Similar outcomes have been reported in studies where anthocyanin-rich formulations positively influenced the gut microbial balance, promoting the proliferation of beneficial microbes [103].

Furthermore, in a Caco-2 and RAW 264.7 co-culture model, HME-MUL-F2 contributed to maintaining intestinal barrier integrity by increasing TEER levels, downregulating pro-inflammatory cytokines (*PGE2*, *IL-1β*, *TNF-α*, *IL-6*), and enhancing the expression of tight junction proteins (*ZO-1*, *occludin*, *JAM-1*, *claudin-1*, *-3*, *-4*), suggesting its potential role in mitigating inflammation-induced epithelial dysfunction. This finding is consistent with those of previous studies demonstrating that anthocyanins can enhance intestinal barrier function by modulating tight junction protein expression [104].

In vivo studies using a DSS-induced colitis mouse model further demonstrated that HME-MUL-F2 could alleviate colitis symptoms, increase body weight and colon length, reduce pro-inflammatory cytokines (*IL-1β*, *TNF-α*, *IL-6*, *MCP-1*), and increase anti-inflammatory cytokines (*IL-10*). This aligns with the results of existing literature highlighting the role of anthocyanins in attenuating inflammation by downregulating pro-inflammatory mediators [105]. Additionally, HME-MUL-F2 appeared to modulate the NF-κB signaling pathway and support gut microbial homeostasis, exhibiting comparable efficacy at a lower dosage (125 mg/kg) relative to that of MUL (250 mg/kg).

Our findings suggest that the observed therapeutic effects of HME-MUL-F2 may be primarily due to enhanced anthocyanin bioavailability and targeted delivery to the colon, leading to improved gut barrier function and modulation of inflammatory pathways, particularly through inhibition of the NF-κB signaling cascade.

These findings suggest that HME-MUL-F2 may serve as a promising formulation for enhancing gut barrier function and modulating the intestinal microbiome in IBD management. However, while improvements were observed in the treatment group, additional studies are required to determine whether these effects are directly attributable to increased anthocyanin delivery to the colon. Notably, its efficacy at a lower dose highlights its potential as an efficient therapeutic alternative. Furthermore, the application of HME technology to improve the stability and bioavailability of natural compounds underscores its broader prospects in regards to functional food development and targeted drug delivery systems.

Future research should focus on pharmacokinetic profiling, long-term safety assessments, and clinical validation to further substantiate the therapeutic potential of HME-

MUL-F2. Continued investigations may facilitate its translation into functional foods, nutraceuticals, or natural therapeutics, while additional studies are warranted to comprehensively evaluate its therapeutic efficacy and clinical feasibility.

Author Contributions: Conceptualization, E.-J.G.; methodology, B.R.R. and G.J.G.; software, Y.R.S. and M.J.K. (Min Ji Kang); formal analysis, M.J.K. (Min Ji Kang) and M.J.K. (Min Jun Kim); resources, J.-S.B.; writing—original draft preparation E.-J.G.; writing—review and editing, J.D.L.; supervision, J.D.L. All authors have read and agreed to the published version of the manuscript.

Funding: This research was supported by the BK21 FOUR, funded by the Ministry of Education (MOE, Republic of Korea), and the National Research Foundation of Korea (NRF).

Institutional Review Board Statement: Animal studies were carried out with permission from Gyeongsang National University's Animal Ethics Committee (approval number: GNU-230303-M0040, 3 March 2023).

Informed Consent Statement: Not applicable.

Data Availability Statement: The original contributions presented in the study are included in the article, further inquiries can be directed to the corresponding author/s.

Conflicts of Interest: The authors declare no conflicts of interest.

References

1. Günther, J.; Koy, M.; Berthold, A.; Schuberth, H.-J.; Seyfert, H.-M. Comparison of the Pathogen Species-Specific Immune Response in Udder Derived Cell Types and Their Models. *Vet. Res.* **2016**, *47*, 22. [CrossRef]
2. Whitsett, J.A.; Alenghat, T. Respiratory Epithelial Cells Orchestrate Pulmonary Innate Immunity. *Nat. Immunol.* **2015**, *16*, 27–35. [CrossRef]
3. Mulder, D.J.; Noble, A.J.; Justinich, C.J.; Duffin, J.M. A Tale of Two Diseases: The History of Inflammatory Bowel Disease. *J. Crohns Colitis* **2014**, *8*, 341–348. [CrossRef]
4. Li, L.; Wang, L.; Wu, Z.; Yao, L.; Wu, Y.; Huang, L.; Liu, K.; Zhou, X.; Gou, D. Anthocyanin-Rich Fractions from Red Raspberries Attenuate Inflammation in Both RAW264. 7 Macrophages and a Mouse Model of Colitis. *Sci. Rep.* **2014**, *4*, 6234.
5. Meng, M.; Klingensmith, N.J.; Coopersmith, C.M. New Insights into the Gut as the Driver of Critical Illness and Organ Failure. *Curr. Opin. Crit. Care* **2017**, *23*, 143–148. [CrossRef] [PubMed]
6. Iacob, S.; Iacob, D.G. Infectious Threats, the Intestinal Barrier, and Its Trojan Horse: Dysbiosis. *Front. Microbiol.* **2019**, *10*, 1676. [CrossRef] [PubMed]
7. Stewart, A.S.; Pratt-Phillips, S.; Gonzalez, L.M. Alterations in Intestinal Permeability: The Role of the "Leaky Gut" in Health and Disease. *J. Equine Vet. Sci.* **2017**, *52*, 10–22. [CrossRef]
8. Kim, J.G.; Lee, S.J.; Kagnoff, M.F. Nod1 Is an Essential Signal Transducer in Intestinal Epithelial Cells Infected with Bacteria That Avoid Recognition by Toll-like Receptors. *Infect. Immun.* **2004**, *72*, 1487–1495. [CrossRef]
9. Rhayat, L.; Maresca, M.; Nicoletti, C.; Perrier, J.; Brinch, K.S.; Christian, S.; Devillard, E.; Eckhardt, E. Effect of Bacillus Subtilis Strains on Intestinal Barrier Function and Inflammatory Response. *Front. Immunol.* **2019**, *10*, 431111. [CrossRef]
10. Vora, P.; Youdim, A.; Thomas, L.S.; Fukata, M.; Tesfay, S.Y.; Lukasek, K.; Michelsen, K.S.; Wada, A.; Hirayama, T.; Arditi, M. β-Defensin-2 Expression Is Regulated by TLR Signaling in Intestinal Epithelial Cells. *J. Immunol.* **2004**, *173*, 5398–5405. [CrossRef]
11. O'Hara, A.M.; Shanahan, F. The Gut Flora as a Forgotten Organ. *EMBO Rep.* **2006**, *7*, 688–693. [PubMed]
12. McDonald, D.; Ackermann, G.; Khailova, L.; Baird, C.; Heyland, D.; Kozar, R.; Lemieux, M.; Derenski, K.; King, J.; Vis-Kampen, C. Extreme Dysbiosis of the Microbiome in Critical Illness. *mSphere* **2016**, *1*, 10-1128.
13. Eun, C.S. Intestinal Microbiota and Inflammatory Bowel Diseases. *J. Korean Med. Assoc.* **2021**, *64*, 588–595. [CrossRef]
14. Tuomela, A.; Hirvonen, J.; Peltonen, L. Stabilizing Agents for Drug Nanocrystals: Effect on Bioavailability. *Pharmaceutics* **2016**, *8*, 16. [CrossRef] [PubMed]
15. Tiţa, B.; Fuliaş, A.; Bandur, G.; Marian, E.; Tiţa, D. Compatibility Study between Ketoprofen and Pharmaceutical Excipients Used in Solid Dosage Forms. *J. Pharm. Biomed. Anal.* **2011**, *56*, 221–227. [CrossRef]
16. Silverstein, R.M.; Webster, F.X.; Kiemle, D.J. *Identificação Espectrométrica de Compostos Orgánicos (7a)*; Grupo Gen-LTC: Milano, Italy, 2010; ISBN 8521615213.
17. Nayak, B.; Liu, R.H.; Tang, J. Effect of Processing on Phenolic Antioxidants of Fruits, Vegetables, and Grains—A Review. *Crit. Rev. Food Sci. Nutr.* **2015**, *55*, 887–918. [CrossRef]

18. Kay, C.D.; Pereira-Caro, G.; Ludwig, I.A.; Clifford, M.N.; Crozier, A. Anthocyanins and Flavanones Are More Bioavailable than Previously Perceived: A Review of Recent Evidence. *Annu. Rev. Food Sci. Technol.* **2017**, *8*, 155–180.
19. Hao, J.; Gao, Y.; Xue, J.; Yang, Y.; Yin, J.; Wu, T.; Zhang, M. Phytochemicals, Pharmacological Effects and Molecular Mechanisms of Mulberry. *Foods* **2022**, *11*, 1170. [CrossRef]
20. Qin, S.; Lv, C.; Hou, D.-X. Biological Functions and Health Benefits of Food Polyphenols. *Funct. Foods Biotechnol.* **2020**, 295–326.
21. Augustin, M.A.; Hemar, Y. Nano-and Micro-Structured Assemblies for Encapsulation of Food Ingredients. *Chem. Soc. Rev.* **2009**, *38*, 902–912. [CrossRef]
22. Cardona, F.; Andrés-Lacueva, C.; Tulipani, S.; Tinahones, F.J.; Queipo-Ortuño, M.I. Benefits of Polyphenols on Gut Microbiota and Implications in Human Health. *J. Nutr. Biochem.* **2013**, *24*, 1415–1422. [CrossRef]
23. Reitz, C.; Kleinebudde, P. Solid Lipid Extrusion of Sustained Release Dosage Forms. *Eur. J. Pharm. Biopharm.* **2007**, *67*, 440–448. [CrossRef] [PubMed]
24. Repka, M.A.; Sejal, S.; Jiannan, L.; Sindhuri, M.; Joe, M.; Ketaki, P.; Mohammed, N.N. Melt Extrusion: Process to Product. *Expert. Opin. Drug Deliv.* **2012**, *9*, 105–125. [CrossRef] [PubMed]
25. Detsi, A.; Kavetsou, E.; Kostopoulou, I.; Pitterou, I.; Pontillo, A.R.N.; Tzani, A.; Christodoulou, P.; Siliachli, A.; Zoumpoulakis, P. Nanosystems for the Encapsulation of Natural Products: The Case of Chitosan Biopolymer as a Matrix. *Pharmaceutics* **2020**, *12*, 669. [CrossRef]
26. Eunsu, L.; Hyeongjeong, K.; Yu, J.; Cho, Y.; Kim, D.; Yuhyeon, S.; Kwon, O.; Bongjeon, A. Anti-Inflammatory Effect of Polygonum Multiflorum Extraction in Activated RAW 264.7 Cells with Lipopolysaccharide. *Food Sci. Preserv.* **2014**, *21*, 740–746. [CrossRef]
27. Choi, S.-J.; Jeon, H.; Lee, C.U.; Yoon, S.H.; Bae, S.K.; Chin, Y.-W.; Yoon, K.D. Isolation and Development of Quantification Method for Cyanidin-3-Glucoside and Cyanidin-3-Rutinoside in Mulberry Fruit by High-Performance Countercurrent Chromatography and High-Performance Liquid Chromatography. *Nat. Product. Sci.* **2015**, *21*, 20–24.
28. Go, E.J.; Ryu, B.R.; Gim, G.J.; Lee, H.Y.; You, H.S.; Kim, H.B.; Lee, H.T.; Lee, J.Y.; Shim, M.S.; Baek, J.-S. Hot-Melt Extrusion Enhances Antioxidant Effects of Mulberry on Probiotics and Pathogenic Microorganisms. *Antioxidants* **2022**, *11*, 2301. [CrossRef] [PubMed]
29. Kura, A.U.; Fakurazi, S.; Hussein, M.Z.; Arulselvan, P. Nanotechnology in Drug Delivery: The Need for More Cell Culture Based Studies in Screening. *Chem. Cent. J.* **2014**, *8*, 46. [CrossRef]
30. Marsousi, N.; Doffey-Lazeyras, F.; Rudaz, S.; Desmeules, J.A.; Daali, Y. Intestinal Permeability and P-glycoprotein-mediated Efflux Transport of Ticagrelor in Caco-2 Monolayer Cells. *Fundam. Clin. Pharmacol.* **2016**, *30*, 577–584. [CrossRef]
31. Chantret, I.; Rodolosse, A.; Barbat, A.; Dussaulx, E.; Brot-Laroche, E.; Zweibaum, A.; Rousset, M. Differential Expression of Sucrase-Isomaltase in Clones Isolated from Early and Late Passages of the Cell Line Caco-2: Evidence for Glucose-Dependent Negative Regulation. *J. Cell Sci.* **1994**, *107*, 213–225. [CrossRef]
32. Mahler, G.J.; Shuler, M.L.; Glahn, R.P. Characterization of Caco-2 and HT29-MTX Cocultures in an in Vitro Digestion/Cell Culture Model Used to Predict Iron Bioavailability. *J. Nutr. Biochem.* **2009**, *20*, 494–502. [PubMed]
33. Yang, M.; Lu, X.; Xu, J.; Liu, X.; Zhang, W.; Guan, R.; Zhong, H. Cellular Uptake, Transport Mechanism and Anti-Inflammatory Effect of Cyanidin-3-Glucoside Nanoliposomes in Caco-2/RAW 264.7 Co-Culture Model. *Front. Nutr.* **2022**, *9*, 995391.
34. Chan, E.P.; Lichtenstein, G.R. Chemoprevention: Risk Reduction with Medical Therapy of Inflammatory Bowel Disease. *Gastroenterol. Clin.* **2006**, *35*, 675–712.
35. Sappington, P.L.; Han, X.; Yang, R.; Delude, R.L.; Fink, M.P. Ethyl Pyruvate Ameliorates Intestinal Epithelial Barrier Dysfunction in Endotoxemic Mice and Immunostimulated Caco-2 Enterocytic Monolayers. *J. Pharmacol. Exp. Ther.* **2003**, *304*, 464–476. [PubMed]
36. Pinto, M.; Robine-Leon, S.; Appay, M.-D.; Kedinger, M.; Triadou, N.; Dussaulx, E.; Lacroix, B.; Simon-Assmann, P.; Haffen, K.; Fogh, J. Enterocyte-like Differentiation and Polarization of the Human Colon Carcinoma Cell Line Caco-2 in Culture. *Biol. Cell* **1983**, *47*, 323–330.
37. Briske-Anderson, M.J.; Finley, J.W.; Newman, S.M. The Influence of Culture Time and Passage Number on the Morphological and Physiological Development of Caco-2 Cells. *Proc. Soc. Exp. Biol. Med.* **1997**, *214*, 248–257. [CrossRef]
38. Jiang, Q.; Yin, J.; Chen, J.; Ma, X.; Wu, M.; Li, X.; Yao, K.; Tan, B.; Yin, Y. 4-Phenylbutyric Acid Accelerates Rehabilitation of Barrier Function in IPEC-J2 Cell Monolayer Model. *Anim. Nutr.* **2021**, *7*, 1061–1069.
39. Valdez, J.C.; Cho, J.; Bolling, B.W. Aronia Berry Inhibits Disruption of Caco-2 Intestinal Barrier Function. *Arch. Biochem. Biophys.* **2020**, *688*, 108409.
40. Umare, V.; Pradhan, V.; Nadkar, M.; Rajadhyaksha, A.; Patwardhan, M.; Ghosh, K.K.; Nadkarni, A.H. Effect of Proinflammatory Cytokines (IL-6, TNF-α, and IL-1β) on Clinical Manifestations in Indian SLE Patients. *Mediat. Inflamm.* **2014**, *2014*, 385297.
41. Jeong, J.W.; Lee, W.S.; Shin, S.C.; Kim, G.Y.; Choi, B.T.; Choi, Y.H. Anthocyanins Downregulate Lipopolysaccharide-Induced Inflammatory Responses in BV2 Microglial Cells by Suppressing the NF-?B and Akt/MAPKs Signaling Pathways. *Int. J. Mol. Sci.* **2013**, *14*, 1502–1515. [CrossRef]

42. Yang, D.; Jones, K.S. Effect of Alginate on Innate Immune Activation of Macrophages. *J. Biomed. Mater. Res. A* **2009**, *90*, 411–418. [CrossRef]
43. Watari, A.; Sakamoto, Y.; Hisaie, K.; Iwamoto, K.; Fueta, M.; Yagi, K.; Kondoh, M. Rebeccamycin Attenuates TNF-α-Induced Intestinal Epithelial Barrier Dysfunction by Inhibiting Myosin Light Chain Kinase Production. *Cell. Physiol. Biochem.* **2017**, *41*, 1924–1934. [CrossRef]
44. Anderson, J.M.; Van Itallie, C.M. Physiology and Function of the Tight Junction. *Cold Spring Harb. Perspect. Biol.* **2009**, *1*, a002584. [CrossRef] [PubMed]
45. Lee, S.H. Intestinal Permeability Regulation by Tight Junction: Implication on Inflammatory Bowel Diseases. *Intest. Res.* **2015**, *13*, 11–18.
46. Huang, Y.; Zhou, W. Microencapsulation of Anthocyanins through Two-Step Emulsification and Release Characteristics during in Vitro Digestion. *Food Chem.* **2019**, *278*, 357–363. [CrossRef]
47. Ni, Y.; Teng, T.; Li, R.; Simonyi, A.; Sun, G.Y.; Lee, J.C. TNFα Alters Occludin and Cerebral Endothelial Permeability: Role of P38MAPK. *PLoS ONE* **2017**, *12*, e0170346.
48. Ershad, M.; Shigenaga, M.K.; Bandy, B. Differential Protection by Anthocyanin-Rich Bilberry Extract and Resveratrol against Lipid Micelle-Induced Oxidative Stress and Monolayer Permeability in Caco-2 Intestinal Epithelial Cells. *Food Funct.* **2021**, *12*, 2950–2961. [CrossRef]
49. Cremonini, E.; Daveri, E.; Mastaloudis, A.; Adamo, A.M.; Mills, D.; Kalanetra, K.; Hester, S.N.; Wood, S.M.; Fraga, C.G.; Oteiza, P.I. Anthocyanins Protect the Gastrointestinal Tract from High Fat Diet-Induced Alterations in Redox Signaling, Barrier Integrity and Dysbiosis. *Redox Biol.* **2019**, *26*, 101269. [CrossRef] [PubMed]
50. Ge, F.; Zhu, L.; Yang, L.; Li, W.; Wei, S.; Tao, Y.; Du, G. The Soluble and Particulate Form of Alginates Positively Regulate Immune Response. *Iran. J. Immunol.* **2018**, *15*, 228–238.
51. Wong, S.W.; Yao, Y.; Hong, Y.; Ma, Z.; Kok, S.H.L.; Sun, S.; Cho, M.; Lee, K.K.H.; Mak, A.F.T. Preventive Effects of Poloxamer 188 on Muscle Cell Damage Mechanics under Oxidative Stress. *Ann. Biomed. Eng.* **2017**, *45*, 1083–1092. [CrossRef]
52. Mo, J.; Ni, J.; Zhang, M.; Xu, Y.; Li, Y.; Karim, N.; Chen, W. Mulberry Anthocyanins Ameliorate DSS-Induced Ulcerative Colitis by Improving Intestinal Barrier Function and Modulating Gut Microbiota. *Antioxidants* **2022**, *11*, 1674. [CrossRef] [PubMed]
53. Sahoo, R.N.; De, A.; Kataria, V.; Mallick, S. Solvent-Free Hot Melt Extrusion Technique in Improving Mesalamine Release for Better Management of Inflammatory Bowel Disease. *Indian. J. Pharm. Educ. Res.* **2019**, *53*, S554–S562. [CrossRef]
54. Jain, A.; Irizarry-Caro, R.A.; Chawla, A.S.; Philip, N.H.; Carroll, K.R.; Katz, J.D.; Oberst, A.; Chervonsky, A.V.; Pasare, C. T Cells Instruct Dendritic Cells to Produce Inflammasome Independent IL-1β Causing Systemic Inflammation. *bioRxiv* **2018**, 475517.
55. Evans, S.; Tzeng, H.-P.; Veis, D.J.; Matkovich, S.; Weinheimer, C.; Kovacs, A.; Barger, P.M.; Mann, D.L. TNF Receptor–Activated Factor 2 Mediates Cardiac Protection through Noncanonical NF-KB Signaling. *JCI Insight* **2018**, *3*, e98278.
56. Allavena, P.; Bianchi, G.; Zhou, D.; Van Damme, J.; Jílek, P.; Sozzani, S.; Mantovani, A. Induction of Natural Killer Cell Migration by Monocyte Chemotactic Protein−1,−2 And−3. *Eur. J. Immunol.* **1994**, *24*, 3233–3236.
57. Sutherland, A.D.; Gearry, R.B.; Frizelle, F.A. Review of Fecal Biomarkers in Inflammatory Bowel Disease. *Dis. Colon. Rectum* **2008**, *51*, 1283–1291.
58. Smith, J.W.; Castro, G.A. Relation of Peroxidase Activity in Gut Mucosa to Inflammation. *Am. J. Physiol.-Regul. Integr. Comp. Physiol.* **1978**, *234*, R72–R79.
59. Sabra, R.; Billa, N.; Roberts, C.J. Cetuximab-Conjugated Chitosan-Pectinate (Modified) Composite Nanoparticles for Targeting Colon Cancer. *Int. J. Pharm.* **2019**, *572*, 118775.
60. Zheng, S.; Zhuang, T.; Tang, Y.; Wu, R.; Xu, T.; Leng, T.; Wang, Y.; Lin, Z.; Ji, M. Leonurine Protects against Ulcerative Colitis by Alleviating Inflammation and Modulating Intestinal Microflora in Mouse Models. *Exp. Ther. Med.* **2021**, *22*, 1199. [CrossRef]
61. Yang, C.; Merlin, D. Unveiling Colitis: A Journey through the Dextran Sodium Sulfate-Induced Model. *Inflamm. Bowel Dis.* **2024**, *30*, 844–853.
62. Landy, J.; Ronde, E.; English, N.; Clark, S.K.; Hart, A.L.; Knight, S.C.; Ciclitira, P.J.; Al-Hassi, H.O. Tight Junctions in Inflammatory Bowel Diseases and Inflammatory Bowel Disease Associated Colorectal Cancer. *World J. Gastroenterol.* **2016**, *22*, 3117. [PubMed]
63. Rawat, M.; Nighot, M.; Al-Sadi, R.; Gupta, Y.; Viszwapriya, D.; Yochum, G.; Koltun, W.; Ma, T.Y. IL1B Increases Intestinal Tight Junction Permeability by Up-Regulation of MIR200C-3p, Which Degrades Occludin MRNA. *Gastroenterology* **2020**, *159*, 1375–1389.
64. Weber, C.R.; Turner, J.R. Inflammatory Bowel Disease: Is It Really Just Another Break in the Wall? *Gut* **2007**, *56*, 6–8. [PubMed]
65. Heller, F.; Florian, P.; Bojarski, C.; Richter, J.; Christ, M.; Hillenbrand, B.; Mankertz, J.; Gitter, A.H.; Bürgel, N.; Fromm, M. Interleukin-13 Is the Key Effector Th2 Cytokine in Ulcerative Colitis That Affects Epithelial Tight Junctions, Apoptosis, and Cell Restitution. *Gastroenterology* **2005**, *129*, 550–564.
66. Edelblum, K.L.; Turner, J.R. The Tight Junction in Inflammatory Disease: Communication Breakdown. *Curr. Opin. Pharmacol.* **2009**, *9*, 715–720. [CrossRef]

67. Zeissig, S.; Bürgel, N.; Günzel, D.; Richter, J.; Mankertz, J.; Wahnschaffe, U.; Kroesen, A.J.; Zeitz, M.; Fromm, M.; Schulzke, J.D. Changes in Expression and Distribution of Claudin 2, 5 and 8 Lead to Discontinuous Tight Junctions and Barrier Dysfunction in Active Crohn's Disease. *Gut* **2007**, *56*, 61–72. [CrossRef]
68. Blair, S.A.; Kane, S.V.; Clayburgh, D.R.; Turner, J.R. Epithelial Myosin Light Chain Kinase Expression and Activity Are Upregulated in Inflammatory Bowel Disease. *Lab. Investig.* **2006**, *86*, 191–201.
69. Cao, M.; Wang, P.; Sun, C.; He, W.; Wang, F. Amelioration of IFN-γ and TNF-α-Induced Intestinal Epithelial Barrier Dysfunction by Berberine via Suppression of MLCK-MLC Phosphorylation Signaling Pathway. *PLoS ONE* **2013**, *8*, e61944.
70. Ghosh, S.; May, M.J.; Kopp, E.B. NF-KB and Rel Proteins: Evolutionarily Conserved Mediators of Immune Responses. *Annu. Rev. Immunol.* **1998**, *16*, 225–260. [PubMed]
71. Beaulieu, L.M.; Freedman, J.E. NFκB Regulation of Platelet Function: No Nucleus, No Genes, No Problem? *J. Thromb. Haemost.* **2009**, *7*, 1329–1332. [PubMed]
72. Karin, M.; Yamamoto, Y.; Wang, Q.M. The IKK NF-KB System: A Treasure Trove for Drug Development. *Nat. Rev. Drug Discov.* **2004**, *3*, 17–26. [CrossRef]
73. Baldwin, A.S., Jr. The NF-KB and IκB Proteins: New Discoveries and Insights. *Annu. Rev. Immunol.* **1996**, *14*, 649–681. [CrossRef]
74. Tsang, S.W.; Ip, S.P.; Wu, J.C.-Y.; Ng, S.-C.; Yung, K.K.-L.; Bian, Z.-X. A Chinese Medicinal Formulation Ameliorates Dextran Sulfate Sodium-Induced Experimental Colitis by Suppressing the Activity of Nuclear Factor-KappaB Signaling. *J. Ethnopharmacol.* **2015**, *162*, 20–30. [CrossRef]
75. Nam, N.-H. Naturally Occurring NF-KB Inhibitors. *Mini Rev. Med. Chem.* **2006**, *6*, 945–951. [CrossRef]
76. Clemente, J.C.; Ursell, L.K.; Parfrey, L.W.; Knight, R. The Impact of the Gut Microbiota on Human Health: An Integrative View. *Cell* **2012**, *148*, 1258–1270. [CrossRef]
77. Franzosa, E.A.; Sirota-Madi, A.; Avila-Pacheco, J.; Fornelos, N.; Haiser, H.J.; Reinker, S.; Vatanen, T.; Hall, A.B.; Mallick, H.; McIver, L.J. Gut Microbiome Structure and Metabolic Activity in Inflammatory Bowel Disease. *Nat. Microbiol.* **2019**, *4*, 293–305. [CrossRef]
78. Michielan, A.; D'Incà, R. Intestinal Permeability in Inflammatory Bowel Disease: Pathogenesis, Clinical Evaluation, and Therapy of Leaky Gut. *Mediat. Inflamm.* **2015**, *2015*, 628157. [CrossRef]
79. Facchin, S.; Vitulo, N.; Calgaro, M.; Buda, A.; Romualdi, C.; Pohl, D.; Perini, B.; Lorenzon, G.; Marinelli, C.; D'Incà, R. Microbiota Changes Induced by Microencapsulated Sodium Butyrate in Patients with Inflammatory Bowel Disease. *Neurogastroenterol. Motil.* **2020**, *32*, e13914. [CrossRef] [PubMed]
80. Manichanh, C.; Rigottier-Gois, L.; Bonnaud, E.; Gloux, K.; Pelletier, E.; Frangeul, L.; Nalin, R.; Jarrin, C.; Chardon, P.; Marteau, P. Reduced Diversity of Faecal Microbiota in Crohn's Disease Revealed by a Metagenomic Approach. *Gut* **2006**, *55*, 205–211. [CrossRef] [PubMed]
81. Jialing, L.; Yangyang, G.; Jing, Z.; Xiaoyi, T.; Ping, W.; Liwei, S.; Simin, C. Changes in Serum Inflammatory Cytokine Levels and Intestinal Flora in a Self-Healing Dextran Sodium Sulfate-Induced Ulcerative Colitis Murine Model. *Life Sci.* **2020**, *263*, 118587. [CrossRef] [PubMed]
82. Lozupone, C.A.; Knight, R. Species Divergence and the Measurement of Microbial Diversity. *FEMS Microbiol. Rev.* **2008**, *32*, 557–578.
83. O'Toole, P.W.; Marchesi, J.R.; Hill, C. Next-Generation Probiotics: The Spectrum from Probiotics to Live Biotherapeutics. *Nat. Microbiol.* **2017**, *2*, 17057. [CrossRef]
84. Litvak, Y.; Byndloss, M.X.; Tsolis, R.M.; Bäumler, A.J. Dysbiotic Proteobacteria Expansion: A Microbial Signature of Epithelial Dysfunction. *Curr. Opin. Microbiol.* **2017**, *39*, 1–6. [CrossRef]
85. Ge, H.; Cai, Z.; Chai, J.; Liu, J.; Liu, B.; Yu, Y.; Liu, J.; Zhang, T. Egg White Peptides Ameliorate Dextran Sulfate Sodium-Induced Acute Colitis Symptoms by Inhibiting the Production of pro-Inflammatory Cytokines and Modulation of Gut Microbiota Composition. *Food Chem.* **2021**, *360*, 129981. [CrossRef] [PubMed]
86. Peng, L.; Gao, X.; Nie, L.; Xie, J.; Dai, T.; Shi, C.; Tao, L.; Wang, Y.; Tian, Y.; Sheng, J. Astragalin Attenuates Dextran Sulfate Sodium (DSS)-Induced Acute Experimental Colitis by Alleviating Gut Microbiota Dysbiosis and Inhibiting NF-KB Activation in Mice. *Front. Immunol.* **2020**, *11*, 2058.
87. Wang, K.; Wan, Z.; Ou, A.; Liang, X.; Guo, X.; Zhang, Z.; Wu, L.; Xue, X. Monofloral Honey from a Medical Plant, Prunella Vulgaris, Protected against Dextran Sulfate Sodium-Induced Ulcerative Colitis via Modulating Gut Microbial Populations in Rats. *Food Funct.* **2019**, *10*, 3828–3838. [CrossRef] [PubMed]
88. Witten, J.; Samad, T.; Ribbeck, K. Selective Permeability of Mucus Barriers. *Curr. Opin. Biotechnol.* **2018**, *52*, 124–133.
89. Alosaimi, A.M.; Alorabi, R.O.; Katowah, D.F.; Al-Thagafi, Z.T.; Alsolami, E.S.; Hussein, M.A.; Qutob, M.; Rafatullah, M. Review on Biomedical Advances of Hybrid Nanocomposite Biopolymeric Materials. *Bioengineering* **2023**, *10*, 279. [CrossRef]
90. Tang, H.Y.; Fang, Z.; Ng, K. Dietary Fiber-Based Colon-Targeted Delivery Systems for Polyphenols. *Trends Food Sci. Technol.* **2020**, *100*, 333–348. [CrossRef]

91. Rashwan, A.K.; Karim, N.; Xu, Y.; Xie, J.; Cui, H.; Mozafari, M.R.; Chen, W. Potential Micro-/Nano-Encapsulation Systems for Improving Stability and Bioavailability of Anthocyanins: An Updated Review. *Crit. Rev. Food Sci. Nutr.* **2023**, *63*, 3362–3385. [CrossRef]
92. Alkhader, E.; Billa, N.; Roberts, C.J. Mucoadhesive Chitosan-Pectinate Nanoparticles for the Delivery of Curcumin to the Colon. *AAPS PharmSciTech* **2017**, *18*, 1009–1018. [CrossRef]
93. Sha, A.; Luo, Y.; Xiao, W.; He, J.; Chen, X.; Xiong, Z.; Peng, L.; Zou, L.; Liu, B.; Li, Q. Plant-Derived Exosome-like Nanoparticles: A Comprehensive Overview of Their Composition, Biogenesis, Isolation, and Biological Applications. *Int. J. Mol. Sci.* **2024**, *25*, 12092. [CrossRef] [PubMed]
94. Ayvaz, H.; Cabaroglu, T.; Akyildiz, A.; Pala, C.U.; Temizkan, R.; Ağçam, E.; Ayvaz, Z.; Durazzo, A.; Lucarini, M.; Direito, R.; et al. Anthocyanins: Metabolic Digestion, Bioavailability, Therapeutic Effects, Current Pharmaceutical/Industrial Use, and Innovation Potential. *Antioxidants* **2022**, *12*, 48. [CrossRef] [PubMed]
95. Cheng, Y.; Watanabe, C.; Ando, Y.; Kitaoka, S.; Egawa, Y.; Takashima, T.; Matsumoto, A.; Murakami, M. Caco-2 Cell Sheet Partially Laminated with HT29-MTX Cells as a Novel In Vitro Model of Gut Epithelium Drug Permeability. *Pharmaceutics* **2023**, *15*, 2338. [CrossRef]
96. Wang, Y.; Cai, M.; Zeng, H.; Zhao, H.; Zhang, M.; Yang, Z. Preparation, Characterization and Iron Absorption by Caco-2 Cells of the Casein Peptides-Iron Chelate. *Int. J. Pept. Res. Ther.* **2022**, *28*, 116. [CrossRef]
97. Wongwanakul, R.; Auewiriyavit, S.; Furihata, T.; Gonil, P.; Sajomsang, W.; Maniratanachote, R.; Jianmongkol, S. Quaternization of High Molecular Weight Chitosan for Increasing Intestinal Drug Absorption Using Caco-2 Cells as an in Vitro Intestinal Model. *Sci. Rep.* **2023**, *13*, 7904. [CrossRef]
98. Wang, X.; Huang, M.; Yang, F.; Sun, H.; Zhou, X.; Guo, Y.; Wang, X.; Zhang, M. Rapeseed Polysaccharides as Prebiotics on Growth and Acidifying Activity of Probiotics in Vitro. *Carbohydr. Polym.* **2015**, *125*, 232–240. [CrossRef]
99. Ishimoto, K.; Miki, S.; Ohno, A.; Nakamura, Y.; Otani, S.; Nakamura, M.; Nakagawa, S. β-Carotene Solid Dispersion Prepared by Hot-Melt Technology Improves Its Solubility in Water. *J. Food Sci. Technol.* **2019**, *56*, 3540–3546. [CrossRef]
100. Cho, N.; Lee, S.G.; Kim, J.O.; Kim, Y.A.; Kim, E.M.; Park, C.; Ji, J.H.; Kim, K.K. Identification of Differentially Expressed Genes Associated with Extracellular Matrix Degradation and Inflammatory Regulation in Calcific Tendinopathy Using RNA Sequencing. *Calcif. Tissue Int.* **2020**, *107*, 489–498. [CrossRef]
101. Kim, H.B.; Go, E.J.; Baek, J.S. Effect of Hot-Melt Extruded Morus Alba Leaves on Intestinal Microflora and Epithelial Cells. *Heliyon* **2024**, *10*, e23954. [CrossRef]
102. Peach, M.; Marsh, N.; MacPhee, D.J. Protein Solubilization: Attend to the Choice of Lysis Buffer. *Methods Mol. Biol.* **2012**, *869*, 37–47. [CrossRef] [PubMed]
103. Láng, L.; McArthur, S.; Lazar, A.S.; Pourtau, L.; Gaudout, D.; Pontifex, M.G.; Müller, M.; Vauzour, D. Dietary (Poly)Phenols and the Gut–Brain Axis in Ageing. *Nutrients* **2024**, *16*, 1500. [CrossRef] [PubMed]
104. Zhang, M.; Zhou, N.; Zhao, L.; Zhao, L. Black Rice Anthocyanins Nanoparticles Based on Bovine Serum Albumin and Hyaluronic Acid: Preparation, Characterization, Absorption and Intestinal Barrier Function Protection in Caco-2 Monolayers. *Int. J. Biol. Macromol.* **2024**, *267*, 131325. [CrossRef]
105. Karpí Nski, M.; Doglio, A.; Zarowski, M.O.; Mosaddad, S.A.; Hussain, A.; Tebyaniyan, H. Green Alternatives as Antimicrobial Agents in Mitigating Periodontal Diseases: A Narrative Review. *Microorganisms* **2023**, *11*, 1269. [CrossRef]

Disclaimer/Publisher's Note: The statements, opinions and data contained in all publications are solely those of the individual author(s) and contributor(s) and not of MDPI and/or the editor(s). MDPI and/or the editor(s) disclaim responsibility for any injury to people or property resulting from any ideas, methods, instructions or products referred to in the content.

pharmaceuticals

MDPI

Review

Role of Polyphenols in Dermatological Diseases: Exploring Pharmacotherapeutic Mechanisms and Clinical Implications

Juan Salazar [1], Ángel Ortega [1], José Luis Pérez [1], Bermary Garrido [1], Raquel Santeliz [1], Néstor Galbán [1], Maria Paula Díaz [1], Raquel Cano [2], Gabriel Cano [3], Julio Cesar Contreras-Velasquez [4] and Maricarmen Chacín [5,*]

[1] Endocrine and Metabolic Diseases Research Center, School of Medicine, University of Zulia, Maracaibo 4004, Venezuela; juanjsv18@hotmail.com (J.S.); angelort94@hotmail.com (Á.O.); joseluispv2811@gmail.com (J.L.P.); bermarygarrido@gmail.com (B.G.); gabrielasanteliz29@gmail.com (R.S.); nestorag17@gmail.com (N.G.); mariadiazalbornoz@hotmail.com (M.P.D.)
[2] Clínica General del Norte, Grupo de Estudio e Investigación en Salud, Barranquilla 080002, Colombia; raquelamiracano@gmail.com
[3] Institut für Pharmazie Königin-Luise, Freie Universität Berlin, Strasse 2-4, 14195 Berlin, Germany; gabriel.simon.cano@fu-berlin.de
[4] Departamento de Productividad e Innovación, Universidad de la Costa, Barranquilla 080002, Colombia; jcontrer30@cuc.edu.co
[5] Centro de Investigaciones en Ciencias de la Vida (CICV), Facultad de Ciencias de la Salud, Universidad Simón Bolívar, Barranquilla 080002, Colombia
* Correspondence: maricarmen.chacing@unisimon.edu.co

Abstract: Although not frequently lethal, dermatological diseases represent a common cause of consultation worldwide. Due to the natural and non-invasive approach of phytotherapy, research for novel alternatives, such as polyphenols, to treat skin disorders is a subject of interest in modern medicine. Polyphenols, in particular, have been considered because of their anti-inflammatory, antitumoral, antimicrobial, and antioxidant properties, low molecular weight, and lipophilic nature that enables the passage of these compounds through the skin barrier. This review discusses the treatment of common dermatological diseases such as acne vulgaris, fungal infections, dermatitis, alopecia, and skin cancer, using polyphenols as therapeutic and prophylactic options. The specific molecules considered for each disorder, mechanisms of action, current clinical trials, and proposed applications are also reviewed.

Keywords: skin disorders; polyphenols; phytotherapy

1. Introduction

For decades, dermatologic diseases have occupied relevant positions as main complaints for medical consultation, cataloged by the Global Burden of Disease (GBD) study as the fourth main cause of non-lethal disease and the eighteenth main cause of disability worldwide [1]. These relevant facts transform these entities into important health issues, affecting all age groups and geographical areas [2].

Due to the prevalence and the socioeconomic burden generated by dermatologic diseases, it is imperative to find new therapeutic alternatives to diminish the consequences of these disorders [3]. For the past years, the study of natural polyphenols and their application in dermatologic diseases has obtained a primary interest. This group of molecules is widely distributed in the environment as secondary metabolites from plant sources, characterized by one or more phenolic rings within its chemical structure. Moreover, these molecules have demonstrated notable antioxidant, anti-inflammatory, antimicrobial, and in vivo as well as in vitro anticarcinogenic activities [4,5].

Likewise, due to their low molecular weight and lipophilic properties similar to the stratum corneum, the cosmetic applications of these compounds have been explored, and topical extracts have been prepared, in order to obtain benefits from the direct effect of phenolic compounds when they penetrate the skin´s natural barrier; therefore, these compounds could represent a potential strategy for the prevention and treatment of frequent skin disorders [6,7]. Thus, this review summarizes current preclinical and clinical evidence of polyphenol-based phytochemicals as a treatment for skin disorders (SDs) and the potential molecular mechanisms involved.

2. Pharmacotherapeutic Mechanisms of Polyphenols in Main Skin Diseases

2.1. Acne Vulgaris (AV)

AV is considered one of the most common chronic dermatologic disorders in the teenage population. This pathology is characterized by its multifactorial etiology, mainly triggered by the proliferation of resident skin bacteria, such as *Propionibacterium acne* and excessive sebum production induced by androgens [8]. In addition, other events, such as the activation of inflammatory cascades leading to hyperkeratinization, increased reactive oxygen species (ROS), and reduced antioxidant activity, provoke hair follicle obstruction, resulting in comedo formation [9]. It is worth mentioning that the high costs and antibiotic resistance observed with conventional treatments have led to the study of numerous plant supplements, which have polyphenols, as an effective therapeutic alternative [10].

In this sense, an anti-inflammatory mechanism of the wild bitter gourd (*Momordica charantia*) total phenolic content leaf extract (TPCLE) has been studied due to its different polyphenolic compounds, such as phenolic acids, myricetin, quercetin, and luteolin as well as its acne-related properties. Clinical evidence indicates that the inhibition of growth of pathogens such as *Propionibacterium acne* is a potential therapeutic target to consider. In consequence, Huang et al. [11] tried to demonstrate this fact through intradermal injections of *Propionibacterium acne*, followed by TPCLE both in vivo and in vitro. TPCLE positively managed to attenuate the secretion of IL-8, IL-1β, and TNFα after inhibiting the expression of the Mitogen-Activated Protein Kinase (MAPK) and, subsequently, the Nuclear Factor Kappa-Light-Chain-Enhancer of activated B cells (NF-kB). Moreover, TPCLE inhibited Matrix Metalloproteinase-9 (MPP-9), an enzyme involved in extracellular matrix degradation and thus in acne lesions, demonstrating the great anti-inflammatory properties of this group of polyphenols [11].

A similar mechanism was found in oregano extracts, *Origanum vulgare* [12], widely distributed in rosmarinic acid, quercetin, carvacrol, and apigenin. In the said mechanism, the inactivation of transcriptional marker signaling responsible for the inhibition of NF-kB was attributed to the inactivation of Toll-Like receptor 2 (TLR2) [12]. Furthermore, the mRNA expression of NOS, ICAM-1, NF-kB, COX-2, and COX-1 [13] was inhibited in human keratinocytes NCTC 2544 with an *M. styphelioides* leaf extract treatment, rich in quercetin, gallic acid, and ellagic acid [14].

Additionally, a flavonoid widely distributed in apples and strawberries, known as phloretin, has been studied for its anti-inflammatory properties and potential antibacterial mechanism. Similarly, phloretin, found in its free form or glycosylated, inhibited the heterodimerization of TLR2/1; however, it also diminished the phosphorylation of the c-Jun N-terminal kinase (JNK) pathway in *HaCaT* keratinocytes stimulated by *P. acnes* in a dose-dependent manner. On the other hand, it was shown that the active site of the 3-ketoacyl-ACP synthase (KAS-III) interacted with rings A and B of the phloretin structure, blocking the reaction between *P. acnes*, KAS-III, and its substrates, and in consequence

inhibiting fatty acid synthesis necessary for bacterial survival [10], therefore, proving the anti-inflammatory effect and great antibacterial potential of certain polyphenols.

In contrast, other studies on *Quercus mongolica* leaf extract (QML) examined the antioxidant activity of flavonoids, tannins, triterpenoids, and phenols, mainly pedunculagin (PD), and a decrease in IL-6 and IL-8 production as well as reduced concentrations of Nitric Acid (NA) were observed in the said studies. These phenomena are caused by diminished TLR-4 mRNA. This effect was also demonstrated in a study performed by Kim et al. [15], in which polyphenols of punicalagin, ellagic acid, and pomegranate peels (PPs) were used [16].

Finally, an enzyme regulatory mechanism involved in androgen metabolism has been studied for its role in the pathogenesis of acne. The 5α-reductase type 1 (5αAR-1) is an enzyme directly implicated in androgen-dependent sebum production and a presumptive therapeutic target. For this reason, Koseki et al. [17] attempted to explain the relationship between polyphenols and 5-AR in both in vivo and in vitro studies, using *Bokusoku* (BK), an extract of *Quercus* cortex, extensively found in gallate polyphenols, such as gallotannin and ellagitannin. In this sense, the inhibition of 5AR-1 and, thus, its implication in sebum production suppression were evidenced. Likewise, BK and one of its strongest phenolic compounds, the *Pentagalloylglucose*, suppressed testosterone-induced lipogenesis, blocking androgen-dependent cellular activity. Therefore, the inhibitory activity of 5αAR-1 and lipogenesis suppression are important therapeutic targets that might reduce sebum production in patients with acne [17,18].

2.2. Dermatitis

Atopic dermatitis (AD) is a chronic inflammatory disease with a notable allergic component, which can appear from early childhood and is prone to recurrences. This pathology is characterized by clinical manifestations such as erythematous, itchy, and lichenified skin [19]. Its pathophysiology is initiated with an altered genotype, leading to intense immunity and hypersensitivity dysregulations mediated by the increased levels of Th2 and IgE [20]; furthermore, certain environmental and psychological triggers exacerbate AD development [21]. Likewise, intestinal dysbiosis has been implicated as an underlying mechanism of AD since the microbiota shapes immune responses systematically, thus alluding to the complex and multifactorial pathophysiology that comprises this disease [22].

As a consequence of AD recurrence, the chronic use of conventional anti-inflammatory therapy such as topical corticosteroids (TCSs) or calcineurin inhibitors (CIs) are not the safest options due to their known side effects. Moreover, the high economic burden, significant morbidity, and poor quality of life demand new therapeutic alternatives with minimum side effects [23]. Based on polyphenol influence through various anti-AD mechanisms, different polyphenolic compounds studied in preclinical trials promise to be innovative options for this disease.

Furthermore, the pro-inflammatory environment generated by increased cytokine levels has been considered a potential therapeutic target. In light of this, preclinical evidence has shown that diosmetin [24], quercetin, and galanin [25] drive a fall in pro-inflammatory cytokines such as IL-4, TNFα, and IL-1β expression via ERK, p38, and JNK, as well as NF-kB translocation inhibition. In addition, other flavonoids, like taxifolin, aromadendrin, padmatin, and chamaejasmine, have been linked to IgE reduction [26], as well as secondary metabolites of plant polyphenols such as 3-aryl isocoumarins and diarylheptanoids, and these compounds have shown modulatory activities on inflammatory pathways such as the inhibition of NF-kB activation [21,27]. Thus, their efficacy in inhibiting pleiotropic cytokines of Th2 cells that regulate isotype changes from different immunoglobulins to IgE makes these flavonoids an alternative to treat inflammatory responses associated with AD.

Recently, another mechanism to attenuate the pruritus caused by AD has been studied. Nevertheless, the pathophysiological mechanism of AD pruritus is still unknown. Studies show that Thymic Stromal Lymphopoietin (TSLP) is directly linked to pruritus and severeness of AD. Consequently, Fitoussi et al. [28] studied the efficacy of *Tambourissa trichophylla* leaf extract (TTLE), with a titration of >40% polyphenols, mainly troxerutin. Inhibition of TSLP secretion was observed, and the said effect was associated with the IL-1α pathway, a cytokine able to induce the expression of TSLP and therefore alter the cutaneous barrier [29]. Likewise, treatment with systemic resveratrol was associated with diminished TSLP expression in skin lesions similar to EA. Therefore, phenolic compounds seem to be potential therapeutic tools to alleviate AD symptoms such as pruritus.

On the other hand, AD has a close relationship to the intestinal microbiota. Interestingly, AD patients present imbalances between *Clostridium* spp. and beneficial bacteria such as *Bifidobacterium* spp. [30]. In this context, the acacia polyphenol (AP) has been studied, and the topical application of this molecule produced pruritus reduction in DA lesions after inhibiting skin inflammation, and, in consequence, creating a systemic influence in the gut–skin axis. This fact has been demonstrated due to increased beneficial bacteria, such as *Bifidobacterium* spp. and *Lactobacillus* spp., after AP use in murine models with AD [30]. Moreover, a similar behavior was observed after the utilization of *Schizonepeta tenuifolia* Briquet (STB) and *Alpinia oxyphylla* Miquel (AOM) extracts, which are rich in flavonoids and gallic acid, and the said compounds induced changes in the microbiome and therefore supported the importance of the gut–skin axis theory [31].

It is important to point out that, currently, only a few preclinical trials focus on the effects of phenolic compounds in contact dermatitis (CD). Contact dermatitis is characterized by extreme hypersensitivity to allergens once they reach the skin. Thus, Jegal et al. [32] employed *Wikstroemia indica* extract, rich in flavonoids, lignans, and coumarins, to assess their efficacy on CD. Quercetin was strongly associated with the suppression of lysosomal enzyme β-hexosaminidase and IL-4 mRNA expression, which are important regulators of immune responses during the initial phase of CD. Even though more preclinical studies are needed in this field, the potential use of polyphenols as a new therapeutic tool for treating CD and AD is highly relevant.

2.3. Skin Fungal Infections

Dermatomycosis comprises a wide range of diseases that target skin, nails, and hair [33]. These are considered the most frequent mycotic infections worldwide and are caused by different etiological agents such as (i) dermatophytes, including the genre *Trichophyton*, *Microsporum*, and *Epidermophyton*, responsible for dermatophytosis and onychomycosis, as well as (ii) yeasts responsible for cutaneous candidiasis and pityriasis versicolor, such as *Candida* spp. and *Malassezia* spp., respectively [34]. A common feature among fungal pathogens of the skin is the production of keratinolytic enzymes responsible for the degradation of the keratinized epithelium and induction of inflammatory responses in the site of infection [35]. The aforementioned process depends on the intensity of inflammatory mediators produced by the strains involved and the host's response to the pathogen [36].

In this context, an effective approach to treat dermatomycosis involves adding topical corticosteroids to an antimycotic therapy to diminish initial inflammatory symptoms and avoid bacterial superinfection. However, the risk of side effects and its high cost are difficulties worth considering [37]. Recently, different phenolic compounds have been proposed as an alternative to this scenario since these molecules can interfere directly with the growth and survival of the fungal species, attenuate inflammatory responses, and regulate ROS production (Figure 1) [37].

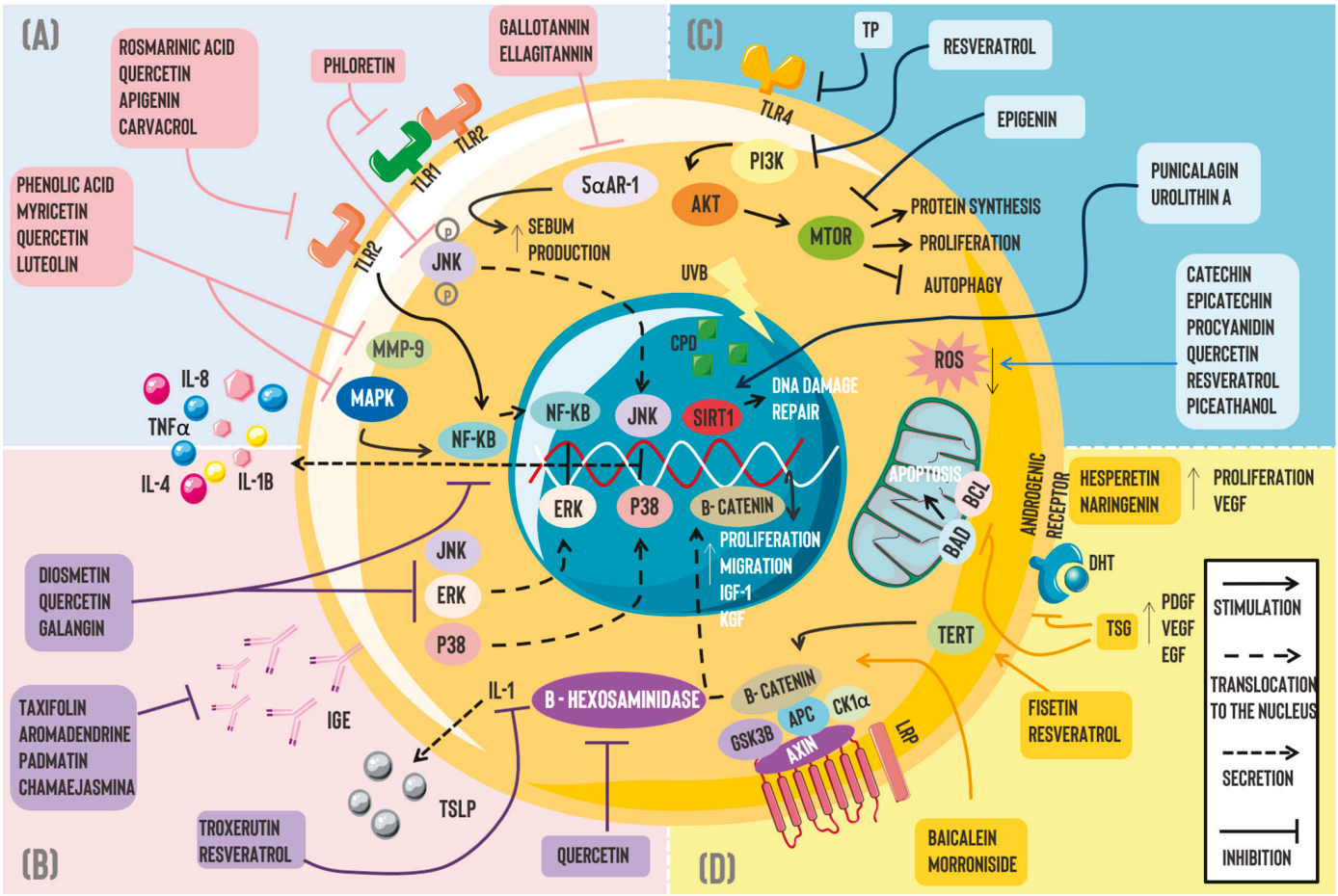

Figure 1. Pharmacotherapeutic mechanisms of polyphenols in skin disorders: Currently, multiple pharmacological mechanisms have been attributed to naturally occurring polyphenols for different skin pathologies, including (**A**) *Acne vulgaris*, where the actions of gallotannin and ellagitannin suppressed sebum production via 5αAR-1 inhibition. Moreover, phloretin's anti-inflammatory properties inhibit TLR2/1 heterodimerization and JNK signaling in human keratinocytes. Phenolic acid, myricetin, quercetin, and luteolin can inhibit MMP-9 and, thus, diminish acne lesions and, in addition, have similar effects to rosmarinic acid, apigenin, and carvacrol over NF-kB by blocking the molecule and decreasing the subsequent IL-8, II,-1B, and TNFα secretion; (**B**) the anti-inflammatory effect of polyphenols is observed in dermatitis where diosmetin, quercetin, and gallatannin inhibit signaling pathways such as ERK, JNK, and p38, as well as NK-kB translocation to the nucleus. Likewise, flavonoids such as taxifolin, aromadendrin, padmatin, and chamaejasmine were linked to IgE decrements. Resveratrol and troxerutin decrease TSLP expression, and this effect is likely associated with the IL-1α pathway. Quercetin has been associated with *β*-hexosaminidase inhibition. (**C**) Skin cancer is linked to ROS overproduction, DNA damage, and UV ray effects. Certain polyphenols such as catechin, epicatechin, procyanidin, quercetin, resveratrol, and piceatannol have demonstrated antioxidant properties by diminishing ROS levels. On the other hand, resveratrol and epigenin possess antitumoral activity through direct or indirect mTOR blockade. A similar effect is observed by inhibiting TLR4 through TP. Punicalagin and urolithin A repair DNA damage induced by UV rays via SIRT1 stimulation. (**D**) Regarding alopecia, morroniside and baicalein induce cellular proliferation as well as migration through the Wnt/β catenin pathway. Furthermore, fisetin and resveratrol promote β-catenin translocation and higher IGF-1 and KGF expression through a TERT-dependent mechanism. Lastly, polyphenols such as hesperetin and naringenin stimulated VEGF expression and proliferation in DPCs. Simultaneously, this molecule promotes PDGF and EGF increments, inhibiting the DHT effect on androgenic receptors. Similarly, TSG diminishes DPC apoptosis via Bcl-2/BAD blockade.

Abbreviations: TLR: Toll-like receptor; JNK: Jun N-terminal kinase; 5αAR-1: 5-alpha reductase; MMP-9: Matrix Metallopeptidase 9; NF-KB: Nuclear Factor Kappa-Light-Chain-Enhancer of activated B cells; MAPK: Mitogen-Activated Protein Kinase; ERK: Extracellular-regulated Kinase; IL: Interleukin; TNFα: Tumor Necrosis Factor Alpha; IgE: Immunoglobulin E; TSLP: Thymic Stromal Lymphopoietin; TERT: telomerase reverse transcriptase; TSG: 2,3,5,4′-tetrahydroxyestilbene-2-*O*-β-D-glucoside; PDGF: Platelet-derived Growth Factor; VEGF: Vascular Endothelial Growth Factor; EGF: Epidermal Growth Factor; DHT: Dihydrotestosterone; BAD: BCL 2-associated agonist of cell death; BCL: B-cell Lymphoma; IGF: insulin-like growth factor; KGF: keratinocyte growth factor; ROS: reactive oxygen species; TP: tea polyphenol; PI3K: Phosphoinositide 3-Kinase; AKT: Protein Kinase B; mTOR: The Mechanistic Target of Rapamycin; UVB: ultraviolet B; CPD: cyclobutane pyrimidine dimer; SIRT: Sirtuin.

The effect of polyphenols on fungal growth occurs through various cellular targets. The inhibition of ergosterol biosynthesis has been documented as one of the mechanisms, considering that this blockade constitutes a key factor that leads to alterations in the plasmatic membrane and a consequent loss of cellular integrity [38]. Along with this perspective, it has been demonstrated that gallic acid (GA) [39] and ellagic acid (EA) [39,40] significantly diminish the ergosterol content in the membrane of *T. rubrum* in vitro by reducing the activity of limiting enzymes of sterol synthesis: sterol 14α-demethylase P450 (CYP51) and squalene epoxidase (SE). This potential antifungal activity of both compounds is equivalent to conventional treatments such as fluconazole and terbinafine.

Similarly, caffeic acid (CA) and Licochalcone A (LicoA) exhibit a powerful antimycotic effect on *T. rubrum*, with a minimum inhibitory concentration (MIC) of 86.59 and 11.52 μM, respectively. The mechanism involved encompasses an inhibition of gene expression related to ergosterol biosynthesis, plasmatic membrane synthesis, and glyoxylate cycle, with the latter process significantly increased with LicoA, suggesting a multimodal role of these agents, which act by interfering with key pathways of *T. rubrum* survival [41]. An additional therapeutic goal to consider is the fatty acid synthase (FAS), whose inhibition reduces fatty acid synthesis and, consequently, alters the mycotic membrane lipidic content [42]. In this sense, the antifungal action of flavonoids, such as gallate of epigallocatechin [43], quercetin, and trans-chalcone [44,45] via FAS blockade, has been reported.

In addition to the effect on fatty acid metabolism, the action of trans-chalcone over different virulence factors produced by *T. rubrum* has been described. In line with this, the downregulation of genes that codify proteases and heat shock proteins (Hsp70, Hdp88, and Hsp90) has been observed. Likewise, this flavonoid can interact with MAPK, Tor, and CDK signaling pathways, which mediate the assembly and maintenance of the plasmatic membrane. These findings suggest a role for the aforementioned compound in several aspects of dermatophyte biology that should be further explored in future investigations [46]. In contrast, Gaziano et al. assessed in silico and in vitro anti-dermatophytic effects of phenolic compounds extracted from *Cardiospermum halicacabum.* Evidence indicated that rutin and luteolin directly affect the growth of *T. rubrum*, in a potential mechanism mediated through the interaction with the ATP domain of *Hsp90*. Interestingly, although both compounds showed a particular effect, it was not superior to the effect demonstrated by the total leaf extract. Thus, it can be inferred that using *Cardiospermum halicacabum* extract could represent a new antifungal strategy to explore as a single agent or in combination with conventional drugs [47].

On the other hand, baicalein and wogonin, two flavones present in root extracts of *Scutellaria baicalensis*, exert a potential antifungal activity against *T. rubrum*, *T. mentagrophytes*, *A. fumigatus*, and *C. albicans*. Moreover, the powerful effect of baicalein against the previously mentioned pathogens has been observed; meanwhile, wogonin inhibited the activity of every pathogen except *C. albicans.* The mechanism of action is associated with

increments in mitochondrial ROS and, therefore, the induction of modifications in mitochondrial membrane potential (MMP), which results in cellular apoptosis [48]. Likewise, isoquercitrin (ISO) exerts a synergic effect with fluconazole and amphotericin B, promoting cellular apoptosis and altering the permeability of *C. albicans* membrane through the inhibition of Superoxide Dismutase (SOD) mitochondrial activity, leading to increments in oxidative stress levels [49].

Lastly, the anti-inflammatory potential of some phenolic compounds represents an attractive therapeutic target to explore in dermatomycosis. In this sense, Gomes et al. evaluated the anti-dermatophytic effect of *Salacia senegalensis* leaf extract, observing the antifungal activity of the plant against *T. rubrum* and *E. floccosum*, and these effects could be partially attributed to the presence of flavanols with potential synergic actions, such as quercetin, myricitrin, and quercitrin. Likewise, the anti-inflammatory effect of the extract stands out in a mechanism dependent on eicosanoid derivates of 5-lipooxygenase (5-LOX). Hence, studying flavonoids in *Salacia senegalensis* extract might represent an alternative to consider when it comes to reducing acute inflammatory responses associated with dermatophytes [50].

2.4. Alopecia

The social stigma generated from hair loss (HL) has made this condition a common complaint in dermatologic appointments [51]. From a clinical perspective, alopecia possesses different etiologies. Androgenic alopecia (AGA) is the most frequent, affecting men and women through different stages of life, with elevated dihydrotestosterone (DHT) levels as its main contributing factor [52]. Furthermore, AGA is a non-scarring alopecia characterized by rounded, flat, alopecic patches and caused by the autoimmune destruction of the hair follicle (HF) [53]. Finally, telogen effluvium (TE) is a heterogeneous entity characterized by sudden and diffuse hair loss that occurs around three months after a triggering event, as a consequence of regular hair growth cycle alteration, abruptly transitioning from the anagen phase (active growth) to telogen phase (rest) [54].

Despite the growing interest in finding new therapeutic strategies to treat HL in recent years, the available pharmacological options are still scarce. The only drugs currently approved by the FDA to manage this condition are minoxidil and finasteride. In addition, due to limited efficacy and potential side effects, the use of these drugs remains controversial [55]. On the contrary, phenolic extracts have emerged as a safer and more economical alternative to treat HL. Significant effects of epigallocatechin [56], quercetin [57], and baicalein [57], among others, have been documented in diverse experimental models.

Several hypotheses have been developed to clarify the potential mechanisms of action of polyphenols to induce hair growth. An attractive target explored is the regulation of hair follicle dermal papilla cell (DPC) activities, a specialized cellular group that controls the proliferation and regeneration of hair follicles by producing different growth factors [58]. Studies indicate that hesperetin and naringenin perform important roles via the stimulation of human DPC proliferation in vitro as well as cellular protection from oxidative stress mediated by hydrogen peroxide (H_2O_2) and increments in VEGF, which is an important angiogenic factor, capable of promoting the restoration of oxygen supply within the growing HF [59].

Furthermore, baicalein exerts a promising role in the modulation of DPC activities. It has been documented that the topical application of this flavonoid promotes follicular growth in Balb/c-null mice through a potential Wnt/β-catenin pathway-dependent mechanism and alkaline phosphatase (ALP) activation in this cellular population [60]. Likewise, this mechanism has been demonstrated with other compounds and cell types. It has been observed that a glycoside extracted from the medicinal plant *Cornus officinalis*

known as morroniside can stimulate the proliferation and migration of the outer root sheath cells (ORSCs), as well as induce HF growth in vitro through the Wnt/β-catenin signaling pathway in a dose-dependent manner. Thus, the regulation of this pathway constitutes a common mechanism used by phenolic extracts to induce the onset of anagen phase and follicular growth [61].

On the other hand, the prolongation of DPC viability represents a key approach to avoid the transition to telogen phase and, as a consequence, attenuate HL [62]. Accordingly, Shin et al. demonstrated that *Polygonum multiflorum* (PM) extract, whose main component is 2,3,5,4′-tetrahydroxyestilbene-2-*O*-β-D-glucoside (TSG), induces an anti-apoptotic effect in human cultured DPCs through the regulation of Bcl-2/BAD, thus extending the anagen phase. Moreover, the extract promotes increments in the production of VEGF, PDGF, and EGF and inhibits the effect mediated by DHT on androgenic receptor (AR) expression. This multimodal mechanism of PM extract on hair growth might represent a potential approach to treating AGA; however, new studies to explore this phenomenon with individual intake of TSG are required [63].

Lastly, fisetin and resveratrol have played a key role in the transition from the telogen to anagen phase and, consequently, in dorsal skin hair growth in mice. In a mechanism involving the telomerase reverse transcriptase, whose overexpression induced β-catenin nuclear translocation, increments in cytokines such as insulin growth factor-1 (IGF-1) and keratinocyte growth factor (KGF), as well as the promotion of stem cell proliferation within the hair follicle, were observed. Therefore, this positive effect of TERT on the anagen phase, induced by these polyphenols, represents a therapeutic mechanism to consider in future investigations [64].

2.5. Skin Cancer

Skin cancer is one of the most common cancers worldwide. The number of new cases has increased alarmingly over the last decade. This increase could be attributed to continuous exposure to sunlight and the ozone layer changes that predispose the earth's surface to higher ultraviolet (UV) radiation [65]. Skin cancer is classified into two subtypes: (i) Non-Melanoma Skin Cancer (NMSC), also known as keratinocyte cancer, which represents the most common malignant neoplasia, with Basal Cell Carcinoma (BCC) and squamous cell carcinoma (SCC) comprising 99% of every NMSC [66], and (ii) Melanoma Skin Cancer (MSC), even though it only represents 3% of all the skin cancer cases, it has the highest mortality rate and poorer prognosis [67].

The economic burden of skin cancer on the health system worldwide has also increased [68], boosting the research to find new, more economical and safer therapeutic strategies. In this context, it has been noted that polyphenols have significant effects on cancer progression through the modification of signaling cascades affected during carcinogenesis [69], proliferation, migration, and invasion [70], as well as angiogenesis [69], therefore improving patients' prognosis.

UV rays can penetrate the epidermis and reach the superior dermis to induce biological side effects, including oxidative stress, inflammation, DNA damage, and premature photoaging [71]. DNA damage results in cyclobutane pyrimidine dimer (CPD) formation. These molecules act as promoters of immunosuppression and trigger photocarcinogenesis [72]. Furthermore, the potential of phenolic compounds extracted from pomegranate (*Punica granatum*), such as punicalagin and urolithin, as DNA repair tools has been documented. These molecules possess powerful properties as SIRT1 inducers, facilitating Nucleotide Excision Repair (NER) through the deacetylation of XPC and XPA genes, finally eliminating previously formed CPDs [73].

Currently, it is known that reactive oxygen species have a major role in cutaneous carcinogenesis via the overactivation of multiple pathways such as MAPK, phosphatidylinositol 3-kinase (PI3K)/kinase protein B (AKT)/mammalian target of rapamycin (mTOR), and NF-kB pathway [74]. Likewise, clinical evidence highlights the bioprotector effect of *Arachis hypogaea* (peanut) polyphenols, which include catechin, epicatechin, procyanidin, and quercetin, against oxidative stress due to their capacity to diminish ROS levels [75]. Moreover, Eskandari et al. monitored reactions between hydrogen peroxide, quercetin, resveratrol, and piceatannol on the skin through an oxygen electrode covered with a cutaneous membrane (SCOE) as a tool in vitro, demonstrating that these polyphenolic compounds promote antioxidant reactions in 2–22 min [76].

In addition, polyphenols, such as resveratrol, have shown antiproliferative effects on tumor cells due to the downregulation of phosphorylated PI3K and AKT [77]. Similarly, epigenin, a natural flavonoid, has proven to inhibit skin cancer induced by UV rays via mTOR blockade, improving keratinocyte autophagy and diminishing its proliferation [78]. These antitumoral effects were observed in an in vitro and in vivo study performed by Chen et al., where tea polyphenols (TPs) showed time- and dose-dependent effects over melanoma cells, significantly inhibiting their proliferative, migrative, and invasive capacity through TLR4 suspension [70].

Polyphenols could contribute to skin cancer prevention and treatment through the induction of malignant cell apoptosis; as highlighted in Arumugam et al.'s preclinical trial, the synergic use of polyphenols such as resveratrol, epigallocatechin-3-gallate, and diallyl trisulfide could play a significant role in apoptosis inhibition. In the said study, A431 cells were used in a human epidermoid carcinoma model, and the application of polyphenolic compounds induced apoptosis inhibition via Bax and Bad upregulation, as well as pre-apoptotic proteins, while molecules such as Bcl2 and caspases 3 and 9 were downregulated [79].

2.6. Rosacea

Rosacea is a chronic inflammatory dermatosis affecting the central face, characterized by persistent erythema, telangiectasia, and papulopustular eruptions. Although its etiology is multifactorial, including genetic and environmental influences, the exact pathophysiological mechanisms remain elusive (Figure 2).

Rosacea is a prevalent inflammatory skin condition predominantly affecting the central face, with symptoms that significantly deteriorate the patient's quality of life [80,81]. It manifests primarily as facial flushing, erythema, telangiectasia, and papules/pustules. The pathogenesis of rosacea is complex and not fully understood, but it likely involves a combination of genetic predisposition and environmental triggers.

Rosacea presents in four distinct subtypes, each with unique clinical features: 1-Erythematotelangiectatic Rosacea (ETR) characterized by persistent facial redness, flushing, and visible blood vessels; 2-Papulopustular Rosacea (PPR) which features small, inflammatory papules and pustules on a backdrop of erythema; 3-Phymatous Rosacea involves skin thickening and irregular surface nodules, most often on the nose (rhinophyma); and 4-Ocular Rosacea that affects the eyes, leading to irritation, redness, and watery eyes [82].

The pathogenesis of rosacea is complex, including an overabundance of *Demodex mites*, particularly *Demodex folliculorum*, associated with triggering inflammatory reactions contributing to rosacea. Evidence suggests that rosacea patients exhibit abnormal immune responses, including increased levels of pro-inflammatory cytokines that contribute to skin inflammation and damage. Environmental triggers such as UV radiation, extreme temperatures, spicy foods, and alcohol have been recognized for exacerbating rosacea symptoms [82].

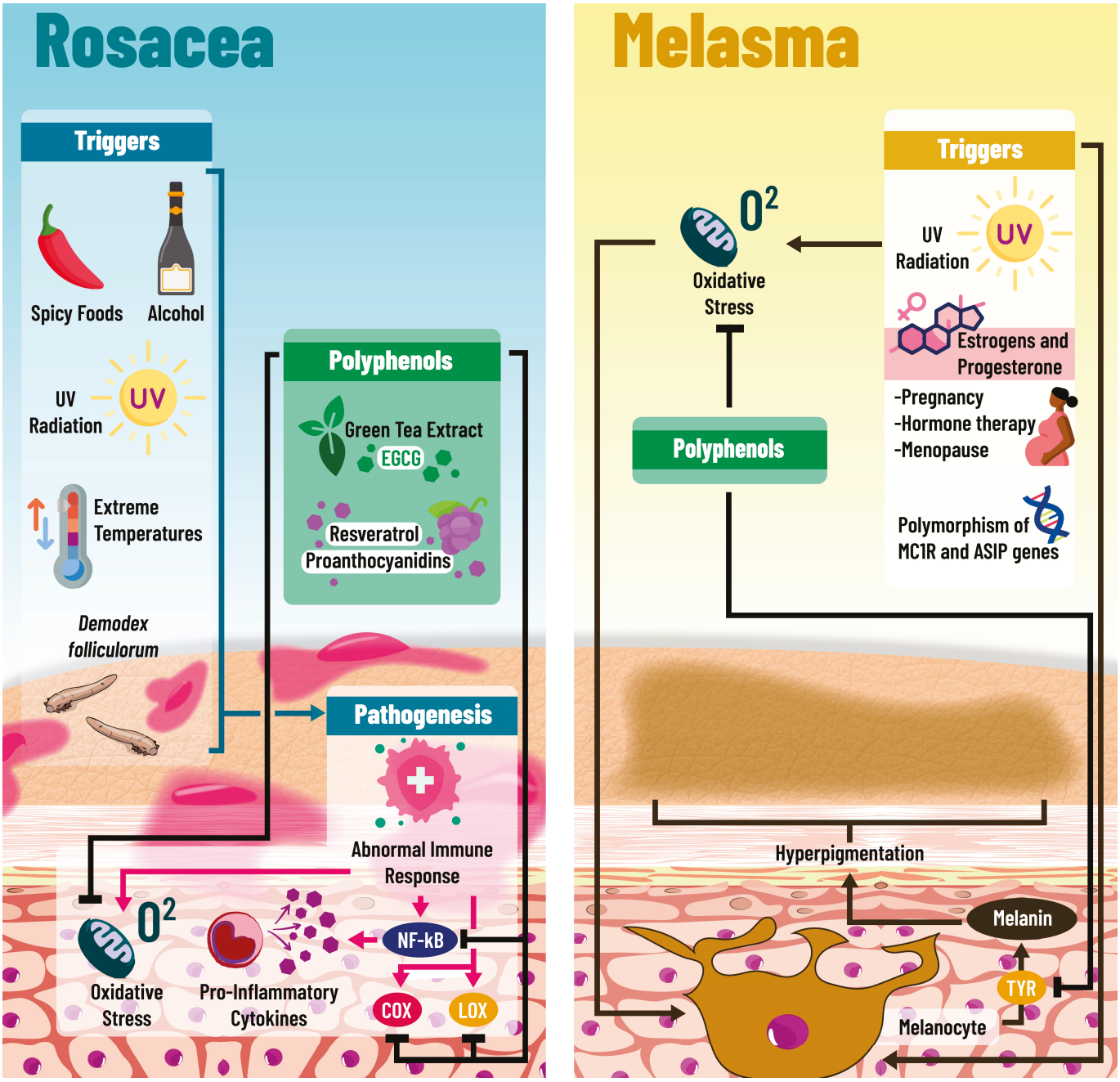

Figure 2. Underlying mechanisms of polyphenols in rosacea and melasma: The pathophysiological basis of rosacea is not completely understood; however, multiple triggers have been identified; among these are the overexposure to the acarus *Demodex folliculorum*, extreme temperatures, UV light exposure, and the consumption of alcohol and spicy foods. All of these elements can promote abnormal responses on the immune system, conditioning a pro-inflammatory state on the skin, characterized by NF-kB expression, pro-inflammatory cytokine secretion, and increased oxidative stress within the cells. It has been observed that polyphenols such as EGCG, resveratrol, and proanthocyanidins may interfere with the inflammatory response of these patients, inhibiting NF-kB expression, pro-inflammatory cytokine secretion, and Cox and Lox activation. Furthermore, because of their antioxidant activities, polyphenols are able to reduce oxidative stress levels. Likewise, polyphenols seem to improve melasma, and this condition is characterized by skin hyperpigmentation and is associated with genes such as MCR1 and ASIP, due to the activation of melanocytes by various factors like UV light and hormones (estrogen and progesterone) in pregnant women and menopausal

women receiving hormone therapy. The potential protective mechanisms of polyphenols in melasma are oxidative stress reduction, inflammatory pathways' downregulation, and potential tyrosinase inhibition. Abbreviations: COX: cyclooxygenase; LOX: lipoxygenase; NF-kB: Nuclear Factor Kappa-B; TYR: Tyrosine; UV: ultraviolet; EGCG: epigallocatechin gallate.

Emerging research suggests that antioxidants and polyphenols, which can neutralize free radicals and reduce oxidative stress, have potential clinical benefits in rosacea treatment. Polyphenols exert anti-inflammatory effects, potentially attenuating inflammatory pathways involved in rosacea. They also enhance the skin's barrier function, which helps protect against environmental irritants. Notable polyphenols with proven efficacy in rosacea management include green tea extract, which contains epigallocatechin gallate (EGCG), known for its strong anti-inflammatory and antioxidant effects. Resveratrol, found in grapes and berries, offers significant anti-inflammatory and antioxidant benefits, making it beneficial in reducing rosacea symptoms. Grape seed extract is known for its high proanthocyanidin content, which has anti-inflammatory and antioxidant capabilities [83].

Aside from polyphenols, rosacea management includes topical treatments such as metronidazole, azelaic acid, and ivermectin, which are widely used. Oral antibiotics like doxycycline and tetracycline are prescribed for more severe cases. Laser and light therapies target vascular and inflammatory components of rosacea, offering symptom improvement [84].

Rosacea is a complex dermatological condition that significantly impacts patients' lives. While the exact cause of rosacea is still under investigation, integrating polyphenols into treatment regimens offers a promising approach due to their antioxidative and anti-inflammatory properties. Comprehensive management, incorporating established and emerging therapies tailored to individual patient needs, remains paramount for effectively controlling and improving rosacea symptoms.

Moreover, the role of polyphenols in dermatology, particularly in the context of inflammatory skin diseases like rosacea, extends beyond their antioxidative and anti-inflammatory properties. Polyphenols have been shown to inhibit the activation of NF-kB, a key transcription factor in the inflammatory response, which leads to the downregulation of various pro-inflammatory cytokines and mediators involved in rosacea [85]. Additionally, polyphenols can modulate the activity of enzymes such as cyclooxygenase and lipoxygenase, further reducing the synthesis of pro-inflammatory eicosanoids, i.e., lipid compounds that exacerbate inflammation. This multifaceted mechanism of action makes polyphenols an attractive component in the holistic management of rosacea, offering potential synergies with other therapeutic modalities to enhance treatment efficacy and patient outcomes [85].

2.7. Melasma

Melasma, an acquired facial hyperpigmentation, predominantly affects women of darker skin and is characterized by symmetrical hyperpigmented patches typically found on the forehead, cheeks, upper lip, and chin, significantly impacting the quality of life [85,86]. These patches can cause emotional distress and affect social interactions, making a thorough understanding of the pathogenic mechanisms and therapeutic options crucial for effective management.

The etiology of melasma is considered multifactorial, involving genetic, hormonal, and environmental components. Genetic predisposition plays a significant role, with a strong concordance observed among twins and family members, and polymorphisms in genes related to melanogenesis, such as MC1R and ASIP, have been linked to an increased risk. Hormonally, estrogen and progesterone, which regulate melanogenesis, are crucial, with a higher prevalence of melasma noted during pregnancy, menopause, and among users of oral contraceptives or hormone therapy. Environmentally, UV radiation is a

primary trigger, stimulating melanin production and exacerbating hyperpigmentation. Other factors like heat, stress, and certain medications also contribute to the onset or worsening of melasma [87,88].

Several risk factors increase the likelihood of developing melasma, including female gender, darker skin phototypes, a family history of melasma, hormonal fluctuations during pregnancy or due to hormone therapy, and excessive UV radiation exposure [88].

Treatment of melasma should be tailored to each individual, considering the severity of the condition, the patient's skin phototype, and clinical characteristics. Commonly employed therapies include depigmenting agents like hydroquinone, azelaic acid, kojic acid, and arbutin, which are effective in lightening hyperpigmented patches. Strict photoprotection is crucial to prevent progression and relapses, with the daily use of broad-spectrum sunscreen being recommended. Laser procedures such as Q-switched lasers, Nd: YAG lasers, and intense pulsed light have shown efficacy for refractory cases. Often, combining depigmenting agents, photoprotection, and laser treatments yields the best results [89,90].

Polyphenols have recently gained attention in melasma management. Their mechanisms include neutralizing free radicals to reduce oxidative stress contributing to melanogenesis, modulating inflammatory pathways to alleviate associated inflammation, and potentially inhibiting tyrosinase, a key enzyme in melanin production. While research into polyphenols' effectiveness in melasma treatment is still developing, initial studies have shown promising results, suggesting that these compounds could significantly manage this complex condition [91,92].

3. Clinical Evidence of Polyphenols in Dermatological Diseases

During the last few years, numerous preclinical and clinical studies have highlighted the therapeutic benefits of polyphenols in dermatologic pathologies. These compounds' mechanistic and pharmacological features indicate their possible influence in acne vulgaris, dermatitis, skin fungal infections, alopecia, and skin cancer pathophysiology [23,24,31,39,70]. Thus, their potential clinical use has become an object of investigation. The following section summarizes key clinical evidence regarding polyphenols' impact in treating multiple skin disorders (Table 1).

Table 1. Summary of key clinical evidence regarding polyphenols and skin disorders.

Author	Skin Disorder	Methodology	Results
Kim et al. [93]	Acne vulgaris	Meta-analysis with five randomized controlled clinical trials evaluated the efficacy and safety of green tea extract for treating acne.	Green tea extract significantly reduced the number of inflammatory lesions (−9.38; 95% CI: −14.13 to −4.63), inflammatory lesion counts (−11.39; 95% CI: −15.91 to −6.86), and non-inflammatory acne lesions (−32.44; 95% CI: −39.27 to −25.62).
Waranuch et al. [94]	Acne vulgaris	A single-center, parallel, randomized controlled trial assessed the anti-acne and anti-blotch activity of a hydrogel formulated with a combination of *Aloe barbadensis* leaf extract and *Garcinia mangostana* peel extract.	There was a reduction in total acne lesions ($p < 0.0001$) and mean acne severity index. Also, a decrease in skin redness ($p < 0.05$) and in mean melanin value ($p = 0.037$) was found.
Ikeda et al. [95]	Skin fungal infection	A double-blind, randomized, placebo-controlled trial evaluating the effects of a foot bath containing green tea polyphenols in patients with interdigital tinea pedis.	The use of a foot bath containing green tea polyphenols for 12 weeks produced a significant reduction in the size of the affected area ($p < 0.001$).

Table 1. *Cont.*

Author	Skin Disorder	Methodology	Results
Loing et al. [96]	Alopecia	A randomized, placebo-controlled study assessed the efficacy of *Trifolium pratense* flower extract and a biomimetic peptide in alopecia.	The anagen/telogen (A/T) ratio increased by +46%, anagen hair increased at an average of +13%, and telogen hair density decreased by −29% after 4 months of treatment.
Takahashi et al. [97]	Alopecia	A double-blind, randomized, placebo-controlled trial evaluated the efficacy of the external application of 0.7% apple procyanidin oligomers in patients with pattern baldness.	There was a significant increase in total number of hair (procyanidin, 3.3 ± 13.0 (mean ± SD)/0.50 cm^2; placebo, −3.6 ± 8.1/0.50 cm^2; $p < 0.001$, two-sample *t*-test).
Mehrbani et al. [98]	Atopic Dermatitis	A double-blind, randomized, placebo, controlled trial assessed the effect of powdered lyophilized milk serum with cuscuta extract to treat AD.	A marked increase in skin humidity and elasticity was observed ($p < 0.001$), along with diminished pruritus ($p < 0.05$) and sleep disturbances ($p < 0.05$).
Zhao et al. [99]	Radiation Dermatitis	A phase II, double-blind, randomized, controlled clinical trial was performed to determine the therapeutic and preventive properties of EGCG on RD patients with breast cancer treated with post-operatory radiotherapy.	EGCG significantly reduced the incidence, severity, and clinical manifestations of RD.

Abbreviations: A/T: anagen/telogen; AD: atopic dermatitis; RD: radiation dermatitis; EGCG: epigallocatechin-3-gallate topical serum.

Firstly, green tea is the most extensively investigated polyphenol in acne vulgaris on a clinical level [93,94,100–106]. In this sense, Kim et al. [93], in a meta-analysis of five randomized controlled studies, reported that the topical application of green tea extract is favorable for acne treatment without significant side effects. Its topical use significantly diminished the cases of inflammatory lesions (−9.38; IC 95%: −14.13 −4.63), the number of inflammatory lesions (−11.39; IC del 95%: −15.91 −6.86), and non-inflammatory lesions (−32.44; IC del 95%: −39.27 −25.62).

Likewise, in a randomized, double-blind, and placebo-controlled trial [106], significant reductions in acne lesions located in the nose, perioral area, and chin were reported after the use of a daily dose of 856 mg of epigallocatechin gallate in women with post-puberty acne. Similarly, Yoon et al. [105] conducted an 8-week randomized, double-blinded, split-face clinical trial, where 1% and 5% epigallocatechin-3-gallate solutions significantly improved inflammatory and non-inflammatory acne lesions. Moreover, Junt et al. [104] reported in a clinical study the significant symptomatic improvement in patients with acne, with reductions in comedones (61%) and blisters (28%) after topical treatment with green tea catechin (polyphenol: 60, 20 mg/mL).

The clinical use of other polyphenols to treat acne vulgaris has also been tested [94,100,101,107]. Waranuch et al. [94], in a single-center, parallel, randomized controlled trial, assessed the anti-acne and anti-blemish properties of a hydrogel formulated with a combination of *Aloe barbadensis* leaf extract, *Garcinia mangostana* peel extract, and *Camellia sinensis* leaf extract. A significant reduction in total acne lesions, severeness index, skin redness, and mean melanin value was reported. Furthermore, in a single-blinded, placebo-controlled, split-face comparative study [107], a considerable reduction in sebum secretions was reported after using green tea lotus extract emulsion.

On the other hand, their potential clinical use in alopecia has gained interest in the last few years. In a randomized controlled placebo study, *Trifolium pratense* flower extract and a biomimetic peptide were applied to thirty patients with mild-to-moderate active HL

for four months [96]. A significant increase (46%) in the treated group was found between the anagen/telogen (A/T) relationship. The anagen hair increased by +13%, and telogen hair density decreased by −29% [96]. Similarly, in a randomized controlled placebo study, Loing et al. [96] analyzed the hair-growing activity of procyanidin oligomers in 43 subjects. The treated subjects showed a significantly improved hair density and number of total scalp hair.

Moreover, Seok et al. [108], in a double-masked, controlled, placebo clinical trial, studied the efficacy of *Cistanche tubulosa* and *Laminaria japonica* to promote hair growth. A significant increase in density (test group: 23.29 n/cm^2 ± 24.26, control: 10.35 n/cm^2 ± 20.08, $p < 0.05$) and diameter (test group: 0.018 mm ± 0.015, control: 0.003 mm ± 0.013, $p < 0.05$) was found in the hair of the treated group. Lastly, Kamimura et al. [109] in a double-blind clinical study reported the effects of procyanidin B-2 in 29 patients, showing a significant augment in the total number of hair (procyanidin B-2, 6.68 ± 5.53 (mean ± ED)/0.25 cm^2; placebo, 0.08 ± 4.56 (mean ± ED)/0.25 cm^2; $p < 0.005$) and terminal hair (procyanidin B-2, 1.99 ± 2.58 (mean ± ED)/0.25 cm^2; placebo, −0.82 ± 3.40 (mean ± ED)/0.25 cm^2; $p < 0.02$).

Concerning skin fungal infections, despite a wide range of preclinical studies in the literature about polyphenol's antifungal activity [41,43,110], the clinical level of the data is very limited [95,111,112]. In this sense, Ikeda et al. [95], in a double-masked, randomized, placebo-controlled trial, observed a significant improvement in tinea pedis. Similar results were reported in diabetic patients with onychomycosis [113]. *Solanum chrysotrichu* has proven to be another useful phyto drug [112,114]. Herrera-Arellano et al. [114], in a controlled and randomized double-masked clinical trial, demonstrated a clinical efficacy of 92.16% in *pityriasis capitis* patients after the use of the extract. In addition, it has been reported that Brazilian green propolis causes a clinical improvement in tinea pedis interdigitalis, tinea corporis [115], tinea capitis, and tinea versicolor [116]. Finally, other polyphenols such as *Ocimum gratissimum* [117], *Acalypha wilkesiana* [118], *Cymbopogon citratus* [119], *Cassia alata* [120], and *Melaleuca alternifolia* [121] have demonstrated improvement in fungal infections.

On the other hand, various clinical studies assessed the efficacy of polyphenols in different types of dermatitis, obtaining mixed results. Two clinical trials related to atopic dermatitis (AD) were found: the first is a monocentric, randomized, controlled, double-blind study [122] that evaluated the efficacy and safety of a vitamin E, gallate, epigallocatechin, and grape seed procyanidin (MD2011001) topical cream in a sample of patients with mild-to-moderate AD for 28 days, in which a statistically significant difference was not observed when compared to placebo.

In a second randomized, double-masked, controlled, placebo trial performed by Mehrbani et al. [98], 52 adult subjects with mild-to-moderate AD were treated with lyophilized powdered milk serum rich in flavonoids, quercetin, kaempferol, and rutin or placebo [98]. The results were promising, with statistically significant improvement compared to placebo, regarding clinical manifestations such as elasticity, hydration, pruritus of affected skin, and diminished sleep disturbances; moreover, it was concluded that these improvements were prolonged 15 days after the treatment. Nevertheless, the data provided by these investigations do not allow us to individually assess the effect of polyphenols on AD [123].

Radiation dermatitis (RD) in oncologic patients has been a focus of polyphenol research. Several studies assessed topical epigallocatechin-3-gallate (EGCG), an active compound of green tea, to prevent and treat this affection. In the research carried out by Zhao et al. [99], the effect of EGCG in RD prevention was evaluated via a second phase, randomized, double-blind, controlled, placebo trial and performed in breast cancer patients treated with postoperative radiotherapy. Following EGCG treatment, the incidence, severity, and

clinical manifestations showed a statistically significant decrease. Moreover, the same authors previously tested the tolerability of the therapy in a phase I clinical trial [124], where no significant increase in adverse effects was observed. In addition, a more recent phase I clinical trial by Xie et al. [125] evaluated the use of EGCG for RD in patients with thoracic cancer, observing improvement in sensibility, pruritus, redness, pain, burning, and traction sensations, with no adverse effects reported.

EGCG is not the only polyphenol studied for RD; silymarin, a flavonoid extracted from *Silybum marianum*, was assessed by Karbasforooshan et al. [126] in a randomized, double blind and controlled placebo clinical trial. In the study, 1% silymarin gel was applied to breast cancer patients for RD prevention. Even though all subjects developed RD by the end of the study, a delayed onset and decreased severity were observed in the silymarin group.

Furthermore, polyphenols are potential therapeutic agents for contact dermatitis (CD). Improvements in inflammation markers were observed, specifically lower levels of INFγ, IL-4, IL-17, pentraxin 3, and NO and augmented levels of IL-10, in women with CD treated with 300 mg of polyphenols per day extracted from red grape seeds [127].

Lastly, regarding the use of polyphenols for treating and preventing skin cancer, even though a growing body of in vitro and in vivo experimental studies with promising results exist, currently, no clinical trials assessing the safety and efficacy of these compounds is available [128].

4. Bioavailability of Polyphenols and Routes of Administration

The bioavailability of polyphenols is a crucial issue in their therapeutic application. Despite their high bioactivity, the performance of polyphenols in vivo may be limited due to low water solubility, low lipophilicity, and inadequate molecular size; therefore, polyphenols suffer from structural instability in biological environments. All these characteristics lead to poor biodistribution, first-pass metabolism, poor penetration, and accumulation in the different organs [129,130].

Nowadays, topical administration has become one of the most attractive routes for the pharmaceutical industry. This method of administration can overcome some of the drawbacks of oral administration, such as low bioavailability, while ensuring the continuous and stable release of the polyphenol at the site of action. However, normal skin possesses a formidable barrier to drug absorption, mainly due to its particular lipid composition and the stratum corneum tissue [129].

Nanomedicine represents a favorable tool to increase the bioavailability and activities of natural products [131]. Nanostructured delivery systems that allow for a more effective delivery of polyphenols to the skin are currently being developed [130]. Nanocarriers can improve the stability, bioavailability, and targeted delivery of active ingredients, allowing better penetration and efficacy in treating specific skin conditions [132–136].

5. Natural Components Other than Polyphenols Being Used in Skin Conditions

While polyphenols represent a promising alternative in various dermatological therapies, other organic compounds, including terpenes and terpenoids, carotenoids, and benzoquinones, also exhibit beneficial properties for skin conditions [137–139].

Terpenes and terpenoids are a broad class of organic compounds found in several plants, as well as in some insects and microorganisms. Due to their anti-inflammatory, anti-microbial, and anti-tumor effects, terpenoids have been studied for their possible effects on inflammatory skin conditions, *Staphylococcus Aureus* infections, impetigo, dermatomycosis, and in the prevention and treatment of skin cancer [137,140]. Fungal terpenes

and terpenoids have demonstrated tyrosinase inhibition, suggesting their potential use in treating skin pigmentation disorders and melanogenesis-related cancers [141–144].

On the other hand, carotenoids constitute a specific type of terpenoid; within this classification, there are compounds such as lutein, canthaxanthin, α-carotene, β-carotene, and lycopene [145]. These molecules possess anti-inflammatory, anti-tumor, and antioxidant properties [138]. Recent interventional studies have proven the effects of lutein on UV light-induced carcinogenesis in animal models, as well as its beneficial effects on physiological skin parameters in humans, including antioxidant protection against UV light irradiation [146–148]. Similarly, clinical trials have confirmed the antioxidant activity of carotenoids and their capacity to improve erythematous affections. [149,150]. Moreover, canthaxanthin has demonstrated its utility in erythropoietic protoporphyria, a genetic disorder characterized by sun sensitivity [151].

Benzoquinones represent a different class of organic compounds, widely distributed in fungus, bacteria, arthropods, and plants. Embelin is a benzoquinone produced by the plant *Embelia ribes*, known by its pharmacological and therapeutic effects, including antioxidant, anti-inflammatory, and anti-tumor properties [152]. Numerous research studies have managed to show its capacity to inhibit leukocyte aggregation, suppressing TNF and IL-1, along with other inflammatory factors, and this ability might be useful in skin conditions such as psoriasis and dermatitis. Simultaneously, a variety of studies have pointed out the pro-apoptotic, anti-proliferative, anti-metastatic, anti-angiogenic, and anti-inflammatory qualities of the said compound, thus, representing a promising alternative for skin cancer treatment and prophylaxis [152–154].

Many natural sources with potential skin benefits remain underexplored. Future studies should prioritize the research of lesser-known plant extracts, marine compounds, and other natural resources to identify novel bioactive ingredients and their therapeutic role in skin disorders.

6. Conclusions

Dermatologic disorders continue to be among the most frequently encountered and challenging medical conditions in contemporary medicine. Due to their intricate and multifaceted pathophysiological mechanisms, researchers have been actively pursuing and evaluating novel therapeutic alternatives for their management over the past several decades. Within this evolving therapeutic landscape, polyphenols have emerged as a particularly promising group of metabolites, distinguished by their remarkable ability to produce a diverse array of beneficial effects—including potent antioxidant, anti-inflammatory, antimicrobial, antitumoral, and DNA-repairing properties—through multiple cellular and molecular mechanisms in various dermatological conditions.

In this dynamic context, the extensive body of preclinical evidence supports and validates the potential therapeutic applications of polyphenols in addressing the underlying pathogenic processes of numerous dermatological conditions, including but not limited to acne vulgaris, various forms of dermatitis, cutaneous fungal infections, different patterns of alopecia, and several types of skin cancer. Despite these positive preclinical findings, the current landscape of clinical trial evidence remains notably limited in scope and depth. Therefore, there exists a pressing need for additional high-quality clinical research studies characterized by larger patient populations, extended follow-up observation periods, and more rigorous methodological frameworks to comprehensively evaluate and definitively establish the clinical efficacy and practical applications of polyphenol-based interventions in the treatment of dermatological disorders. Furthermore, the development of novel approaches dedicated to boost the natural properties of these molecules by enhancing

characteristics such as absorption, solubility, and bioavailability, among others, represents a promising field of research in modern phytotherapy.

Author Contributions: Conceptualization: Á.O., J.S., J.L.P., R.S., B.G. and M.P.D.; methodology J.S., Á.O., J.L.P. and M.C.; investigation Á.O., J.L.P., R.S., N.G., B.G. and M.P.D.; writing—review and editing Á.O., J.L.P., M.P.D., R.S., N.G., B.G., J.C.C.-V., R.C., G.C. and M.C.; supervision M.C., J.C.C.-V., R.C. and G.C. All authors have read and agreed to the published version of the manuscript.

Funding: This research was funded by Universidad Simón Bolívar, Vicerrectoría de Investigación, Extensión e Innovación, Internal funds for Research Strengthening, Barranquilla, Colombia.

Conflicts of Interest: The authors declare no conflicts of interest.

Abbreviations

The following abbreviations are used in this manuscript:

GBD	Global Burden Disease
SD	Skin disorders
AV	Acne vulgaris
ROS	Reactive oxygen species
TPCLE	Total phenolic content leaf extract
IL-8	Interleukin-8
IL-1β	Interleukin-1β
TNFα	Tumor Necrosis Factor Alpha
MAPK	Mitogen-Activated Protein Kinase
NF-kB	Nuclear Factor Kappa-Light-Chain-Enhancer of activated B cells
MPP-9	Matrix Metalloproteinase 9
TLR2	Toll-like receptor 2
mRNA	Messenger RNA
NOS	Nitrous Oxide
ICAM-1	Intercellular Adhesion Molecule-1
COX-2	Cyclooxygenase-2
COX-1	Cyclooxygenase-1
JNK	c-Jun N-terminal kinase
KAS-III	3-Ketoacyl ACP synthase
QML	Quercus mongolica leaf extract
PD	Pedunculagin
IL-6	Interleukin-6
PP	Pomegranate peels
5αAR-1	5α reductase type 1
BK	Bokusoku
AD	Atopic dermatitis
TCS	Topical corticosteroids
CI	Calcineurin inhibitors
IL-4	Interleukin-4
ERK	Extracellular Signal-Regulated Kinase
IgE	Immunoglobulin E
TSLP	Thymic Stromal Lymphopoietin
TTLE	*Tambourissa trichophylla* leaf extract
AP	Acacia polyphenol
STB	*Schizonepeta tenuifolia* Briquet
AOM	*Alpinia oxyphylla* Miquel
CD	Contact dermatitis

mTOR	Mammalian Target of Rapamycin
TLR4	Toll-like receptor 4
SIRT1	Sirtuin 1
IGF-1	Insulin-like Growth Factor 1
KGF	Keratinocyte growth factor
TERT	Telomerase reverse transcriptase
VEGF	Vascular Endothelial Growth Factor
DPC	Dermal papilla cell
PDGF	Platelet-derived Growth Factor
EGF	Epidermal Growth Factor
DHT	Dihydrotestosterone
GA	Gallic acid
EA	Ellagic acid
CYP51	Sterol 14α-demethylase P450
SE	Squalane Epoxidase
CA	Caffeic Acid
LicoA	Licochalcone A
FAS	Fatty acid synthase
CDK	Cyclin-Dependent Kinase
ATP	Adenosine triphosphate
MMP	Mitochondrial membrane potential
ISO	Isoquercitrin
SOD	Superoxide Dismutase
5-LOX	5-Lipooxygenase
HL	Hair loss
AGA	Androgenic alopecia
HF	Hair follicle
TE	Telogen effluvium
H_2O_2	Hydrogen peroxide
ALP	Alkaline phosphatase
ORSC	Outer root sheath cells
PM	Polygonum multiflorum
TSG	2,3,5,4-Tetrahydroxystilbene-2-*O*-β-D-glucoside
AR	Androgenic receptor
UV	Ultraviolet
NMSC	Non-Melanoma Skin Cancer
BCC	Basal Cell Carcinoma
SCC	Squamous cell carcinoma
MSC	Melanoma Skin Cancer
CPD	Cyclobutane pyrimidine dimer
NER	Nucleotide Excision Repair
PI3K	Phosphatidylinositol 3 Kinase
AKT	Kinase protein B
TP	Tea polyphenol
ETR	Erythematotelangiectatic Rosacea
PPR	Papulopustular Rosacea
EGCG	Epigallocatechin gallate
RD	Radiation dermatitis
INFγ	Interferon-Gamma
IL-17	Interleukin-17
IL-10	Interleukin-10

References

1. Ortiz, A.; Herrera, T.; del Molino, C.P.; Piñeiro, F.; Perales, M.L.; Muñoz, P. Epidemiología de las enfermedades dermatologicas en atencion primaria. *Rev. Española Salud Pública* **1992**, *66*, 71–82.
2. Hay, R.J.; Johns, N.E.; Williams, H.C.; Bolliger, I.; Dellavalle, R.P.; Margolis, D.J.; Marks, R.; Naldi, L.; Weinstock, M.A.; Wulf, S.K.; et al. The global burden of skin disease in 2010: An analysis of the prevalence and impact of skin conditions. *J. Investig. Dermatol.* **2014**, *134*, 1527–1534. [CrossRef] [PubMed]
3. Chu, S.; Mehrmal, S.; Uppal, P.; Giesey, R.L.; Delost, M.E.; Delost, G.R. Burden of skin disease and associated socioeconomic status in Europe: An ecologic study from the Global Burden of Disease Study 2017. *JAAD Int.* **2020**, *1*, 95–103. [CrossRef] [PubMed]
4. Salazar, J.; Cano, C.; Pérez, J.L.; Castro, A.; Díaz, M.P.; Garrido, B.; Carrasquero, R.; Chacín, M.; Velasco, M.; D'marco, L.; et al. Role of Dietary Polyphenols in Adipose Tissue Browning: A Narrative Review. *Curr. Pharm. Des.* **2020**, *26*, 4444–4460. [CrossRef] [PubMed]
5. Działo, M.; Mierziak, J.; Korzun, U.; Preisner, M.; Szopa, J.; Kulma, A. The Potential of Plant Phenolics in Prevention and Therapy of Skin Disorders. *Int. J. Mol. Sci.* **2016**, *17*, 160. [CrossRef] [PubMed] [PubMed Central]
6. de Lima Cherubim, D.J.; Buzanello Martins, C.V.; Oliveira Fariña, L.; da Silva de Lucca, R.A. Polyphenols as natural antioxidants in cosmetics applications. *J. Cosmet. Dermatol.* **2020**, *19*, 33–37. [CrossRef]
7. Kosina, P.; Paloncýová, M.; Rajnochová Svobodová, A.; Zálešák, B.; Biedermann, D.; Ulrichová, J.; Vostálová, J. Dermal Delivery of Selected Polyphenols from *Silybum marianum*. Theoretical and Experimental Study. *Molecules* **2018**, *24*, 61. [CrossRef] [PubMed]
8. Chilicka, K.; Gold, M.H.; Nowicka, D. Acne vulgaris and the most popular and new cosmetological treatments. *J. Cosmet. Dermatol.* **2023**, *22*, 1946–1950. [CrossRef]
9. Vasam, M.; Korutla, S.; Bohara, R.A. Acne vulgaris: A review of the pathophysiology, treatment, and recent nanotechnology based advances. *Biochem. Biophys. Rep.* **2023**, *36*, 101578. [CrossRef] [PubMed]
10. Cheon, D.; Kim, J.; Jeon, D.; Shin, H.-C.; Kim, Y. Target Proteins of Phloretin for Its Anti-Inflammatory and Antibacterial Activities Against Propionibacterium acnes-Induced Skin Infection. *Molecules* **2019**, *24*, 1319. [CrossRef]
11. Huang, W.-C.; Tsai, T.-H.; Huang, C.-J.; Li, Y.-Y.; Chyuan, J.-H.; Chuang, L.-T.; Tsai, P.-J. Inhibitory Effects of Wild Bitter Melon Leaf Extract on *Propionibacterium acnes*-Induced Skin Inflammation in Mice and Cytokine Production In Vitro. *Food Funct.* **2015**, *6*, 2550–2560. [CrossRef] [PubMed]
12. Chuang, L.-T.; Tsai, T.-H.; Lien, T.-J.; Huang, W.-C.; Liu, J.-J.; Chang, H.; Chang, M.-L.; Tsai, P.-J. Ethanolic Extract of *Origanum vulgare* Suppresses *Propionibacterium acnes*-Induced Inflammatory Responses in Human Monocyte and Mouse Ear Edema Models. *Molecules* **2018**, *23*, 1987. [CrossRef] [PubMed]
13. Chrząszcz, M.; Miazga-Karska, M.; Klimek, K.; Granica, S.; Tchórzewska, D.; Ginalska, G.; Szewczyk, K. Extracts from *Cephalaria Uralensis* (Murray) Roem. & Schult. and *Cephalaria Gigantea* (Ledeb.) Bobrov as Potential Agents for Treatment of Acne Vulgaris: Chemical Characterization and In Vitro Biological Evaluation. *Antioxidants* **2020**, *9*, 796. [CrossRef]
14. Albouchi, F.; Avola, R.; Dico, G.M.L.; Calabrese, V.; Graziano, A.C.E.; Abderrabba, M.; Cardile, V. *Melaleuca styphelioides* Sm. Polyphenols Modulate Interferon Gamma/Histamine-Induced Inflammation in Human NCTC 2544 Keratinocytes. *Molecules* **2018**, *23*, 2526. [CrossRef] [PubMed]
15. Kim, M.; Yin, J.; Hwang, I.H.; Park, D.H.; Lee, E.K.; Kim, M.J.; Lee, M.W. Anti-Acne Vulgaris Effects of Pedunculagin from the Leaves of *Quercus mongolica* by Anti-Inflammatory Activity and 5α-Reductase Inhibition. *Molecules* **2020**, *25*, 2154. [CrossRef]
16. Du, L.; Li, J.; Zhang, X.; Wang, L.; Zhang, W.; Yang, M.; Hou, C. Pomegranate peel polyphenols inhibits inflammation in LPS-induced RAW264.7 macrophages via the suppression of TLR4/NF-κB pathway activation. *Food Nutr. Res.* **2019**, *63*, 3392. [CrossRef]
17. Koseki, J.; Matsumoto, T.; Matsubara, Y.; Tsuchiya, K.; Mizuhara, Y.; Sekiguchi, K.; Nishimura, H.; Watanabe, J.; Kaneko, A.; Hattori, T.; et al. Inhibition of Rat 5α-Reductase Activity and Testosterone-Induced Sebum Synthesis in Hamster Sebocytes by an Extract of Quercus acutissima Cortex. *Evid.-Based Complement. Alternat. Med.* **2015**, *2015*, 853846. [CrossRef] [PubMed]
18. Lee, D.Y.; Lee, H.J.; Ryu, J.-H. Prenylated Polyphenols from *Broussonetia kazinoki* as Inhibitors of Nitric Oxide Production. *Molecules* **2018**, *23*, 639. [CrossRef]
19. Tanei, R. Atopic Dermatitis in Older Adults: A Review of Treatment Options. *Drugs Aging* **2020**, *37*, 149–160. [CrossRef]
20. Bridgman, A.C.; Qureshi, A.; Li, T.; Tabung, F.K.; Cho, E.; Drucker, A.M. Inflammatory dietary pattern and incident psoriasis, psoriatic arthritis, and atopic dermatitis in women: A cohort study. *J. Am. Acad. Dermatol.* **2019**, *80*, 1682–1690. [CrossRef] [PubMed]
21. Ji, H.; Li, X.-K. Oxidative Stress in Atopic Dermatitis. *Oxid. Med. Cell. Longev.* **2016**, *2016*, 2721469. [CrossRef]
22. Kingkaw, A.; Nakphaichit, M.; Suratannon, N.; Nitisinprasert, S.; Wongoutong, C.; Chatchatee, P.; Krobthong, S.; Charoenlappanit, S.; Roytrakul, S.; Vongsangnak, W. Analysis of the infant gut microbiome reveals metabolic functional roles associated with healthy infants and infants with atopic dermatitis using metaproteomics. *PeerJ* **2020**, *8*, e9988. [CrossRef] [PubMed]
23. Gil, T.-Y.; Kang, Y.-M.; Eom, Y.-J.; Hong, C.-H.; An, H.-J. Anti-Atopic Dermatitis Effect of *Seaweed Fulvescens* Extract via Inhibiting the STAT1 Pathway. *Mediat. Inflamm.* **2019**, *2019*, 3760934. [CrossRef]

24. Lee, D.H.; Park, J.K.; Choi, J.; Jang, H.; Seol, J.W. Anti-inflammatory effects of natural flavonoid diosmetin in IL-4 and LPS-induced macrophage activation and atopic dermatitis model. *Int. Immunopharmacol.* **2020**, *89*, 107046. [CrossRef]
25. Lee, H.N.; Shin, S.A.; Choo, G.S.; Kim, H.J.; Park, Y.S.; Kim, B.S.; Kim, S.K.; Cho, S.D.; Nam, J.S.; Choi, C.S.; et al. Anti-inflammatory effect of quercetin and galangin in LPS-stimulated RAW264.7 macrophages and DNCB-induced atopic dermatitis animal models. *Int. J. Mol. Med.* **2018**, *41*, 888–898. [CrossRef] [PubMed]
26. Jegal, J.; Park, N.-J.; Kim, T.-Y.; Choi, S.; Lee, S.W.; Hang, J.; Kim, S.-N.; Yang, M.H. Effect of Topically Applied *Wikstroemia dolichantha* Diels on the Development of Atopic Dermatitis-Like Skin Symptoms in Mice. *Nutrients* **2019**, *11*, 914. [CrossRef] [PubMed]
27. Sudarshan, K.; Yarlagadda, S.; Sengupta, S. Recent Advances in the Synthesis of Diarylheptanoids. *Chem. Asian J.* **2024**, *19*, e202400380. [CrossRef] [PubMed]
28. Fitoussi, J.; Virassamynaïk, S.; Callejon, S.; Weber, S.; Collet, E.; Scalia, J.; Chavagnac-Bonneville, M.; Trompezinski, S.; Sayag, M. Inhibition of thymic stromal lymphopoietin production to improve pruritus and quality of life in infants and children with atopic dermatitis. *J. Cosmet. Dermatol.* **2020**, *19*, 2061–2069. [CrossRef]
29. Sozmen, S.C.; Karaman, M.; Micili, S.C.; Isik, S.; Ayyildiz, Z.A.; Bagriyanik, A.; Uzuner, N.; Karaman, O. Resveratrol ameliorates 2,4-dinitrofluorobenzene-induced atopic dermatitis-like lesions through effects on the epithelium. *PeerJ* **2016**, *4*, e1889. [CrossRef] [PubMed]
30. Ikarashi, N.; Fujitate, N.; Togashi, T.; Takayama, N.; Fukuda, N.; Kon, R.; Sakai, H.; Kamei, J.; Sugiyama, K. Acacia Polyphenol Ameliorates Atopic Dermatitis in Trimellitic Anhydride-Induced Model Mice via Changes in the Gut Microbiota. *Foods* **2020**, *9*, 773. [CrossRef]
31. Zhang, T.; Qiu, J.; Wu, X.; Huang, S.; Yuan, H.; Park, S. *Schizonepeta tenuifolia* with *Alpinia oxyphylla* Alleviates Atopic Dermatitis and Improves the Gut Microbiome in Nc/Nga Mice. *Pharmaceutics* **2020**, *12*, 722. [CrossRef]
32. Jegal, J.; Park, N.-J.; Lee, S.-Y.; Jo, B.-G.; Bong, S.-K.; Kim, S.-N.; Yang, M.H. Quercitrin, the Main Compound in *Wikstroemia indica*, Mitigates Skin Lesions in a Mouse Model of 2,4-Dinitrochlorobenzene-Induced Contact Hypersensitivity. *Evid.-Based Complement. Altern. Med.* **2020**, *2020*, 4307161. [CrossRef] [PubMed]
33. Kim, S.-H.; Cho, S.-H.; Youn, S.-K.; Park, J.-S.; Choi, J.T.; Bak, Y.-S.; Yu, Y.-B.; Kim, Y.K. Epidemiological Characterization of Skin Fungal Infections Between the Years 2006 and 2010 in Korea. *Osong Public Health Res. Perspect.* **2015**, *6*, 341–345. [CrossRef] [PubMed]
34. White, T.C.; Findley, K.; Dawson, T.L.; Scheynius, A.; Boekhout, T.; Cuomo, C.A.; Xu, J.; Saunders, C.W. Fungi on the Skin: Dermatophytes and Malassezia. *Cold Spring Harb. Perspect. Med.* **2014**, *4*, a019802. [CrossRef]
35. Hube, B.; Hay, R.; Brasch, J.; Veraldi, S.; Schaller, M. Dermatomycoses and inflammation: The adaptive balance between growth, damage, and survival. *J. Mycol. Med.* **2015**, *25*, e44–e58. [CrossRef] [PubMed]
36. Martinez-Rossi, N.M.; Peres, N.T.A.; Rossi, A. Pathogenesis of Dermatophytosis: Sensing the Host Tissue. *Mycopathologia* **2017**, *182*, 215–227. [CrossRef] [PubMed]
37. Al Aboody, M.S.; Mickymaray, S. Anti-Fungal Efficacy and Mechanisms of Flavonoids. *Antibiotics* **2020**, *9*, 45. [CrossRef]
38. Jordá, T.; Puig, S. Regulation of Ergosterol Biosynthesis in *Saccharomyces cerevisiae*. *Genes* **2020**, *11*, 795. [CrossRef]
39. Li, Z.-J.; Liu, M.; Dawuti, G.; Dou, Q.; Ma, Y.; Liu, H.-G.; Aibai, S. Antifungal Activity of Gallic Acid In Vitro and In Vivo. *Phytother. Res.* **2017**, *31*, 1039–1045. [CrossRef] [PubMed]
40. Li, Z.J.; Guo, X.; Dawuti, G.; Aibai, S. Antifungal Activity of Ellagic Acid In Vitro and In Vivo. *Phytother. Res.* **2015**, *29*, 1019–1025. [CrossRef]
41. Cantelli, B.A.M.; Bitencourt, T.A.; Komoto, T.T.; Beleboni, R.O.; Marins, M.; Fachin, A.L. Caffeic acid and licochalcone A interfere with the glyoxylate cycle of Trichophyton rubrum. *Biomed. Pharmacother.* **2017**, *96*, 1389–1394. [CrossRef] [PubMed]
42. Maier, T.; Leibundgut, M.; Boehringer, D.; Ban, N. Structure and function of eukaryotic fatty acid synthases. *Q. Rev. Biophys.* **2010**, *43*, 373–422. [CrossRef]
43. Da Silva, C.R.; De Andrade-Neto, J.B.; Campos, R.D.S.; Figueiredo, N.S.; Sampaio, L.S.; Magalhães, H.I.F.; Cavalcanti, B.C.; Gaspar, D.M.; De Andrade, G.M.; Lima, I.S.P.; et al. Synergistic effect of the flavonoid catechin, quercetin, or epigallocatechin gallate with fluconazole induces apoptosis in Candida tropicalis resistant to fluconazole. *Antimicrob. Agents Chemother.* **2014**, *58*, 1468–1478. [CrossRef]
44. Bitencourt, T.A.; Komoto, T.T.; Massaroto, B.G.; Miranda, C.E.S.; Beleboni, R.O.; Marins, M.; Fachin, A.L. Trans-chalcone and quercetin down-regulate fatty acid synthase gene expression and reduce ergosterol content in the human pathogenic dermatophyte Trichophyton rubrum. *BMC Complement. Altern. Med.* **2013**, *13*, 229. [CrossRef]
45. Bitencourt, T.A.; TakahasiKomoto, T.; Marins, M.; Fachin, A.L. Antifungal activity of flavonoids and modulation of expression of genes of fatty acid synthesis in the dermatophyte Trichophyton rubrum. *BMC Proc.* **2014**, *8* (Suppl. S4), 53. [CrossRef]
46. Bitencourt, T.A.; Macedo, C.; Franco, M.E.; Rocha, M.C.; Moreli, I.S.; Cantelli, B.A.M.; Sanches, P.R.; Beleboni, R.O.; Malavazi, I.; Passos, G.A.; et al. Trans-chalcone activity against Trichophyton rubrum relies on an interplay between signaling pathways related to cell wall integrity and fatty acid metabolism. *BMC Genom.* **2019**, *20*, 411. [CrossRef]

47. Gaziano, R.; Campione, E.; Iacovelli, F.; Marino, D.; Pica, F.; Di Francesco, P.; Aquaro, S.; Menichini, F.; Falconi, M.; Bianchi, L. Antifungal activity of *Cardiospermum halicacabum* L. (Sapindaceae) against Trichophyton rubrum occurs through molecular interaction with fungal Hsp90. *Drug Des. Dev. Ther.* **2018**, *12*, 2185–2193. [CrossRef]
48. Da, X.; Nishiyama, Y.; Tie, D.; Hein, K.Z.; Yamamoto, O.; Morita, E. Antifungal Activity and Mechanism of Action of Ou-gon (*Scutellaria* Root Extract) Components Against Pathogenic Fungi. *Sci. Rep.* **2019**, *9*, 1683. [CrossRef]
49. Kim, S.; Woo, E.; Lee, D.G. Synergistic Antifungal Activity of Isoquercitrin: Apoptosis and Membrane Permeabilization Related to Reactive Oxygen Species in *Candida albicans*. *IUBMB Life* **2019**, *71*, 283–292. [CrossRef]
50. Gomes, N.G.M.; Oliveira, A.P.; Cunha, D.; Pereira, D.M.; Valentão, P.; Pinto, E.; Araújo, L.; Andrade, P.B. Flavonoid Composition of *Salacia senegalensis* (Lam.) DC. Leaves, Evaluation of Antidermatophytic Effects, and Potential Amelioration of the Associated Inflammatory Response. *Molecules* **2019**, *24*, 2530. [CrossRef]
51. Tosti, A.; Gray, J. Assessment of Hair and Scalp Disorders. *J. Investig. Dermatol. Symp. Proc.* **2007**, *12*, 23–27. [CrossRef] [PubMed]
52. Mysore, V.; Parthasaradhi, A.; Kharkar, R.; Ghoshal, A.; Ganjoo, A.; Ravichandran, G.; Saraswat, A.; Shah, Y.; Singh, M.; Remadevi, T.; et al. Expert consensus on the management of androgenetic alopecia in India. *Int. J. Trichology* **2019**, *11*, 101–106. [CrossRef] [PubMed]
53. Simakou, T.; Butcher, J.P.; Reid, S.; Henriquez, F.L. Alopecia areata: A multifactorial autoimmune condition. *J. Autoimmun.* **2019**, *98*, 74–85. [CrossRef]
54. Malkud, S. Telogen Effluvium: A Review. *J. Clin. Diagn. Res.* **2015**, *9*, WE01–WE03. [CrossRef] [PubMed]
55. Santos, Z.; Avci, P.; Hamblin, M.R. Drug discovery for alopecia: Gone today, hair tomorrow. *Expert Opin. Drug Discov.* **2015**, *10*, 269–292. [CrossRef] [PubMed]
56. Kwon, O.S.; Han, J.H.; Yoo, H.G.; Chung, J.H.; Cho, K.H.; Eun, H.C.; Kim, K.H. Human hair growth enhancement in vitro by green tea epigallocatechin-3-gallate (EGCG). *Phytomedicine* **2007**, *14*, 551–555. [CrossRef] [PubMed]
57. Wikramanayake, T.C.; Villasante, A.C.; Mauro, L.M.; Perez, C.I.; Schachner, L.A.; Jimenez, J.J. Prevention and treatment of alopecia areata with quercetin in the C3H/HeJ mouse model. *Cell. Stress. Chaperones* **2012**, *17*, 267–274. [CrossRef]
58. Driskell, R.R.; Clavel, C.; Rendl, M.; Watt, F.M. Hair follicle dermal papilla cells at a glance. *J. Cell Sci.* **2011**, *124 Pt 8*, 1179–1182. [CrossRef]
59. Madaan, A.; Joshi, V.; Kishore, A.; Verma, R.; Singh, A.; Jaggi, M.; Sung, Y.K. In vitro Hair Growth Promoting Effects of Naringenin and Hesperetin on Human Dermal Papilla Cells and Keratinocytes. *Am. J. Dermatol. Venereol.* **2017**, *6*, 51–57.
60. Xing, F.; Yi, W.J.; Miao, F.; Su, M.Y.; Lei, T.C. Baicalin increases hair follicle development by increasing canonical Wnt/β-catenin signaling and activating dermal papillar cells in mice. *Int. J. Mol. Med.* **2018**, *41*, 2079–2085. [CrossRef]
61. Zhou, L.; Wang, H.; Jing, J.; Yu, L.; Wu, X.; Lu, Z. Morroniside regulates hair growth and cycle transition via activation of the Wnt/β-catenin signaling pathway. *Sci. Rep.* **2018**, *8*, 13785. [CrossRef] [PubMed]
62. Han, J.H.; Kwon, O.S.; Chung, J.H.; Cho, K.H.; Eun, H.C.; Kim, K.H. Effect of minoxidil on proliferation and apoptosis in dermal papilla cells of human hair follicle. *J. Dermatol. Sci.* **2004**, *34*, 91–98. [CrossRef]
63. Shin, J.Y.; Choi, Y.-H.; Kim, J.; Park, S.Y.; Nam, Y.J.; Lee, S.Y.; Jeon, J.H.; Jin, M.H.; Lee, S. Polygonum multiflorum extract support hair growth by elongating anagen phase and abrogating the effect of androgen in cultured human dermal papilla cells. *BMC Complement. Med. Ther.* **2020**, *20*, 144. [CrossRef]
64. Kubo, C.; Ogawa, M.; Uehara, N.; Katakura, Y. Fisetin Promotes Hair Growth by Augmenting TERT Expression. *Front. Cell Dev. Biol.* **2020**, *8*, 566617. [CrossRef] [PubMed]
65. Khazaei, Z.; Ghorat, F.; Jarrahi, A.M.; Adineh, H.A.; Sohrabivafa, M.; Goodarzi, E. Global incidence and mortality of skin cancer by histological subtype and its relationship with the human development index (HDI); an ecology study in 2018. *World Cancer Res. J.* **2019**, *6*, e1265. [CrossRef]
66. Fahradyan, A.; Howell, A.C.; Wolfswinkel, E.M.; Tsuha, M.; Sheth, P.; Wong, A.K. Updates on the Management of Non-Melanoma Skin Cancer (NMSC). *Healthcare* **2017**, *5*, 82. [CrossRef] [PubMed]
67. Mohammadbeigi, A.; Khazaei, S.; Veisani, Y.; Delpisheh, A.; Jenabi, E. Global inequality in the incidence and mortality rate of melanoma skin cancer according to human development index: A country-level analysis. *Egypt. J. Dermatol. Venerol.* **2021**, *41*, 26. [CrossRef]
68. Chen, J.T.; Kempton, S.J.; Rao, V.K.M. The Economics of Skin Cancer: An Analysis of Medicare Payment Data. *Plast. Reconstr. Surg. Glob. Open* **2016**, *4*, e868. [CrossRef] [PubMed]
69. Sajadimajd, S.; Bahramsoltani, R.; Iranpanah, A.; Patra, J.K.; Das, G.; Gouda, S.; Rahimi, R.; Rezaeiamiri, E.; Cao, H.; Giampieri, F.; et al. Advances on Natural Polyphenols as Anticancer Agents for Skin Cancer. *Pharmacol. Res.* **2020**, *151*, 104584. [CrossRef]
70. Chen, X.; Chang, L.; Qu, Y.; Liang, J.; Jin, W.; Xia, X. Tea polyphenols inhibit the proliferation, migration, and invasion of melanoma cells through the down-regulation of TLR4. *Int. J. Immunopathol. Pharmacol.* **2018**, *32*, 394632017739531. [CrossRef] [PubMed]

71. Swalwell, H.; Latimer, J.; Haywood, R.M.; Birch-Machin, M.A. Investigating the role of melanin in UVA/UVB- and hydrogen peroxide-induced cellular and mitochondrial ROS production and mitochondrial DNA damage in human melanoma cells. *Free Radic. Biol. Med.* **2012**, *52*, 626–634. [CrossRef]
72. Ikehata, H.; Mori, T.; Kamei, Y.; Douki, T.; Cadet, J.; Yamamoto, M. Wavelength- and Tissue-dependent Variations in the Mutagenicity of Cyclobutane Pyrimidine Dimers in Mouse Skin. *Photochem. Photobiol.* **2020**, *96*, 94–104. [CrossRef] [PubMed]
73. Chong, Z.; Matsuo, H.; Onoue, S.; Yamamoto, H.; Ito, H.; Katakura, Y. Identification of polyphenols that repair the ultraviolet-B-induced DNA damage via SIRT1-dependent XPC/XPA activation. *J. Funct. Foods* **2019**, *54*, 119–127. [CrossRef]
74. Xian, D.; Lai, R.; Song, J.; Xiong, X.; Zhong, J. Emerging Perspective: Role of Increased ROS and Redox Imbalance in Skin Carcinogenesis. *Oxid. Med. Cell. Longev.* **2019**, *2019*, 8127362. [CrossRef]
75. Rossi, Y.E.; Bohl, L.P.; Braber, N.L.V.; Ballatore, M.B.; Escobar, F.M.; Bodoira, R.; Maestri, D.M.; Porporatto, C.; Cavaglieri, L.R.; Montenegro, M.A. Polyphenols of peanut (*Arachis hypogaea* L.) skin as bioprotectors of normal cells. Studies of cytotoxicity, cytoprotection and interaction with ROS. *J. Funct. Foods* **2020**, *67*, 103862. [CrossRef]
76. Eskandari, M.; Rembiesa, J.; Startaitė, L.; Holefors, A.; Valančiūtė, A.; Faridbod, F.; Ganjali, M.R.; Engblom, J.; Ruzgas, T. Polyphenol-hydrogen peroxide reactions in skin: In vitro model relevant to study ROS reactions at inflammation. *Anal. Chim. Acta* **2019**, *1075*, 91–97. [CrossRef]
77. Ko, J.-H.; Sethi, G.; Um, J.-Y.; Shanmugam, M.K.; Arfuso, F.; Kumar, A.P.; Bishayee, A.; Ahn, K.S. The Role of Resveratrol in Cancer Therapy. *Int. J. Mol. Sci.* **2017**, *18*, 2589. [CrossRef] [PubMed]
78. Bridgeman, B.B.; Wang, P.; Ye, B.; Pelling, J.C.; Volpert, O.V.; Tong, X. Inhibition of mTOR by apigenin in UVB-irradiated keratinocytes: A new implication of skin cancer prevention. *Cell. Signal.* **2016**, *28*, 460–468. [CrossRef] [PubMed]
79. Arumugam, G.; Yadav, S.A. Synergistic inhibitory actions of resveratrol, epigallocatechin-3-gallate, and diallyl trisulfide against skin cancer cell line A431 through mitochondrial caspase dependent pathway: A combinational drug approach. *Med. Oncol.* **2024**, *41*, 64. [CrossRef]
80. Zujko-Kowalska, K.; Masłowska, J.; Knaś-Dawidziuk, M.; Hamulka, J.; Zujko, M.E. Dietary Antioxidants May Support Cosmetic Treatment in Patients with Rosacea. *Antioxidants* **2024**, *13*, 381. [CrossRef]
81. Searle, T.; Ali, F.R.; Carolides, S.; Al-Niaimi, F. Rosacea and Diet: What is New in 2021? *J. Clin. Aesthet. Dermatol.* **2021**, *14*, 49–54.
82. Paiva-Santos, A.C.; Gonçalves, T.; Peixoto, D.; Pires, P.C.; Velsankar, K.; Jha, N.K.; Chavda, V.P.; Mohammad, I.S.; Cefali, L.C.; Mazzola, P.G.; et al. Rosacea Topical Treatment and Care: From Traditional to New Drug Delivery Systems. *Mol. Pharm.* **2023**, *20*, 3804–3828. [CrossRef]
83. Zhang, H.; Tang, K.; Wang, Y.; Fang, R.; Sun, Q. Rosacea Treatment: Review and Update. *Dermatol. Ther.* **2021**, *11*, 13–24. [CrossRef]
84. Maden, S. Epidermal Skin Barrier and Skin Care in Rosacea: A Narrative Review. *Dermis* **2024**, *4*, 15. [CrossRef]
85. Dall'Oglio, F.; Nasca, M.R.; Gerbino, C.; Micali, G. Advances in pharmacotherapy for rosacea: What is the current state of the art? *Expert Opin. Pharmacother.* **2022**, *23*, 1845–1854. [CrossRef]
86. Espósito, A.C.C.; Cassiano, D.P.; da Silva, C.N.; Lima, P.B.; Dias, J.A.F.; Hassun, K.; Bagatin, E.; Miot, L.D.B.; Miot, H.A. Update on Melasma—Part I: Pathogenesis. *Dermatol. Ther.* **2022**, *12*, 1967–1988. [CrossRef] [PubMed]
87. Artzi, O.; Horovitz, T.; Bar-Ilan, E.; Shehadeh, W.; Koren, A.; Zusmanovitch, L.; Mehrabi, J.N.; Salameh, F.; Nelkenbaum, G.I.; Zur, E.; et al. The pathogenesis of melasma and implications for treatment. *J. Cosmet. Dermatol.* **2021**, *20*, 3432–3445. [CrossRef]
88. Doolan, B.J.; Gupta, M. Melasma. *Aust. J. Gen. Pract.* **2021**, *50*, 880–885. [CrossRef]
89. Cassiano, D.P.; Espósito, A.C.C.; Da Silva, C.N.; Lima, P.B.; Dias, J.A.F.; Hassun, K.; Miot, L.D.B.; Miot, H.A.; Bagatin, E. Update on Melasma—Part II: Treatment. *Dermatol. Ther.* **2022**, *12*, 1989–2012. [CrossRef]
90. Liu, W.; Chen, Q.; Xia, Y. New Mechanistic Insights of Melasma. *Clin. Cosmet. Investig. Dermatol.* **2023**, *16*, 429–442. [CrossRef] [PubMed]
91. Bs, K.M.B.; Babbush, R.A.; Khachemoune, A. Treatment of melasma: A review of less commonly used antioxidants. *Int. J. Dermatol.* **2021**, *60*, 166–173. [CrossRef]
92. AlSalem, S.; Alexis, A. Melasma hyperpigmentation: An overview of current topical therapeutics. *Dermatol. Rev.* **2022**, *4*, 38–52. [CrossRef]
93. Kim, S.; Park, T.H.; Kim, W.I.; Park, S.; Kim, J.H.; Cho, M.K. The effects of green tea on acne vulgaris: A systematic review and meta-analysis of randomized clinical trials. *Phytother. Res.* **2020**, *35*, 374–383. [CrossRef] [PubMed]
94. Waranuch, N.; Phimnuan, P.; Yakaew, S.; Nakyai, W.; Grandmottet, F.; Onlom, C.; Srivilai, J.; Viyoch, J. Antiacne and antiblotch activities of a formulated combination of Aloe barbadensis leaf powder, Garcinia mangostana peel extract, and Camellia sinensis leaf extract. *Clin. Cosmet. Investig. Dermatol.* **2019**, *12*, 383–391. [CrossRef] [PubMed]
95. Ikeda, S.; Kanoya, Y.; Nagata, S. Effects of a foot bath containing green tea polyphenols on interdigital tinea pedis. *Foot* **2013**, *23*, 58–62. [CrossRef]
96. Loing, E.; Lachance, R.; Ollier, V.; Hocquaux, M. A new strategy to modulate alopecia using a combination of two specific and unique ingredients. *J. Cosmet. Sci.* **2013**, *64*, 45–58.

97. Takahashi, T.; Kamimura, A.; Kagoura, M.; Toyoda, M.; Morohashi, M. Investigation of the topical application of procyanidin oligomers from apples to identify their potential use as a hair-growing agent. *J. Cosmet. Dermatol.* **2005**, *4*, 245–249. [CrossRef] [PubMed]
98. Mehrbani, M.; Choopani, R.; Fekri, A.; Mehrabani, M.; Mosaddegh, M.; Mehrabani, M. The efficacy of whey associated with dodder seed extract on moderate-to-severe atopic dermatitis in adults: A randomized, double-blind, placebo-controlled clinical trial. *J. Ethnopharmacol.* **2015**, *172*, 325–332. [CrossRef] [PubMed]
99. Zhao, H.; Zhu, W.; Zhao, X.; Li, X.; Zhou, Z.; Zheng, M.; Meng, X.; Kong, L.; Zhang, S.; He, D.; et al. Efficacy of Epigallocatechin-3-Gallate in Preventing Dermatitis in Patients with Breast Cancer Receiving Postoperative Radiotherapy: A Double-Blind, Placebo-Controlled, Phase 2 Randomized Clinical Trial. *JAMA Dermatol.* **2022**, *158*, 779. [CrossRef]
100. Sharquie, K.E.; Noaimi, A.A.; Al-Salih, M.M. Topical therapy of acne vulgaris using 2% tea lotion in comparison with 5% zinc sulphate solution. *Saudi Med. J.* **2008**, *29*, 1757–1761. [PubMed]
101. Sharquie, K.E.; Al-Turfi, I.A.; Al-Shimary, W.M. Treatment of acne vulgaris with 2% topical tea lotion. *Saudi Med. J.* **2006**, *27*, 83–85. [PubMed]
102. Elsaie, M.L.; Abdelhamid, M.F.; Elsaaiee, L.T.; Emam, H.M. The efficacy of topical 2% green tea lotion in mild-to-moderate acne vulgaris. *J. Drugs Dermatol.* **2009**, *8*, 358–364. [PubMed]
103. Mahmood, T.; Akhtar, N.; Khan, B.A.; Khan, H.M.S.; Saeed, T. Outcomes of 3% green tea emulsion on skin sebum production in male volunteers. *Bosn. J. Basic Med. Sci.* **2010**, *10*, 260–264. [CrossRef] [PubMed]
104. Jung, M.K.; Ha, S.; Son, J.-A.; Song, J.H.; Houh, Y.; Cho, E.; Chun, J.H.; Yoon, S.R.; Yang, Y.; Ban, S.I.; et al. Polyphenon-60 displays a therapeutic effect on acne by suppression of TLR2 and IL-8 expression via down-regulating the ERK1/2 pathway. *Arch. Dermatol. Res.* **2012**, *304*, 655–663. [CrossRef] [PubMed]
105. Yoon, J.Y.; Kwon, H.H.; Min, S.U.; Thiboutot, D.M.; Suh, D.H. Epigallocatechin-3-gallate improves acne in humans by modulating intracellular molecular targets and inhibiting *P. acnes*. *J. Investig. Dermatol.* **2013**, *133*, 429–440. [CrossRef]
106. Lu, P.; Hsu, C. Does supplementation with green tea extract improve acne in post-adolescent women? A randomized, double-blind, and placebo-controlled clinical trial. *Complement. Ther. Med.* **2016**, *25*, 159–163. [CrossRef]
107. Mahmood, T.; Akhtar, N.; Moldovan, C. A comparison of the effects of topical green tea and lotus on facial sebum control in healthy humans. *Hippokratia* **2013**, *17*, 64–67.
108. Seok, J.; Kim, T.S.; Kwon, H.J.; Lee, S.P.; Kang, M.H.; Kim, B.J.; Kim, M.N. Efficacy of *Cistanche Tubulosa* and *Laminaria Japonica* Extracts (MK-R7) Supplement in Preventing Patterned Hair Loss and Promoting Scalp Health. *Clin. Nutr. Res.* **2015**, *4*, 124–131. [CrossRef]
109. Kamimura, A.; Takahashi, T.; Watanabe, Y. Investigation of topical application of procyanidin B-2 from apple to identify its potential use as a hair growing agent. *Phytomedicine* **2000**, *7*, 529–536. [CrossRef]
110. Sharma, B.; Kumar, P.; Joshi, S.C. Topical Treatment of Dermatophytic Lesion on Mice (*Mus musculus*) Model. *Indian J. Microbiol.* **2011**, *51*, 217–222. [CrossRef]
111. Romero-Cerecero, O.; Rojas, G.; Navarro, V.; Herrera-Arellano, A.; Zamilpa-Álvarez, A.; Tortoriello, J. Effectiveness and tolerability of a standardized extract from *Ageratina pichinchensis* on patients with tinea pedis: An explorative pilot study controlled with ketoconazole. *Planta Medica* **2006**, *72*, 1257–1261. [CrossRef]
112. Herrera-Arellano, A.; Rodríguez-Soberanes, A.; de los Angeles Martínez-Rivera, M.; Martínez-Cruz, E.; Zamilpa, A.; Alvarez, L.; Tortoriello, J. Effectiveness and tolerability of a standardized phytodrug derived from *Solanum chrysotrichum* on *Tinea pedis*: A controlled and randomized clinical trial. *Planta Med.* **2003**, *69*, 390–395. [PubMed]
113. Romero-Cerecero, O.; Islas-Garduño, A.L.; Zamilpa, A.; Tortoriello, J. Effectiveness of an encecalin standardized extract of *Ageratina pichinchensis* on the treatment of onychomycosis in patients with diabetes mellitus. *Phytother. Res.* **2020**, *34*, 1678–1686. [CrossRef] [PubMed]
114. Herrera-Arellano, A.; Jiménez-Ferrer, E.; Vega-Pimentel, A.M.; de los Angeles Martínez-Rivera, M.; Hernández-Hernández, M.; Zamilpa, A.; Tortoriello, J. Clinical and mycological evaluation of therapeutic effectiveness of *Solanum chrysotrichum* standardized extract on patients with *Pityriasis capitis* (dandruff). A double blind and randomized clinical trial controlled with ketoconazole. *Planta Med.* **2004**, *70*, 483–488. [CrossRef] [PubMed]
115. Ngatu, N.R.; Saruta, T.; Hirota, R.; Eitoku, M.; Luzitu, N.S.; Muzembo, B.A.; Matsui, T.; Suganuma, N. Brazilian green propolis extracts improve *Tinea pedis* interdigitalis and Tinea corporis. *J. Altern. Complement. Med.* **2012**, *18*, 8–9. [CrossRef] [PubMed]
116. Ngatu, N.R.; Saruta, T.; Hirota, R.; Eitoku, M.; Muzembo, B.A.; Matsui, T.; Nangana, L.S.; Mbenza, M.A.; Kumagai, N.; Suganuma, N. Antifungal efficacy of Brazilian green propolis extracts and honey on Tinea capitis and Tinea versicolor. *Eur. J. Integr. Med.* **2011**, *3*, e281–e287. [CrossRef]
117. Obot, M.J.; Aluyi, H.S. Treatment of superficial mycoses with *Ocimum gratissimum*. *Int. J. Infect. Dis.* **2002**, *6*, 151. [CrossRef] [PubMed]
118. Oyelami, O.A.; Onayemi, O.; Oladimeji, F.A.; Ogundaini, A.O.; Olugbade, T.A.; Onawunmi, G.O. Clinical evaluation of Acalypha ointment in the treatment of superficial fungal skin diseases. *Phytother. Res.* **2003**, *17*, 555–557. [CrossRef]

119. Carmo, E.S.; Pereira, F.d.O.; Cavalcante, N.M.; Gayoso, C.W.; Lima, E.d.O. Treatment of pityriasis versicolor with topical application of essential oil of *Cymbopogon citratus* (DC) Stapf—Therapeutic pilot study. *An. Bras. Dermatol.* **2013**, *88*, 381–385. [CrossRef]
120. Damodaran, S.; Venkataraman, S. A study on the therapeutic efficacy of *Cassia alata*, Linn. leaf extract against *Pityriasis versicolor*. *J. Ethnopharmacol.* **1994**, *42*, 19–23. [CrossRef]
121. Buck, D.S.; Nidorf, D.M.; Addino, J.G. Comparison of two topical preparations for the treatment of onychomycosis: Melaleuca alternifolia (tea tree) oil and clotrimazole. *J. Fam. Pract.* **1994**, *38*, 601–605.
122. Patrizi, A.; Raone, B.; Neri, I.; Gurioli, C.; Carbonara, M.; Cassano, N.; Vena, G.A. Randomized, controlled, double-blind clinical study evaluating the safety and efficacy of MD2011001 cream in mild-to-moderate atopic dermatitis of the face and neck in children, adolescents and adults. *J. Dermatol. Treat.* **2016**, *27*, 346–350. [CrossRef] [PubMed]
123. Brasiel, P.G.d.A.; Guimarães, F.V.; Rodrigues, P.M.; Bou-Habib, D.C.; Carvalho, V.d.F. Therapeutic Efficacy of Flavonoids in Allergies: A Systematic Review of Randomized Controlled Trials. *J. Immunol. Res.* **2022**, *2022*, 8191253. [CrossRef]
124. Zhao, H.; Zhu, W.; Jia, L.; Sun, X.; Chen, G.; Zhao, X.; Li, X.; Meng, X.; Kong, L.; Xing, L.; et al. Phase I study of topical epigallocatechin-3-gallate (EGCG) in patients with breast cancer receiving adjuvant radiotherapy. *Br. J. Radiol.* **2016**, *89*, 20150665. [CrossRef]
125. Xie, J.; Jia, L.; Xie, P.; Yin, X.; Zhu, W.; Zhao, H.; Wang, X.; Meng, X.; Xing, L.; Zhao, H.; et al. Efficacy and safety of epigallocatechin-3-gallate in treatment acute severe dermatitis in patients with cancer receiving radiotherapy: A phase I clinical trial. *Sci. Rep.* **2023**, *13*, 13865. [CrossRef] [PubMed]
126. Karbasforooshan, H.; Hosseini, S.; Elyasi, S.; Pakdel, A.F.; Karimi, G. Topical silymarin administration for prevention of acute radiodermatitis in breast cancer patients: A randomized, double-blind, placebo-controlled clinical trial. *Phytother. Res.* **2019**, *33*, 379–386. [CrossRef]
127. Magrone, T.; Jirillo, E.; Magrone, M.; Russo, M.A.; Romita, P.; Massari, F.; Foti, C. Red Grape Polyphenol Oral Administration Improves Immune Response in Women Affected by Nickel-Mediated Allergic Contact Dermatitis. *Endocr. Metab. Immune Disord.-Drug Targets* **2021**, *21*, 374–384. [CrossRef]
128. Costa, A.; Bonner, M.Y.; Arbiser, J.L. Use of Polyphenolic Compounds in Dermatologic Oncology. *Am. J. Clin. Dermatol.* **2016**, *17*, 369–385. [CrossRef]
129. Liu, H.-M.; Cheng, M.-Y.; Xun, M.-H.; Zhao, Z.-W.; Zhang, Y.; Tang, W.; Cheng, J.; Ni, J.; Wang, W. Possible Mechanisms of Oxidative Stress-Induced Skin Cellular Senescence, Inflammation, and Cancer and the Therapeutic Potential of Plant Polyphenols. *Int. J. Mol. Sci.* **2023**, *24*, 3755. [CrossRef] [PubMed]
130. Trindade, L.R.; da Silva, D.V.T.; Baião, D.d.S.; Paschoalin, V.M.F. Increasing the Power of Polyphenols through Nanoencapsulation for Adjuvant Therapy against Cardiovascular Diseases. *Molecules* **2021**, *26*, 4621. [CrossRef] [PubMed]
131. Bilia, A.R.; Piazzini, V.; Risaliti, L.; Vanti, G.; Casamonti, M.; Wang, M.; Bergonzi, M.C. Nanocarriers: A Successful Tool to Increase Solubility, Stability and Optimise Bioefficacy of Natural Constituents. *Curr. Med. Chem.* **2019**, *26*, 4631–4656. [CrossRef]
132. Iqubal, M.K.; Iqubal, A.; Imtiyaz, K.; Rizvi, M.M.A.; Gupta, M.M.; Ali, J.; Baboota, S. Combinatorial lipid-nanosystem for dermal delivery of 5-fluorouracil and resveratrol against skin cancer: Delineation of improved dermatokinetics and epidermal drug deposition enhancement analysis. *Eur. J. Pharm. Biopharm.* **2021**, *163*, 223–239. [CrossRef]
133. Menaa, F.; Menaa, A.; Menaa, B. Polyphenols Nano-Formulations for Topical Delivery and Skin Tissue Engineering. In *Polyphenols in Human Health and Disease*; Elsevier: Amsterdam, The Netherlands, 2014; pp. 839–848. [CrossRef]
134. Qadir, A.; Aqil, M.; Ali, A.; Warsi, M.H.; Mujeeb, M.; Ahmad, F.J.; Ahmad, S.; Beg, S. Nanostructured lipidic carriers for dual drug delivery in the management of psoriasis: Systematic optimization, dermatokinetic and preclinical evaluation. *J. Drug Deliv. Sci. Technol.* **2020**, *57*, 101775. [CrossRef]
135. Hasan, N.; Imran, M.; Nadeem, M.; Jain, D.; Haider, K.; Alam Rizvi, M.M.; Sheikh, A.; Kesharwani, P.; Jain, G.K.; Ahmad, F.J. Formulation and development of novel lipid-based combinatorial advanced nanoformulation for effective treatment of non-melanoma skin cancer. *Int. J. Pharm.* **2023**, *632*, 122580. [CrossRef]
136. Gupta, N.K.; Dixit, V.K. Development and evaluation of vesicular system for curcumin delivery. *Arch. Dermatol. Res.* **2011**, *303*, 89–101. [CrossRef] [PubMed]
137. Trepa, M.; Sułkowska-Ziaja, K.; Kała, K.; Muszyńska, B. Therapeutic Potential of Fungal Terpenes and Terpenoids: Application in Skin Diseases. *Molecules* **2024**, *29*, 1183. [CrossRef] [PubMed]
138. Stevanović, Z.D.; Aligiannis, N.; Graikou, K.; Bilia, A.R.; Kolašinac, S.; Kilibarda, S. Bioactivity of carotenoids and their role in skin disorders: From tradition to application. *Maced. Pharm. Bull.* **2022**, *68*, 149–150. [CrossRef]
139. Maurya, S.K.; Divakar, S.; Patil, U.K. Potentials of plant derived products for the treatment of skin disorders. *Ger. J. Pharm. Biomater.* **2023**, *2*, 9–31. [CrossRef]
140. Park, J.; Nguyen, T.M.N.; Park, H.-A.; Nguyen, M.T.T.; Lee, N.-Y.; Ban, S.-Y.; Park, K.-B.; Lee, C.-K.; Kim, J.; Park, J.-T. Protective Effects of Lanostane Triterpenoids from Chaga Mushroom in Human Keratinocytes, HaCaT Cells, against Inflammatory and Oxidative Stresses. *IJMS* **2023**, *24*, 12803. [CrossRef]

141. Yan, Z.F.; Yang, Y.; Tian, F.H.; Mao, X.X.; Li, Y.; Li, C.T. Inhibitory and Acceleratory Effects of *Inonotus obliquus* on Tyrosinase Activity and Melanin Formation in B16 Melanoma Cells. *Evid.-Based Complement. Altern. Med.* **2014**, *2014*, 259836. [CrossRef]
142. Kreuzenbeck, N.B.; Dhiman, S.; Roman, D.; Burkhardt, I.; Conlon, B.H.; Fricke, J.; Guo, H.; Blume, J.; Görls, H.; Poulsen, M.; et al. Isolation, (bio)synthetic studies and evaluation of antimicrobial properties of drimenol-type sesquiterpenes of *Termitomyces* fungi. *Commun. Chem.* **2023**, *6*, 79. [CrossRef]
143. Ahmad, M.F. Ganoderma lucidum: A rational pharmacological approach to surmount cancer. *J. Ethnopharmacol.* **2020**, *260*, 113047. [CrossRef]
144. Ren, Q.; Lu, X.-Y.; Han, J.-X.; Aisa, H.A.; Yuan, T. Triterpenoids and phenolics from the fruiting bodies of *Inonotus hispidus* and their activations of melanogenesis and tyrosinase. *Chin. Chem. Lett.* **2017**, *28*, 1052–1056. [CrossRef]
145. Darvin, M.E.; Sterry, W.; Lademann, J.; Vergou, T. The Role of Carotenoids in Human Skin. *Molecules* **2011**, *16*, 10491–10506. [CrossRef]
146. I Ibiebele, T.; van der Pols, J.C.; Hughes, M.C.; Marks, G.C.; Williams, G.M.; Green, A.C. Dietary pattern in association with squamous cell carcinoma of the skin: A prospective study. *Am. J. Clin. Nutr.* **2007**, *85*, 1401–1408. [CrossRef]
147. Fortes, C.; Mastroeni, S.; Melchi, F.; A Pilla, M.; Antonelli, G.; Camaioni, D.; Alotto, M.; Pasquini, P. A protective effect of the Mediterranean diet for cutaneous melanoma. *Leuk. Res.* **2008**, *37*, 1018–1029. [CrossRef]
148. Heinen, M.M.; Hughes, M.C.; Ibiebele, T.I.; Marks, G.C.; Green, A.C.; van der Pols, J.C. Intake of antioxidant nutrients and the risk of skin cancer. *Eur. J. Cancer* **2007**, *43*, 2707–2716. [CrossRef]
149. Palombo, P.; Fabrizi, G.; Ruocco, V.; Ruocco, E.; Fluhr, J.; Roberts, R.; Morganti, P. Beneficial Long-Term Effects of Combined Oral/Topical Antioxidant Treatment with the Carotenoids Lutein and Zeaxanthin on Human Skin: A Double-Blind, Placebo-Controlled Study. *Ski. Pharmacol. Physiol.* **2007**, *20*, 199–210. [CrossRef]
150. Heinrich, U.; Wiebusch, M.; Tronnier, H.; Gärtner, C.; Eichler, O.; Sies, H.; Stahl, W. Supplementation with β-Carotene or a Similar Amount of Mixed Carotenoids Protects Humans from UV-Induced Erythema. *J. Nutr.* **2003**, *133*, 98–101. [CrossRef]
151. Biskanaki, F.; Kalofiri, P.; Tertipi, N.; Sfyri, E.; Andreou, E.; Kefala, V.; Rallis, E. Carotenoids and Dermoaesthetic Benefits: Public Health Implications. *Cosmetics* **2023**, *10*, 120. [CrossRef]
152. Wróbel-Biedrawa, D.; Grabowska, K.; Galanty, A.; Sobolewska, D.; Żmudzki, P.; Podolak, I. Anti-melanoma potential of two benzoquinone homologues embelin and rapanone—A comparative in vitro study. *Toxicol. In Vitro* **2020**, *65*, 104826. [CrossRef] [PubMed]
153. Babu, A.; Laila, S.P.; Fernandez, A. A Fluoro Derivative of Embelin, as Potent B-RAF Inhibitor in Melanoma. *Anti-Cancer Agents Med. Chem.* **2021**, *21*, 2066–2074. [CrossRef] [PubMed]
154. Kamath, A.J.; Chandy, A.S.; Joseph, A.A.; Gorantla, J.N.; Donadkar, A.D.; Nath, L.R.; Sharifi-Rad, J.; Calina, D. Embelin: A multifaceted anticancer agent with translational potential in targeting tumor progression and metastasis. *EXCLI J.* **2023**, *22*, 1311–1329. [CrossRef]

Disclaimer/Publisher's Note: The statements, opinions and data contained in all publications are solely those of the individual author(s) and contributor(s) and not of MDPI and/or the editor(s). MDPI and/or the editor(s) disclaim responsibility for any injury to people or property resulting from any ideas, methods, instructions or products referred to in the content.

pharmaceuticals

MDPI

Article

Effects of Hispidulin on the Osteo/Odontogenic and Endothelial Differentiation of Dental Pulp Stem Cells

Yeon Kim [1,2,3], Hyun-Joo Park [1,2,3], Mi-Kyoung Kim [1,2], Hyung Joon Kim [1,2,3], Yong-Il Kim [3,4], Soo-Kyung Bae [2,3,5] and Moon-Kyoung Bae [1,2,3,*]

[1] Department of Oral Physiology, School of Dentistry, Pusan National University, Yangsan 50612, Republic of Korea; hjoonkim@pusan.ac.kr (H.J.K.)
[2] Periodontal Disease Signaling Network Research Center (MRC), School of Dentistry, Pusan National University, Yangsan 50612, Republic of Korea; skbae@pusan.ac.kr
[3] Dental and Life Science Institute, School of Dentistry, Pusan National University, Yangsan 50612, Republic of Korea
[4] Department of Orthodontics, School of Dentistry, Pusan National University, Yangsan 50612, Republic of Korea
[5] Department of Dental Pharmacology, School of Dentistry, Pusan National University, Yangsan 50612, Republic of Korea
* Correspondence: mkbae@pusan.ac.kr; Tel.: +82-51-510-8239; Fax.: +82-51-510-8238

Abstract: Background: Human dental pulp stem cells (HDPSCs) with multi-lineage differentiation potential and migration ability are required for HDPSC-based bone and dental regeneration. Hispidulin is a naturally occurring flavonoid with diverse pharmacological activities, but its effects on biological properties of HDPSCs remain unknown. Therefore, we investigated the effects of hispidulin on the differentiation potential and migration ability of HDPSCs and elucidated their underlying mechanisms. **Methods:** The osteo/odontogenic capacity of HDPSCs was assessed using the alkaline phosphatase (ALP) and Alizarin Red S (ARS) staining. The migration ability of HDPSCs was evaluated using a scratch wound assay. Furthermore, the endothelial differentiation of HDPSCs was examined by using a capillary sprouting assay and by assessing CD31 expression. **Results:** Hispidulin significantly enhanced the osteo/odontogenic differentiation of HDPSCs with increased expression of osteo/odontogenic differentiation markers. Hispidulin increased the migration of HDPSCs, which was mediated by the upregulation of C-X-C chemokine receptor type 4 (CXCR4). The treatment of HDPSCs with hispidulin enhanced the differentiation of HDPSCs into endothelial cells, as evidenced by increased capillary sprouting and endothelial marker expression. In addition, we demonstrated that hispidulin activated the ERK1/2 signaling, and its inhibition by U0126 significantly suppressed the hispidulin-induced endothelial differentiation of HDPSCs. **Conclusions:** These findings demonstrate that hispidulin effectively promotes the osteo/odontogenic and endothelial differentiation, and migration of HDPSCs. These results suggest that hispidulin may have potential therapeutic applications in dental pulp regeneration and tissue engineering.

Keywords: hispidulin; dental pulp stem cells; differentiation

1. Introduction

Human dental pulp stem cells (HDPSCs) are derived from the connective soft tissue within the dental pulp chamber surrounding hard tissues [1]. HDPSCs have emerged as promising sources of mesenchymal stem cells for regenerative medicine due to their proliferative capacity, ready accessibility from extracted teeth, and remarkable multipotency [2]. Their potential for both osteogenic and odontogenic differentiation increases their value for the regeneration of mineralized tissues, such as bone and dentin [2]. Moreover, recent studies have highlighted the endothelial differentiation capacity of HDPSCs, revealing their ability to express endothelial-specific markers, such as CD31 and the von Willebrand

factor, and form capillary-like sprouting structures in vitro [3]. The capacity of HDPSCs to differentiate into both osteo/odontogenic and endothelial cells is particularly significant for tissue engineering applications, enabling the simultaneous development of mineralized structures and essential vessel networks within bioengineered tissues [4,5].

Hispidulin (chemically known as 4′,5,7-trihydroxy-6-methoxyflavone) is a naturally occurring flavonoid found in various medicinal plants such as *Arrabidaea chica*, *Salvia involucrata*, and *Saussurea involucrata* [6,7]. Hispidulin has recently significant attention owing to its diverse pharmacological properties including anti-inflammatory, antioxidant, anticancer, and neuroprotective effects [8–12]. Some flavonoids, including isocoumarin and icariin, have been demonstrated to play crucial roles in bone metabolism by regulating osteoblast and osteoclast differentiation [13,14]. Recent studies have demonstrated that hispidulin represses bone resorption in receptor activator of the nuclear factor κB (NF-κB) ligand (RANKL)-stimulated osteoclast precursor cells and promotes osteoblastic differentiation in MC3T3E1 cells [15]. However, its effects on the biological properties of HDPSCs, including their proliferation, migration, and differentiation, remain unclear.

We investigated the effects of hispidulin on the osteo/odontogenic and endothelial differentiation of HDPSCs and elucidated the underlying mechanisms by which hispidulin has influences on the differentiation process.

2. Results

2.1. Hispidulin Accelerates the Osteo/Odontogenic Differentiation of HDPSCs

We first investigated the effects of hispidulin on the osteo/odontogenic differentiation of HDPSCs, for which we examined their mineralization activity using alkaline phosphatase (ALP) staining. HDPSCs cultured in the osteogenic differentiation medium (ODM) exhibited increased ALP activity compared with those cultured in the basic growth medium. This effect was significantly enhanced by hispidulin treatment, as evidenced by the increased staining intensity at both the 7- and 14-day time points (Figure 1A). Furthermore, Alizarin Red S (ARS) staining was performed to confirm the mineralization-promoting effects of hispidulin. Hispidulin treatment markedly enhanced calcium nodule formation in HDPSCs cultured in the ODM for 14 and 21 days (Figure 1B). In addition, we examined the expression of osteo/odontogenic differentiation-related markers. Real-time polymerase chain reaction (PCR) revealed that hispidulin treatment significantly upregulated the expression of ALP, osteocalcin, Runt-related transcription factor 2 (Runx-2), and dentin matrix protein-1 (DMP-1) in ODM-cultured HDPSCs (Figure 1C). Notably, treatment with 10 μM of hispidulin resulted in more pronounced effects, inducing approximately 2.3-fold, 2.3-fold, 2.4-fold, and 2.5-fold increases in the expression of *ALP*, *osteocalcin*, *Runx-2*, and *DMP-1*, respectively, compared to untreated ODM-cultured HDPSCs.

2.2. Hispidulin Increases the Migration Ability of HDPSCs

We adopted the scratch wound migration assay to investigate the migratory capacity of HDPSCs in response to hispidulin treatment. Both 1 μM and 5 μM hispidulin treatment significantly enhanced cell migration by approximately 180% and 210%, respectively, compared to untreated controls (Figure 2A). Based on the important role of C-X-C chemokine receptor type 4 (CXCR4) in the migration and recruitment of HDPSCs [16], we examined whether hispidulin affects the expressions of CXCR4 in HDPSCs. The treatment of HDPSCs with hispidulin increased the mRNA and protein expression of CXCR4 in HDPSCs, as demonstrated by qRT-PCR and western blotting (Figure 2B,C). We treated HDPSCs with AMD3100, a specific CXCR4 antagonist, to address the involvement of CXCR4 signaling in hispidulin-induced migration [17]. As shown in Figure 2D, treatment with AMD3100 caused a 47% reduction in hispidulin-induced HDPSC migration.

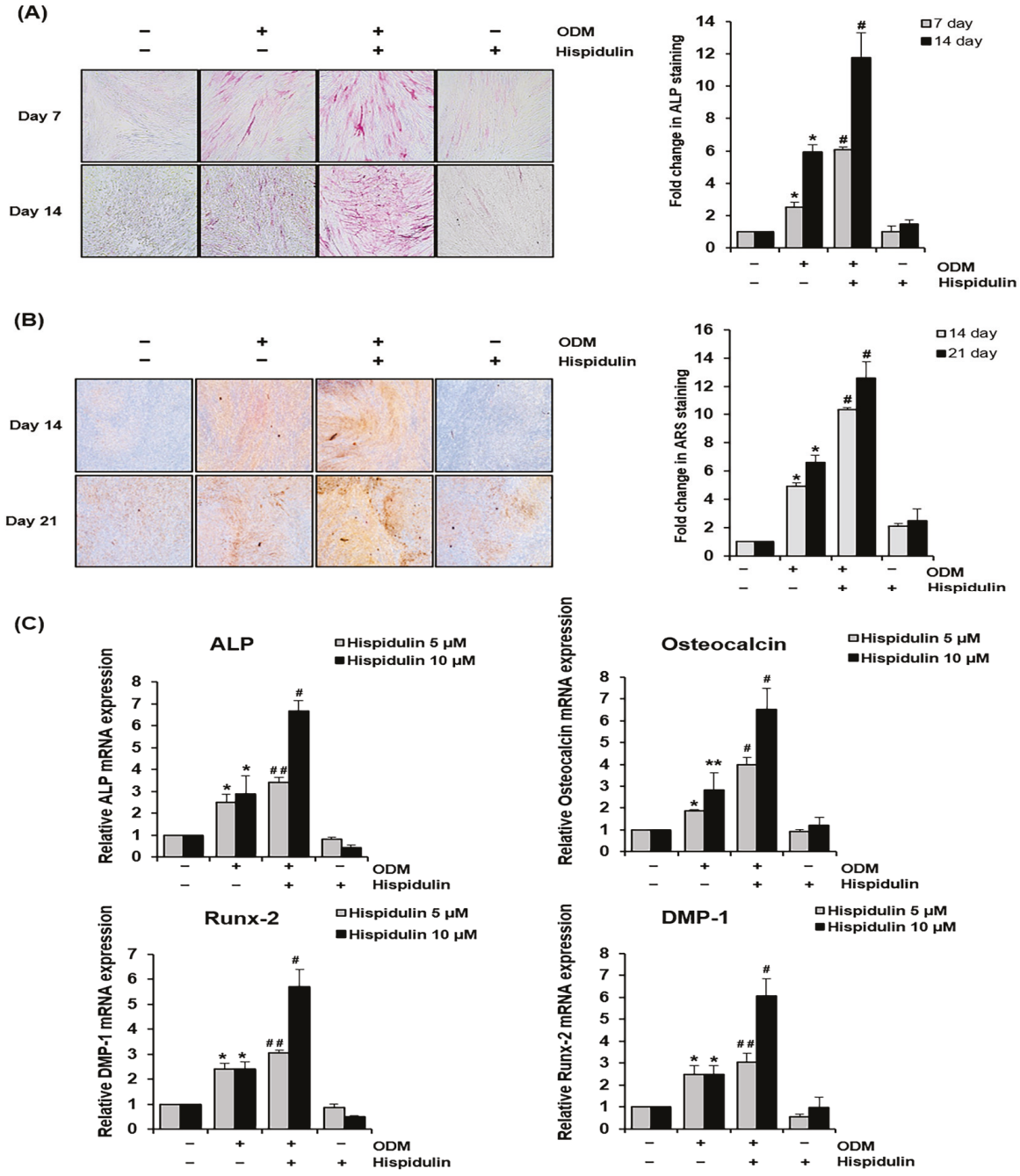

Figure 1. Effect of hispidulin on osteo/odontogenic differentiation and expression of osteo/odontogenic-related markers in HDPSCs. (**A**) HDPSCs were either cultured in the basic growth medium or osteogenic differentiation medium (ODM) with or without hispidulin (5 μM). ALP staining was performed on days 7 and 14. Stained cells were photographed using a phase contrast microscope at 100× magnification. ALP-positive areas were quantified by densitometry in triplicates. * $p < 0.01$ compared to control. # $p < 0.05$ compared to ODM. (**B**) The formation of mineralized nodules was evaluated by ARS staining and quantified through densitometric analysis in triplicate at days 14 and 21. The stained cells were imaged under 100× magnification. * $p < 0.01$ compared to control. # $p < 0.01$ compared to ODM. (**C**) HDPSCs were cultured with or without ODM in the presence of hispidulin for 14 days. The mRNA expression of *ALP*, *osteocalcin*, *DMP-1*, *and Runx-2* were assessed through real-time PCR analysis. All values were normalized to β-actin mRNA levels, and the expression level of the control group was designated as 1.0. * $p < 0.01$ compared to control. ** $p < 0.05$ compared to control. # $p < 0.01$ compared to ODM. ## $p < 0.05$ compared to ODM.

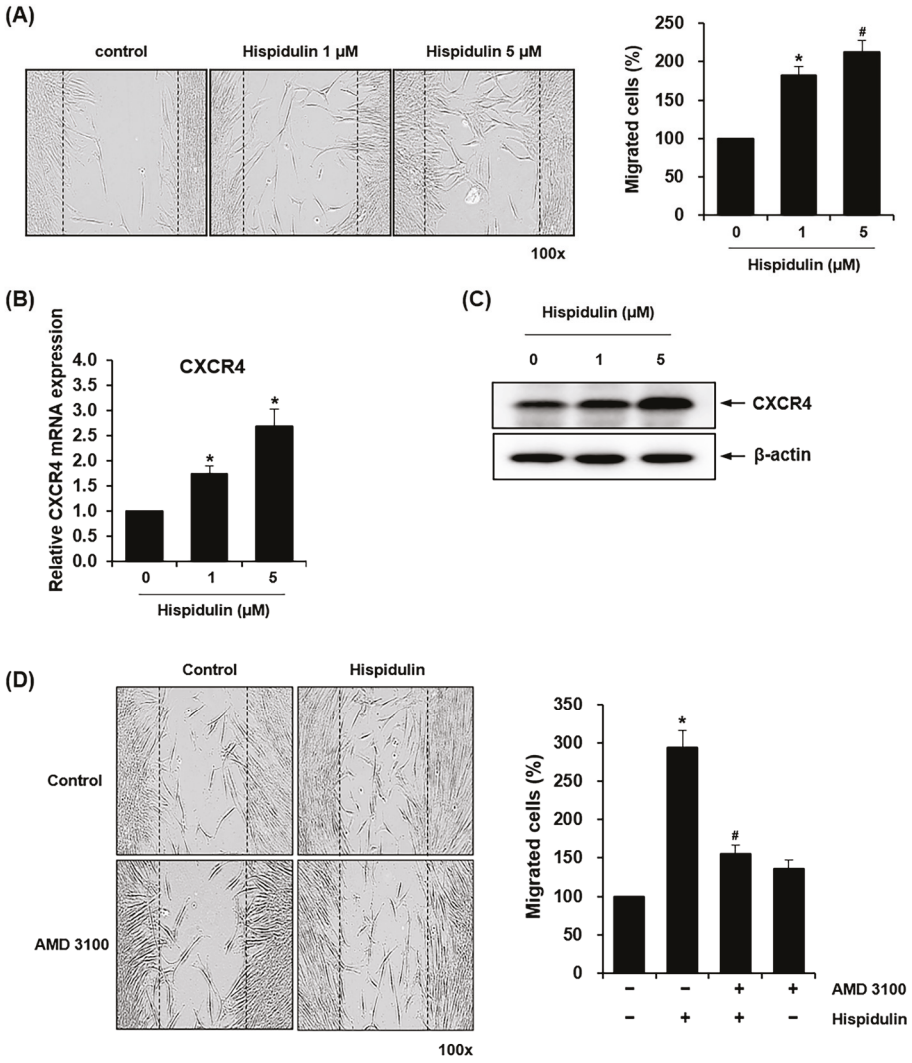

Figure 2. Effect of hispidulin on the migration of HDPSCs. (**A**) Scratch wound migration assays were performed on HDPSCs cultured without or with hispidulin (1 or 5 μM) for 24 h. Cell migration into the scratch wound area was photographed at 100× magnification and quantified. Results are expressed as the mean values from three independent experiments per group. * $p < 0.05$ compared with control. # $p < 0.01$ compared with control. (**B**) HDPSCs were treated with hispidulin (1 or 5 μM) for 24 h, and the expression of CXCR4 was analyzed with real-time qPCR. All values were normalized to β-actin mRNA levels, with the control group expression set as 1.0. * $p < 0.05$ compared with control. (**C**) Protein expression of CXCR4 was observed by western blotting using an anti-CXCR4 antibody (upper) and densitometric analysis (lower). β-actin was used as the loading control. (**D**) HDPSCs were incubated with 1 μM hispidulin alone or in combination with AMD3100 (50 μg/mL) for 24 h. Migrated cells beyond the reference line were photographed at 100× magnification and quantified. * $p < 0.01$ compared with control. # $p < 0.01$ compared to hispidulin.

2.3. Hispidulin Enhances the Endothelial Differentiation of HDPSCs via CD31 Expression

We used a capillary sprouting assay to assess the endothelial differentiation potential of HDPSCs [18,19]. HDPSCs were cultured in an endothelial differentiation medium (EGM-2MV) supplemented with hispidulin. HDPSCs treated with hispidulin demonstrated increased capillary sprouting compared with the control group. Quantitative analysis revealed progressive capillary sprouting at days 3, 5, and 7 of hispidulin treatment, with the most pronounced effect observed on day 7 (Figure 3A). We examined the expression of the endothelial marker CD31 using western blotting and fluorescence-activated cell sorting (FACS) analysis to further elucidate the effect of hispidulin on the endothelial

differentiation of HDPSCs. Western blotting demonstrated that CD31 protein expression increased in hispidulin-treated HDPSCs (Figure 3B). The cell surface expression of CD31 was further confirmed by flow cytometry to quantify the antigenic activity of proteins on the cell surface. The percentage of CD31-positive cells gradually increased from 1.43% under control conditions to 8.23%, 10.39%, and 23.17% after 3, 5, and 7 days of hispidulin treatment, respectively (Figure 3C).

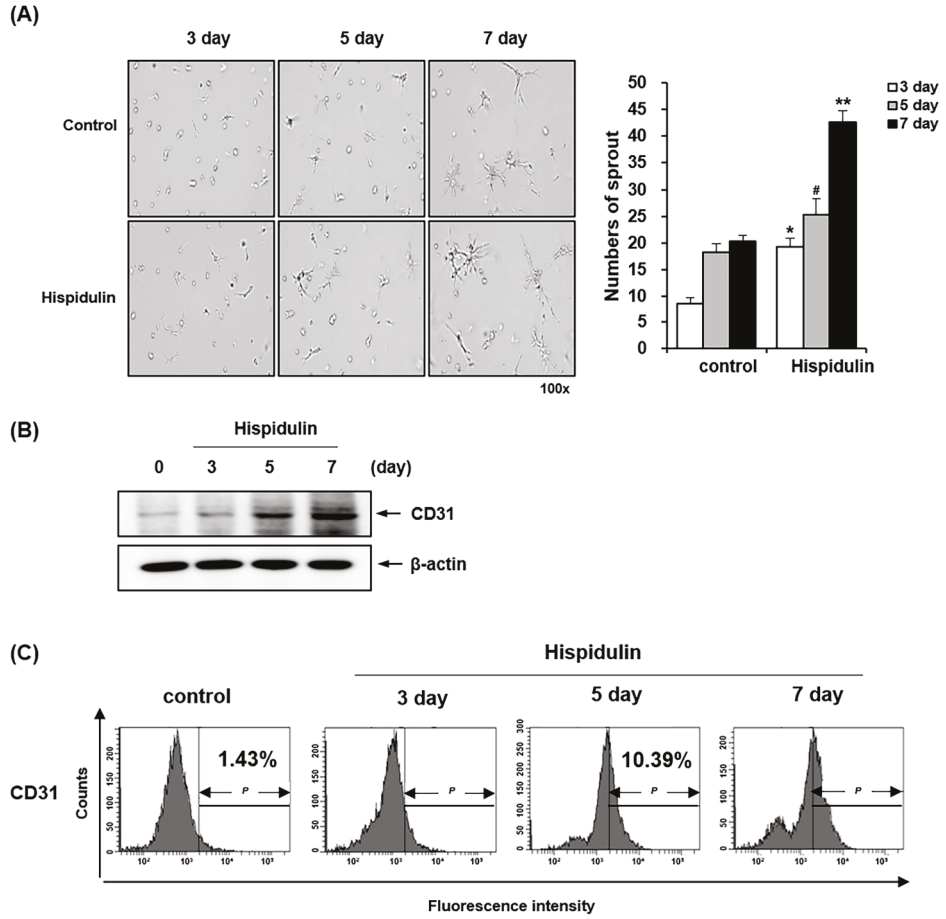

Figure 3. Effect of hispidulin on endothelial differentiation of HDPSCs. (**A**) HDPSCs implanted on a Matrigel-coated plate were treated with 1 μM hispidulin for 3, 5, and 7 days in the EGM-2MV. The numbers of sprouts were counted and imaged under 100× magnification. Each result represents the mean value of triplicate experiments in each group. * $p < 0.01$ compared with the 3-days control. # $p < 0.05$ compared with 5-dayscontrol. ** $p < 0.01$ compared with the 7-days control. (**B**) The protein expression of CD31 was analyzed by western blotting. β-actin was used as a loading control. (**C**) HDPSCs were treated with 1 μM hispidulin for 3, 5, and 7 days. CD31 was measured by flow cytometry.

2.4. ERK1/2 Mediates Hispidulin-Induced Endothelial Differentiation of HDPSCs

We investigated whether hispidulin treatment activated the ERK1/2 signaling pathway during the endothelial differentiation of HDPSCs. It has been previously reported that the ERK1/2 signaling plays a pivotal role in regulating the differentiation of HDPSCs into endothelial cells [20]. Western blotting revealed that the levels of phosphorylated ERK1/2 peaked 15 min after hispidulin treatment (Figure 4A). Pretreatment of HDPSCs with U0126, a mitogen-activated protein kinase (MAPK)/ERK kinase-specific inhibitor, blocked CD31 protein expression induced by hispidulin (Figure 4B). To investigate the role of ERK1/2 in hispidulin-induced endothelial differentiation of HDPSCs, HDPSCs were pretreated with U0126 before hispidulin treatment. As shown in Figure 4C, U0126 significantly suppressed hispidulin-induced sprouting formation in HDPSCs.

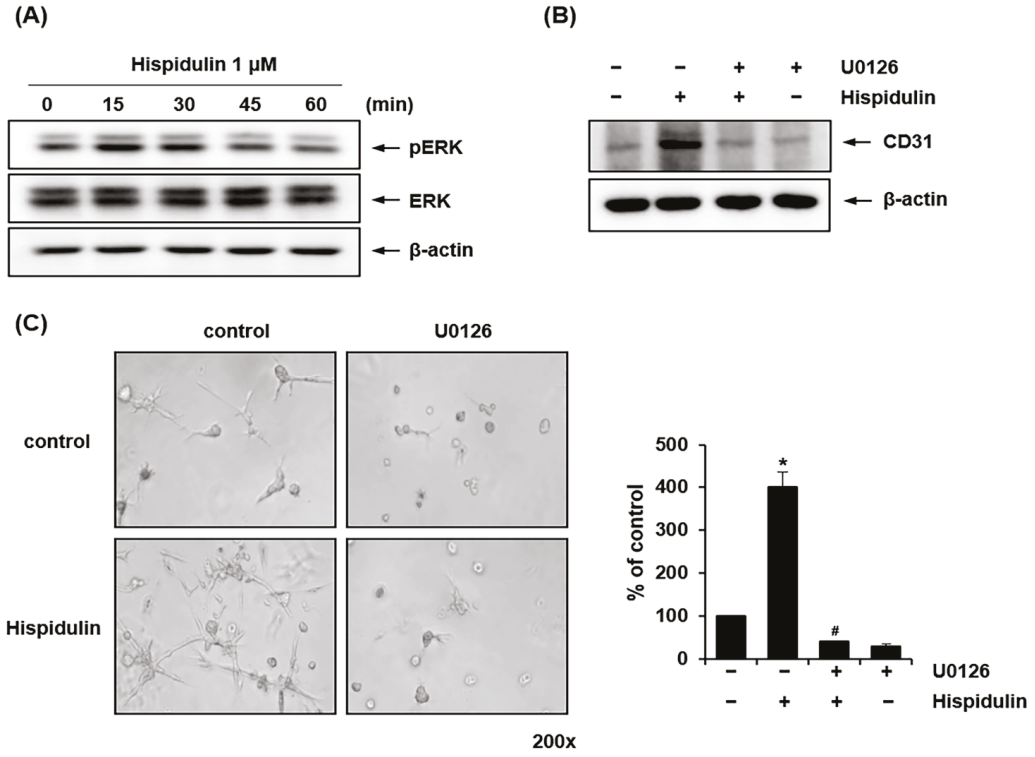

Figure 4. Effect of hispidulin on the ERK signaling pathway in endothelial differentiation of HDPSCs. (**A**) HDPSCs were treated with hispidulin (1 μM) for the indicated times in EGM-2MV. Cell lysates were immunoblotted with antibodies against phospho-ERK and total ERK. β-actin was used as a loading control. (**B**) HDPSCs were treated with hispidulin (1 μM) alone or in combination with U0126 (10 μM). After 7 days, CD31 protein expression was analyzed by western blotting. β-actin was used as a loading control. (**C**) HDPSCs were seeded on Matrigel-coated plates and treated with hispidulin (1 μM) alone or in combination with U0126 (10 μM) in EGM-2MV. Capillary sprouting was observed after 7 days (200× magnification). Images are representative of three independent experiments. * $p < 0.01$ compared to control. # $p < 0.01$ compared to hispidulin.

3. Discussion

Hispidulin, a naturally occurring flavone found in several medicinal plants, is a highly promising bioactive compound with a remarkable spectrum of pharmacological activities, including antioxidant, antifungal, antitumor, anti-inflammatory, and neuroprotective properties [8–12]. Recently, the inhibitory effects of hispidulin on RANKL-induced osteoclastogenesis and bone resorption have been demonstrated [15]. Hispidulin increased the ALP activity of MC3T3E1 cells while simultaneously inhibiting osteoclast formation in RAW 264.7 cells and bone marrow-derived macrophages (BMMs), thereby maintaining bone homeostasis [15]. We found that hispidulin promoted the osteogenic/odontogenic differentiation of HDPSCs by upregulating osteo/odontogenic-related proteins. These observations indicate that hispidulin exerts its regulatory effects on bone homeostasis by influencing both bone resorption and formation. This finding may provide a promising therapeutic potential for bone-related disorders.

Flavonoids have a remarkable ability to promote the osteogenic and endothelial differentiation of mesenchymal stem cells derived from various tissue sources, including bone marrow, adipose tissue, and dental tissues [21,22]. Naringenin, a flavanone-type flavonoid, has been reported to enhance both osteogenic and endothelial differentiation of human periodontal ligament stem cells, contributing to alveolar bone regeneration [23]. Similarly, icariin, a prenylated flavonol glycoside, has demonstrated the ability to promote bone regeneration under diabetic conditions through simultaneous activation of osteogenesis and angiogenesis in bone marrow mesenchymal stem cells [24]. Given that the coupling of

osteogenesis and neovascularization is crucial for successful bone regeneration [25], our findings suggest that hispidulin may facilitate bone regeneration through its dual effects on osteogenic and endothelial differentiation.

In addition to their osteogenic/odontogenic differentiation capacity, HDPSCs possess vasculogenic differentiation potential, highlighting their promising utility in regenerative medicine and tissue engineering [26,27]. In particular, HDPSCs naturally differentiate into odontoblast-like cells at the injury site in the dental pulp to produce reparative dentin as a protective barrier [28]. In addition, HDPSCs can differentiate into vascular endothelial lineages, forming vascular networks essential for delivering oxygen and nutrients [29,30]. We observed that hispidulin promoted capillary sprouting of HDPSCs in Matrigel and increased the protein expression of endothelial cell markers, particularly CD31, in HDPSCs, suggesting a stimulatory effect of hispidulin on the endothelial differentiation of HDPSCs in vitro. Research has shown that the tooth slice/scaffold model provides a valuable in vivo approach to assess the impact of bioactive compounds, such as flavonoids and growth factors, on the differentiation potential of dental pulp stem cells [17,31,32]. Although our findings demonstrated promising effects of hispidulin on osteogenic/odontogenic and endothelial differentiation, further in vivo studies using tooth slice/scaffold models are warranted to validate these results and evaluate the functional integration of differentiated cells within the host tissue.

Our results demonstrated that hispidulin enhanced ERK1/2 phosphorylation in HDPSCs cultured in the EGM-2MVmedium, and the inhibition of MAPK/ERK kinase suppressed both, hispidulin-induced endothelial cell marker expression and hispidulin-stimulated formation of sprout-like structures in HDPSCs. The MAPK/ERK pathway plays a crucial role in mediating endothelial differentiation of different mesenchymal stem cells, including adipose tissue-derived stem cells, bone marrow mesenchymal stem cells, and stem cells from exfoliated deciduous teeth (SHEDs) [20,33,34]. Previous study has demonstrated that hispidulin treatment inhibits transforming growth factor-β1 (TGF-β1)-induced Smad2/3 signaling in cancer cell lines [35]. Furthermore, the inhibition of TGF-β signaling has been shown to enhance endothelial differentiation in SHEDs [36]. Based on these findings, we hypothesize that hispidulin may enhance endothelial differentiation of HDPSCs through the inhibition of TGF-β1-induced Smad2/3 signaling pathway. In addition, the activation of Wnt/β-catenin signaling is involved in vasculogenic differentiation of dental stem cells [37]. We are investigating whether hispidulin regulates glycogen synthase kinase-3β (GSK-3β) activity and β-catenin expression in HDPSCs during endothelial differentiation. Although our findings establish the MAPK/ERK pathway as a key mediator of hispidulin-induced endothelial differentiation, future studies are required to investigate potential interactions between hispidulin and these other critical signaling pathways, particularly the Wnt/β-catenin and TGF-β pathways, to comprehensively understand the molecular mechanisms underlying hispidulin's effects on endothelial differentiation of HDPSCs.

In conclusion, our study demonstrated the multifaceted potential of hispidulin in dental tissue engineering through its ability to enhance both the osteo/odontogenic and endothelial differentiation of HDPSCs and promote their migration. These comprehensive findings are summarized in the schematic diagram (Figure 5). While these findings suggest hispidulin's promising therapeutic potential in for dental pulp regeneration and tissue engineering, future in vivo studies and clinical trials will be necessary to fully validate its efficacy and safety for clinical applications.

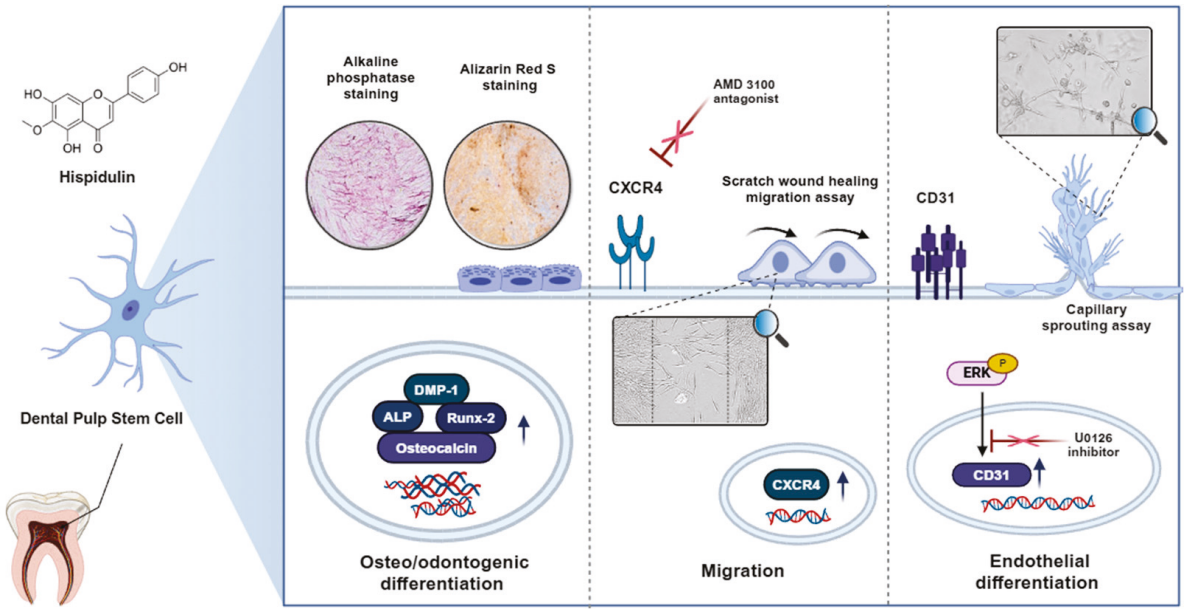

Figure 5. Schematic diagram illustrating the regulatory mechanisms of hispidulin in promoting osteo/odontogenic and endothelial differentiation, and migration of HDPSCs.

4. Materials and Methods

4.1. Reagents and Antibodies

Hispidulin, AMD3100, U0126, β-glycerophosphate disodium salt pentahydrate, ascorbic acid, dexamethasone, and methyl-thiazolyl-tetrazolium (MTT) were supplied by Sigma-Aldrich (St. Louis, MO, USA). Anti-human CD31, CXCR4, and β-actin antibodies were procured from Santa Cruz (Dallas, TX, USA), Thermo Fisher Scientific (Waltham, MA, USA), and Bioworld Technology (St. Louis Park, MN, USA), respectively. Anti-human ERK and phospho-ERK antibodies were obtained from Cell Signaling Technology (Danvers, MA, USA).

4.2. Cell Culture

HDPSCs were acquired from Lonza (Basel, Switzerland) and grown in α-modification of Eagle's minimum essential medium (α-MEM, Thermo Fisher Scientific, Waltham, MA, USA), supplemented with 10% fetal bovine serum (FBS; Merck Millipore, Burlington, MA, USA), 1% penicillin-streptomycin, and 5 μg/mL plasmocin (InvivoGen, San Diego, CA, USA). HDPSCs were incubated at 37 °C in a humidified atmosphere with 5% CO_2. For osteogenic differentiation, HDPSCs were cultured in the ODM containing 10mM β-glycerophosphate, 50 μg/mL ascorbic acid, and 0.1mM dexamethasone for 7–21days. The ODM was replaced every 2 days.

4.3. Cell Proliferation

The proliferation of HDPSCs was analyzed after 24, 48, and 72 h of culture growth. At the end of the culture period, cells were added in 500 μL of fresh medium containing 0.5 mg/mL MTT solution and were incubated for 4 h at 37 °C in a humidified atmosphere with 5% CO_2. The medium was changed with 200 μL of dimethyl sulfoxide (DMSO, Sigma-Aldrich, St. Louis, MO, USA) for 3 min. Subsequently, formazan absorbance was measured at 540 nm using a microplate reader (Allsheng, Hangzhou, China).

4.4. ALP Staining

An ALP staining kit (Sigma-Aldrich, St. Louis, MO, USA) was used according to the manufacturer's instructions on days 7 and 14. HDPSCs were fixed with an ALP-fixing solution, washed with distilled water, and stained with an alkaline dye mixture.

Images of each sample were acquired using a Nikon ECLIPSE 55i microscope (Korea Lab Technology, Seungnam, Republic of Korea). Each experiment was performed in duplicates and three separate experiments were performed for each group.

4.5. ARS Staining

After osteogenic induction for 14 and 21 days, the HDPSCs were fixed with 4% paraformaldehyde for 15 min, stained with 2% ARS (Sigma-Aldrich) solution for 30 min at room temperature, and washed twice with distilled water. Images of the stained mineralized nodules were acquired in three separate wells using a Nikon ECLIPSE 55i microscope (Nikon, Minato, Tokyo, Japan) and analyzed using the ImageJ software version 1.53o to calculate the mean and standard deviation.

4.6. Scratch Wound Healing Migration Assay

HDPSCs were seeded in plates containing a basic growth medium until they formed an adherent monolayer. A wound line was created by scratching the plates with a 10 μL pipette tip, and the floating cells were removed twice with 10% α-MEM. After incubating the cells with 1 μM hispidulin alone or in combination with AMD3100 (50 μg/mL) for 24 h, cell migration into the scratched area was photographed using a Nikon ECLIPSE 55i microscope (Nikon, Minato, Tokyo, Japan). The average width of the gaps was calculated from images captured using a microscope at four different sites from each wound line (n = 4).

4.7. Reverse Transcription-Quantitative PCR

The total RNA was extracted with a RiboEx kit (GeneAll, Seoul, Republic of Korea) and reverse transcribed using a reverse transcription kit (Promega; Madison, WI, USA). Real-time PCR was then performed with SYBR Green premix (Enzynomics, Daejeon, Republic of Korea) using Applied Biosystems (Waltham, MA, USA). The oligonucleotide primers listed below were used: β-actin: 5′-ACTCTTCCAGCCTTCCTTCC-3′ and 5′-TGTTGGCGTACAGGTCTTTG-3′; ALP: 5′-ATTTCTCTTGGGCAGGCAGAGAGT-3′ and5′-ATCCAGAATGTTCCACGGAGGCTT-3′; osteocalcin: 5′-CAGCGAGGTAGTGAAGAGAC-3′ and 5′-TGAAAGCCGATGTGGTCAG-3′; DMP-1: 5′-AGGAAGTCTCGCATCTCAGAG-3′ and 5′-TGGAGTTGCTGTTTTCTGTAGAG-3′; Runx-2:5′-CTCTACTATGGCACTTCGTC AGG-3′ and 5′-GCTTCCATCAGCGTCAACAC-3′. The cycling conditions consisted of an initial amplification cycle at 95 °C for 10 min, followed by 40 amplification cycles at 95 °C for 15 s, 60 °C for 60 s, and 72 °C for 7 s. The expression levels of target genes were calculated using the $2^{-\Delta\Delta Ct}$ method, with the β-actin gene used as a housekeeping control.

4.8. Western Immunoblotting

Equal amounts of the samples (20 μg) were loaded on gels for sodium dodecyl sulfate-polyacrylamide gel electrophoresis (SDS/PAGE) and transferred to a nitrocellulose membrane (GE Healthcare, Chicago, IL, USA). The membrane was blocked with 5% skim milk in TBS containing 0.1% Tween-20 for 1 h at room temperature and probed with appropriate antibodies (anti-human β-actin, anti-human CXCX4, anti-human CD31, anti-human ERK, and anti-phospho-ERK) overnight at 4 °C. The signal was developed using an enhanced chemiluminescence solution (ECL; GE Healthcare, Chicago, IL, USA) and monitored using the Azure 300 Chemiluminescent Western Blot Imaging System (Azure Biosystems, Dublin, CA, USA).

4.9. Flow Cytometry Analysis

HDPSCs were incubated with 1 μM hispidulin for 3, 5, and 7 days. After incubation, HDPSCs were washed with PBS and treated with PBS containing PE anti-human CD31 (BD Biosciences, Bedford, MA, USA) at 4 °C. After 1 h, the cells were washed twice with PBS and analyzed by flow cytometry using a fluorescence-activated cell sorter (Becton Dickinson and Company, Franklin Lakes, NJ, USA).

4.10. Capillary Sprouting Assay

A sprouting assay was performed as described by Sakai et al. [18]. Before adding HDPSCs, thawed growth factor reduced Matrigel (Corning, Inc., Corning, NY, USA) was added in a 24-well plate for 60 min at 37 °C. HDPSCs were seeded on these Matrigel-coated wells and treated with 1 μM hispidulin for 3, 5, and 7 days in the EGM-2MV (Lonza, Basel, Switzerland). After the completion of sprouting, three representative images were captured from each well using a Nikon ECLIPSE 55i microscope (Nikon, Minato, Tokyo, Japan).

4.11. Statistical Analysis

Data are shown as the mean ± standard deviation (SD) obtained from at least three independent experiments. Statistical comparisons between groups were conducted using a one-way analysis of variance (ANOVA), followed by a Student's *t*-test.

Author Contributions: Conceptualization, M.-K.B.; methodology, H.-J.P., M.-K.K. and Y.K.; resources, H.J.K. and Y.-I.K.; investigation, H.-J.P., Y.K. and M.-K.K.; data curation, H.-J.P. and Y.K.; formal analysis, H.-J.P. and S.-K.B.; writing—original draft, Y.K. and M.-K.B.; writing—review and editing, Y.K. and M.-K.B.; funding acquisition, M.-K.B.; project administration, M.-K.B.; supervision, M.-K.B. All authors have read and agreed to the published version of the manuscript.

Funding: This research was supported by grants from the National Research Foundation of Korea, funded by the Korean government (MSIT, NRF-2018R1A5A2023879 and 2021R1A2C1003687).

Institutional Review Board Statement: Not applicable.

Informed Consent Statement: Not applicable.

Data Availability Statement: The data presented in this study are available on request from the corresponding author.

Conflicts of Interest: The authors declare no conflicts of interest.

References

1. Sui, B.; Wu, D.; Xiang, L.; Fu, Y.; Kou, X.; Shi, S. Dental Pulp Stem Cells: From Discovery to Clinical Application. *J. Endod.* **2020**, *46*, S46–S55. [CrossRef] [PubMed]
2. Honda, M.; Ohshima, H. Biological Characteristics of Dental Pulp Stem Cells and their Potential use in Regenerative Medicine. *J. Oral Biosci.* **2022**, *64*, 26–36. [CrossRef] [PubMed]
3. Katata, C.; Sasaki, J.I.; Li, A.; Abe, G.L.; Nör, J.E.; Hayashi, M.; Imazato, S. Fabrication of Vascularized DPSC Constructs for Efficient Pulp Regeneration. *J. Dent. Res.* **2021**, *100*, 1351–1358. [CrossRef] [PubMed]
4. Cordeiro, M.M.; Dong, Z.; Kaneko, T.; Zhang, Z.; Miyazawa, M.; Shi, S.; Smith, A.J.; Nör, J.E. Dental Pulp Tissue Engineering with Stem Cells from Exfoliated Deciduous Teeth. *J. Endod.* **2008**, *34*, 962–969. [CrossRef]
5. Piva, E.; Silva, A.F.; Nör, J.E. Functionalized Scaffolds to Control Dental Pulp Stem Cell Fate. *J. Endod.* **2014**, *40*, 33. [CrossRef]
6. Atif, M.; Ali, I.; Hussain, A.; Hyder, S.V.; Niaz, B.; Khan, F.A.; Maalik, A.; Farooq, U. Pharmacological Assessment of Hispidulin--a Natural Bioactive Flavone. *Acta Pol. Pharm.* **2015**, *72*, 829–842. [PubMed]
7. Patel, K.; Patel, D.K. Medicinal Importance, Pharmacological Activities, and Analytical Aspects of Hispidulin: A Concise Report. *J. Tradit. Complement. Med.* **2016**, *7*, 360–366. [CrossRef] [PubMed]
8. Ashaq, A.; Maqbool, M.F.; Maryam, A.; Khan, M.; Shakir, H.A.; Irfan, M.; Qazi, J.I.; Li, Y.; Ma, T. Hispidulin: A Novel Natural Compound with Therapeutic Potential Against Human Cancers. *Phytother. Res.* **2021**, *35*, 771–789. [CrossRef]
9. Kut, K.; Bartosz, G.; Soszyński, M.; Sadowska-Bartosz, I. Antioxidant Properties of Hispidulin. *Nat. Prod. Res.* **2022**, *36*, 6401–6404. [CrossRef] [PubMed]
10. Kim, Y.; Lee, H.; Park, H.; Kim, M.; Kim, Y.; Kim, H.J.; Bae, S.; Kim, Y.; Bae, M. Hispidulin Inhibits the Vascular Inflammation Triggered by Porphyromonas Gingivalis Lipopolysaccharide. *Molecules* **2023**, *28*, 6717. [CrossRef] [PubMed]
11. Mustapha, S.; Magaji, R.A.; Magaji, M.G.; Gaya, I.B.; Umar, B.; Yusha'u, Y.; Daku, A.B.; Chiroma, S.M.; Jaafar, A.; Mehat, M.Z.; et al. Neuroprotective Roles of Flavonoid "Hispidulin" in the Central Nervous System: A Review. Iran. *J. Basic Med. Sci.* **2024**, *27*, 1077–1084.
12. Jeong, S.; Kim, Y.; Lee, D.; Kim, S.; Lee, S. Hispidulin Alleviates Mast Cell-Mediated Allergic Airway Inflammation through FcεR1 and Nrf2/HO-1 Signaling Pathway. *Antioxidants* **2024**, *13*, 528. [CrossRef] [PubMed]
13. Du, J.; Wang, Y.; Wu, C.; Zhang, X.; Zhang, X.; Xu, X. Targeting Bone Homeostasis Regulation: Potential of Traditional Chinese Medicine Flavonoids in the Treatment of Osteoporosis. *Front. Pharmacol.* **2024**, *15*, 1361864. [CrossRef]
14. Liu, M.; Zhou, D.; Liu, Q.; Xie, F.; Xiang, D.; Tang, G.; Luo, S. Osteogenesis Activity of Isocoumarin a through the Activation of the PI3K-Akt/Erk Cascade-Activated BMP/RUNX2 Signaling Pathway. *Eur. J. Pharmacol.* **2019**, *858*, 172480. [CrossRef] [PubMed]

15. Nepal, M.; Choi, H.J.; Choi, B.; Yang, M.; Chae, J.; Li, L.; Soh, Y. Hispidulin Attenuates Bone Resorption and Osteoclastogenesis Via the RANKL-Induced NF-κB and NFATc1 Pathways. *Eur. J. Pharmacol.* **2013**, *715*, 96–104. [CrossRef]
16. Li, M.; Sun, X.; Ma, L.; Jin, L.; Zhang, W.; Xiao, M.; Yu, Q. SDF-1/CXCR4 Axis Induces Human Dental Pulp Stem Cell Migration through FAK/PI3K/Akt and GSK3β/B-Catenin Pathways. *Sci. Rep.* **2017**, *7*, 40161. [CrossRef]
17. Kim, Y.; Park, H.; Kim, M.; Kim, Y.; Kim, H.J.; Bae, S.; Nör, J.E.; Bae, M. Naringenin Stimulates Osteogenic/Odontogenic Differentiation and Migration of Human Dental Pulp Stem Cells. *J. Dent. Sci.* **2023**, *18*, 577–585. [CrossRef] [PubMed]
18. Sakai, V.T.; Zhang, Z.; Dong, Z.; Neiva, K.G.; Machado, M.A.A.M.; Shi, S.; Santos, C.F.; Nör, J.E. SHED Differentiate into Functional Odontoblasts and Endothelium. *J. Dent. Res.* **2010**, *89*, 791–796. [CrossRef]
19. Li, A.; Sasaki, J.I.; Inubushi, T.; Abe, G.L.; Nör, J.E.; Yamashiro, T.; Imazato, S. Role of Heparan Sulfate in Vasculogenesis of Dental Pulp Stem Cells. *J. Dent. Res.* **2023**, *102*, 207–216. [CrossRef]
20. Bento, L.W.; Zhang, Z.; Imai, A.; Nör, F.; Dong, Z.; Shi, S.; Araujo, F.B.; Nör, J.E. Endothelial Differentiation of SHED Requires MEK1/ERK Signaling. *J. Dent. Res.* **2013**, *92*, 51–57. [CrossRef] [PubMed]
21. Zhang, J.; Liu, Z.; Luo, Y.; Li, X.; Huang, G.; Chen, H.; Li, A.; Qin, S. The Role of Flavonoids in the Osteogenic Differentiation of Mesenchymal Stem Cells. *Front. Pharmacol.* **2022**, *13*, 849513. [CrossRef]
22. Sudarshan, K.; Boda, A.K.; Dogra, S.; Bose, I.; Yadav, P.N.; Aidhen, I.S. Discovery of an Isocoumarin Analogue that Modulates Neuronal Functions Via Neurotrophin Receptor TrkB. *Bioorg. Med. Chem. Lett.* **2019**, *29*, 585–590. [CrossRef] [PubMed]
23. Zhang, L.; He, H.; Zhang, M.; Wu, Y.; Xu, X.; Yang, M.; Mei, L. Assessing the Effect and Related Mechanism of Naringenin on the Proliferation, Osteogenic Differentiation and Endothelial Differentiation of Human Periodontal Ligament Stem Cells. *Biochem. Biophys. Res. Commun.* **2021**, *534*, 337–342. [CrossRef] [PubMed]
24. Zheng, S.; Hu, G.; Li, J.; Zheng, J.; Li, Y. Icariin Accelerates Bone Regeneration by Inducing Osteogenesis-Angiogenesis Coupling in Rats with Type 1 Diabetes Mellitus. *World J. Diabetes* **2024**, *15*, 769–782. [CrossRef]
25. Grellier, M.; Granja, P.L.; Fricain, J.; Bidarra, S.J.; Renard, M.; Bareille, R.; Bourget, C.; Amédée, J.; Barbosa, M.A. The Effect of the Co-Immobilization of Human Osteoprogenitors and Endothelial Cells within Alginate Microspheres on Mineralization in a Bone Defect. *Biomaterials* **2009**, *30*, 3271–3278. [CrossRef]
26. Li, A.; Sasaki, J.; Abe, G.L.; Katata, C.; Sakai, H.; Imazato, S. Vascularization of a Bone Organoid Using Dental Pulp Stem Cells. *Stem Cells Int.* **2023**, *2023*, 5367887. [CrossRef] [PubMed]
27. Mantesso, A.; Zhang, Z.; Warner, K.A.; Herzog, A.E.; Pulianmackal, A.J.; Nör, J.E. Pulpbow: A Method to Study the Vasculogenic Potential of Mesenchymal Stem Cells from the Dental Pulp. *Cells* **2021**, *10*, 2804. [CrossRef] [PubMed]
28. Duncan, H.F.; Cooper, P.R.; Smith, A.J. Dissecting Dentine-Pulp Injury and Wound Healing Responses: Consequences for Regenerative Endodontics. *Int. Endod. J.* **2019**, *52*, 261–266. [CrossRef]
29. Yi, B.; Dissanayaka, W.L.; Zhang, C. Growth Factors and Small-Molecule Compounds in Derivation of Endothelial Lineages from Dental Stem Cells. *J. Endod.* **2020**, *46*, S63–S70. [CrossRef]
30. Li, J.; Zhu, Y.; Li, N.; Wu, T.; Zheng, X.; Heng, B.C.; Zou, D.; Xu, J. Upregulation of ETV2 Expression Promotes Endothelial Differentiation of Human Dental Pulp Stem Cells. *Cell Transplant.* **2021**, *30*, 963689720978739. [CrossRef]
31. Sakai, V.T.; Cordeiro, M.M.; Dong, Z.; Zhang, Z.; Zeitlin, B.D.; Nör, J.E. Tooth Slice/Scaffold Model of Dental Pulp Tissue Engineering. *Adv. Dent. Res.* **2011**, *23*, 325–332. [CrossRef]
32. Prescott, R.S.; Alsanea, R.; Fayad, M.I.; Johnson, B.R.; Wenckus, C.S.; Hao, J.; John, A.S.; George, A. In Vivo Generation of Dental Pulp-Like Tissue by using Dental Pulp Stem Cells, a Collagen Scaffold, and Dentin Matrix Protein 1 After Subcutaneous Transplantation in Mice. *J. Endod.* **2008**, *34*, 421–426. [CrossRef]
33. Xu, J.; Liu, X.; Jiang, Y.; Chu, L.; Hao, H.; Liua, Z.; Verfaillie, C.; Zweier, J.; Gupta, K.; Liu, Z. MAPK/ERK Signaling Mediates VEGF-Induced Bone Marrow Stem Cell Differentiation into Endothelial Cell. *J. Cell. Mol. Med.* **2008**, *12*, 2395–2406. [CrossRef] [PubMed]
34. Almalki, S.G.; Agrawal, D.K. ERK Signaling is Required for VEGF-A/VEGFR2-Induced Differentiation of Porcine Adipose-Derived Mesenchymal Stem Cells into Endothelial Cells. *Stem Cell Res. Ther.* **2017**, *8*, 113–114. [CrossRef] [PubMed]
35. Kim, H.A.; Lee, J. Hispidulin Modulates Epithelial-Mesenchymal Transition in Breast Cancer Cells. *Oncol. Lett.* **2021**, *21*, 155. [CrossRef] [PubMed]
36. Xu, J.G.; Gong, T.; Wang, Y.Y.; Zou, T.; Heng, B.C.; Yang, Y.Q.; Zhang, C.F. Inhibition of TGF-β Signaling in SHED Enhances Endothelial Differentiation. *J. Dent. Res.* **2018**, *97*, 218–225. [CrossRef] [PubMed]
37. Zhang, Z.; Nör, F.; Oh, M.; Cucco, C.; Shi, S.; Nör, J.E. Wnt/B-Catenin Signaling Determines the Vasculogenic Fate of Postnatal Mesenchymal Stem Cells. *Stem Cells* **2016**, *34*, 1576–1587. [CrossRef]

Disclaimer/Publisher's Note: The statements, opinions and data contained in all publications are solely those of the individual author(s) and contributor(s) and not of MDPI and/or the editor(s). MDPI and/or the editor(s) disclaim responsibility for any injury to people or property resulting from any ideas, methods, instructions or products referred to in the content.

pharmaceuticals

MDPI

Article

Isoorientin Improves Excisional Skin Wound Healing in Mice

Aline B. Hora [1], Laiza S. Biano [2], Ana Carla S. Nascimento [2], Zaine T. Camargo [3], Greice I. Heiden [4], Ricardo L. C. Albulquerque-Júnior [4], Renata Grespan [2], Jessica M. D. A. Aragão [2] and Enilton A. Camargo [1,2,*]

[1] Graduate Program in Health Sciences, Federal University of Sergipe, São Cristóvão 49060-676, Brazil
[2] Graduate Program in Physiological Sciences, Federal University of Sergipe, São Cristóvão 49107-230, Brazil
[3] Graduate Program in Chemistry, Federal University of Sergipe, São Cristóvão 49107-230, Brazil
[4] Graduate Program in Dentistry, Federal University of Santa Catarina, Florianópolis 88040-900, Brazil
* Correspondence: eniltoncamargo@academico.ufs.br; Tel.: +55-79-3198-6644

Abstract: Background/Objectives: Wound healing relies on a coordinated process with the participation of different mediators. Natural products are a source of active compounds with healing potential. Isoorientin is a natural flavone recognized as having several pharmacological properties, such as anti-inflammatory effects, making it a potential treatment for wounds. We investigated the effect of isoorientin on the healing of excisional skin wounds. **Methods**: Male Swiss mice were subjected to the induction of excisional skin wounds (6 mm diameter) and treated with a vehicle (2% dimethyl sulfoxide in propylene glycol) or 2.5% isoorientin applied topically once a day for 14 days. The wound area was measured on days 0, 3, 7, and 14. Histopathological analyses were performed on the cicatricial tissue after 14 days. The myeloperoxidase activity and the interleukin-1β, tumoral necrosis factor (TNF)-α, and interleukin-6 concentrations were determined on the third day. **Results**: We observed that 3 days after the topical application of isoorientin, the lesion area was significantly smaller when compared to those of the vehicle ($p < 0.01$) and control ($p < 0.05$) groups. No difference was observed after 7 and 14 days of induction. Despite this, on day 14, histological analysis of cicatricial tissue from the animals treated with isoorientin showed reduced epidermal thickness ($p < 0.001$) and increased collagen deposition ($p < 0.001$). These effects were accompanied by decreased myeloperoxidase activity and interleukin-1β concentration on the third day of induction, without alteration in TNF-α and interleukin-6. **Conclusions**: The treatment with isoorientin promoted better tissue repair in excisional wounds in mice, which may be linked to the modulation of the early inflammatory response.

Keywords: flavone; tissue repair; collagen deposition; epidermal thickness

1. Introduction

Skin wounds have a significant impact on the health and quality of life of patients [1], not only due to the disruption of skin integrity and the primary outcomes of this situation, but also due to other factors such as sleep disturbances, fatigue, job loss, low self-esteem, and depression [2].

The main causes of skin wounds are physical, chemical, or thermal injuries that lead to the disruption of skin integrity. Many wounds present impaired healing, both acutely and chronically, as alterations can occur in the normal stages of healing, such as those caused by infectious conditions [3]. The healing of skin wounds is regulated by a standard succession of coordinated events, involving the phases of hemostasis, inflammation, proliferation, and remodeling [4].

Wound treatment involves numerous conventional resources that are generally used topically, such as essential fatty acids, alginates, antiseptics, activated charcoal, proteolytic enzymes, hydrocolloids, hydrogels, hydropolymers, silver sulfadiazine, growth factors, and skin substitutes, among others [5]. However, for most of these treatments, there is a need

for greater accessibility to the population, as well as simpler and less costly production [6]. Furthermore, there are controversies about the safety and efficacy of wound treatment [7,8].

Thus, new approaches are needed to treat skin wounds, and natural products are a historically relevant alternative for treating various diseases [9,10]. Within the scope of natural products, flavonoids are polyphenolic compounds that have been widely studied for their anti-inflammatory and antioxidant properties [11,12]. According to previous studies, flavonoids have been mentioned as promising therapeutic agents for the healing of wounds [13], since they can modulate the nuclear factor (NF)-κB signaling pathway, which regulates the expression of inflammatory genes and is closely associated with chronic inflammation [12,14].

Isoorientin is a natural flavonoid that belongs to the flavones subclass. This compound is found in various plants, such as passion fruit, corn, wheat, and barley, and is used in traditional medicine in some cultures [15]. It has attracted attention due to its potential healing properties, which may be associated with various biological mechanisms. At the cellular level, it exerts anti-inflammatory effects by inhibiting pro-inflammatory mediators, such as the cytokines tumoral necrosis factor (TNF)-α, interleukin (IL)-1β, and IL-6 [16,17]. A previous study showed that Swiss 3T3 albino mouse fibroblast exposure to isoorientin improved in vitro wound closure by enhancing cell migration [18]. These authors suggested that isoorientin stimulated cellular nutrition and collagen synthesis, which is crucial for reconstructing damaged tissue. However, the potential of isoorientin for wound healing in vivo has not been previously evaluated. In the present study, we explored the effect of topically applied isoorientin on the healing of excisional wounds induced in mice. We showed for the first time that this isoflavone produces a beneficial effect on the wound healing process in mice, especially when linked with its anti-inflammatory action.

2. Results

2.1. Isoorientin Reduces the Wound Area during the Inflammatory Phase

Wounds were inflicted on day 0 and treated over 14 days, according to the experimental design (Figure 1A). The areas of the wounds were similar at day 0. However, the group treated with isoorientin (2.5% Iso) showed a smaller wound area on the third day, as observed in the representative images (Figure 1B) and the quantitative data (Figure 1C), compared to the vehicle ($p < 0.01$) and control ($p < 0.05$) groups. This parameter remained similar in all groups on the seventh and fourteenth days (Figure 1B,C).

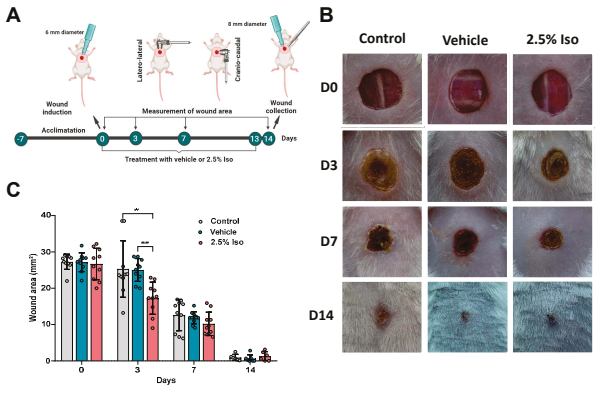

Figure 1. The effect of isoorientin on the skin wound area at different time points. Mice were divided into control (no treatment), vehicle (2% dimethyl sulfoxide (DMSO) in propylene glycol), and 2.5% isoorientin (2.5% Iso) groups. The area of each skin lesion was measured at days 0, 3, 7, and 14 after induction, according to the experimental design (**A**). Representative images of the skin lesions of the groups at different time points are shown (**B**). The area of the skin lesions (**C**) is expressed as mean ± SD (n = 10/group at D0, 3, and 7, and n = 6/group at D14). Two-way analysis of variance (ANOVA) and the Bonferroni post hoc test were used. * $p < 0.05$ or ** $p < 0.01$ compared to the control or vehicle group, as indicated. Created in BioRender.com.

2.2. The Administration of Isoorientin Enhances the Quality of Wound Healing

The control and vehicle groups exhibited similar histopathological features after 14 days, with intense epidermal acanthosis occurring and the papillary/reticular dermis presenting relatively thick residual granulation tissue consisting of numerous capillary vessels with an irregular distribution, supported by collagen fibrils arranged in a reticular pattern (Figure 2A–F). Additionally, a thicker and deeper band of granulation tissue was observed in these groups compared to the narrow subepidermal band seen in the 2.5% Iso group (Figure 2G–I). The granulation tissue was highly vascularized in the control and vehicle groups and was more fibrocellular in the 2.5% Iso group, but was absent in normal skin (Figure 2).

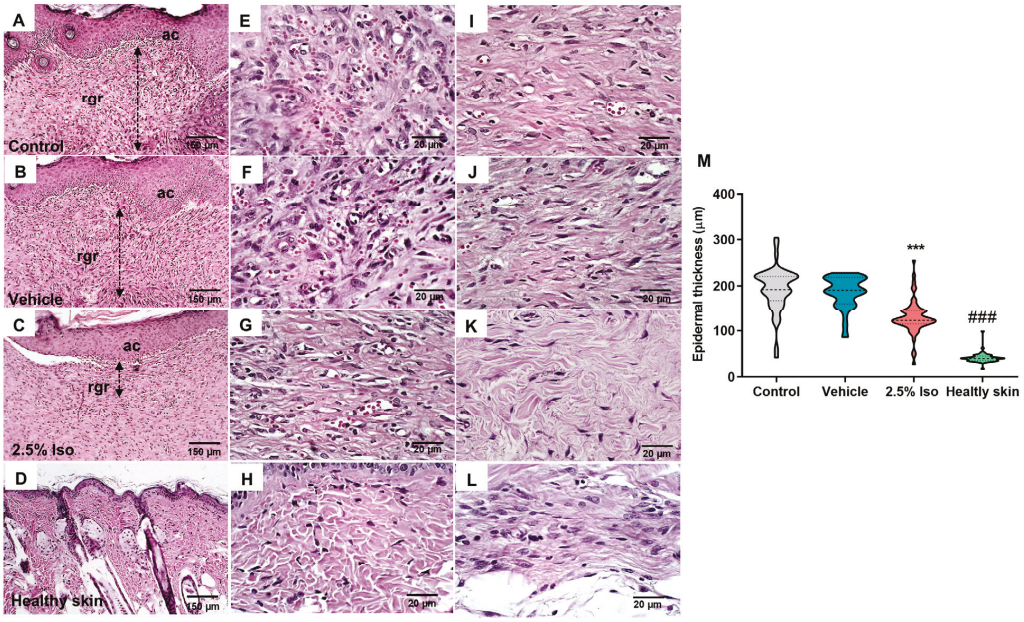

Figure 2. Representative images of the wound tissues 14 days after induction and quantification of the epidermal thickness. Histological sections stained with hematoxylin and eosin represent each experimental group's epidermis and papillary/reticular dermis. Panoramic views of the groups—control (**A**), vehicle (**B**), 2.5% Iso (**C**), and healthy skin (**D**)—show the measurement of the granulation reaction depth (dotted lines with double arrows), epidermal acanthosis (ac), and residual granulation reaction (rgr) in the lamina propria (100×). Details of the granulation reaction and the deeper dermal portion in the control (**E**,**I**), vehicle (**F**,**J**), 2.5% Iso (**G**,**K**), and healthy skin (**H**,**L**) groups (400×) are shown. A violin plot shows the measurement of the mean epidermal thickness in the experimental groups (**M**), n = 6 animals with 6–8 measurements each. The Kruskal–Wallis and Dunn's post hoc tests were used. *** $p < 0.001$ and ### $p < 0.001$ compared to the control or vehicle groups.

The epidermal thicknesses in the control and vehicle groups were statistically similar ($p > 0.05$), but both were significantly thicker than in the 2.5% Iso group and healthy skin ($p < 0.001$, Figure 2M).

2.3. Isoorientin Promotes Greater Collagen Deposition in Injured Tissue

The collagen fibers deposited in the dermis were identified by blue staining, using Masson's trichrome stain (Figure 3A–H), after 14 days. The control and vehicle groups showed a similar pattern of scar collagenization, represented by thin bundles of varying lengths and irregular arrangement of collagen fibers. The 2.5% Iso group also exhibited thin, delicate fibers, but they were more densely packed and arranged in parallel patterns (Figure 3G). Healthy skin displayed a dense and compact collagenization, consisting of thick and coarse bundles of collagen fibers arranged in an intertwined pattern (Figure 3H).

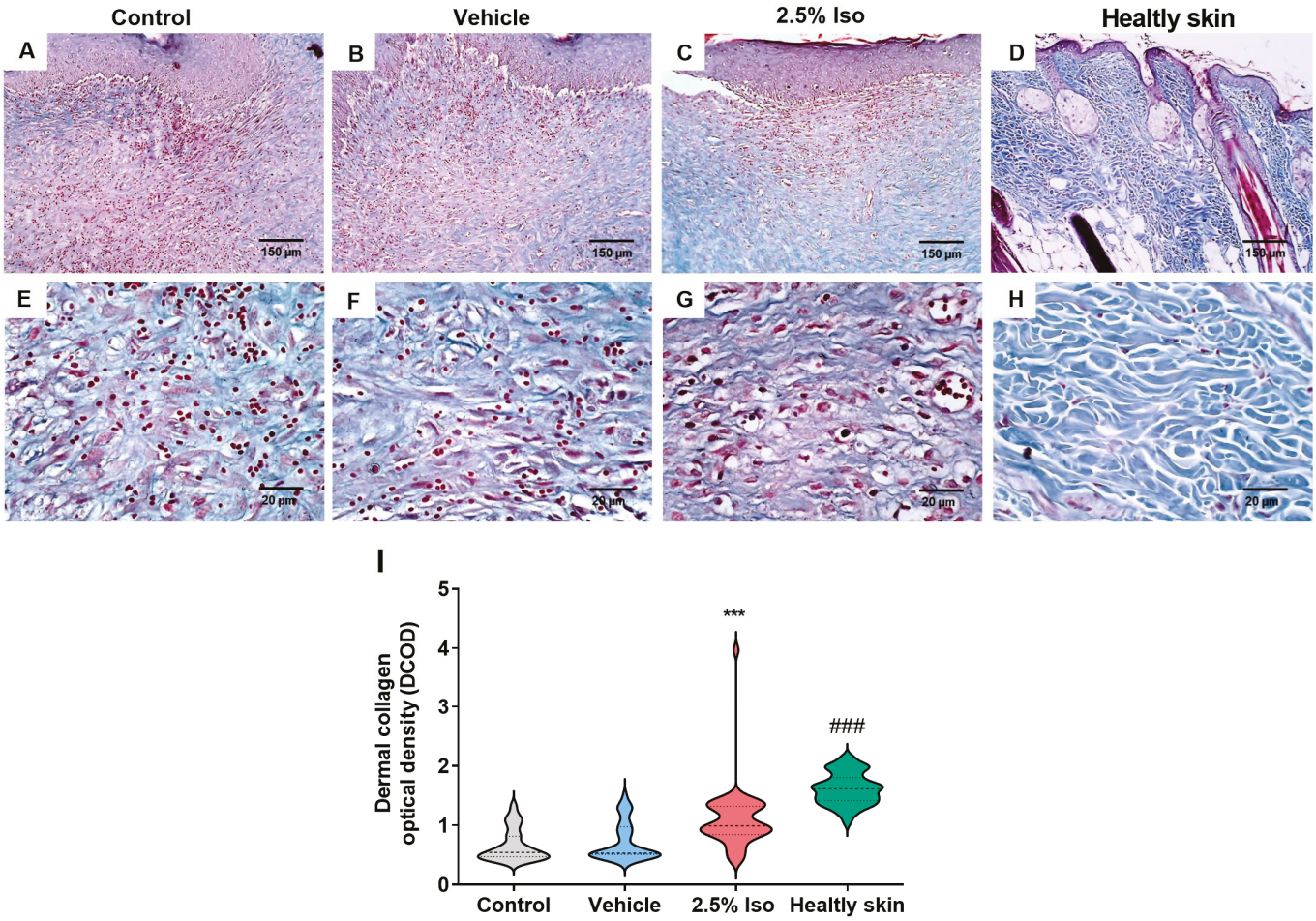

Figure 3. Representative images of Masson's trichrome staining, and quantification of collagen deposition in the wound tissues 14 days after induction. Histological sections stained with Masson's trichrome represent each experimental group's papillary/reticular dermis area. Panoramic views of the control (**A**), vehicle (**B**), 2.5% Iso (**C**), and healthy tissue (**D**) groups (100×) are shown, along with the histological appearances of collagen fibers in the experimental groups and normal skin (**E**–**H**) (400×). The violin plot demonstrates the dermal collagen optical density (DCOD) determination in the experimental groups (**I**), n = 6 animals with 7–10 measurements each. Data are expressed as the median and minimum to maximum. Kruskal–Wallis and Dunn's post hoc tests were used. *** $p < 0.001$ and ### $p < 0.001$ compared to the control or vehicle groups.

The control and vehicle groups exhibited similar density values for the collagenization density. However, the 2.5% Iso group and healthy skin showed a higher density of collagen deposition compared to the control and vehicle groups ($p < 0.001$) (Figure 3I).

2.4. Inflammatory Markers Are Reduced in the Wounds of Animals Treated with Isoorientin

The activity of the myeloperoxidase (MPO) enzyme was evaluated on the third day, to indirectly determine the neutrophil infiltrate in the wounds. Since we did not observe differences between the healing parameters in the control and vehicle groups, only the vehicle group was used for comparison with the 2.5% Iso group. We found a reduction in MPO activity in the wounds of the 2.5% Iso group ($p = 0.0003$) compared to the vehicle group (Figure 4A).

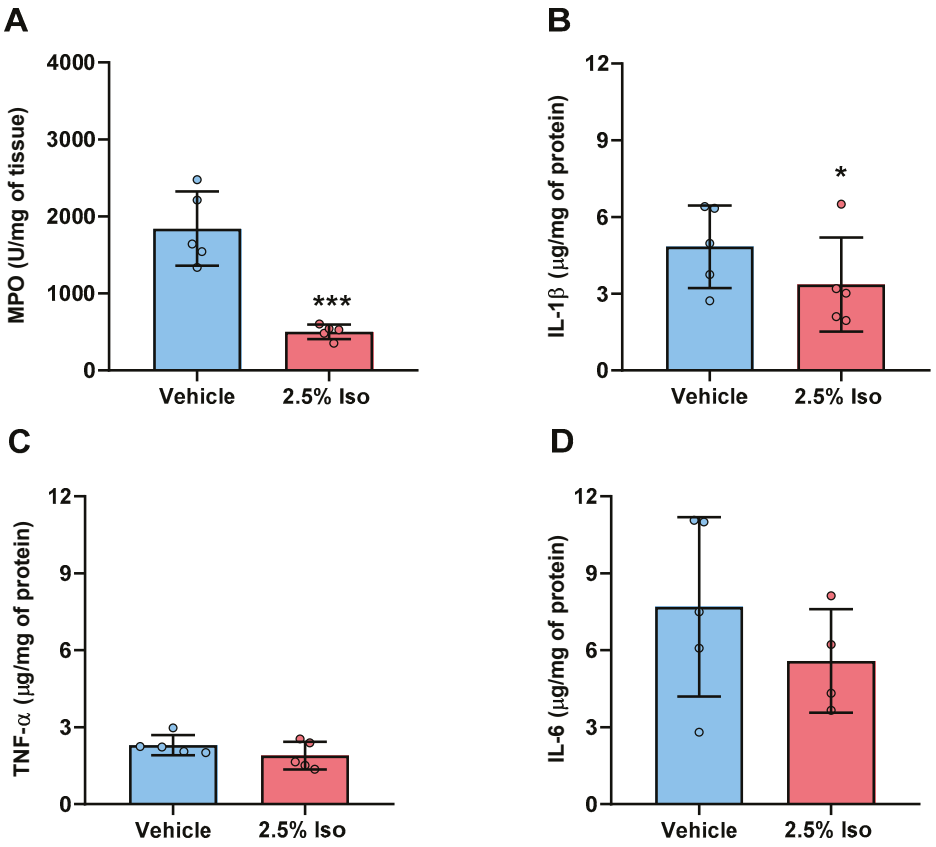

Figure 4. The effect of isoorientin on the myeloperoxidase activity and pro-inflammatory cytokine production in the wound tissues 3 days after induction. Mice were treated daily according to their respective groups: control (no treatment), vehicle (2% DMSO in propylene glycol), or Iso (2.5% Isoorientin). The wounds were analyzed on the third day to measure MPO activity (**A**) and the concentrations of IL-1β (**B**), TNF-α (**C**), and IL-6 (**D**). Data are expressed as mean ± SD (n = 5). Two-way ANOVA and the Bonferroni post hoc test were used. * $p < 0.05$ and *** $p < 0.0001$, respectively, compared to the vehicle group.

Furthermore, the pro-inflammatory cytokines IL-1β, TNF-α, and IL-6 were measured in the wounds on the third day. Treatment with isoorientin reduced the amount of IL-1β ($p = 0.029$; Figure 4B) compared to the vehicle group. However, this effect was not observed for the TNF-α and IL-6 cytokines (Figure 4C,D).

3. Discussion

In this study, we showed for the first time that isoorientin exhibits wound-healing activity in vivo. Our data suggest that this effect might be linked to its anti-inflammatory activity.

For this, we used the excisional skin wound model in mice. The analysis was initially focused on wound closure by secondary intention, using previously established parameters [19]. The healing of these excisional wounds significantly differs from the process associated with incisional wounds. Due to their extent and the lack of approximation of the wound edges, the closure of excisional wounds relies on tissue contraction, requiring increased cell proliferation, granulation tissue formation, and extracellular matrix deposition in the affected area [19].

Natural products have long been used for wound treatment to improve healing [20]. Isoorientin has several pharmacological properties, including antioxidant and anti-inflammatory effects [21]. Based on these properties, isoorientin seems to be of interest for the healing process as it possibly acts through various biological mechanisms that facilitate tissue repair.

In this study, we observed a reduction in wound area in animals treated with isoorientin at a concentration of 2.5% during the inflammatory phase. The healing of these lesions can be impaired both in the short and long term due to potential disruptions in the normal stages of recovery, such as those caused by infections [22]. The gross features of the wounds also showed that the crust formed in the treated group was thinner, with less fibrin deposition used for its formation. By the third day after the injury, lesions from all groups were neither edematous nor presenting surrounding necrotic areas. Thus, the reduction in wound area during the inflammatory phase aided the repair over the closing time (14 days). The relevance of this finding is amplified by the knowledge that cutaneous lesions resulting from a diverse range of damages can have their recovery compromised by factors that alter the normal stages of healing, including exacerbated inflammation, which delays the recovery process [23–25]. Inflammation, as a natural response to injury, plays a crucial role in this context, involving a complex interplay of mediators that, if dysregulated, can lead to significant disturbances [3,22,26]. This emphasizes the importance of effective therapeutic approaches, as observed for isoorientin.

The impact of isoorientin's action in the initial period of the wound healing process seemed to contribute to a better histological pattern of the cicatricial tissue. Although all groups achieved re-epithelialization on day 14 after wound induction, it is important to note that treatment with isoorientin promoted better reorganization of collagen fibers. Of interest is the fact that some flavonoids have been recognized by their wound-healing effects and their influence on collagen reorganization in diabetic animals [27], such as quercetin in mice [28] and a flavonoid-rich fraction from *Martynia annua* Linn or luteolin in rats [29].

The effectiveness of wound healing depends on the multifactorial phenomenon. It encompasses initial hemostasis, essential for containing blood loss and controlling inflammation, which precedes the repair stage [4]. The decrease in epidermal thickness and the increase in the density of collagen deposition observed after treatment with isoorientin suggest positive modulation in cell proliferation and migration, neovascularization, and epithelial growth, emphasizing the impact of this flavone on wound healing and dermal restructuring. Additionally, the wounds treated with isoorientin presented attenuated inflammatory infiltrate and a marked reduction in interstitial thickening. These data suggest that isoorientin favors collagen reorganization and wound healing by modulating the inflammatory response and tissue remodeling.

Skin lesion repair is characterized by angiogenesis, fibroplasia, and re-epithelialization, and it involves the migration and proliferation of many cells, including fibroblasts, endothelial cells, and epithelial cells; the deposition of connective tissue; and wound contraction [30]. It is known that the movement of macrophages and fibroblasts to the wound area is desirable for building complete functional tissue. Monocyte infiltration into the wound area, following the migration of polymorphonuclear leukocytes and the subsequent stimulation of macrophage differentiation, causes the secretion of key growth factors and cytokines [3].

Pro-inflammatory cytokines, such as IL1-β, IL-6, and TNF-α, play a central role in wound healing mechanisms [16]. Isoorientin reduced neutrophil migration (detected through the MPO activity) and the concentration of IL1-β in treated wounds after 3 days of induction, indicating that it can modulate the responses of cells involved in the initial stages of the inflammatory process, accelerating tissue repair. However, we did not find significative alteration in the TNF-α and IL-6 levels of the group treated with isoorientin. It is hard to explain why the effect of isoorientin on the IL-1β levels was more prominent. One could suggest that a differential effect on the NOD-like Receptor Pyrin Domain Containing 3 (NLRP3) pathway would be a reasonable explanation for these findings, since this is a pathway that is important for the formation of IL-1β [31]. Some studies have shown that the anti-inflammatory action of isoorientin is related to the inhibition of the NLRP3 pathway in models of lipopolysaccharide (LPS)-induced acute lung injury in rats [32] and trinitrobenzene sulfonic acid (TNBS)-induced colitis in mice [33], although, even in these

studies, the effects of isoorientin extend to other pro-inflammatory cytokines. So, it is difficult to explain these facts clearly from a mechanistic perspective. Despite this, we can securely correlate the reduction in MPO activity, along with the decrease in IL-1β, with the anti-inflammatory effect of isoorientin at the wound site, and these results are consistent with the findings from other authors [34], who have demonstrated reduced infiltration of cells linked to the inflammatory process in mice undergoing treatment with isoorientin. Furthermore, the expression of inflammatory mediators, including cyclooxygenase-2, TNF-α, IL-1β, inducible nitric oxide synthase, and 5-lypoxygenase, decreased in response to treatment with isoorientin in a mice macrophage lineage (Raw 264.7), as well as in vivo in carrageenan-induced air pouch leukocyte recruitment and paw edema models [34].

Thus, our data show that isoorientin modulates the inflammatory response by reducing the release of pro-inflammatory cytokines, which helps prevent excessive inflammation that could impair efficient wound healing. Furthermore, in vitro and in vivo studies [17] have shown that this isoflavone exerts potent antioxidant effects, neutralizing reactive oxygen species (ROS) and reducing oxidative stress at the injury site [35], which may take place through the positive modulation of the nuclear factor erythroid 2-related factor 2 (Nrf2) pathway, as proposed by other authors in mice models such as LPS-induced lung injury [32], ovalbumin-induced asthma [36], and TNBS-induced colitis [33]. A more recent study [37] has also shown that ISO can prevent redox damage to RAW264.7 cells, stimulated by the receptor activation of nuclear factor-κB ligand (RANKL), through a mechanism related to Nrf2. This action may also be crucial for the healing process, as excessive formation of ROS can cause additional tissue damage and delay repair [38].

4. Materials and Methods

4.1. Groups and Treatments

All procedures were conducted according to the guidelines of the National Council for Control of Animal Experimentation and approved by the Ethics Committee on Animal Use of the Federal University of Sergipe (protocol number 4639261223).

Male Swiss mice (25–30 g) were obtained from the Animal Center of the Federal University of Sergipe. All animals had similar baseline characteristics and were housed in appropriate boxes (dimensions 29 × 18 × 16 cm), with a maximum of 6 animals per box. The distribution of the boxes in the room was aleatory and the mice were kept under standard conditions (22 ± 1 °C, humidity 60 ± 5%, and 12/12 h light/dark cycle) and fed standard laboratory chow and tap water ad libitum.

The animals were individually housed and acclimatized for 7 days before wound induction. We randomly allocated the animals into three experimental groups: control, vehicle, and 2.5% Iso. For the treatment, isoorientin (ChemFaces, Wuhan, China, 98% purity), at a concentration of 2.5%, was applied as a volume of 30 μL (750 μg of the compound) dissolved in DMSO (2%) and propylene glycol (98%) solution. This concentration of isoorientin was based on a previous study [6]. The vehicle was chosen after preliminary tests, considering the poor water solubility of isoorientin. Thus, the vehicle group was treated with 2% DMSO in propylene glycol. The control group did not receive any treatment.

The animals were euthanized 3 (n = 10), 7 (n = 10), or 14 (n = 6) experimental days after the induction (Figure 1A). Experimental procedures were performed in the afternoon.

4.2. Wound Healing Model

We selected a mouse model of excisional wounds because it is one of the most used models and it is considered to mimic acute clinical wounds that heal by second intention [39]. This model has been extensively used in prior studies, providing a robust framework for understanding the mechanisms involved in wound healing [19].

For wound induction, mice were anesthetized with ketamine (100 mg/kg, i.p.) and xylazine (10 mg/kg, i.p.). Trichotomy of the dorsothoracic region was performed, followed by antisepsis with 0.5% alcoholic chlorhexidine. Subsequently, cutaneous excision was induced with a 6 mm circular metallic punch. Treatment and vehicle were applied (30 μL)

daily from day 0 to day 13 (Figure 1A). On the 14th day, the wound collection was performed with an 8 mm circular metallic punch, encompassing the entire area of the lesion and some healthy tissue, as previously described [40].

The cranio-caudal and latero-lateral diameters of the wounds were measured using a digital caliper on days 0, 3, 7, and 14 (Figure 1A). The wound area was calculated according to the following equation: Wound area (mm^2) = π.R.r (π = 3.1416), where R = cranio-caudal radius, and r = latero-lateral radius [41]. The researcher responsible for handling the treatments and measurement was not aware of the identity of each group.

4.3. Histopathology

The wounds (8 mm diameter) were collected 14 days into the experiment and fixed in 10% formalin for subsequent routine staining with hematoxylin and eosin or Masson's trichrome. In these experiments, we added a naïve control group (healthy skin) for comparison.

Histological evaluation of the average epidermal tissue thickness was performed on sections stained with hematoxylin and eosin. Three histological fields (100×) in each section were analyzed, and the measurements of epidermal thickness (stratified squamous epithelium lining, excluding the superficial keratin layer) were taken from each field. Morphometric measurements were obtained using ImageJ software (version 1.44).

The analysis of Dermal Collagen Optical Density (DCOD) OCD was performed using ImageJ software (version 1.44). Initially, a photomicrograph (400×) of the tissues stained with Masson's trichrome was transformed into an 8-bit grayscale system. Next, the software was calibrated using a color palette ranging from white to black. The optical density (OD) values obtained were matched to the corresponding values provided by the software system (standard) through a fitted curve equation (R^2 = 0.9924), used to calculate collagen OD based on its equivalence to previously calibrated grayscale values. After adjusting the software calibration for the micrometer, optical densities were measured within a circumference of 0.1256 mm^2 in the papillary/reticular dermis region. For each photomicrograph (100×), OD measurement was carried out in the central area. We performed the measurements in three histological fields in each section of each animal. The pathologist responsible for the measurement was blinded to the groups' identities.

4.4. MPO Activity

Neutrophil infiltration in wounds was indirectly measured by assaying MPO activity as a quantitative marker of the activity of this cell type [42]. Briefly, tissue samples (n = 5 mice) were homogenized in sodium phosphate buffer and 0.5% hexadecyltrimethylammonium bromide (Merck, Darmstadt, Germany), 1 mL/100 mg of tissue. Subsequently, the samples were centrifuged for 2 min at 8000× *g*. The supernatant (20 µL) was added to 200 µL of O-dianisidine (Merck, Darmstadt, Germany) solution, and each sample's absorbance was determined at 460 nm over 2 min at 25 °C on a plate spectrophotometer (SynergyMx®, Biotek, Bad Friedrichshall, Germany).

4.5. Determination of Cytokine Concentrations

The samples from 5 mice were homogenized in cytokine extraction buffer containing phosphate-buffered saline (10 mM, pH 7.4), a cocktail of protease inhibitors (1:1000 *v*/*v*; Merck, Darmstadt, Germany), phenylmethylsulfonyl fluoride (0.1 mM), NaCl (150 mM), EDTA (1 mM), and Tween 20 (0.05%), and centrifuged at 10,000× *g*. Subsequently, TNF-α, IL-1β, and IL-6 concentrations in the supernatant were determined using commercially available enzyme-linked immunosorbent assay kits, following the manufacturer's protocol (Invitrogen, Waltham, MA, USA).

4.6. Statistical Analysis

GraphPad Prism 8.0 was utilized for statistical analysis. The Shapiro–Wilk normality test was applied to the data. Data from the wound area (Figure 1B) showed parametric distribution, and two-way ANOVA, followed by the Bonferroni post hoc test, was used.

Data regarding the MPO activity and cytokine levels (Figure 4) were also parametric, and a t-test was used. Data concerning the epidermal thickness (Figure 2M) and collagen density (Figure 3I) did not show parametric distribution, and the Kruskal–Wallis test, followed by Dunn's post hoc test, was used. Data were expressed as the mean ± SD or the median and interquartile range. Values of $p < 0.05$ were considered statistically significant.

5. Conclusions

Our data show that isoorientin can improve the healing of excised skin by producing an anti-inflammatory effect in the initial stages of the wound healing process, which results in better epidermal thickness and collagen deposition in the closed wound. These findings reinforce the therapeutic value of isoorientin as an anti-inflammatory agent and an important modulator of fundamental cellular processes for wound healing.

Author Contributions: Conceptualization: A.B.H., Z.T.C. and E.A.C.; provision of study materials: E.A.C., R.G. and Z.T.C.; collection and assembly of data: A.B.H., A.C.S.N., L.S.B., J.M.D.A.A., G.I.H. and R.L.C.A.-J.; data analysis and interpretation: J.M.D.A.A., R.G. and R.L.C.A.-J.; manuscript writing: A.B.H., J.M.D.A.A. and E.A.C. All authors have read and agreed to the published version of the manuscript.

Funding: This research was conducted with financial support from the Coordination for the Improvement of Higher Education Personnel (CAPES, Social Demand Program), the National Council for Scientific and Technological Development (CNPq, n° 315369/2021-3), and Fundação de Amparo à Pesquisa e à Inovação Tecnológica do Estado de Sergipe (FAPITEC/SE, Edital 04/2021).

Institutional Review Board Statement: The Institutional Review Board (or Ethics Committee) approved the animal study protocol of the Ethics Committee on Animal Use of the Federal University of Sergipe (protocol number 4639261223) on 26 December 2023.

Informed Consent Statement: Not applicable.

Data Availability Statement: Data are contained within the article.

Acknowledgments: The authors thank the funding agencies.

Conflicts of Interest: The authors declare no conflict of interest.

References

1. Sen, C.K. Human Wound and Its Burden: Updated 2020 Compendium of Estimates. *Adv. Wound Care* **2021**, *10*, 281–292. [CrossRef] [PubMed]
2. Do, H.T.T.; Edwards, H.; Finlayson, K. Identifying Relationships between Symptom Clusters and Quality of Life in Adults with Chronic Mixed Venous and Arterial Leg Ulcers. *Int. Wound J.* **2016**, *13*, 904–911. [CrossRef] [PubMed]
3. Wilkinson, H.N.; Hardman, M.J. Wound Healing: Cellular Mechanisms and Pathological Outcomes. *Open Biol.* **2020**, *10*, 200223. [CrossRef]
4. Sorg, H.; Sorg, C.G.G. Skin Wound Healing: Of Players, Patterns, and Processes. *Eur. Surg. Res.* **2023**, *64*, 141–157. [CrossRef]
5. Shaydakov, M.E.; Ting, W.; Sadek, M.; Aziz, F.; Diaz, J.A.; Raffetto, J.D.; Marston, W.A.; Lal, B.K.; Welch, H.J.; Shaydakov, M.; et al. Review of the Current Evidence for Topical Treatment for Venous Leg Ulcers. *J. Vasc. Surg. Venous Lymphat. Disord.* **2022**, *10*, 241–247.e15. [CrossRef] [PubMed]
6. Duque, A.P.d.N.; Pinto, N.d.C.C.; Mendes, R.d.F.; da Silva, J.M.; Aragão, D.M.d.O.; Castañon, M.C.M.N.; Scio, E. In Vivo Wound Healing Activity of Gels Containing Cecropia Pachystachya Leaves. *J. Pharm. Pharmacol.* **2016**, *68*, 128–138. [CrossRef]
7. Okonkwo, U.A.; DiPietro, L.A. Diabetes and Wound Angiogenesis. *Int. J. Mol. Sci.* **2017**, *18*, 1419. [CrossRef]
8. Rosen, J.; Landriscina, A.; Kutner, A.; Adler, B.L.; Krausz, A.E.; Nosanchuk, J.D.; Friedman, A.J. Silver Sulfadiazine Retards Wound Healing in Mice via Alterations in Cytokine Expression. *J. Investig. Dermatol.* **2015**, *135*, 1459–1462. [CrossRef] [PubMed]
9. Wang, X.; Izzo, A.A.; Papapetropoulos, A.; Alexander, S.P.H.; Cortese-Krott, M.; Kendall, D.A.; Martemyanov, K.A.; Mauro, C.; Panettieri, R.A.; Patel, H.H.; et al. Natural Product Pharmacology: The British Journal of Pharmacology Perspective. *Br. J. Pharmacol.* **2024**, *181*, 3547–3555. [CrossRef]
10. Harvey, A.L.; Edrada-Ebel, R.; Quinn, R.J. The Re-Emergence of Natural Products for Drug Discovery in the Genomics Era. *Nat. Rev. Drug Discov.* **2015**, *14*, 111–129. [CrossRef]
11. Al-Khayri, J.M.; Sahana, G.R.; Nagella, P.; Joseph, B.V.; Alessa, F.M.; Al-Mssallem, M.Q. Flavonoids as Potential Anti-Inflammatory Molecules: A Review. *Molecules* **2022**, *27*, 2901. [CrossRef]

12. Choy, K.W.; Murugan, D.; Leong, X.-F.; Abas, R.; Alias, A.; Mustafa, M.R. Flavonoids as Natural Anti-Inflammatory Agents Targeting Nuclear Factor-Kappa B (NFκB) Signaling in Cardiovascular Diseases: A Mini Review. *Front. Pharmacol.* **2019**, *10*, 1295. [CrossRef] [PubMed]
13. Sychrová, A.; Škovranová, G.; Čulenová, M.; Fialová, S.B. Prenylated Flavonoids in Topical Infections and Wound Healing. *Molecules* **2022**, *27*, 4491. [CrossRef]
14. González, R.; Ballester, I.; López-Posadas, R.; Suárez, M.D.; Zarzuelo, A.; Martínez-Augustin, O.; Medina, F.S.D. Effects of Flavonoids and Other Polyphenols on Inflammation. *Crit. Rev. Food Sci. Nutr.* **2011**, *51*, 331–362. [CrossRef] [PubMed]
15. Fan, X.; Wei, W.; Huang, J.; Liu, X.; Ci, X. Isoorientin Attenuates Cisplatin-Induced Nephrotoxicity Through the Inhibition of Oxidative Stress and Apoptosis via Activating the SIRT1/SIRT6/Nrf-2 Pathway. *Front. Pharmacol.* **2020**, *11*, 264. [CrossRef] [PubMed]
16. Yuan, L.; Wu, Y.; Ren, X.; Liu, Q.; Wang, J.; Liu, X. Isoorientin Attenuates Lipopolysaccharide-Induced pro-Inflammatory Responses through down-Regulation of ROS-Related MAPK/NF-κB Signaling Pathway in BV-2 Microglia. *Mol. Cell Biochem.* **2014**, *386*, 153–165. [CrossRef]
17. Yuan, L.; Han, X.; Li, W.; Ren, D.; Yang, X. Isoorientin Prevents Hyperlipidemia and Liver Injury by Regulating Lipid Metabolism, Antioxidant Capability, and Inflammatory Cytokine Release in High-Fructose-Fed Mice. *J. Agric. Food Chem.* **2016**, *64*, 2682–2689. [CrossRef]
18. Wedler, J.; Daubitz, T.; Schlotterbeck, G.; Butterweck, V. In Vitro Anti-Inflammatory and Wound-Healing Potential of a Phyllostachys Edulis Leaf Extract–Identification of Isoorientin as an Active Compound. *Planta Med.* **2014**, *80*, 1678–1684. [CrossRef]
19. Sami, D.G.; Heiba, H.H.; Abdellatif, A. Wound Healing Models: A Systematic Review of Animal and Non-Animal Models. *Wound Med.* **2019**, *24*, 8–17. [CrossRef]
20. Criollo-Mendoza, M.S.; Contreras-Angulo, L.A.; Leyva-López, N.; Gutiérrez-Grijalva, E.P.; Jiménez-Ortega, L.A.; Heredia, J.B. Wound Healing Properties of Natural Products: Mechanisms of Action. *Molecules* **2023**, *28*, 598. [CrossRef]
21. Ziqubu, K.; Dludla, P.V.; Joubert, E.; Muller, C.J.F.; Louw, J.; Tiano, L.; Nkambule, B.B.; Kappo, A.P.; Mazibuko-Mbeje, S.E. Isoorientin: A Dietary Flavone with the Potential to Ameliorate Diverse Metabolic Complications. *Pharmacol. Res.* **2020**, *158*, 104867. [CrossRef] [PubMed]
22. Peña, O.A.; Martin, P. Cellular and Molecular Mechanisms of Skin Wound Healing. *Nat. Rev. Mol. Cell Biol.* **2024**, *25*, 599–616. [CrossRef] [PubMed]
23. Altoé, L.S.; Alves, R.S.; Sarandy, M.M.; Morais-Santos, M.; Novaes, R.D.; Gonçalves, R.V. Does Antibiotic Use Accelerate or Retard Cutaneous Repair? A Systematic Review in Animal Models. *PLoS ONE* **2019**, *14*, e0223511. [CrossRef] [PubMed]
24. Ebaid, H. Neutrophil Depletion in the Early Inflammatory Phase Delayed Cutaneous Wound Healing in Older Rats: Improvements Due to the Use of Un-Denatured Camel Whey Protein. *Diagn. Pathol.* **2014**, *9*, 46. [CrossRef]
25. Hassanshahi, A.; Moradzad, M.; Ghalamkari, S.; Fadaei, M.; Cowin, A.J.; Hassanshahi, M. Macrophage-Mediated Inflammation in Skin Wound Healing. *Cells* **2022**, *11*, 2953. [CrossRef]
26. Boniakowski, A.E.; Kimball, A.S.; Jacobs, B.N.; Kunkel, S.L.; Gallagher, K.A. Macrophage-Mediated Inflammation in Normal and Diabetic Wound Healing. *J. Immunol.* **2017**, *199*, 17–24. [CrossRef]
27. Antunes-Ricardo, M.; Gutiérrez-Uribe, J.; Serna-Saldívar, S.O. Anti-Inflammatory Glycosylated Flavonoids as Therapeutic Agents for Treatment of Diabetes-Impaired Wounds. *Curr. Top. Med. Chem.* **2015**, *15*, 2456–2463. [CrossRef]
28. Kant, V.; Jangir, B.L.; Sharma, M.; Kumar, V.; Joshi, V.G. Topical Application of Quercetin Improves Wound Repair and Regeneration in Diabetic Rats. *Immunopharmacol. Immunotoxicol.* **2021**, *43*, 536–553. [CrossRef]
29. Lodhi, S.; Singhai, A.K. Wound Healing Effect of Flavonoid Rich Fraction and Luteolin Isolated from *Martynia annua* Linn. on Streptozotocin Induced Diabetic Rats. *Asian Pac. J. Trop. Med.* **2013**, *6*, 253–259. [CrossRef]
30. Landén, N.X.; Li, D.; Ståhle, M. Transition from Inflammation to Proliferation: A Critical Step during Wound Healing. *Cell. Mol. Life Sci.* **2016**, *73*, 3861–3885. [CrossRef]
31. Ding, Y.; Ding, X.; Zhang, H.; Li, S.; Yang, P.; Tan, Q. Relevance of NLRP3 Inflammasome-Related Pathways in the Pathology of Diabetic Wound Healing and Possible Therapeutic Targets. *Oxid. Med. Cell Longev.* **2022**, *2022*, 9687925. [CrossRef] [PubMed]
32. Zhang, L.; Zhu, X.-Z.; Badamjav, R.; Zhang, J.-Z.; Kou, J.-P.; Yu, B.-Y.; Li, F. Isoorientin Protects Lipopolysaccharide-Induced Acute Lung Injury in Mice via Modulating Keap1/Nrf2-HO-1 and NLRP3 Inflammasome Pathways. *Eur. J. Pharmacol.* **2022**, *917*, 174748. [CrossRef] [PubMed]
33. Cheng, Q.; Yu, X.; Zhang, R.; Chen, L. Isoorientin Alleviates Inflammatory Bowel Disease by Inhibiting NLRP3 Inflammasome Activation through Nrf2/NQO1 Pathway. *Curr. Top. Nutraceutical Res.* **2020**, *18*, 392–397. [CrossRef]
34. Anilkumar, K.; Reddy, G.V.; Azad, R.; Yarla, N.S.; Dharmapuri, G.; Srivastava, A.; Kamal, M.A.; Pallu, R. Evaluation of Anti-Inflammatory Properties of Isoorientin Isolated from Tubers of *Pueraria tuberosa*. *Oxid. Med. Cell Longev.* **2017**, *2017*, 5498054. [CrossRef]
35. Zhao, Y.; He, C.; Hu, S.; Ni, H.; Tan, X.; Zhi, Y.; Yi, L.; Na, R.; Li, Y.; Du, Q.; et al. Anti-Oxidative Stress and Cognitive Improvement of a Semi-Synthetic Isoorientin-Based GSK-3β Inhibitor in Rat Pheochromocytoma Cell PC12 and Scopolamine-Induced AD Model Mice via AKT/GSK-3β/Nrf2 Pathway. *Exp. Neurol.* **2024**, *380*, 114881. [CrossRef]
36. Liang, S.; Zhao, Y.; Chen, G.; Wang, C. Isoorientin Ameliorates OVA-Induced Asthma in a Murine Model of Asthma. *Exp. Biol. Med.* **2022**, *247*, 1479–1488. [CrossRef]

37. Zhang, B.; Qu, Z.; Hui, H.; He, B.; Wang, D.; Zhang, Y.; Zhao, Y.; Zhang, J.; Yan, L. Exploring the Therapeutic Potential of Isoorientin in the Treatment of Osteoporosis: A Study Using Network Pharmacology and Experimental Validation. *Mol. Med.* **2024**, *30*, 27. [CrossRef]
38. Dunnill, C.; Patton, T.; Brennan, J.; Barrett, J.; Dryden, M.; Cooke, J.; Leaper, D.; Georgopoulos, N.T. Reactive Oxygen Species (ROS) and Wound Healing: The Functional Role of ROS and Emerging ROS-Modulating Technologies for Augmentation of the Healing Process. *Int. Wound J.* **2017**, *14*, 89–96. [CrossRef]
39. Masson-Meyers, D.S.; Andrade, T.A.M.; Caetano, G.F.; Guimaraes, F.R.; Leite, M.N.; Leite, S.N.; Frade, M.A.C. Experimental Models and Methods for Cutaneous Wound Healing Assessment. *Int. J. Exp. Pathol.* **2020**, *101*, 21–37. [CrossRef]
40. Canesso, M.C.C.; Vieira, A.T.; Castro, T.B.R.; Schirmer, B.G.A.; Cisalpino, D.; Martins, F.S.; Rachid, M.A.; Nicoli, J.R.; Teixeira, M.M.; Barcelos, L.S. Skin Wound Healing Is Accelerated and Scarless in the Absence of Commensal Microbiota. *J. Immunol.* **2014**, *193*, 5171–5180. [CrossRef]
41. Ramsey, D.T.; Pope, E.R.; Wagner-Mann, C.; Berg, J.N.; Swaim, S.F. Effects of Three Occlusive Dressing Materials on Healing of Full-Thickness Skin Wounds in Dogs. *Am. J. Vet. Res.* **1995**, *56*, 941–949. [CrossRef] [PubMed]
42. Bradley, P.P.; Priebat, D.A.; Christensen, R.D.; Rothstein, G. Measurement of Cutaneous Inflammation: Estimation of Neutrophil Content with an Enzyme Marker. *J. Investig. Dermatol.* **1982**, *78*, 206–209. [CrossRef] [PubMed]

Disclaimer/Publisher's Note: The statements, opinions and data contained in all publications are solely those of the individual author(s) and contributor(s) and not of MDPI and/or the editor(s). MDPI and/or the editor(s) disclaim responsibility for any injury to people or property resulting from any ideas, methods, instructions or products referred to in the content.

pharmaceuticals

MDPI

Article

Anti-Alzheimer's Potency of Rich Phenylethanoid Glycosides Extract from *Marrubium vulgare* L.: In Vitro and In Silico Studies

Mahmoud Emam [1], Samah A. El-Newary [2], Hanan Y. Aati [3], Bin Wei [4], Mohamed Seif [5,*] and Abeer Y. Ibrahim [2,*]

[1] Phytochemistry and Plant Systematics Department, National Research Centre, Dokki, Giza 12622, Egypt; mahmoudemamhegazy2020@gmail.com
[2] Medicinal and Aromatic Plants Research Department, Pharmaceutical and Drug Industries Research Institute, National Research Centre, 33 El Bohouth St., Dokki, Giza 12622, Egypt; samahelnewary@yahoo.com
[3] Pharmacognosy Department, College of Pharmacy, King Saud University, P.O. Box 22452, Riyadh 11495, Saudi Arabia; hati@ksu.edu.sa
[4] College of Pharmaceutical Science & Collaborative Innovation Center of Yangtze River Delta Region Green Pharmaceuticals, Zhejiang University of Technology, Hangzhou 310014, China; binwei@zjut.edu.cn
[5] Food Toxicology and Contaminants Department, Food Industries and Nutrition Research Institute, National Research Centre, Dokki, Giza 12622, Egypt
* Correspondence: seif.eg@gmail.com (M.S.); abeeryousry@yahoo.com (A.Y.I.)

Abstract: Background/Objectives: *Marrubium vulgare* L. (*M. vulgare*), the white horehound, is well known for treating inflammation-related diseases. Methods: In this context, we investigated the efficacy of *M. vulgare* ingredients in treating Alzheimer's disease using various in vitro and in silico antioxidant, anti-inflammatory, anti-cholinesterase, and anti-tyrosinase mechanisms. Results: In our results, sixty-one components were tentatively identified using gas and liquid chromatography (GC-MS and LC-MS^n) and categorized as hydrocarbons, fatty acids, and polyphenolics. The extract inhibited linoleic oxidation with an IC_{50} value of 114.72 µg/mL, captured iron (Fe^{2+}) ions with an IC_{50} value of 164.19 µg/mL, and displayed reducing power. In addition, the extract showed radical-scavenging ability towards $DPPH^{\bullet}$, $NO^{\bullet}$, $ABTS^{\bullet+}$, and H_2O_2 assays compared to L-ascorbic acid and butylated hydroxytoluene. The $DPPH^{\bullet}$ was scavenged by 77.62% at 100 µg/mL, and $NO^{\bullet}$, $ABTS^{\bullet+}$, and H_2O_2 were scavenged with IC_{50} values of 531.66, 117.51, and 143.10 µg/mL, respectively. *M. vulgare* also exhibited discriminating anti-inflammatory potency against cyclooxygenase (COX-2) with IC_{50} values of 619.15 µg/mL compared to celecoxib ($p > 0.05$). Notably, three Alzheimer's biomarkers, acetylcholinesterase (AChE), butyrylcholinesterase (BChE), and tyrosinase were significantly inhibited. The molecular docking study supposed that the phenylethanoid glycosides of samioside and forsythoside B inhibited AChE and tyrosinase enzymes with low binding affinities of −9.969 and −8.804 kcal/mol, respectively. Marruboside was a proper inhibitor of COX and BChE enzymes with a binding score of −10.218 and −10.306 kcal/mol, respectively. Conclusions: *M. vulgare* extract showed significant inhibitory actions, which suggest that it could have a promising potential as an anti-Alzheimer agent.

Keywords: anti-inflammatory; anti-cholinesterase; antioxidant; anti-tyrosinase; *Marrubium vulgare*; molecular docking

1. Introduction

Marrubium vulgare L. (*M. vulgare*) (Family *Lamiaceae*), is a grey-leaved non-woody perennial plant with stems that belongs to the *Lamiaceae* family. *M. vulgare* is commonly known as white horehound or common horehound. It grows in warm climates, including Europe, North Africa, and Central Asia. The plant is tall and typically reaches 1.5–2.4 m. It has hairy roots, multiple stems, long oval leaves, and white flowers [1].

Marrubium is a Latin word derived from the Hebrew word marrob, which means bitter juice, and vulgare meaning 'common' or 'well known'. The English phrase 'horehound' is derived from the Old English terms har and hune, which mean a downy plant [1]. White horehound has been linked to folk medicine from at least the first century BC, when it was mentioned as a remedy for respiratory issues in the treatise *De Medicina* by Roman encyclopedist Aulus Cornelius Celsus [2]. Also, it is recommended to treat the teeth, digestion, skin problems, boils, rheumatism, inflammation, sore eyes, hypertension, hyperglycemia, and night blindness. In addition, its volatile oil is a relaxant and can be used for heart palpitations [3].

In recent years, several studies have confirmed the remarkable pharmacological activities of *M. vulgare* both in vivo and in vitro. The plant exhibited noteworthy analgesic activity, anti-edematogenic activity, anti-inflammatory activity, sedative activity, antidiabetic activity, anti-spasmodic activity, anti-ulcer effects, hypolipemic activity, anti-hypertensive action, a hepatoprotective effect, immunomodulatory activity, antimicrobial and anti-*Helicobacter pylori* effects, antiviral activity, and is anti-tumorigenic against human colorectal cancer cells [1,3–7]. Also, different *M. vulgare* extracts showed antiparasitic activity, antiprotozoal activity, antiplasmodial activity, and anthelmintic activity [1], and can be a significant source of natural herbicides to control weeds in crop fields [8]. These pharmacological activities were attributed to the presence of many interesting metabolites that have been isolated from *M. vulgare* as an essential oil, terpenes, flavonoids, coumarins, phenolic acids, and phenylpropanoids [1].

Globally, *M. vulgare* is described in German Commission E publications as a cold remedy, digestive, and choleretic. The plant produces the popular horehound candy, which is said to alleviate coughs, hoarseness, and bronchitis thanks to its pleasant flavor. It is generally deemed safe in the United States and is widely used as a flavoring agent. Currently, some *M. vulgare* herbal medicinal formulations are used as an expectorant in cold-related coughs, and for symptomatic treatment of minor dyspeptic issues such as bloating and gas and a brief lack of appetite [9]. Even though there are just 33 licensed pharmaceutical formulations containing white horehound in India, it is well-known in the United States [5]. In 2015, *M. vulgare* formulations were the best-selling herbal dietary supplements, generating around USD 106 million in commercial sales [10].

For millennia, medicinal and aroma plants, particularly those having ethnopharmacological applications, have been used as natural sources of treatments and healthcare against contemporary problems [11]. One of these is the prevalent type of dementia known as Alzheimer's disease (AD), which accounts for at least two-thirds of cases in individuals aged 65 and older [12].

Alzheimer's disease (AD) is disorder that is a degenerative defect, which leads to brain cell damage and eventual cell death. Early symptoms of the disease include short-term memory loss and impaired conversation skills. Late-stage symptoms include significant memory loss and difficulties in performing simple daily tasks [13]. Currently, there is no cure for Alzheimer's, but existing medications can improve brain function in some patients, allowing them to remain independent for many years. Nevertheless, these drugs are associated with severe side effects [14]. Therefore, it is essential to search for new remedies with fewer side effects. Several intriguing natural products for Alzheimer's have been extracted from medicinal plants like *Balanites aegyptiaca* dates' hydroethanolic extract [15], *Calendula Suffruticosa* Vahlsubsp. boissieri Lanza [16], and *Olea dioica* [17].

In addition, tyrosinase is the enzyme that catalyzes L-tyrosine to convert to 3,4-dihydroxyphenylalanine (DOPA). L-Dopa is the precursor to dopamine, norepinephrine (noradrenaline), and epinephrine (adrenaline). Dopamine plays numerous essential roles in the brain and body [18]. On the other hand, tyrosinase can impair neurons by generating dopamine quinones, highly reactive and toxic species, through the oxidation of the catechol ring of dopamine. Dopamine quinones may bind to the sulfhydryl active functional groups of cysteine amino acids in the cytosol, forming protein adducts that can irreversibly alter or decrease protein activity. Dopamine oxidation also affects the dopamine transporter,

glutamate transport, and mitochondrial respiration. Cytosolic quinones can also reach the nucleus and cause covalent DNA changes [19]. Tyrosinase activity also increases the induction of H_2O_2, acting as an enhancer of cellular oxidative stress [20]. Greggio et. al. [19] concluded that tyrosinase may be damaging to catecholaminergic neurons by raising the concentration of dopamine-derived reactive species during oxidative stress situations. Tyrosinase blockers are a class of medicines that obstruct tyrosinase action. Even though there are numerous tyrosinase inhibitors available, only some are currently promoted as "safe". Therefore, the quest for novel tyrosinase blockers is crucial [21]. Tyrosinase blockers derived from natural sources have sparked widespread interest among researchers due to their decreased toxicity and improved bioavailability. Microorganisms and plants have steadily emerged as exploration hotspots for tyrosinase inhibitor extraction. Some plant-derived bioactive components limit tyrosinase potency, although at higher doses than recognized blockers such as pyran-4-one derivative (kojic acid), nonanedioic acid (azelaic acid), and hydroquinone-β-D-glucopyranoside (arbutin) [22].

As well, acetylcholine (ACh) functions as a neurotransmitter in the human brain and body, sending signals to other cells such as neurons, muscle cells, and gland cells. ACh regulates memory by influencing the acquisition, encoding, consolidation, reconsolidation, extinction, and recovery of memory [23]. The cholinesterase (ChE) enzyme, either acetylcholinesterase or butyrylcholinesterase, aids in its breakdown to choline and acetate at cholinergic synapses. Unfortunately, the brains of individuals with Alzheimer's disease have lower levels of acetylcholine compared to healthy individuals, which is associated with increased AChE activity [24]. Thus, inhibiting AChE preserves acetylcholine levels and improves cholinergic function. Consequently, AChE inhibitors are often considered an ideal treatment for Alzheimer's syndrome. AChE inhibitors are indeed the most effective treatments for the cognitive symptoms of Alzheimer's syndrome, senility, dyskinesia, and paralysis agitans [25,26].

The current investigation sought to identify new sources of active medicines from *M. vulgare* aerial parts extract to prevent or treat Alzheimer's syndrome and illustrate their possible mechanistic action. In addition, its effect on neurotransmitter degradation and tyrosinase suppression was investigated. Also, its anti-inflammatory and antioxidant potencies were examined in vitro and further explained with molecular docking studies. This study introduces *M. vulgare*'s phenylethanoid glycoside metabolites as a viable adjuvant therapy for Alzheimer's disease.

2. Results

2.1. Phytochemical Composition of the M. vulgare Extract

Preliminary assays of the *M. vulgare* extract revealed the presence of 61.96 $\pm$ 5.15 mg/g of alkaloids, 240.46 $\pm$ 12.19 mg of Gallic acid/g of polyphenols, and 100.95 $\pm$ 3.77 mg/g of tannins in the extract.

Also, the nonpolar constituents of *M. vulgare* extract were introduced into GC-MS analysis after different chemical treatments to bring the metabolites to a suitable form of derivatization for analysis (Tables 1 and 2). The lipoidal matter (USM) was analyzed using GC-MS analysis after the silylation process was carried out (Table 1). It was ascertained that steroidal structures represent 93.56% of the total identified components, while oxygenated hydrocarbons and sesquiterpenes represent 2.42% and 2.6%, respectively. Traces of polyunsaturated fatty acids were liberated into the solution after silylation and detected at 1.42%.

On the other hand, Table 2 illustrates the relative concentration percentage of saturated and unsaturated fatty acid methyl esters as 2.59% and 1.62%, respectively. In addition, benzoic acid derivatives were the major identified saponified matter in *M. vulgare*, accounting for 95.5%.

In addition, the polar constituents of *M. vulgare* extract were fractionated into butanol and aqueous fractions before injection in the LC/MS^n. Thirty-seven metabolites were identified based on their molar masses, and their fragment ions belong to phenolic acids,

flavonoid glycosides, aglycones, a diterpenoid lactone, phenylethanoid glycoside, and flavonoid (*O* and *C*) high glycosides (Tables 3 and 4).

Table 1. The relative percentage of hydrocarbons and sterols identified by the GC-MS analysis of *M. vulgare* extract.

Peak	t_R (min)	Name	Formula	Chemical Class	Conc.
1	3.12	Desogestrel	$C_{22}H_{30}O$	Steroid	2.92
2	3.16	1-Heptatriacotanol	$C_{37}H_{76}O$	OHC	2.42
3	3.40	Cholest-22-ene-21-ol, 3,5-dehydro-6-methoxy-, pivalate	$C_{33}H_{54}O_3$	Steroid	1.41
4	3.78	3-Ethyl-3-hydroxy-, (5.α.)-androstan-17-one	$C_{21}H_{34}O_2$	Steroid	81.39
5	4.07	Ageratriol, trimethyl ether	$C_{18}H_{30}O_3$	Sesquiterpene	2.60
6	4.37	Cholestan-3-ol, 2-methylene-, (3β, 5.α.)-	$C_{28}H_{48}O$	Steroid	3.97
7	6.62	Stigmasterol	$C_{29}H_{48}O$	Steroid	1.83
8	6.97	(3β, 24S)-Stigmast-5-en-3-ol	$C_{29}H_{50}O$	Steroid	2.05
9	7.83	Doconexent	$C_{22}H_{32}O_2$	PUSFA	1.42

OHC: oxygenated hydrocarbons, PUSFA: polyunsaturated fatty acid, t_R: retention time, Conc.: concentration, % = % of individual peak area/total sum of peak areas × 100.

Table 2. Chemical compositions of saponifiable matter of *M. vulgare* identified by GC-MS analysis.

Peak	t_R (min)	Name	Chemical Formula	Conc. %
1	11.269	Benzoic acid, 2-ethylhexyl ester	$C_{15}H_{22}O_2$	0.11
2	11.618	Hexadecanoic acid, methyl ester	$C_{17}H_{34}O_2$	1.94
3	13.473	Methyl stearate	$C_{19}H_{38}O_2$	0.27
4	13.682	9-Octadecenoic acid (*Z*)-, methyl ester	$C_{19}H_{36}O_2$	0.27
5	14.256	9,12-Octadecadienoic acid (*Z*, *Z*)-, methyl ester	$C_{19}H_{34}O_2$	0.56
6	14.633	Methyl 5,6-octadecadienoate	$C_{19}H_{34}O_2$	0.34
7	15.188	9,12,15-Octadecatrienoic acid, methyl ester, (*Z*,*Z*,*Z*)-	$C_{19}H_{32}O_2$	0.33
8	16.625	17-Octadecynoic acid, methyl ester	$C_{19}H_{34}O_2$	0.06
9	16.778	Methyl 9-cis,11-trans-octadecadienoate	$C_{19}H_{34}O_2$	0.06
10	19.038	Methyl 2-ethylhexyl phthalate	$C_{17}H_{24}O_4$	2.95
11	19.392	Phthalic acid, cyclohexyl methyl ethyl ester	$C_{17}H_{22}O_4$	0.08
12	29.567	Phthalic acid, di(2-propylpentyl) ester	$C_{24}H_{38}O_4$	92.25
13	33.184	Decanedioic acid, bis(2-ethylhexyl) ester	$C_{26}H_{50}O_4$	0.24
14	34.048	Octadecanoic acid, 9,10-dihydroxy-, methyl ester	$C_{19}H_{38}O_4$	0.14
15	35.18	1,3-Benzenedicarboxylic acid, bis(2-ethylhexyl) ester	$C_{24}H_{38}O_4$	0.4
		Sum		100
		SAT. FAME		2.59
		UNSAT. SFAME		1.62
		Benzoic acid derivatives		95.79

Retention time (t_R), SAT: saturated, UNSAT: unsaturated; FAME: fatty acid methyl ester.

Table 3. Identified compounds of *M. vulgare* butanol fraction using LC/MS^n.

Peak	t_R (min)	Identified Metabolites	$[M-H]^-$	Ms/Ms
1	1.7	Quinic acid #	191	173, 127, 111
2	3.13	Aconitic acid #	173	85, 129
3	4.19	Methyl gallic acid #	183	169, 139, 125
4	4.99	Malic acid #	133	115, 87, 71
5	5.93	Apigenin-7-*O*-xyloside	401	287, 269, 221, 219,113
6	6.6	Protocatechuic acid #	153	109
7	7.41	Cinnamic acid	147	103, 77
8	7.73	Ferulic acid	193	134

Table 3. *Cont.*

Peak	t_R (min)	Identified Metabolites	$[M-H]^-$	Ms/Ms
9	8.35	Caffeic acid #	179	135
10	8.90	4-hydroxy benzoic acid #	137	93, 65
11	9.55	Gallic acid #	169	125
12	10.50	Vanillin #	151	136, 135, 92
13	10.88	Vitexin " Apigenin-8-*C*-glucoside" *	431	341, 311, 283, 269
14	12.631	Catechin	289	245, 221, 109
15	12.65	Apigenin-7-*O*-xyloside	401	287, 269, 221, 219, 113
16	12.97	*p*-Coumaric acid #	163	119, 93
17	14.67	Quercetin *	301	273, 257
18	14.75	Naringenin #	271	151, 119
19	15.13	Apigenin-7-*O*-xyloside	401	287, 269, 221, 219, 113
20	15.15	Apigenin *	269	151, 117
21	25.24	luteolin-7-glucoside *	447	285
22	25.67	Luteolin *	285	151, 133
23	28.17	luteolin-7-*O*-lactate *	357	285, 269, 223
24	29.4	Chrysoeriol *	299	285, 284, 269
25	32.2	Apigenin *	269	151, 117
26	35.14	Chrysin #	253	143, 119

t_R = retention time: $[M-H]^-$ = precursor mass; # identified previously from the same genus [27], * isolated previously [28].

Table 4. Identified phenylethanoid glycoside and high (*O* and *C*) glycoside compounds of *M. vulgare* aqueous fraction using LC/MS^n.

Peak	t_R (min)	Identified Metabolites	$[M-H]^-$	Ms/Ms
1	6.36	Marruboside ♦	887	725, 593
2	6.51	Verbascoside ♦	623	461, 315
3	6.80	Forsythoside B ♦	755	593, 461, 447
4	7.00	Samioside ♦	755	593, 461
5	7.45	Apigenin-7-*O*-neohesperidoside #	577	431, 269
6	8.00	Apigenin-7-*O*-diglucuronide-*O*-hexoside	783	737, 607, 431, 269
7	8.59	Apigenin-7-*O*-diglucuronide-*O*-hexoside	783	737, 607, 431, 269
8	9.00	Isoscutellarein-7-*O*-(6-*O*-acetylallosyl) glucoside #	651	591, 489, 285, 257, 217, 175
9	9.49	Apigenin-7-*O*-neohesperidoside #	577	431, 269
10	10.45	Vicenin II (apigenin 6,8-di-C-glycoside) #	593	503, 383
11	14.82	Marrubiin ♦	331	313, 303, 287, 285

♦ Identified previously from the same species [29], # identified previously from the same genus [30,31].

After injecting a butanol sample, 26 molecules were identified as phenolic acids, aglycones, and mono glycosides (Figure 1 and Table 3).

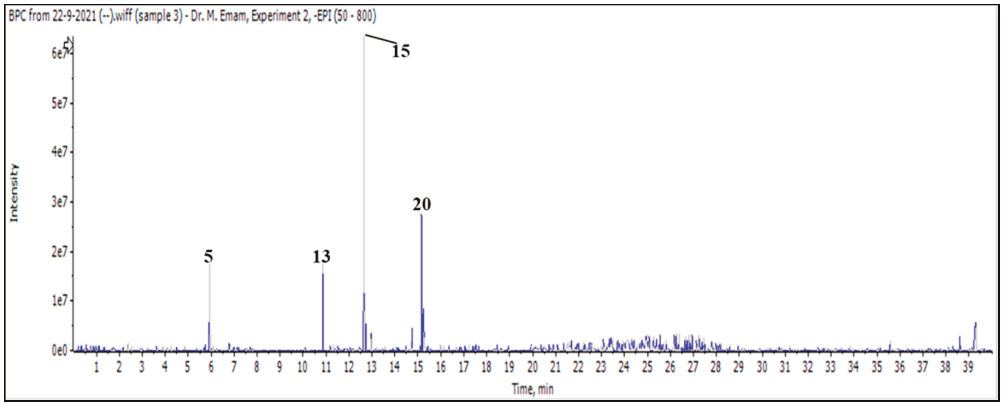

Figure 1. LC/MS2 base peak chromatogram (BPC) of *M. vulgare* extract for butanol fraction.

In addition, the injection of an aqueous sample led to the identification of 11 compounds classified as phenylethanoid glycoside, flavonoid (*O* and *C*) high glycoside, and a diterpenoid lactone (Figure 2 and Table 3).

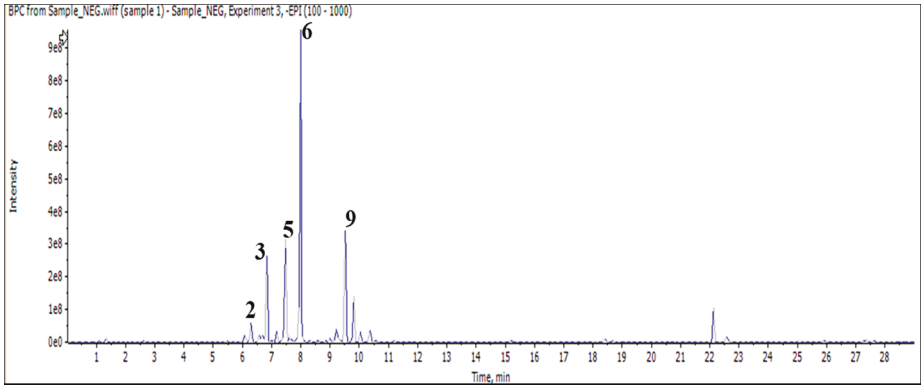

Figure 2. LC/MS^2 base peak chromatogram (BPC) of *M. vulgare* extract for aqueous fraction.

2.2. Biological Activities of the M. vulgare Extract

2.2.1. Antioxidant Potencies of the *M. Vulgare* Extract

Inhibition of Lipid Peroxidation

At 100 µg/mL, *M. vulgare* extract inhibited linoleic oxidation by 46.89% ± 1.98, which rose to 76.91% ± 1.95 at a concentration of 1000 µg/mL with an IC_{50} value of 114.72 µg/mL compared to the 28.64 and 39.30 µg/mL of ascorbic acid and BHT, respectively (Figure 3).

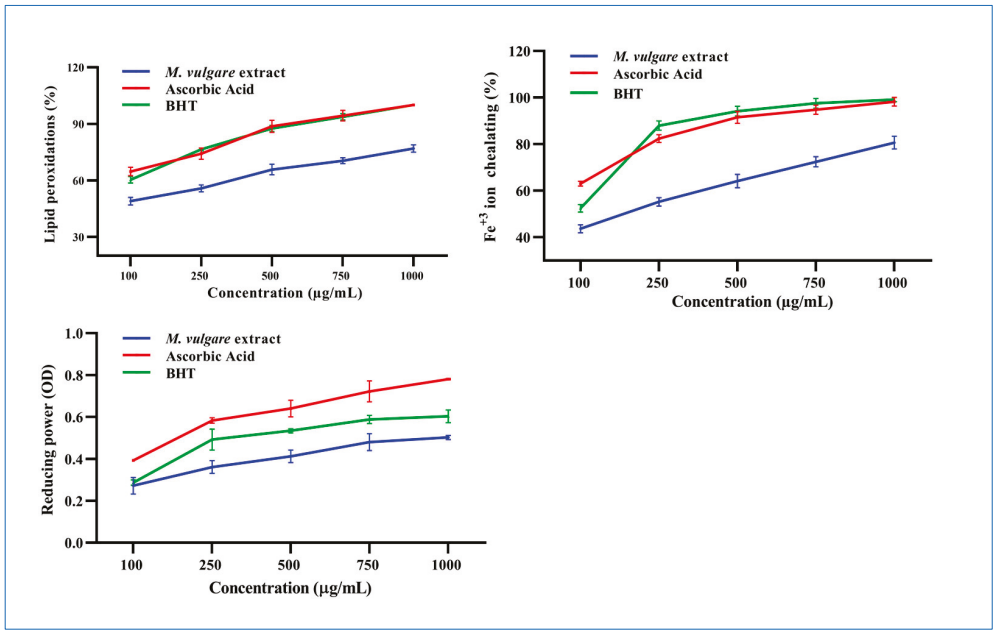

Figure 3. The *M. vulgare* extract and reference materials, ascorbic acid and butylated hydroxytoluene (BHT), were tested at various concentrations (100–1000 µg/mL) for lipid peroxidation inhibition, Fe^{+2} ion chelation capacity, and reducing power capability. The data are displayed as average ± SE ($n = 3$, $p < 0.05$).

Fe^{2+} Chelation Ability

The Fe^{2+} chelation ability of *M. vulgare* was determined based on its ability to prevent the formation of the Fe^{2+}–ferrozine complex. At a concentration of 100 µg/mL, the *M. vulgare* extract captured 43.62% ± 1.70 of the Fe^{2+} ions from the reaction medium, which increased to 80.64% ± 2.70 at a concentration of 1000 µg/mL with an IC_{50} value of

164.91 µg/mL. This was compared to 26.36 and 68.88 µg/mL for ascorbic acid and BHT, respectively (Figure 3).

Reducing Power of *M. vulgare*

The reducing power of *M. vulgare* was indicated by the transformation of Fe^{3+} ions to Fe^{2+}. The Fe^{3+} ion reduction capacity of the extract was estimated by absorbance measurements. Collectively, the *M. vulgare* extract exhibited relatively moderate reducing power compared with ascorbic acid and BHT (Figure 3).

2.2.2. Scavenging Activity

DPPH• Scavenging Activity

M. vulgare extract displayed potent DPPH• scavenging activity and neutralized the radical to the stable form with a percent inhibition of 77.62% ± 2.00 at 100 µg/mL, which increased to 90.44% ± 1.56 at 1000 µg/mL (Figure 4).

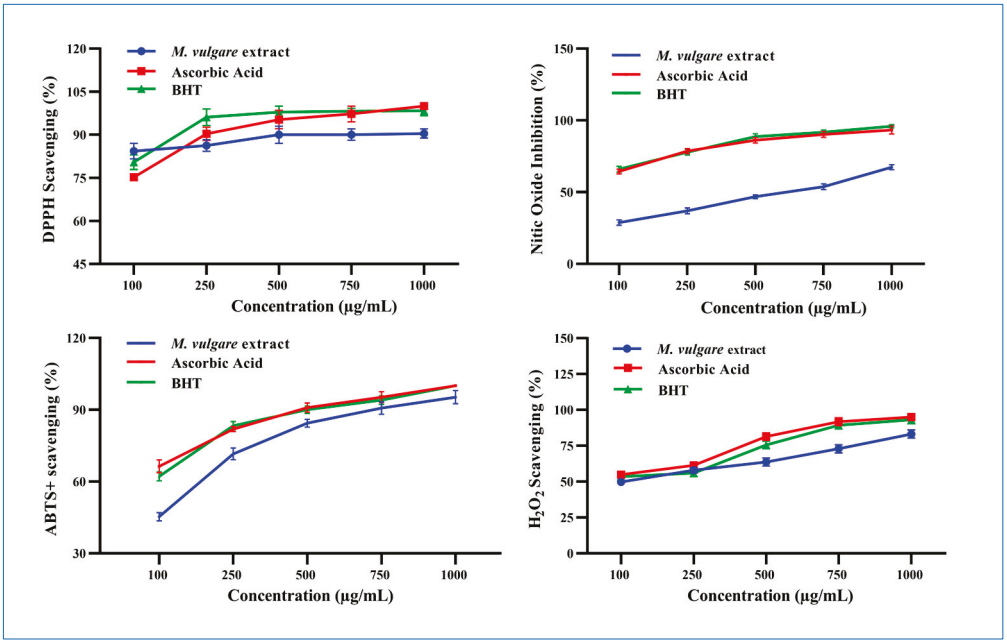

Figure 4. The scavenging properties of *M. vulgare* extract and reference materials including ascorbic acid and BHT at various doses (100–1000 µg/mL) for DPPH•, NO• scavenging, $ABTS^{\bullet+}$, and H_2O_2. BHT: butylated hydroxytoluene, DPPH: 1,1 diphenyl-2-picryl-hydrazyl free radical, $ABTS^{+}$: 2,2-azinobis (3-ethylbenzthiazoline-6-sulfonic acid), NO: nitric oxide, and H_2O_2: hydrogen peroxide. The statistics are presented as average ± SD. The data were analyzed using an independent *t*-test ($n = 3$, $p < 0.05$).

NO• Scavenging Activity

M. vulgare extract inhibited the liberation of NO• from the SNP reaction in a concentration-dependent manner with an IC_{50} value of 531.66 µg/mL (Figure 4). Approximately 28.79% ± 1.80 of NO• was captured in a reaction medium containing 100 µg/mL of *M. vulgare* extract, compared to ascorbic acid and BHT (64.39% ± 1.61 and 65.99% ± 2.00, respectively). NO• scavenging increased to 67.35% ± 1.65 by increasing the concentration of the *M. vulgare* extract to 1000 µg/mL compared to the 93.27% ± 2.73 and 95.88% ± 1.89 of ascorbic acid and BHT, respectively.

$ABTS^{\bullet+}$ Scavenging Power

The *M. vulgare* extract exhibited ABTS radical cation-scavenging ability with an IC_{50} value of 117.51 µg/mL compared to L-ascorbic acid and BHT (Figure 4). At 100 µg/mL, the extract neutralized 45.28% ± 1.72 of the ABTS radical cations in the reaction medium.

Moreover, increasing the concentration of the extract to 1000 µg/mL enhanced the neutralization to 95.51% ± 2.74, close to the scavenging activity recorded for L-ascorbic acid and BHT (i.e., 100% ± 0.00).

H_2O_2 Scavenging Activity

At 100 µg/mL, *M. vulgare* extract reduced H_2O_2 molecules in the medium by 49.73% ± 2.14 compared to the 54.92% ± 1.95 and 53.47% ± 2.53 of L-ascorbic acid and BHT, respectively (Figure 4). By increasing the extract concentration to 1000 µg/mL, the percentage of scavenged H_2O_2 molecules increased to 83.16% ± 2.24 compared to the 95.00% ± 2.50 and 93.16% ±2.84 of L-ascorbic acid and BHT, respectively. *M. vulgare* extract reduced H_2O_2 with an IC_{50} value of 143.10 µg/mL compared to the 91.92 and 129.98 µg/mL of L-ascorbic acid and BHT, respectively.

2.2.3. Anti-Inflammatory Effects of the Crude *M. vulgare* Extract

COX-1 Inhibition

M. vulgare extract had an insignificant inhibitory result on COX-1 ($p > 0.05$) compared to celecoxib. At 100 µg/mL, *M. vulgare* suppressed COX-1 activity by 7.04% ± 0.50, which increased to 26.64% ± 1.70 at 1000 µg/mL (Figure 5), with an IC_{50} value of 2412.25 µg/mL compared to the 64.22 µg/mL of celecoxib.

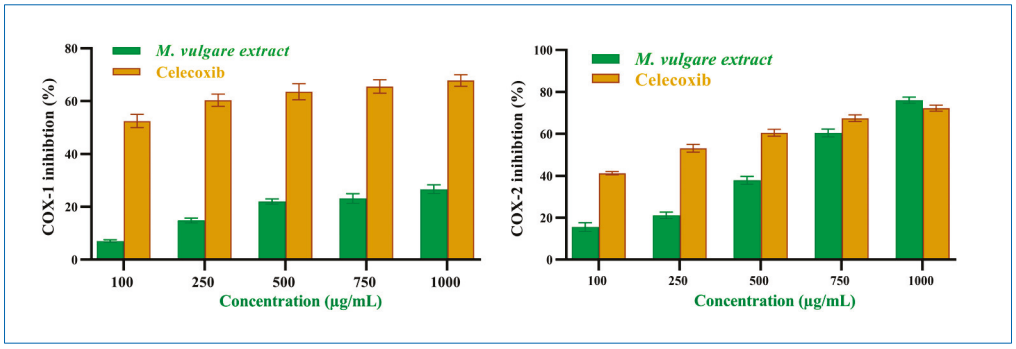

Figure 5. *M. vulgare* extract and celecoxib at varying dosages (100–1000 µg/mL) inhibit COX-1 and COX-2 enzymes. Statistics provided as average ± SD ($n = 3$, $p < 0.05$).

COX-2 Inhibition

On the other hand, *M. vulgare* extract exhibited potent inhibitory effects towards COX-2 (Figure 5) with an IC_{50} value of 619.15 µg/mL, compared to the 221.72 µg/mL of celecoxib. It showed moderate inhibition with 15.59% ± 2.09 at 100 µg/mL, which increased to 76.07% ± 1.41 at 1000 µg/mL. Compared to celecoxib, 41.23% ± 0.77 and 72.49% ± 1.51 inhibitions were established at the same concentrations with $p > 0.05$. Notably, the percentage of COX-2 inhibition at a high extract concentration of 750 and 1000 µg/mL was similar to that of celecoxib. Based on the IC_{50} values of the extract, it was determined that the crude extract of *M. vulgare* has specific anti-inflammatory actions against COX-2.

2.2.4. Effect of *M. vulgare* on the Alzheimer's Syndrome Biological Markers

The anti-Alzheimer's syndrome activities of *M. vulgare* were investigated by elucidating its role in preventing neurotransmitter degradation and the inhibiting of neurofibrillary tangle formation.

Inhibition of Neurotransmitter Degradation

1. Acetylcholinesterase Inhibition

M. vulgare extract significantly inhibited acetylcholinesterase by 35.41% ± 1.54 and 86.24% ± 1.76 at doses of 100 and 1000 µg/mL, respectively (Figure 6), with an IC_{50} value of 321.16 µg/mL.

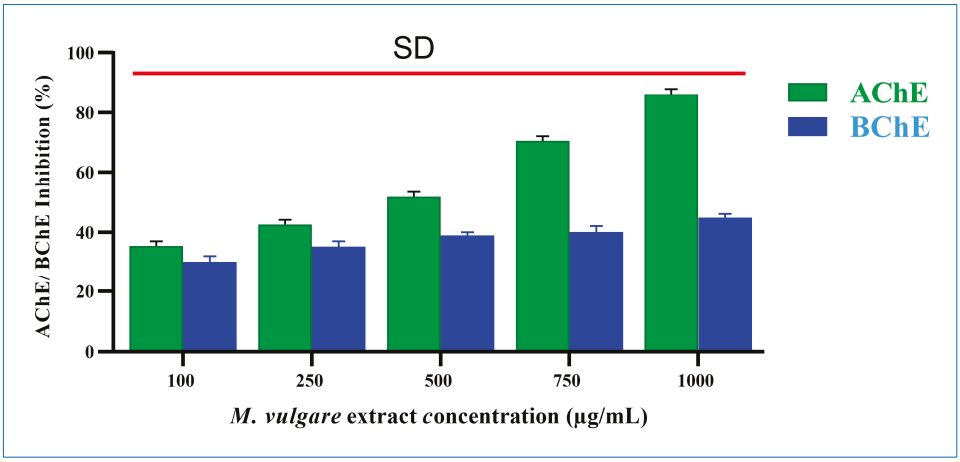

Figure 6. *M. vulgare* extract was tested at various concentrations (100–1000 µg/mL) for anti-cholinesterase activity. Statistics shown as average ± SD (n = 3), $p < 0.05$.

2. Butyrylcholinesterase Inhibition

The *M. vulgare* extract inhibited butyrylcholinesterase activity in a dose-dependent manner with an IC_{50} value of 2195.35 µg/mL. At 100 µg/mL, butyrylcholinesterase activity was decreased by 30.24% ± 1.76. The percentage of inhibition grew progressively as the concentration of the extract increased. The highest inhibition, with a value of 44.76% ± 1.24%, was recorded at 1000 µg/mL (Figure 6).

Inhibition of Tyrosine (Neurofibrillary Tangle Formation)

The *M. vulgare* extract also showed inhibitory tyrosinase effects, which were enhanced by increasing the incubation time and extract concentration (Figure 7). At the lowest extract concentration of 100 µg/mL, tyrosinase was inhibited by 3.54% ± 0.22 after incubation for 10 min. After 20 min of incubation, the inhibition percentage reached 29.58% ± 0.66, whereas, after 40 min, a 34.78% ± 2.05 inhibition was achieved. At the same concentration and incubation times, kojic acid resulted in 9.34% ± 0.66, 37.55% ± 1.45, and 70.32% ± 1.68 inhibitions, respectively.

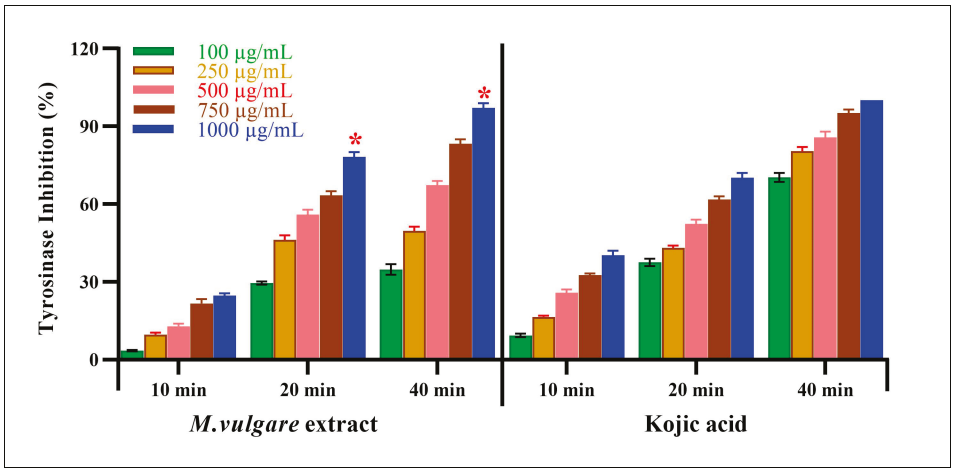

Figure 7. *M. vulgare* extract was examined for anti-tyrosinase activity at varying doses (100–1000 µg/mL). Statistics are presented as average ± SD (n = 3, $p < 0.05$). Statistics are marked with (*), indicating a remarkable change with kojic acid.

Notably, at the highest concentration of the *M. vulgare* extract, i.e., at 1000 µg/mL, the inhibitory tyrosinase activity increased to 24.73% ± 0.84, 78.15% ± 1.85, and 97.14% ± 1.86 after 10, 20, and 40 min of incubation, respectively. In the case of kojic acid, at the same

concentration and incubation times, 40.35% ± 1.65, 70.23% ± 1.77, and 100.00% ± 0.00 inhibition was achieved. At different incubation times of 10, 20, and 40 min, *M. vulgare* extract had lower IC_{50} values of 2.15, 23.05, and 12.19 µg/mL compared to the kojic acid IC_{50} values of 6.00, 29.62, and 62.97 µg/mL, respectively.

2.3. Molecular Docking Simulation

A molecular docking analysis was conducted to understand the interactions between the compounds and the target enzymes and predict the potential binding sites and binding modes, providing theoretical support for the experimental results. As shown in Supplementary Table S1, all the compounds demonstrated varying degrees of binding affinities to the active sites of cyclooxygenase (COX-2), acetylcholinesterase, butyrylcholinesterase, and tyrosinase. Notably, marruboside, samioside, and forsythoside B exhibited the lowest binding affinities, suggesting their potential as effective inhibitors in crude extract samples. To contextualize these findings, we compared the binding affinities and interaction patterns of these compounds with well-known inhibitors of the respective enzymes (Figure 8).

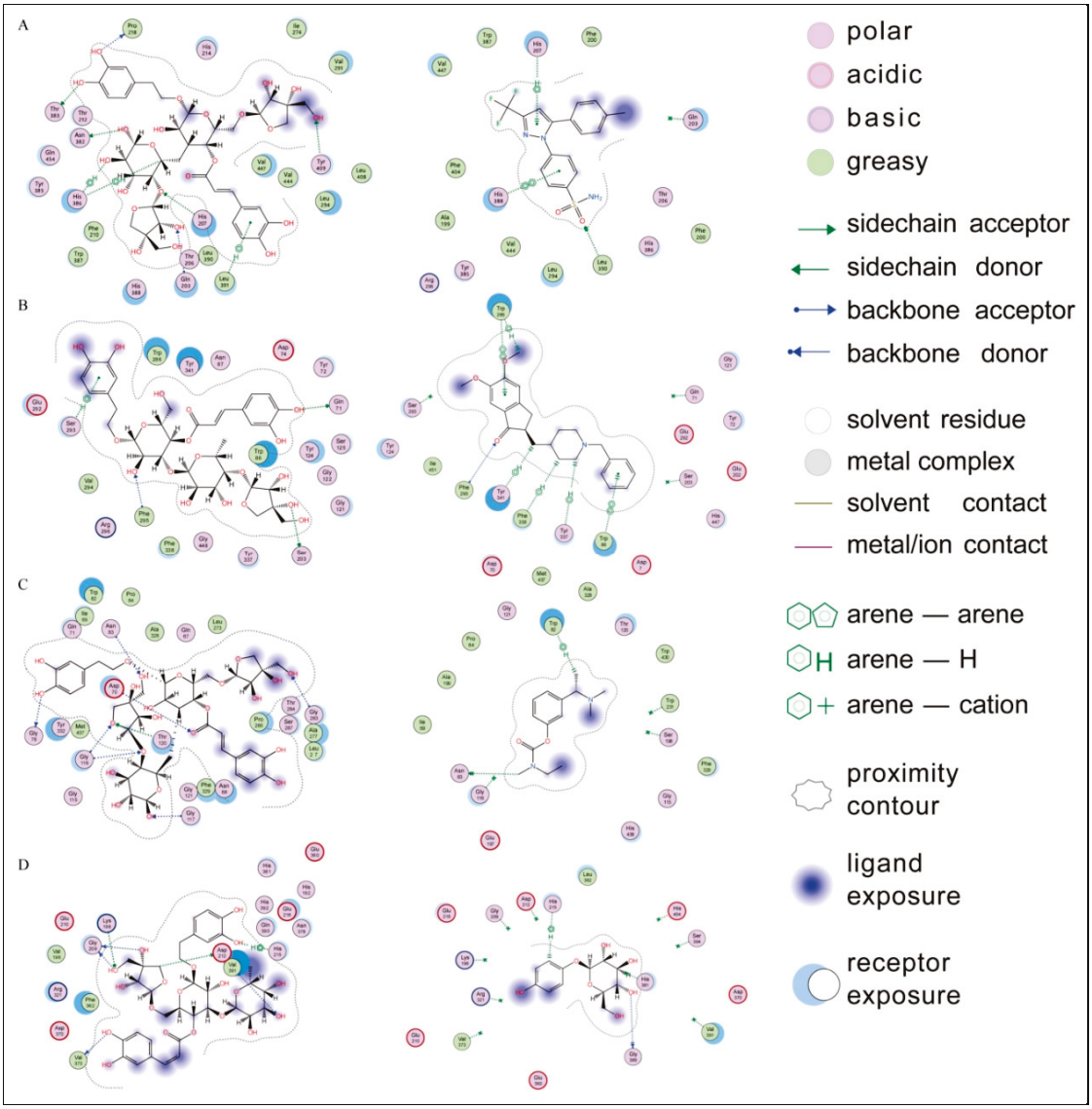

Figure 8. Ligand interactions of (**A**) marruboside and celecoxib, (**B**) samioside and Donepezil, (**C**) marruboside and Rivastigmine, and (**D**) forsythoside and arbutin with the active sites of cyclooxygenase (COX-2), acetylcholinesterase, butyrylcholinesterase, and tyrosinase, respectively.

For COX-2, marruboside showed significant interactions, forming four hydrogen bonds with His^{207}, Asn^{382}, Thr^{383}, and Tyr^{409}, along with three H-π interactions with His^{386} and Leu^{391}. These interactions are comparable to those observed with selective COX-2 inhibitors such as celecoxib and Meloxicam, which are FDA-approved nonsteroidal anti-inflammatory drugs (NSAIDs) known for their improved gastric safety. Celecoxib forms H-π interactions with His^{207}, while Meloxicam forms hydrogen bonds with His^{207} and His^{386} in the active site. This suggests that marruboside may exhibit inhibitory effects similar to these established COX-2 inhibitors.

Similarly, Donepezil and Rivastigmine are potent, selective, non-competitive, and rapidly reversible inhibitors of both acetylcholinesterase and butyrylcholinesterase, and are approved for the treatment of Alzheimer's disease. Therefore, these two drugs were used as reference compounds. Samioside demonstrated robust docking results with acetylcholinesterase, forming hydrogen bonds with Gln^{71}, Ser^{203}, Ser^{293}, and Phe^{295}, as well as hydrophobic interactions with Trp^{86}, Trp^{286}, and Tyr^{341}. Donepezil also forms hydrophobic interactions with Trp286 and Tyr^{341}, while Rivastigmine forms hydrogen bonds with Phe^{295} and hydrophobic interactions with Trp^{286}. This comparison indicates that samioside could potentially serve as an effective acetylcholinesterase inhibitor.

Marruboside also exhibited strong affinity for the active site of butyrylcholinesterase, forming multiple interactions with key residues such as Asp^{70}, Gly^{78}, Asn^{83}, Gly^{116}, Gly^{117}, Thr^{120}, and Gly^{283}. Donepezil forms hydrogen bonds with Gly^{116}, while Rivastigmine forms hydrogen bonds with Asn^{83}. Therefore, marruboside may act as a dual inhibitor for COX-2 and butyrylcholinesterase. Finally, forsythoside B primarily interacted with tyrosinase through an H-π interaction with His^{215} and six hydrogen bonds with Lys^{198}, Gly^{209}, Asp^{212}, Val^{373}, and Val^{393}. This interaction pattern is similar to that of arbutin, which forms an H-π interaction with His^{215}. Thus, forsythoside B could have potential applications in inhibiting tyrosinase activity.

The docking results not only highlight the potential inhibitory effects of marruboside, samioside, and forsythoside B but also provide a mechanistic understanding of how these compounds might exert their biological activity. Comparing these results with known inhibitors further validates the potential of these compounds as leads for drug development, underscoring the importance of molecular docking in identifying promising anti-Alzheimer agents.

3. Discussion

Many plant extracts and phytochemical compounds have been found to exert anti-Alzheimer's activities [32–35]. In the current study, the crude extract of *M. vulgare* displayed potent antioxidant capability and selective anti-inflammatory effects against COX-2, as well as a significant inhibition of cholinesterase and tyrosinase.

Previously, Neganova et al. [36] found a correlation between Fe^{2+} binding activity and the presence of a free nitrogen atom in the modified alkaloid derivatives. Also, a remarkable relationship was found between antioxidant power and the total polyphenol content, which can eliminate radicals to form stable radical intermediates due to hydrogen-donating ability [37]. In addition, flavonoids show unique antioxidant activities, including the inhibition of oxidant generation, preventing oxidants from attacking cells, eliminating oxidative stress, and supporting the cell's antioxidant defense. The free radical-scavenging ability of flavonoids results from rapid hydrogen donation to radical species. Flavonoids inhibit the lipid peroxidation and Fe^{2+}-catalyzed oxidation of glutamine synthase through free radical scavenging and metal ions from the catalytic sites via chelation [38].

In the current study, the total alkaloid and phenolic contents of the *M. vulgare* extract were 6.20% and 24.05%, which explained the antioxidant capability of the *M. vulgare* extract.

Moreover, the discriminating anti-inflammatory capabilities of the *M. vulgare* extract discovered in this study may be related to the extract's antioxidant and anti-inflammatory potencies, particularly its NO-scavenging capacity. Under normal physiological conditions, NO is an anti-inflammatory mediator; however, an excessive production of NO promotes

inflammation. The inducible nitric oxide synthase enzyme (iNOS) catalyzes the synthesis of NO in biological tissues [39]. Moreover, the up-regulation of COX-2 in endothelial cells is often accompanied by an elevation in iNOS levels. Thus, NO inhibition is considered an important therapeutic strategy for controlling inflammatory diseases [40]. The current findings displayed that *M. vulgare* extract succeeded in inhibiting NO compared to the tested standard.

In addition, acetylcholinesterase is the enzyme responsible for the breakdown of acetylcholine into choline and acetate. Inhibiting the activity of this enzyme is considered advantageous in the management of Alzheimer's disease. Alzheimer's disease is characterized by low acetylcholine levels in the brain and myasthenia gravis. Hence, utilizing acetylcholinesterase inhibitors is the most effective approach to treating the cognitive disorders associated with Alzheimer's disease [40]. Galantamine, donepezil, rivastigmine, and memantine are natural product derivatives commonly used to treat Alzheimer's disease as acetylcholinesterase inhibitors [26] for one of two binding sites. The first binding site interacts with positively charged nitrogen atoms in alkaloids, while the second interacts with non-alkaloid components like phenols [41].

So, the inhibitory acetylcholinesterase effects of the *M. vulgare* extract demonstrated in this study were consistent with the outcomes previously reported by Schlemper et al. [42]. They attributed the anti-spasmodic activity of the extract to its inhibitory effects on neurotransmitters, including acetylcholine, prostaglandin E, histamine, bradykinin, and oxytocin, with advanced selectivity for cholinergic levels. The evident anti-acetylcholinesterase and anti-butyrylcholinesterase effects of the *M. vulgare* extract obtained in the current study were attributed to its alkaloid, phenol, and flavonoid content. The hydroxyl (OH) groups on the aromatic ring (B-ring) of flavonoids react with the amino acid residues in the enzyme's peripheral anionic site, blocking the active site [43]. Increasing the number of OH or/and OCH_3 groups on the phenol ring enhances the inhibitory effects on acetylcholinesterase (e.g., cinnamic acid and derivatives). Additionally, the presence of a propenoic (CH=CHCOOH) group as caffeic acid increases the anti-acetylcholinesterase effects [44].

Our results were in agreement with those published before by Neagu et al. [45] that reported how the hydroxycinnamic acid, rutin, and caffeic acid of *Centarium umbellatum* and *Pulmonaria officinalis* exhibited anti-acetylcholinesterase activities [46]. Moreover, trihydroxybenzoic acid and pentahydroxyflavone exhibited anti-acetylcholinesterase and anti-butyrylcholinesterase effects, while 5-caffeoylquinic acid and naringenin displayed anti-butyrylcholinesterase activity [47]. 4-hydroxy-3-methoxycinnamic acid isolated from the ethyl acetate extract of *Impatiens bicolor* Linn showed significant anti-acetylcholinesterase effects [48]. Also, Heoa et al. [49] reported that naringenin isolated from *Citrus junos* exhibits inhibitory acetylcholinesterase activity. It was also demonstrated that coumarin interacts with the catalytic sites of the enzymes via the rings at the 3- and 4-positions [50], resulting in the effective inhibition of acetylcholinesterase and butyrylcholinesterase. By contrast, most recognized blockers have nitrogen atoms such as the isolated galantamine alkaloid structure from *Galanthus nivalis* that inhibit acetylcholinesterase through their complex nitrogen-containing configurations [51].

Another, tyrosinase is a Cu-based oxidase found in fauna and flora tissues. It is the enzyme that limits the pace of melanin formation. Tyrosinase is also involved in the synthesis of neuromelanin and the neuronal damage associated with Parkinson's disease [46]. L-Dopa, a precursor to dopamine, is created when tyrosine hydroxylase acts on tyrosine. In Alzheimer's syndrome, the accumulation of the A-peptide causes the formation of amyloid plaque, which is monitored by neurodegenerative alterations. Previous research has shown that L-Dopa and dopamine liquefy A-peptide fibrils and reduce protein tangle formation. Furthermore, Storga et al. [51] demonstrated the dopaminergic deficit in Alzheimer's disease brain samples [52].

The analyzed flora extracts inhibited tyrosinase activity, albeit at higher doses than recognized blockers such as kojic acid, azelaic acid, and arbutin [53]. Numerous studies

have been conducted to regulate tyrosinase activity utilizing metal chelators such as 5-Hydroxy-2-(hydroxymethyl)-4-pyrone, 1,2-dihydroxybenzene, 2,5-dihydroxybenzoic acid, flavonol, and hydroxamic acid, taking into account the copper structure of tyrosinase [54]. In general, flavonoids containing a hydroxyl (-OH) moiety at the A and B rings are potent tyrosinase blockers. Their mechanism of action involves Cu^{2+} chelate formation [55]. In addition, quercetin and kaempferol have also been shown to interfere with tyrosinase activity through the chelation of copper in the enzyme's active site [21]. Hence, the iron (II)-chelating activity of *M. vulgare* is of great significance, because it has been proposed as anti-tyrosinase activity, preventing the metal ions' transition that can contribute to oxidative damage in neurodegenerative disorders like Alzheimer's and Parkinson's disease [56]. These results explain the anti-tyrosinase action of the *M. vulgare* phytochemical constituents.

Among the phytochemical constituents identified in *M. vulgare* extract, chrysin is reported to improve memory in the aging brain by slowing the growth of reactive species and also to protect hippocampal neurons from injury and restore memory deficits in mice with chronic cerebral hypoperfusion. Chrysin can reduce apoptosis and memory problems associated with traumatic brain damage [57]. Apigenin ameliorates AD-associated memory impairment, reduces the Aβ plaque burden, and inhibits oxidative stress [58]. Luteolin has potential benefits for the central nervous system, including reduced microglia activation, neuronal damage, and high antioxidant activity. In vivo studies on rat models have shown that tetrahydroxyflavone protects against the cognitive impairment caused by prolonged cerebral hypoperfusion. Luteolin's antioxidant activity also reduces the Zn-induced hyperphosphorylation of the protein τ in SH-SY5Y cells and protects obese mice from cognitive impairments due to a high-fat diet [59]. Vanillin can reduce ROS levels and metalloproteinase-9 expression in LPS-stimulated macrophages, suggesting its potential in defending against neurodegeneration and oxidative stress [60]. D-(-)-Quinic acid can prevent aluminum-induced memory impairment by inhibiting AChE activity, promoting DNA repair, and inhibiting NF-κB [61]. In an in vitro model of ischemia, hydroxycinnamic acid derivatives enhanced synaptic transmission recovery following re-oxygenation after oxygen–glucose deprivation and reduced oxidative stress-related cell damage in cell culture models [62]. Additionally, phenylethanoid glycosides (PhGs) reduced neuroinflammation through neuroprotective and anti-inflammatory properties, reducing neuroinflammation and cognitive impairment in transgenic models of Alzheimer's disease [63]. According to the docking results and the previous literature, the anti-Alzheimer's efficacy of *M. vulgare* extract could be mediated by PhGs [64,65].

Finally, we conclude that the active ingredients identified by LC/MS in the hydroethanolic extract of *M. vulgare* fought Alzheimer's through several mechanisms, including (i) suppression of AChE overexpression that prevents ACh hydrolysis, (ii) inhibition of tyrosinase, (iii) suppression of oxidative stress, and (iv) the inhibition of COX-2 and activation of COX-1.

4. Materials and Methods

4.1. M. vulgare Assemblage and Extract Preparations

M. vulgare L. aboveground parts were obtained from the organic farm of Heliopolis University in July 2019 (Tahaweyah, Bilbeis, Al-Sharqia Governorate 7048302, Egypt) (Figure 9). The plants were validated by Prof. Dr. Kamal Zaied, Plant Department, Faculty of Science, Cairo University, Egypt. At room temperature, the aerial segments were dried in the shade, and the powder (1 kg) was macerated with solvent (70% ethanol) for 21 days. The filtrates were mixed and then dried to yield 130 g powder extract using Rotavapor® (Heizbad Hei-VAP, Heidolph, Schwabach, Germany). The lyophilized extract (Christ, Osterode am Harz, Germany) was deposited at −20 °C.



Figure 9. *M. vulgare* plant (Tahaweyah, Bilbeis, Al-Sharqia Governorate 7048302).

4.2. Phytochemical Analysis

4.2.1. Preliminary Chemical Composition of the *M. vulgare* Extract

The total amount of phenolics and tannins was determined using the Folin–Ciocalteu technique [65] and a standard Broadhurst and Jones method [66], respectively. In addition, the alkaloids were determined by Onwuka's gravimetric method [67].

4.2.2. GCMS Analysis

The nonpolar components of unsaponifiable matter (USM) and saponifiable matter (SM) were extracted, derivatized, and analyzed using Agilent GC-MS technology systems. Wiley and NIST Mass Spectral Libraries data were used for identification.

Unsaponifiable Matter (USM)

M. vulgare's *n*-hexane fraction (0.657 g) was saponified under reflux with 10 mL of 10% potassium hydroxide (KOH) and 4 mL of toluene for 24 h to guarantee full hydrolysis [68]. The saponified solution was concentrated using a rotary evaporator and suspended in 100 mL of distilled water, then extracted with peroxide-free diethyl ether (50 mL × 3) [69]. The mixed ethereal extracts were collected, rinsed with distilled water to remove alkalinity, dried on anhydrous sodium sulfate, and evaporated until dry to yield USM (0.36 g ~ 54.95%).

Bis(trimethylsilyl) trifluoroacetamide $(BSTFA)^+$ trimethylchlorosilane (TMCS) (99:1) was used to convert the functional groups of the dried USM sample into trimethylsilyl groups (TMS) [70] before the injection into the GC-MS Agilent technology system that was described previously [71].

Saponifiable Matter (SM) Analysis and the Preparation of the Fatty Acid Methyl Esters (FAMEs)

The aqueous alkaline solution that was left after the separation of the USM matter was acidified with diluted hydrochloric acid to liberate the free fatty acids, extracted with peroxide-free diethyl ether (4 × 50 mL), washed with distilled water to eliminate acidity, and dehydrated over anhydrous sodium sulfate [68,72] to yield fatty acid methyl ester (0.295 g~45.05%). The FAME sample was injected into the GCMS system (Agilent Technologies, Santa Clara, CA, USA) as described previously [73].

4.2.3. LC-ESI-MS/MS Analysis

The polar components of the *M. vulgare* sample were analyzed using liquid chromatography–electrospray ionization–tandem mass spectrometry (LC-ESI-MS/MS) (AB Sciex ExionLC AC HPLC coupled with a SCIEX Triple Quad™ 5500 LC-MS/MS system) as described previously [74].

4.3. Biological Potencies of the M. vulgare Extract

4.3.1. Antioxidant Potencies of the *M. vulgare*

The extracted samples and reference materials (i.e., BHT and ascorbic acid) were prepared as methanolic solutions of serial concentrations, specifically 100, 250, 500, 750, and 1000 μg/mL, and were used for all antioxidant determination methods. Antioxidant capacities were spectrophotometrically assayed (Jasco V630, Tokyo, Japan).

Lipid Peroxidation-[NH4] SCN (Ammonium Thiocyanate)

The potency of the *M. vulgare* extract to obstruct lipid peroxidation (LP) was assessed according to Duh et al. [75]. An amount of 175 μg Tween-20, 155 μL linoleic acid, and 0.04 mol/L potassium phosphate buffer (pH 7.0) was mixed to make a lineolate emulsion. Samples and standards at different concentrations (1 mL) were added to 4.1 mL linoleate emulsion, 0.02 mol/L phosphate buffer (pH = 7.8), and distilled water (DW), then kept warm in the dark at 40 °C. An amount of 0.1 mL of a mixture of each series was added to 9.7 mL ammonium thiocyanate (75%) and incubated for three minutes, and then 0.1 mL of $FeCl_3$ (0.02 mol/L in 3.5% HCl) was added. The peroxide concentration was determined daily at 500 nm. The lipid peroxidation inhibition calculation was designed as the following equation:

$$Inhibition\ \% = ((A_{\ control} - A_{\ sample})/A_{\ control}) \times 100$$

Reduction of Ferric Ions (Fe^{3+})

The ability of the *M. vulgare* extract and the reference compounds to reduce Fe^{3+} ions was described previously [76]. A fixed volume of each tested sample (2.5 mL) was mixed with the same volume of phosphate buffer (0.2 mol/L, pH 6.6) and 1% of $K_3Fe(CN)_6$, and then incubated for 20 min. Subsequently, the same volume of (10%) trichloroacetic acid was introduced to the solution, followed by centrifugation for 10 min at 1000× *g* (MSE Mistral 2000; Sanyo Gallenkamp PLC, Leicestershire, UK, serial no.: S693/02/444). Finally, 2.5 mL of the upper layer was added to 2.5 mL methanol and 0.5 mL ferric chloride ($FeCl_3$, 0.1%) and read at 700 nm.

Ferrous Ions (Fe^{2+})-Chelating Capacity

The Fe^{2+} chelating capacity of the extract and the standard materials were assayed based on the technique of Dinis et al. (1994) [77]. An amount of 0.05 mL $FeCl_2$ (2 mmol/L) was added to each sample. The experiment was initiated by introducing 0.2 mL ferrozine (5 mmol/L), and the mixture was agitated strongly and left to stand at room temperature for 10 min before being measured at 562 nm. The formula provided the percentage of the inhibition of ferrozine-Fe^{2+} complex formation:

$$Inhibition\ (\%) = ((A_{\ control} - A_{\ sample})/A_{\ control}) \times 100$$

4.3.2. Scavenging Properties

$NO^{\bullet}$ Radical-Scavenging Power

The capability of the *M. vulgare* extract and the reference compounds to capture NO• was evaluated based on the method of Marcocci et al. [78]. $NO^{\bullet}$ generated from sodium nitroprusside (SNP) was detected using the Griss mixture, which consisted of 1% sulfanilamide in 5% ortho-H_3PO_4 and 0.1% naphthylethylene diamine dihydrochloride. Initially, 2 mL of each sample was added to SNP (10 mmol/L) and then incubated at 25 °C for 150 min. Subsequently, 1 mL of the mixture was diluted with 1 mL of Griess reagent, and the absorbance was measured at 540 nm against a standard solution.

$DPPH^{\bullet}$ Radical-Scavenging Power

The capacity of *M. vulgare* to neutralize $DPPH^{\bullet}$ radicals was estimated based on the protocol of Yamaguchi et al. [79]. An amount of 1 mL of DPPH• reagent (0.1 mmol/L

DPPH• in methanol) was add to 3 mL of each trial, mixed vigorously, and left to remain at room temperature for 30 min before a reading at 517 nm. The control was prepared using the same process but without the sample. The DPPH• radical content was calculated using the following formula:

$$DPPH^{\bullet}\ radical\ scavenging\ power\ (\%) = 100 - ((A_{\ control} - A_{\ sample})/A_{\ control} \times 100)$$

ABTS Radical Cation Capture Power

The capacity of *M. vulgare* to capture the ABTS radical cations was assayed using the technique developed by Miller and Rice-Evans [80] and modified by Arnao et al. [81]. An amount of 0.2 mL of peroxidase (4.4 U/mL), 0.2 mL of H_2O_2 (50 µmol/L), 0.2 mL of ABTS (100 µmol/L), and 1 mL of methanol was added and kept in the dark for 1 h to form a bluish-green complex. Then, 1 mL of each sample was added to the complex, and the absorbance was measured at 734 nm. The ABTS radical cation capture power was calculated as follows:

$$ABTS_{\bullet}\ radical\ scavenging\ power\ (\%) = (1 - (A_{\ sample}/A_{\ control})) \times 100$$

H_2O_2 Scavenging Activity

The H_2O_2 scavenging ability of *M. vulgare* extract or the standard compounds were assessed using the method described by Ruch et al. [82]. Samples and standard concentrations were added to 0.6 mL H_2O_2 (40 mmol/L) and then read at 230 nm after 10 min against a phosphate buffer blank without H_2O_2. The H_2O_2 scavenging capacity was calculated as follows:

$$H_2O_2\ \% = Inhibition\ (\%) = ((A_{\ control} - A_{\ sample})/A_{\ control}) \times 100$$

4.3.3. Anti-Inflammatory Activity Assay

Cyclooxygenase Inhibition Protocol

The cyclooxygenase reduction protocol was carried out based on the method of Larsen et al. [83], and celecoxib was employed as a reference drug. Leuco-2, 7-dichlorofluorescein diacetate (5 mg) was hydrolyzed at room temperature in 50 µL sodium hydroxide (NaOH, 1M) for 10 min, then 30 µL HCl (1M) was mixed to neutralize excess NaOH, before the resulting 1-DCF was diluted in 0.1 M Tris buffer, pH 8. The cyclooxygenase enzyme (COX-1 or COX-2) was diluted in 0.1 M Tris buffer, pH 8. The examined samples (20 µL) were incubated with the enzyme at room temperature for 5 min in the presence of hematin. To initiate the reaction, phenol (500 µM), 1-DCF (20 µM), and hematin (1 µM) were added to a 1 mL final volume of 0.1 M Tris buffer, pH8. The reaction was monitored for 1 min at 502 nm. The blank contained all of the reaction components except the enzyme.

4.3.4. In Vitro Evaluation of the Anti-Alzheimer Effectiveness of the *M. vulgare* Extract

Inhibition of Acetylcholinesterase

The acetylcholinesterase activities (AChE and BChE) were analyzed based on the methods of Ingkaninan et al. [84]. The *M. vulgare* serial concentrations in methyl alcohol (100, 250, 500, 750, and 1000 µg/mL) were first organized. Also, the rest of the protocol steps were followed as described previously [15,84]. The measurement was conducted in triplicate, and the mean absorbance was used to calculate the inhibition percentage. The IC_{50} values were calculated using the log–probit analysis [15].

Inhibition of Tyrosinase

Liu et al. [85] conducted the tyrosinase inhibition assessment. The absorbance was calculated at 475 nm using a spectrophotometer. *M. vulgare* extract (40 µL) was liquefied in methanol and added to each well. Each well received 80 µL of phosphate buffer (pH 6.8), 40 µL of tyrosinase, and 40 µL of L-Dopa. The blank included all the constituents except

L-Dopa. Kojic acid was considered a common inhibitor. The percentage of tyrosinase reduction in the extract and standard was determined three times [15].

4.4. Molecular Docking Study

To explore the molecular basis of the *M. vulgare* extract in combating Alzheimer's disease, all 56 components identified in the extract were subjected to molecular docking studies with enzymes related to Alzheimer's disease. As mentioned in a current report, docking experiments were designed by MOE software (Version 2014. 09, Chemical Computing Group Inc., Montreal, Canada) [86]. X-ray crystal structures of cyclooxygenase (PDB ID: 3mdl), acetylcholinesterase (PDB ID: 4ey7), butyrylcholinesterase (PDB ID: 1xlu), and tyrosinase (PDB ID: 5m8t) were restored from the Protein Data Bank (https://www.rcsb.org, access on 1 April 2024) and created with MOE. Water molecules located farther than 4.5 Å from the ligand or receptor were deleted, and structure preparation was performed to address protonation issues in the protein, using default settings in QuickPrep. The co-crystallized ligand was removed from the prepared protein and redocked into the binding site to validate the docking protocol by analyzing the RMSD and docking parameters. Both ligand and receptor molecules were energy-minimized using the Amber10:EHT force field. The Triangular Matching docking approach was used to dock all compounds into the active sites of the four enzymes. The number of docking iterations was set to 300, while the default values were used for the remaining parameters, resulting in five descriptions of each ligand–protein complex. The docking mode with the lowest energy was selected, and the docking findings were manually examined to determine the interactions of the drugs with binding pockets.

4.5. Statistical Analysis

The results are shown as mean ± SD. In vitro antioxidant data were analyzed using a one-way *t*-test ($n = 4$). The *p*-value was less than 0.05, indicating statistical significance.

5. Conclusions

In the current study, the crude extract of *M. vulgare* suppressed acetylcholinesterase and butyrylcholinesterase degradation, which are essential enzymes involved in correctly functioning processes related to memory and learning. It may also prevent the aggregation of neurofibrillary tangles by reducing tyrosinase activity. Additionally, *M. vulgare* has shown potential as a selective antioxidant and anti-inflammatory agent, which can prevent the cascade of amyloid-β and senile plaque formation. The antioxidant activity of *M. vulgare* can ultimately lead to the suppression of lipid peroxidation and the formation of amyloid-β. The current study effectively demonstrated the comprehensive role of the crude *M. vulgare* extract in treating Alzheimer's syndrome according to its anti-acetylcholinesterase and anti-butyrylcholinesterase effects, anti-tyrosinase activities, and antioxidant and anti-inflammatory properties. In addition, the molecular docking studies introduced the phenylethanoid glycoside metabolites of marruboside, samioside, and forsythoside B as promising potential anti-Alzheimer agents with the lowest binding affinities towards the investigated enzymes.

Supplementary Materials: The following supporting information can be downloaded at: https://www.mdpi.com/article/10.3390/ph17101282/s1, Table S1: molecular docking results.

Author Contributions: M.E.: Project administration, Conceptualization, Formal analysis, Methodology, Data curation, Investigation, Software, Visualization, Writing—review and editing. S.A.E.-N.: Supervision, Data curation, Resources, Writing—original draft. H.Y.A.: Formal analysis, Investigation, Writing—original draft, Funding. B.W.: Methodology, Data curation, Investigation, Software, Visualization. M.S.: Project administration, Conceptualization, Formal analysis, Methodology, Investigation, Validation, Software, Writing—review and editing. A.Y.I.: Conceptualization, Methodology, Supervision, Data curation, Validation, Writing—original draft. All authors have read and agreed to the published version of the manuscript.

Funding: The authors thank the Researcher-Supporting Project, number (RSP2024R504), King Saud University, Riyadh, Saudi Arabia.

Institutional Review Board Statement: Not applicable.

Informed Consent Statement: Not applicable.

Data Availability Statement: Data is contained within the article or Supplementary Material.

Acknowledgments: The authors wish to express the Researcher-Supporting Project, number (RSP2024R504), King Saud University, Riyadh, Saudi Arabia. As well as the authors continue thanks to the National Research Centre of Egypt for supporting this work.

Conflicts of Interest: The authors declare no conflicts of interest.

References

1. Aćimović, M.; Jeremić, K.; Salaj, N.; Gavarić, N.; Kiprovski, B.; Sikora, V.; Zeremski, T. *Marrubium vulgare* L.: A phytochemical and pharmacological overview. *Molecules* **2020**, *25*, 2898. [CrossRef] [PubMed]
2. Sewidan, N.; Khalaf, R.A.; Mohammad, H. In-vitro studies on selected Jordanian plants as dipeptidyl peptidase-IV inhibitors for management of diabetes mellitus. *Iran. J. Pharm. Res.* **2020**, *19*, 95. [PubMed]
3. Lodhi, S.; Vadnere, G.P.; Sharma, V.K.; Usman, M.R. *Marrubium vulgare* L.: A review on phytochemical and pharmacological aspects. *J. Intercult. Ethnopharmacol.* **2017**, *6*, 429–452. [CrossRef]
4. Paula de Oliveira, A.; Santin, J.R.; Lemos, M.; Klein Júnior, L.C.; Couto, A.G.; Meyre da Silva Bittencourt, C.; Filho, V.C.; Faloni de Andrade, S. Gastroprotective activity of methanol extract and marrubiin obtained from leaves of *Marrubium vulgare* L. (Lamiaceae). *J. Pharm. Pharmacol.* **2011**, *63*, 1230–1237. [CrossRef] [PubMed]
5. Akther, N.; Shawl, A.; Sultana, S.; Chandan, B.; Akhter, M. Hepatoprotective activity of *Marrubium vulgare* against paracetamol induced toxicity. *J. Pharm. Res.* **2013**, *7*, 565–570. [CrossRef]
6. Robles-Zepeda, R.E.; Velázquez-Contreras, C.A.; Garibay-Escobar, A.; Gálvez-Ruiz, J.C.; Ruiz-Bustos, E. Antimicrobial activity of Northwestern Mexican plants against *Helicobacter pylori*. *J. Med. Food* **2011**, *14*, 1280–1283. [CrossRef]
7. Dallali, S.; Rouz, S.; Aichi, H.; Hassine, H.B. Phenolic contentand allelopathic potential of leavesand rhizosphere soilaqueous extracts of white horehound (*Maribum vulgare* L.). *J. New Sci.* **2017**, *39*, 3.
8. Yabrir, B. Essential oil of *Marrubium vulgare*: Chemical composition and biological activities. A review. *Nat. Prod. Sci.* **2019**, *25*, 81–91. [CrossRef]
9. Evans, W.C. *Trease and Evans' Pharmacognosy*; Elsevier Health Sciences: Amsterdam, The Netherlands, 2009.
10. Izzo, A.A.; Hoon-Kim, S.; Radhakrishnan, R.; Williamson, E.M. A critical approach to evaluating clinical efficacy, adverse events and drug interactions of herbal remedies. *Phytother. Res.* **2016**, *30*, 691–700. [CrossRef]
11. Chaachouay, N.; Zidane, L. Plant-derived natural products: A source for drug discovery and development. *Drugs Drug Candidates* **2024**, *3*, 184–207. [CrossRef]
12. Kumar, A.; Sidhu, J.; Goyal, A.; Tsao, J.W.; Doerr, C. *Alzheimer Disease (Nursing)*; StatPearls Publishing: Treasure Island, FL, USA, 2021.
13. Health, U.D.o.; Services, H. *Alzheimer's Disease Fact Sheet. National Institute on Aging*; US Department of Health and Human Services: Washington, DC, USA, 2019.
14. Alzheimer's Association. 2018 Alzheimer's disease facts and figures. *Alzheimer's Dement.* **2018**, *14*, 367–429. [CrossRef]
15. Ibrahim, A.; El-Newary, S.; Hendawy, S.F.; Ibrahim, A.E. *Balanites aegyptiaca* extract to treat risk factors of Alzheimer's disease: An in vitro study. *Egypt. J. Chem.* **2021**, *64*, 781–792. [CrossRef]
16. Samai, Z.; Toudert, N.; Djilani, S.E.; Dadda, N.; Zakkad, F.; Hamel, T. Chemical composition and in vitro antioxidant, anti-alzheimer, anti-diabetic, anti-tyrosinase, and antimicrobial properties of essential oils and extracts derived from various parts of the algerian *Calendula suffruticosa* vahlsubsp. *boissieri Lanza. Chem. Biodivers.* **2023**, *20*, e202200620. [CrossRef] [PubMed]
17. Kenchappa, P.G.; Karthik, Y.; Vijendra, P.D.; Hallur, R.L.; Khandagale, A.S.; Pandurangan, A.K.; Jayanna, S.G.; Alshehri, M.A.; Alasmari, A.; Sayed, S. In vitro evaluation of the neuroprotective potential of *Olea dioica* against Aβ peptide-induced toxicity in human neuroblastoma SH-SY5Y cells. *Front. Pharmacol.* **2023**, *14*, 1139606. [CrossRef] [PubMed]
18. Speranza, L.; Di Porzio, U.; Viggiano, D.; de Donato, A.; Volpicelli, F. Dopamine: The neuromodulator of long-term synaptic plasticity, reward and movement control. *Cells* **2021**, *10*, 735. [CrossRef]
19. Greggio, E.; Bergantino, E.; Carter, D.; Ahmad, R.; Costin, G.E.; Hearing, V.J.; Clarimon, J.; Singleton, A.; Eerola, J.; Hellström, O. Tyrosinase exacerbates dopamine toxicity but is not genetically associated with Parkinson's disease. *J. Neurochem.* **2005**, *93*, 246–256. [CrossRef]
20. Rodboon, T.; Palipoch, S.; Okada, S.; Charoenchon, N.; Nakornpakdee, Y.; Suwannalert, P. Oxyresveratrol inhibits cellular tyrosinase-related oxidative stress-induced melanogenesis in B16 melanoma cells. *J. Appl. Pharm. Sci.* **2020**, *10*, 008–013.
21. Guillen Quispe, Y.N.; Hwang, S.H.; Wang, Z.; Lim, S.S. Screening of peruvian medicinal plants for tyrosinase inhibitory properties: Identification of tyrosinase inhibitors in *Hypericum laricifolium* Juss. *Molecules* **2017**, *22*, 402. [CrossRef]

22. Qu, Y.; Zhan, Q.; Du, S.; Ding, Y.; Fang, B.; Du, W.; Wu, Q.; Yu, H.; Li, L.; Huang, W. Catalysis-based specific detection and inhibition of tyrosinase and their application. *J. Pharm. Anal.* **2020**, *10*, 414–425. [CrossRef]
23. Tiwari, P.; Dwivedi, S.; Singh, M.P.; Mishra, R.; Chandy, A. Basic and modern concepts on cholinergic receptor: A review. *Asian Pac. J. Trop. Dis.* **2013**, *3*, 413–420. [CrossRef]
24. Liu, M.-Y.; Zeng, F.; Shen, Y.; Wang, Y.-Y.; Zhang, N.; Geng, F. Bioguided isolation and structure identification of acetylcholinesterase enzyme inhibitors from Drynariae rhizome. *J. Anal. Methods Chem.* **2020**, *2020*, 2971841. [CrossRef]
25. Braak, H.; Del Tredici, K. Alzheimer's pathogenesis: Is there neuron-to-neuron propagation? *Acta Neuropathol.* **2011**, *121*, 589–595. [CrossRef]
26. Usman, K. Medicinal plants anticholinesterase activity and the potential for Alzheimer's disease treatment. *J. Dis. Med. Plants* **2017**, *3*, 68–82.
27. Bursal, E.; Aras, A.; Kılıç, Ö. Evaluation of antioxidant capacity of endemic plant *Marrubium astracanicum* subsp. *macrodon*: Identification of its phenolic contents by using HPLC-MS/MS. *Nat. Prod. Res.* **2019**, *33*, 1975–1979. [CrossRef]
28. Nawwar, M.A.; El-Mousallamy, A.M.; Barakat, H.H.; Buddrus, J.; Linscheid, M. Flavonoid lactates from leaves of *Marrubium vulgare*. *Phytochemistry* **1989**, *28*, 3201–3206. [CrossRef]
29. Amri, B.; Martino, E.; Vitulo, F.; Corana, F.; Ben-Kaâb, L.B.; Rui, M.; Rossi, D.; Mori, M.; Rossi, S.; Collina, S. *Marrubium vulgare* L. leave extract: Phytochemical composition, antioxidant and wound healing properties. *Molecules* **2017**, *22*, 1851. [CrossRef]
30. Hashemi, M.; Kharazian, N. Identification of flavonoids from *Marrubium* and *Ballota* species (Lamiaceae) and determination of chemotaxonomic markers using high performance liquid chromatography mass spectrometer. *J. Sci. Islam. Repub. Iran* **2021**, *32*, 305–320.
31. Abdelhameed, R.F.; Ali, A.I.; Elhady, S.S.; Abo Mansour, H.E.; Mehanna, E.T.; Mosaad, S.M.; Ibrahim, S.A.; Hareeri, R.H.; Badr, J.M.; Eltahawy, N.A. *Marrubium alysson* L. ameliorated methotrexate-induced testicular damage in mice through regulation of apoptosis and miRNA-29a expression: LC-MS/MS metabolic profiling. *Plants* **2022**, *11*, 2309. [CrossRef]
32. Liu, L.; Gao, Q.; Zhang, Z.; Zhang, X. *Elsholtzia rugulosa*: Phytochemical profile and antioxidant, anti-Alzheimer's disease, antidiabetic, antibacterial, cytotoxic and hepatoprotective activities. *Plant Foods Hum. Nutr.* **2022**, *77*, 62–67. [CrossRef]
33. Rahman, M.M.; Sayeed, M.S.B.; Haque, M.A.; Hassan, M.M.; Islam, S.A. Phytochemical screening, antioxidant, anti-Alzheimer and anti-diabetic activities of *Centella asiatica*. *J. Nat. Prod. Plant Resour.* **2012**, *2*, 504–511.
34. Paul, A.; Zothantluanga, J.H.; Rakshit, G.; Celik, I.; Rudrapal, M.; Zaman, M.K. Computational simulations reveal the synergistic action of phytochemicals of *Morus alba* to exert anti-Alzheimer activity via inhibition of acetylcholinesterase and glycogen synthase kinase-3β. *Polycycl. Aromat. Compd.* **2023**, *44*, 3476–3500. [CrossRef]
35. Lopa, S.S.; Al-Amin, M.Y.; Hasan, M.K.; Ahammed, M.S.; Islam, K.M.; Alam, A.; Tanaka, T.; Sadik, M.G. Phytochemical analysis and cholinesterase inhibitory and antioxidant activities of *Enhydra fluctuans* relevant in the management of Alzheimer's disease. *Int. J. Food Sci.* **2021**, *2021*, 8862025. [CrossRef]
36. Neganova, M.; Afanas'eva, S.; Klochkov, S.; Shevtsova, E. Mechanisms of antioxidant effect of natural sesquiterpene lactone and alkaloid derivatives. *Bull. Exp. Biol. Med.* **2012**, *152*, 720. [CrossRef]
37. Malinowska, P. Effect of flavonoids content on antioxidant activity of commercial cosmetic plant extracts. *Herba Pol.* **2013**, *59*, 63–75. [CrossRef]
38. Kondratyuk, T.P.; Pezzuto, J.M. Natural product polyphenols of relevance to human health. *Pharm. Biol.* **2004**, *42*, 46–63. [CrossRef]
39. Bogdan, C. Nitric oxide and the immune response. *Nat. Immunol.* **2001**, *2*, 907–916. [CrossRef]
40. Bendlin, B.; Carlsson, C.; Gleason, C.; Johnson, S.; Sodhi, A.; Gallagher, C.; Puglielli, L.; Engelman, C.; Ries, M.; Xu, G. Midlife predictors of Alzheimer's disease. *Maturitas* **2010**, *65*, 131–137. [CrossRef]
41. Quinn, D.M. Acetylcholinesterase: Enzyme structure, reaction dynamics, and virtual transition states. *Chem. Rev.* **1987**, *87*, 955–979. [CrossRef]
42. Schlemper, V.; Ribas, A.; Nicolau, M.; Cechinel Filho, V. Antispasmodic effects of hydroalcoholic extract of *Marrubium vulgare* on isolated tissues. *Phytomedicine* **1996**, *3*, 211–216. [CrossRef] [PubMed]
43. Khan, M.T.H.; Orhan, I.; Şenol, F.; Kartal, M.; Şener, B.; Dvorská, M.; Šmejkal, K.; Šlapetová, T. Cholinesterase inhibitory activities of some flavonoid derivatives and chosen xanthone and their molecular docking studies. *Chem. Biol. Interact.* **2009**, *181*, 383–389. [CrossRef]
44. Szwajgier, D. Anticholinesterase activity of phenolic acids and their derivatives. *Z. Naturforschung C* **2013**, *68*, 125–132. [CrossRef]
45. Neagu, E.; Radu, G.L.; Albu, C.; Paun, G. Antioxidant activity, acetylcholinesterase and tyrosinase inhibitory potential of *Pulmonaria officinalis* and *Centarium umbellatum* extracts. *Saudi J. Biol. Sci.* **2018**, *25*, 578–585. [CrossRef] [PubMed]
46. Orhan, I.; Kartal, M.; Tosun, F.; Şener, B. Screening of various phenolic acids and flavonoid derivatives for their anticholinesterase potential. *Z. Naturforschung C* **2007**, *62*, 829–832. [CrossRef] [PubMed]
47. Shahwar, D.; Rehman, S.U.; Raza, M.A. Acetyl cholinesterase inhibition potential and antioxidant activities of ferulic acid isolated from *Impatiens bicolor* Linn. *J. Med. Plants Res* **2010**, *4*, 260–266.
48. Heo, K.S.; Lee, S.J.; Ko, J.H.; Lim, K.; Lim, K.T. Glycoprotein isolated from *Solanum nigrum* L. inhibits the DNA-binding activities of NF-κB and AP-1, and increases the production of nitric oxide in TPA-stimulated MCF-7 cells. *Toxicol. Vitr.* **2004**, *18*, 755–763. [CrossRef]

49. Anand, P.; Singh, B.; Singh, N. A review on coumarins as acetylcholinesterase inhibitors for Alzheimer's disease. *Bioorg. Med. Chem.* **2012**, *20*, 1175–1180. [CrossRef]
50. Konrath, E.L.; Passos, C.d.S.; Klein-Júnior, L.C.; Henriques, A.T. Alkaloids as a source of potential anticholinesterase inhibitors for the treatment of Alzheimer's disease. *J. Pharm. Pharmacol.* **2013**, *65*, 1701–1725. [CrossRef]
51. Storga, D.; Vrecko, K.; Birkmayer, J.; Reibnegger, G. Monoaminergic neurotransmitters, their precursors and metabolites in brains of Alzheimer patients. *Neurosci. Lett.* **1996**, *203*, 29–32. [CrossRef] [PubMed]
52. Zengin, G.; Guler, G.O.; Aktumsek, A.; Ceylan, R.; Picot, C.M.N.; Mahomoodally, M.F. Enzyme inhibitory properties, antioxidant activities, and phytochemical profile of three medicinal plants from Turkey. *Adv. Pharmacol. Pharm. Sci.* **2015**, *2015*, 410675. [CrossRef]
53. Baek, H.S.; Rho, H.S.; Yoo, J.W.; Ahn, S.M.; Lee, J.Y.; Jeonga-Lee, J.-L.; Kim, M.-K.; Kim, D.H.; Chang, I.S. The inhibitory effect of new hydroxamic acid derivatives on melanogenesis. *Bull. Korean Chem. Soc.* **2008**, *29*, 43–46.
54. Salah, N.M.; Souleman, A.M.; Shaker, K.H.; Hawary, S.; El-Hady, F. Acetylcholinesterase, alpha-glucosidase and tyrosinase inhibitors from Egyptian propolis. *Int. J. Pharmacogn. Phytochem. Res.* **2017**, *9*, 528–536. [CrossRef]
55. Aparadh, V.; Naik, V.; Karadge, B.A. Antioxidative properties (TPC, DPPH, FRAP, metal chelating ability, reducing power and TAC) within some *Cleome* species. *Ann. Bot.* **2012**, *2*, 49–56.
56. Prajit, R.; Sritawan, N.; Suwannakot, K.; Naewla, S.; Aranarochana, A.; Sirichoat, A.; Pannangrong, W.; Wigmore, P.; Welbat, J.U. Chrysin protects against memory and hippocampal neurogenesis depletion in D-galactose-induced aging in rats. *Nutrients* **2020**, *12*, 1100. [CrossRef] [PubMed]
57. Balez, R.; Steiner, N.; Engel, M.; Muñoz, S.S.; Lum, J.S.; Wu, Y.; Wang, D.; Vallotton, P.; Sachdev, P.; O'Connor, M. Neuroprotective effects of apigenin against inflammation, neuronal excitability and apoptosis in an induced pluripotent stem cell model of Alzheimer's disease. *Sci. Rep.* **2016**, *6*, 31450. [CrossRef] [PubMed]
58. Rehfeldt, S.C.H.; Silva, J.; Alves, C.; Pinteus, S.; Pedrosa, R.; Laufer, S.; Goettert, M.I. Neuroprotective effect of luteolin-7-O-glucoside against 6-OHDA-induced damage in undifferentiated and RA-differentiated SH-SY5Y Cells. *Int. J. Mol. Sci.* **2022**, *23*, 2914. [CrossRef] [PubMed]
59. Zhong, L.; Tong, Y.; Chuan, J.; Bai, L.; Shi, J.; Zhu, Y. Protective effect of ethyl vanillin against Aβ-induced neurotoxicity in PC12 cells via the reduction of oxidative stress and apoptosis. *Exp. Ther. Med.* **2019**, *17*, 2666–2674. [CrossRef] [PubMed]
60. Liu, L.; Liu, Y.; Zhao, J.; Xing, X.; Zhang, C.; Meng, H. Neuroprotective effects of D-(-)-quinic acid on aluminum chloride-induced dementia in rats. *Evid. Based Complement. Altern. Med.* **2020**, *2020*, 5602597. [CrossRef] [PubMed]
61. Fernandes, M.Y.D.; Dobrachinski, F.; Silva, H.B.; Lopes, J.P.; Gonçalves, F.Q.; Soares, F.A.; Porciúncula, L.O.; Andrade, G.M.; Cunha, R.A.; Tomé, A.R. Neuromodulation and neuroprotective effects of chlorogenic acids in excitatory synapses of mouse hippocampal slices. *Sci. Rep.* **2021**, *11*, 10488. [CrossRef]
62. Shao, S.-Y.; Zhang, F.; Yang, Y.-N.; Feng, Z.-M.; Jiang, J.-S.; Zhang, P.-C. Neuroprotective and anti-inflammatory phenylethanoid glycosides from the fruits of Forsythia suspensa. *Bioorganic Chem.* **2021**, *113*, 105025. [CrossRef]
63. Yang, J.; Ju, B.; Hu, J. Effects of phenylethanoid glycosides extracted from *Herba cistanches* on the learning and memory of the APP/PSI transgenic mice with Alzheimer's disease. *BioMed Res. Int.* **2021**, *2021*, 1291549. [CrossRef]
64. Ji, S.; Wu, Y.; Zhu, R.; Guo, D.; Jiang, Y.; Huang, L.; Ma, X.; Yu, L. Novel Phenylethanoid glycosides improve hippocampal synaptic plasticity via the cyclic adenosine monophosphate-CREB-brain-derived neurotrophic growth factor pathway in APP/PS1 transgenic mice. *Gerontology* **2023**, *69*, 1065–1075. [CrossRef] [PubMed]
65. Singleton, V.L.; Orthofer, R.; Lamuela-Raventós, R.M. Analysis of total phenols and other oxidation substrates and antioxidants by means of Folin-Ciocalteu reagent. *Methods Enzymol.* **1999**, *299*, 152–178.
66. Broadhurst, R.B.; Jones, W.T. Analysis of condensed tannins using acidified vanillin. *J. Sci. Food Agric.* **1978**, *29*, 788–794. [CrossRef]
67. Onwuka, G. Soaking, boiling and antinutritional factors in pigeon peas (*Cajanus cajan*) and cowpeas (*Vigna unguiculata*). *J. Food Process. Preserv.* **2006**, *30*, 616–630. [CrossRef]
68. Ahmed, W.; Kamal, A.; Ibrahim, R. Phytochemical screening and chemical investigation of lipoidal matter of *Arenga engleri* leaves. *J. Adv. Pharm. Res.* **2019**, *3*, 83–89. [CrossRef]
69. Johnson, A.R.; Davenport, J.B. *Biochemistry and Methodology of Lipids*; John Wiley & Sons, Inc.: Hoboken, NJ, USA, 1971.
70. Fang, K.; Pan, X.; Huang, B.; Liu, J.; Wang, Y.; Gao, J. Simultaneous derivatization of hydroxyl and ketone groups for the analysis of steroid hormones by GC–MS. *Chromatographia* **2010**, *72*, 949–956. [CrossRef]
71. Seif, M.; Aati, H.; Amer, M.; Ragauskas, A.J.; Seif, A.; El-Sappah, A.H.; Aati, A.; Madboli, A.E.-N.A.; Emam, M. Mitigation of hepatotoxicity via boosting antioxidants and reducing oxidative stress and inflammation in carbendazim-treated rats using *Adiantum capillus-veneris* L. Extract. *Molecules* **2023**, *28*, 4720. [CrossRef] [PubMed]
72. Vogel, I. *Practical Organic Chemistry*; CiteSeer: Princeton, NJ, USA, 1974.
73. Hassan, M.; Mohdaly, A.; Elneairy, N.; Mahmoud, A. Influence of extraction systems on oil yield, wastes and olive oil properties. *Fayoum J. Agric. Res. Dev.* **2022**, *36*, 1–11. [CrossRef]
74. Farid, M.M.; Aboul Naser, A.F.; Salem, M.M.; Ahmed, Y.R.; Emam, M.; Hamed, M.A. Chemical compositions of *Commiphora opobalsamum* stem bark to alleviate liver complications in streptozotocin-induced diabetes in rats: Role of oxidative stress and DNA damage. *Biomarkers* **2022**, *27*, 671–683. [CrossRef]

75. Duh, P.-D.; Tu, Y.-Y.; Yen, G.-C. Antioxidant activity of water extract of Harng Jyur (*Chrysanthemum morifolium* Ramat). *LWT-Food Sci. Technol.* **1999**, *32*, 269–277. [CrossRef]
76. Oyaizu, M. Studies on products of browning reaction: Antioxidative activities of products of browning reaction prepared from glucosamine. *Jpn. J. Nutr. Diet* **1986**, *44*, 307–315. [CrossRef]
77. Dinis, T.C.; Madeira, V.M.; Almeida, L.M. Action of phenolic derivatives (acetaminophen, salicylate, and 5-aminosalicylate) as inhibitors of membrane lipid peroxidation and as peroxyl radical scavengers. *Arch. Biochem. Biophys.* **1994**, *315*, 161–169. [CrossRef] [PubMed]
78. Marcocci, L.; Maguire, J.J.; Droylefaix, M.T.; Packer, L. The nitric oxide-scavenging properties of *Ginkgo biloba* extract EGb 761. *Biochem. Biophys. Res. Commun.* **1994**, *201*, 748–755. [CrossRef] [PubMed]
79. Yamaguchi, T.; Takamura, H.; Matoba, T.; Terao, J. HPLC method for evaluation of the free radical-scavenging activity of foods by using 1, 1-diphenyl-2-picrylhydrazyl. *Biosci. Biotechnol. Biochem.* **1998**, *62*, 1201–1204. [CrossRef] [PubMed]
80. Miller, N.J.; Rice-Evans, C.A. The relative contributions of ascorbic acid and phenolic antioxidants to the total antioxidant activity of orange and apple fruit juices and blackcurrant drink. *Food Chem.* **1997**, *60*, 331–337. [CrossRef]
81. Arnao, M.B.; Cano, A.; Acosta, M. The hydrophilic and lipophilic contribution to total antioxidant activity. *Food Chem.* **2001**, *73*, 239–244. [CrossRef]
82. Ruch, R.J.; Cheng, S.-j.; Klaunig, J.E. Prevention of cytotoxicity and inhibition of intercellular communication by antioxidant catechins isolated from Chinese green tea. *Carcinogenesis* **1989**, *10*, 1003–1008. [CrossRef] [PubMed]
83. Larsen, L.; Dahl, E.; Bremer, J. Peroxidative oxidation of leuco-dichlorofluorescein by prostaglandin H synthase in prostaglandin biosynthesis from polyunsaturated fatty acids. *Biochim. Biophys. Acta Lipids Lipid Metab.* **1996**, *1299*, 47–53. [CrossRef] [PubMed]
84. Ingkaninan, K.; Temkitthawon, P.; Chuenchom, K.; Yuyaem, T.; Thongnoi, W. Screening for acetylcholinesterase inhibitory activity in plants used in Thai traditional rejuvenating and neurotonic remedies. *J. Ethnopharmacol.* **2003**, *89*, 261–264. [CrossRef]
85. Liu, J.; Cao, R.; Yi, W.; Ma, C.; Wan, Y.; Zhou, B.; Ma, L.; Song, H. A class of potent tyrosinase inhibitors: Alkylidenethiosemicarbazide compounds. *Eur. J. Med. Chem.* **2009**, *44*, 1773–1778. [CrossRef]
86. Li, Y.-S.; He, M.; Zhou, T.-S.; Wang, Q.; He, L.; Wang, S.-J.; Hu, B.; Wei, B.; Wang, H.; Cui, Z.-N. 2, 5-Disubstituted furan derivatives containing 1, 3, 4-thiadiazole moiety as potent α-glucosidase and *E. coli* β-glucuronidase inhibitors. *Eur. J. Med. Chem.* **2021**, *216*, 113322. [CrossRef] [PubMed]

Disclaimer/Publisher's Note: The statements, opinions and data contained in all publications are solely those of the individual author(s) and contributor(s) and not of MDPI and/or the editor(s). MDPI and/or the editor(s) disclaim responsibility for any injury to people or property resulting from any ideas, methods, instructions or products referred to in the content.

pharmaceuticals

Article

Antibacterial Activity and Mechanisms of Plant Flavonoids against Gram-Negative Bacteria Based on the Antibacterial Statistical Model

Yu Yan [1,2,†], Xuexue Xia [1,2,†], Aiman Fatima [1], Li Zhang [2], Ganjun Yuan [1,2,*], Fengxian Lian [2] and Yu Wang [2]

[1] Biotechnological Engineering Center for Pharmaceutical Research and Development, Jiangxi Agricultural University, Nanchang 330045, China
[2] Laboratory of Natural Medicine and Microbiological Drug, College of Bioscience and Bioengineering, Jiangxi Agricultural University, Nanchang 330045, China
* Correspondence: gyuan@jxau.edu.cn; Tel.: +86-0791-83813459
† These authors contributed equally to this work.

Abstract: The antimicrobial quantitative structure–activity relationship of plant flavonoids against Gram-positive bacteria was established in our previous works, and the cell membrane was confirmed as a major site of action. To investigate whether plant flavonoids have similar antibacterial effects and mechanisms against both Gram-negative and Gram-positive bacteria, here, the minimum inhibitory concentrations (MICs) of 37 plant flavonoids against *Escherichia coli* were determined using the microdilution broth method, and then the correlation between their lipophilic parameter ACD/LogP or $LogD_{7.40}$ value and their MIC was analyzed. Simultaneously, the correlation between the ACD/LogP or $LogD_{7.40}$ value and the MIC of 46 plant flavonoids reported in the literature against *E. coli* was also analyzed. Both sets of results showed that there is a significant correlation between the LogP value and the MIC of plant flavonoids against Gram-negative bacteria. However, it is difficult to effectively predict the MIC of plant flavonoids against Gram-negative bacteria from their lipophilic parameters. By comparing two regression curves derived from plant flavonoids against Gram-negative and Gram-positive bacteria, it was further discovered that the antibacterial activities of most plant flavonoids against Gram-negative bacteria are stronger than those against Gram-positive bacteria when their LogP values are less than approximately 3.0, but the opposite is true when their LogP values are more than approximately 3.6. Moreover, this comparison also suggests that unlike mainly acting on the cell membrane of Gram-positive bacteria, plant flavonoids have multiple mechanisms against Gram-negative species, while the cell membrane is also an important action site among them. Combined with the correlation analyses between the enzyme inhibitory activity and the LogP value of the reported flavonoids, it was further suggested that DNA gyrase is another important target of plant flavonoids against Gram-negative bacteria.

Keywords: action mode; antimicrobial; *Escherichia coli*; flavonoids; Gram-negative bacteria; Gram-positive bacteria; lipophilicity; LogP; MIC; statistical model

1. Introduction

Antimicrobial resistance (AMR) has been seriously threatening public health and global economic development, and the COVID-19 pandemic has worsened this issue [1]. Therefore, there is an urgent need to discover new antimicrobial agents, especially those against Gram-negative bacteria [2–5]. Due to the unique structure of the cell envelope, the development of antibacterial agents against Gram-negative bacteria has always been a challenge [3,4]. Fortunately, via the structural modification of tetracyclines, quinolones, aminoglycosides, etc., several antibiotics have been approved for marketing, such as plazomicin and delafloxacin [4–6]. Simultaneously, some natural antibacterial products have also been undergoing clinical research [5,6]. Eventually, the resistant mutants will

emerge after they spend some time circulating in practice, especially in hospitals [7]. Meanwhile, some plant secondary metabolites have been gradually gaining attention since they not only have antimicrobial activities but also show a good safety profile [8,9]. Among these, plant flavonoids are increasingly gaining widespread recognition [10–15].

Flavonoids are an important class of secondary metabolites widely distributed in various plants, and many of them have different degrees of inhibitory activity against numerous pathogenic bacteria. Above all, some of them can enhance the antimicrobial activities of antimicrobial agents and/or even reverse AMR [16,17]. Various antibacterial mechanisms, involving the inhibition of DNA, proteins, and cell envelope biosynthesis, and the damage to the cell membrane, have been reported for plant flavonoids [16,17]. Simultaneously, many structure–activity relationships have been summarized, while some of them contradict one another [17–19]. Recently, the antimicrobial quantitative relationship of plant flavonoids against Gram-positive bacteria has been established that [20], through the statistical analyses and validation of large sample sets. Based on this relationship, the minimum inhibitory concentration (MIC) of plant flavonoids against Gram-positive bacteria can be predicted from their lipophilic physicochemical parameter LogP (Log_{10} of partition coefficient) or $LogD_{7.40}$ (Log_{10} of distribution coefficient at pH 7.40), which is calculated from their chemical structures using the software ACD/Labs. Moreover, it has been indicated that the cell membrane is the major action site of plant flavonoids against Gram-positive bacteria, which includes damage to phospholipid bilayers and respiratory chain inhibition [20,21]. Also, experiments interfering with menaquinone-4 or menaquinones extracted from *Staphylococcus aureus* further suggest that the quinone pool is a key target [22].

Considering the difficulties and biological obstacles in discovering natural products with strong antibacterial activity toward Gram-negative bacteria, it was spontaneously wondered from above whether the antimicrobial activities of plant flavonoids against Gram-negative bacteria are also related to their lipophilicities, and whether the antimicrobial quantitative relationship could also be established. In addition, do plant flavonoids have similar antibacterial effects and mechanisms against both Gram-negative and Gram-positive bacteria? The aim to explore these above will enable the prediction of Gram-negative bacteria MIC values and speed up the discovery of novel antimicrobial compounds. Therefore, the correlation between the lipophilic physicochemical parameter (LogP or $LogD_{7.40}$) and the MIC, the antibacterial quantitative structure–activity relationship, and the possible mechanisms of plant flavonoids against Gram-negative bacteria were further explored by following a procedure similar to those used to explore Gram-positive species.

2. Results

2.1. Structure, Antibacterial Activity, and Physicochemical Parameters

A total of 37 plant flavonoids (Table 1 and Figure 1), with seven structural subtypes, namely, dihydroflavones, flavones, flavonols, chalcones, isoflavones, isoflavanes, and xanthones, were selected for the antimicrobial susceptibility assay and correlation analyses of the antimicrobial activity MIC and the lipophilic physicochemical parameter LogP or $LogD_{7.40}$. Their MIC values (μM) against Escherichia coli and *S. aureus* were determined, and they are listed in Table 1, along with their calculated LogP and $LogD_{7.40}$ values. The results show that all these flavonoids had very weak antimicrobial activities against *E. coli*, with the MIC ranging from 1206.15 to more than 6820.53 μM. This indicates that these plant flavonoids, with LogP and $LogD_{7.40}$ values ranging from 1.26 to 6.70, have weak inhibitory activity against Gram-negative bacteria. However, they presented various degrees of antibacterial activities against *S. aureus*, with the MIC ranging from 9.42 to 13,552.14 or more than 7578.45 μM. According to the previously reported antimicrobial quantitative relationship, the MIC values of these plant flavonoids against Gram-positive bacteria *S. aureus* were simultaneously calculated, and the results show that 81.1% of the calculated MIC values fell into the acceptable range of 1/8 to 8 of the test MIC ones (Table 1). This

further confirms that the antimicrobial activity of plant flavonoids against Gram-positive bacteria can be effectively calculated or predicted.

Table 1. Tested plant flavonoids together with their structure types, physicochemical parameters and antibacterial activities.

Compounds (No.) [a]	Structure Types	LogP [b]	$LogD_{7.40}$ [b]	*E. coli* ATCC 25922		*S. aureus* ATCC 25923	
				MIC (μM) [c]	Log_{10} (MIC)	MIC (μM) [c]	Predicted MIC (μM) [d]
Sophoraflavanone G (**1**)	Dihydroflavones	6.52	6.33	1206.15	3.0814	9.42	16.37
Neohesperidin (**2**)	Dihydroflavones	2.44	1.99	1677.12	3.2246	>1677.12	1816.01
Naringin (**3**)	Dihydroflavones	2.73	2.30	1763.88	3.2465	>1763.88	1151.90
Hesperidin (**4**)	Dihydroflavones	1.78	1.33	1677.12	3.2246	>1677.12	4440.63
Methyl hesperidin (**5**)	Dihydroflavones	2.54	2.10	3278.95	3.5157	>3278.95	8410.66
Eriodictyol (**6**)	Dihydroflavones	2.59	2.34	7104.70	3.8515	>7104.70	1442.76
Eriocitrin (**7**)	Dihydroflavones	1.47	1.03	>3433.13	>3.5357	>3433.13	6397.02
Hesperitin (**8**)	Dihydroflavones	2.90	2.65	6775.18	3.8309	>6775.18	863.94
Naringenin (**9**)	Dihydroflavones	3.19	2.96	7527.47	3.8766	3763.74	509.64
didymin (**10**)	Dihydroflavones	2.72	2.29	3444.51	3.5371	>3444.51	1170.98
Narirutin (**11**)	Dihydroflavones	2.07	1.65	3527.75	3.5475	>3527.75	3063.61
Baicalein (**12**)	Flavones	3.31	2.60	>3789.22	>3.5785	>3789.22	404.47
Licoflavone C (**13**)	Flavones	4.20	3.77	3026.36	3.4809	3026.36	85.1
Tangeritin (**14**)	Flavones	2.73	2.73	2749.95	3.4393	>2749.95	1151.9
Nobiletin (**15**)	Flavones	2.8	2.80	2544.73	3.4056	>2544.74	1025.21
Vitexin (**16**)	Flavones	1.28	0.45	2368.29	3.3744	2368.29	7888.23
Isovitexin (**17**)	Flavones	1.28	0.15	>2368.29	>3.3744	2368.29	7888.23
Diosmin (**18**)	Flavones	2.05	1.23	1682.69	3.2260	>1682.69	3146.25
Rhoifolin (**19**)	Flavones	1.72	0.91	3540.07	3.5490	>3540.07	4777.21
Apigenin (**20**)	Flavones	2.10	1.57	7578.45	3.8796	>7578.45	2942.82
Diosmetin (**21**)	Flavones	3.10	2.55	>6820.53	>3.8338	>6820.53	603.30
5-Demethylnobiletin (**22**)	Flavones	2.60	2.28	5273.32	3.7221	>5273.32	1420.23
4′,5,7-Trimethoxyflavone (**23**)	Flavones	3.35	3.35	6557.38	3.8167	>6557.38	373.96
Sinensetin (**24**)	Flavones	3.40	3.40	5499.91	3.7404	>5499.91	338.78
Orientin (**25**)	Flavones	1.58	0.72	>4567.55	>3.6597	>4567.55	5639.27
Isoorientin (**26**)	Flavones	1.58	0.41	4567.55	3.6597	>4567.55	5639.27
Quercetin (**27**)	Flavonols	2.07	1.40	>3388.04	>3.5299	13552.14	3063.61
Galangin (**28**)	Flavonols	2.83	2.16	3789.22	3.5785	>3789.22	974.47
Icaritin (**29**)	Flavonols	5.09	4.54	2779.66	3.4430	2779.66	75.22
Rutin (**30**)	Flavonols	1.95	1.22	>1677.26	>3.2246	1677.26	3585.77
Quercitrin (**31**)	Flavonols	2.36	1.63	4567.55	3.6597	>4567.55	2043.95
Isoliquiritigenin (**32**)	Chalcones	3.40	3.26	3995.94	3.6016	3995.94	338.78
Licochalcone A (**33**)	Chalcones	4.95	4.85	3026.00	3.4809	11.82	74.44
Formononetin (**34**)	Isoflavones	3.15	2.91	3817.05	3.5817	>3817.04	549.61
Puerarin (**35**)	Isoflavones	2.14	1.59	4918.58	3.6918	614.82	2787.56
Glabridin (**36**)	Isoflavanes	4.18	4.18	3156.79	3.4992	49.32	86.81
α-Mangostin (**37**)	Xanthones	6.70	6.10	2494.70	3.3970	4.87	8.17

[a]: The structures of these compounds are shown in Figure S1 in Supplementary Materials. [b]: The LogP and $LogD_{7.40}$ values were calculated using the software ACD/Labs 6.0. [c]: MIC, minimum inhibitory concentration. [d]: The MIC values of plant flavonoids were predicted from the equation $y = -0.1285\ x^6 + 0.7944\ x^5 + 51.785\ x^4 - 947.64\ x^3 + 6638.7\ x^2 - 21{,}273\ x + 26{,}087$ [20], where y is the antimicrobial activity (MIC) of pant flavonoids against *S. aureus*; and x is the LogP value of corresponding pant flavonoids, also calculated using the software ACD/Labs 6.0.

Also, the MIC values of 52 plant flavonoids (Figure S1) against Gram-negative bacteria *E. coli* were collected from 16 papers in order to use additional data to obtain more reliable conclusions, and they are presented in Table 2. These plant flavonoids include eight structural subtypes, such as dihydroflavones, flavones, biflavones, flavonols, chalcones, isoflavones and xanthones. As intuitively observed from Table 2, the flavonoids with LogP values ranging from 1.53 to 8.03 presented various degrees of antibacterial activities against E. coli, with the reported MIC values ranging from 1.49 to 3308.19 or more than 1722.53 μM.

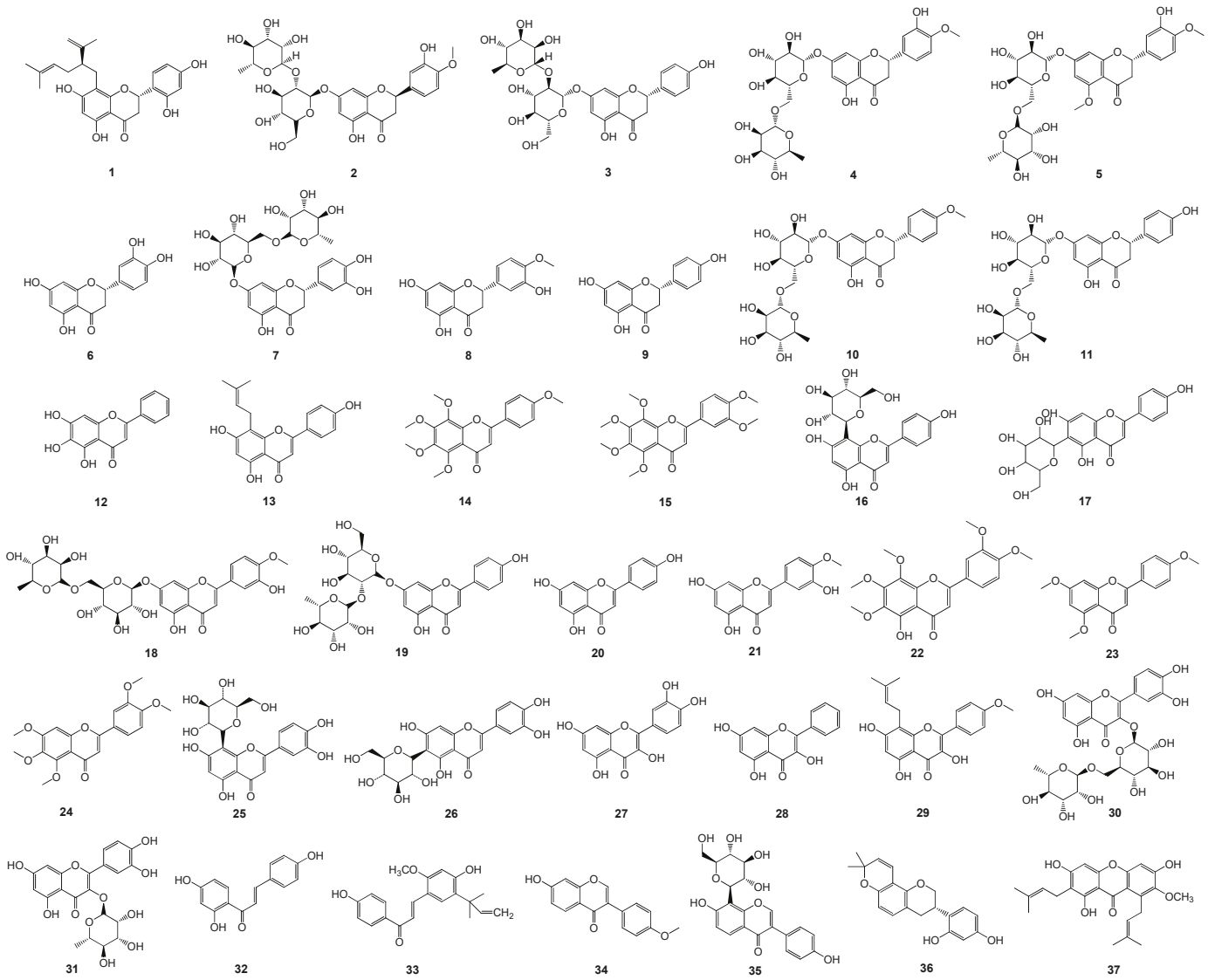

Figure 1. Chemical structures of 37 tested plant flavonoids.

Table 2. Reported plant flavonoids together with their structure types, physicochemical parameters, and inhibitory activities against *E. coli* ATCC 25922 [23–38].

Compounds (No.) [a]	Structure Types	LogP [b]	$LogD_{7.40}$ [b]	MIC (μM) [c]	Log_{10}(MIC) [c]	References
Candidone (**38**)	Dihydroflavones	5.64	5.64	11.35	1.0540	[23]
Atalantoflavone (**39**)	Flavones	4.31	3.58	761.13	2.8815	[23]
2′-hydroxyatalantoflavone (**40**)	Flavones	3.87	3.10	726.57	2.8613	[23]
Neocyclomorusin (**41**)	Flavones	4.30	2.87	18.33	1.2632	[23]
Neobavaisoflavone (**42**)	Isoflavones	4.68	4.69	23.64	1.3736	[23]
Daidzein (**43**)	Isoflavones	3.14	2.61	236.83	2.3744	[23]
Isowighteone (**44**)	Isoflavones	4.78	4.23	380.57	2.5804	[23]
Isoneorautenol (**45**)	Dihydroisoflavones	4.16	4.16	794.14	2.8999	[23]
Abyssione-V 4′-*O*-methyl ether (**46**)	Dihydroflavones	8.03	7.79	9.23	0.9652	[24]
6,8-diprenylgenistein (**47**)	Isoflavones	7.33	7.16	19.19	1.2831	[24]
Alpinumisoflavone (**48**)	Isoflavones	5.80	4.93	11.60	1.0645	[24]
Eriodictyol (**49**)	Dihydroflavones	2.59	2.34	867.27	2.9382	[25]
Hesperetin (**50**)	Dihydroflavones	2.90	2.65	3308.19	3.5196	[25]
Neohesperidin (**51**)	Dihydroflavones	2.44	1.99	>1637.81	>3.2143	[25]
Neoeriocitrin (**52**)	Dihydroflavones	2.13	1.68	1341.07	3.1275	[25]
Naringin (**53**)	Dihydroflavones	2.73	2.30	>1722.53	>3.2362	[25]
Naringenin (**54**)	Dihydroflavones	3.19	2.96	2938.37	3.4681	[25]
5-hydroxy-7,4′-dimethoxyflavone (**55**)	Flavones	3.40	2.78	167.62	2.2243	[26]
Genkwanin (**56**)	Flavones	2.36	1.75	351.78	2.5463	[26]

Table 2. *Cont.*

Compounds (No.) [a]	Structure Types	LogP [b]	$LogD_{7.40}$ [b]	MIC (μM) [c]	Log_{10}(MIC) [c]	References
Quercetin-5,3′-dimethylether (**57**)	Flavonols	2.30	1.74	151.38	2.1801	[26]
Rhamnazin (**58**)	Flavonols	2.51	1.73	302.76	2.4811	[26]
Rhamnocitrin (**59**)	Flavonols	2.56	1.82	166.52	2.2215	[26]
7,4′, 7″, 4‴-tetramethoxy amentoflavone (TMA) (**60**)	Bioflavones	5.80	4.10	420.47	2.6237	[27]
Isoginkgetin (IGG) (**61**)	Bioflavones	5.68	4.32	242.29	2.3843	[27]
Podocarpusflavone A (PFA) (**62**)	Bioflavones	4.15	2.53	452.5	2.6556	[27]
Nobiletin (**63**)	Flavones	2.80	2.80	439.86	2.6433	[28]
Kaempferol (**64**)	Flavonols	2.05	1.40	87.34	1.9412	[28]
Licoflavone C (**65**)	Flavones	4.20	3.77	23.08	1.3632	[29]
Derrone (**66**)	Isoflavones	5.55	4.82	23.22	1.3659	[29]
Epimedokoreanin B (**67**)	Flavones	6.59	6.14	>151.49	>2.1804	[30]
Auriculasin (**68**)	Isoflavones	7.70	6.89	9.51	0.9782	[30]
Pomiferin (**69**)	Isoflavones	7.44	7.06	19.03	1.2794	[30]
Gancaonin L (**70**)	Isoflavones	5.03	4.58	22.58	1.3537	[30]
Mopanin (**71**)	Flavonols	1.94	1.04	>214.59	>2.3316	[30]
Luteolin (**72**)	Flavones	2.40	1.85	349.36	2.5433	[31]
Quercetin (**73**)	Flavonols	2.07	1.40	1323.45	3.1217	[32]
Quercetin 3-*O*-*β*-D-glucosyl (1→4)-*α*-L-rhamnoside (**74**)	Flavonols	2.92	2.20	40.02	1.6023	[33]
Quercetin-3-*O*-*α*-L-rhamnoside or quercitrin (**75**)	Flavonols	2.51	1.78	108.13	2.0339	[33]
Entadanin (**76**)	Flavonols	2.00	0.086	36.31	1.5600	[33]
Kaempferide (**77**)	Flavonols	3.00	2.33	333.03	2.5225	[34]
Kaempferide-3-*O*-*β*-D-glucoside (**78**)	Flavonols	2.31	1.60	432.52	2.6360	[34]
Galangin (**79**)	Flavonols	2.83	2.16	370.04	2.5682	[34]
Tiliroside (**80**)	Flavonols	4.02	3.32	3.36	0.5263	[35]
Quercetin-3,7-*O*-*α*-L-dirhamnoside (**81**)	Flavonols	1.53	0.53	3.36	0.5263	[35]
Kaempferol-3,7-*O*-*α*-L-dirhamnoside (**82**)	Flavonols	1.73	0.76	3.46	0.5391	[35]
Scandenone (**83**)	Isoflavones	7.90	7.12	4.94	0.6937	[35]
Angusticornin B (**84**)	Chalcones	4.31	4.07	2.87	0.4579	[36]
Bartericin A (**85**)	Chalcones	5.46	5.77	1.49	0.1732	[36]
2′,4′,2-$(OH)_3$-chalcone (**86**)	Chalcones	3.95	3.66	476.08	2.6777	[37]
2′,4′,3-$(OH)_3$-chalcone (**87**)	Chalcones	3.35	3.05	179.51	2.2541	[37]
Isobavachalcone (**88**)	Chalcones	5.49	5.44	>394.6	>2.5962	[38]
α-Mangostin (**89**)	Xanthones	6.70	6.10	>311.84	>2.4939	[38]

[a]: The structures of these compounds are shown in Figure S1 in Supplementary Materials. [b]: The LogP and $LogD_{7.40}$ values were calculated using the software ACD/Labs 6.0. [c]: MIC, minimum inhibitory concentration.

2.2. Correlation and Regression Analyses of the Antibacterial Activity and the Physicochemical Parameter

To examine the correlations between the physicochemical parameter (LogP or $LogD_{7.40}$) and the MIC of plant flavonoids against Gram-negative bacteria, the flavonoids mentioned in Tables 1 and 2 were selected for statistical analyses. Since the antimicrobial activities of a compound against different pathogenic bacteria vary, even against the same one under different determination conditions, the correlation and regression analyses of the lipophilic parameter LogP or $LogD_{7.40}$ (x) and the MIC or $\log_{10}$(MIC) (y) were individually performed for the tested and reported flavonoids. The regression equations, together with their correlation coefficients (r) and coefficients of determination (R^2), are listed in Table 3, and the regression curves from the LogP and the MIC or $\log_{10}$(MIC) are shown in Figure 2. According to statistics, the closer the r value to 1, the stronger the correlation. Whether there is a significant correlation between two events or not should be tested with r-test. An r value higher than the critical value of $r_{0.975}(n-2)$ or $r_{0.995}(n-2)$ indicates that there is a significant correlation between two events. It could be determined from Table 3 that all the r values for Equations (1)–(6) were higher than the corresponding critical values of $r_{0.975}(35)$ and $r_{0.975}(44)$. This indicates that there are significant correlations between the lipophilic parameter LogP or $LogD_{7.40}$ (x) and the MIC or $\log_{10}$(MIC) (y) of plant flavonoids against *E. coli*. However, the LogP presents a better correlation than the $LogD_{7.40}$ with the MIC, as the r value of equation (1) was higher than that of Equation (3). This was also confirmed by the fact that there was no significant correlation between the $LogD_{7.40}$ and the MIC of reported plant flavonoids against *E. coli*, as the r value of regression Equation (7) was less than the critical one of $r_{0.975}(44)$. Therefore, the above results, from whether plant flavonoids tested in the current study or those reported in the literature, indicated that the antibacterial activities of plant flavonoids against Gram-negative bacteria are related to their lipophilicities. However, all R^2 values for Equations (1)–(6) were less than 0.45 and far

less than 1.0. According to statistics, the closer R^2 to 1, the higher the goodness of fit, and the closer the calculated value, on the whole, to the actual one. Thus, the smaller R^2 values indicate that the goodness of fit of these regression equations is too low to be effectively used to predict the MIC values of a certain plant flavonoid against Gram-negative bacteria.

Table 3. Regression equations for the correlation between the physicochemical parameter (x) and the antimicrobial activity (y) against Gram-negative bacteria especially *E. coli*, of plant flavonoids.

Equation Number	Sample Numbers (n)	Parameters [a] (x)	Regression Equation (r [b])	Coefficient of Determination (R^2)
(1)	37	LogP	$y = 154.74x^4 - 2328.1x^3 + 11{,}774x^2 - 23{,}630x + 20{,}574$ (0.3736) [c]	0.1396
(2)			$y = -0.0022x^6 + 0.0574x^5 - 0.5624x^4 + 2.6776x^3 - 6.4916x^2 + 7.5985x + 0.2396$ (0.4714) [d]	0.2222
(3)	37	$LogD_{7.40}$	$y = 51.533x^4 - 648.46x^3 + 2399.6x^2 - 2834x + 5407.4$ (0.3412) [c]	0.1164
(4)	46	LogP	$y = 3.4251x^6 - 99.079x^5 + 1128.5x^4 - 6389x^3 + 18{,}606x^2 - 25{,}841x + 13{,}552$ (0.4108) [c]	0.1688
(5)			$y = -0.0358x^4 + 0.7264x^3 - 5.2356x^2 + 15.438x - 13.244$ (0.6670) [d]	0.4449
(6)			$y = 0.0621x^3 - 0.9417x^2 + 4.0824x - 2.9354$ (0.5875) [d]	0.3452
(7)	46	$LogD_{7.40}$	/ [e]	/

[a]: The physicochemical parameter (x) was calculated using the software ACD/Labs 6.0. [b]: r, correlation coefficient; the significant level α was set as 0.05, and the critical values of $r_{0.975}(35)$ and $r_{0.975}(44)$ were equal to 0.33 and 0.29, respectively. [c]: The antimicrobial activity (y) was the MIC of a certain flavonoid against Gram-negative bacteria, especially *E. coli*. [d]: The antimicrobial activity (y) was the $\log_{10}$(MIC) of a certain flavonoid against Gram-negative bacteria, especially *E. coli*. [e]: No regression equation could be established since the r values are less than the critical one of $r_{0.975}(44)$.

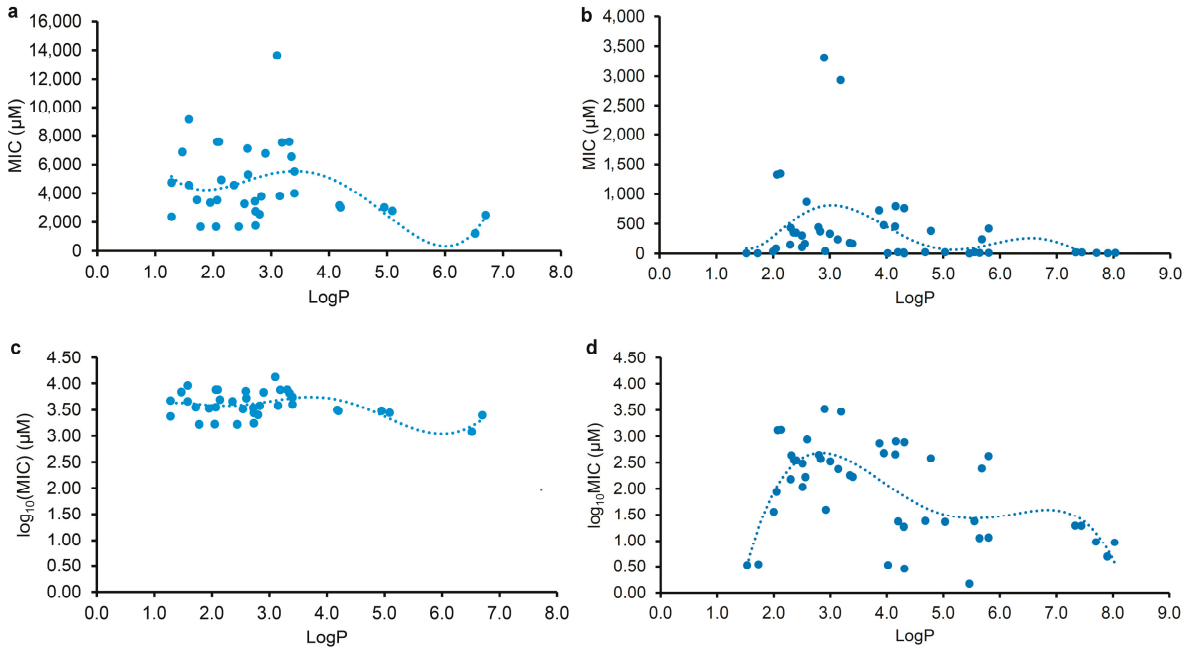

Figure 2. Polynomial regression analyses for the physicochemical parameter LogP (x) and the MIC (up) or $\log_{10}$(MIC) (down) (y) against Gram-negative bacteria, mainly *E. coli*, of plant flavonoids tested ((**a**,**c**), n = 37) and reported ((**b**,**d**), n = 46).

As shown in Figure 2, both regression curves (Figure 2a,c) from the MIC or $\log_{10}$(MIC) and LogP value of the tested plant flavonoids present a biconcave character, and they have two minimum values. However, another two regression curves (Figure 2b,d) from those of reported plant flavonoids have three minimum values. Excluding the difference in the range of the LogP value, it was found that all of them presented similar characters when the LogP values of the plant flavonoids were less than 7.0. Specifically, the left two

curves had minimum MIC or $\log_{10}$(MIC) values when the LogP values of the tested plant flavonoids were approximately 2.0 and 6.0, whereas the right two curves had minimum MIC or $\log_{10}$(MIC) values when the LogP values of the reported plant flavonoids were approximately 1.5 and 5.5. Differently, the right two curves had the third minimum MIC or $\log_{10}$(MIC) values. This was mainly attributed to the fact that the LogP values of some of the reported plant flavonoids were more than 7.0. Although there was a slight difference between the curve shapes in Figure 2a,c, another effective fitting equation, Equation (6), with a smaller r and R^2 than Equation (5) could also be established from the LogP and $\log_{10}$(MIC) of the reported plant flavonoids, and its regression curve (Figure S2) was similar to that in Figure 2c. Therefore, this indicates that maintaining appropriate lipophilicity, probably with a LogP value of approximately 2.0 (or 1.5), 6.0 (or 5.5), or 7.8, is necessary for plant flavonoids to obtain stronger antibacterial activities against Gram-negative bacteria, unlike against Gram-positive bacteria, in which case the higher the LogP value (from 2.0 to 8.9), the stronger the antimicrobial activity presented overall.

2.3. Different Antibacterial Effects and Mechanisms of Plant Flavonoids against Gram-Negative and Gram-Positive Bacteria

Due to various factors, including the method and details of the MIC test, which influence the experimental results, it is usual to observe a significant variation in the MIC values against the same pathogen in different labs. Therefore, the MIC data tested in our lab should be more consistent than the data collected from the literature, and so the regression curve in Figure 2c was further selected for comparison with that from the LogP and $\log_{10}$(MIC) of plant flavonoids against Gram-positive bacteria in our previous study [20] to determine their differences.

As observed in Figure 3, the obvious difference between both curves is that most flavonoids likely have stronger antimicrobial activities against Gram-negative bacteria than Gram-positive species when the LogP value is less than approximately 3.0. However, most flavonoids likely have stronger antimicrobial activities against Gram-positive bacteria than Gram-negative species when the LogP value was more than approximately 3.6. Moreover, the biconcave (Figure 3a) or even triple concave (Figure 2d) character of the regression curve indicates that there are probably multiple action mechanisms of plant flavonoids against Gram-negative bacteria, while the mechanism of plant flavonoids mainly acting on the cell membrane of Gram-positive bacteria only presents a single concave character. As both curves exhibit a similar decreasing trend with the increase in the LogP values ranging from approximately 3.6 to 6.0 (Figure 3), the cell membrane is most likely an important target site for some plant flavonoids against Gram-negative bacteria, especially for those with LogP values ranging from approximately 3.6 to 6.0 (Figure 2c or Figure 3a) or approximately 2.8 to 6.0 (Figure 2d).

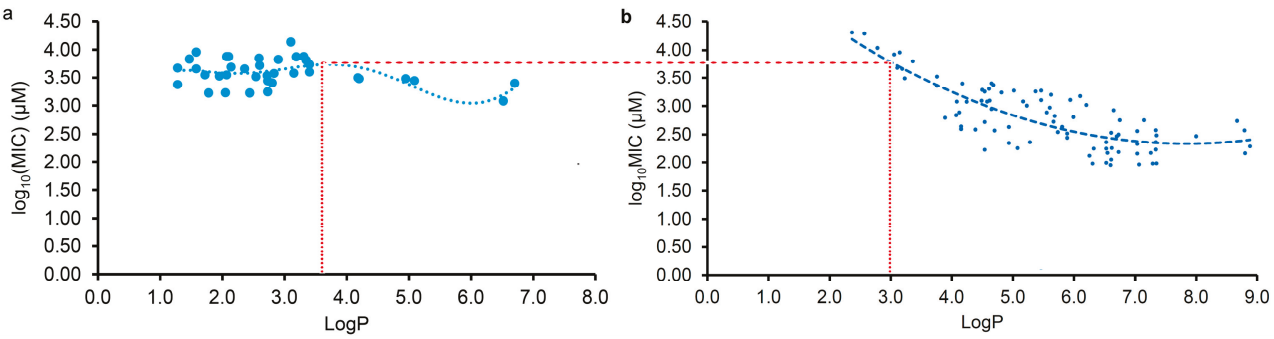

Figure 3. Comparing the regression curves from the LogP and $\log_{10}$(MIC) of plant flavonoids against Gram-negative (**a**) and Gram-positive bacteria (**b**). (**a**) same to Figure 2c; (**b**) same to the left figure on Figure 3 of our previous work [20].

3. Discussion

To predict the antimicrobial activities of plant flavonoids against Gram-negative bacteria and to discover compounds with effective inhibitory activity against Gram-negative bacteria, correlation and regression analyses were performed individually using 37 tested and 46 reported data pairs comprising the LogP (or $LogD_{7.40}$) values and MICs of plant flavonoids against Gram-positive bacteria. The results indicate that, similar to those against Gram-positive bacteria, the antibacterial activities of plant flavonoids against Gram-negative species are related to their lipophilicities. However, the antimicrobial quantitative relationship could not be established for plant flavonoids against Gram-negative bacteria, and so their antimicrobial activities against Gram-negative bacteria could not be predicted from their LogP values. Moreover, different from mainly acting on the cell membrane of Gram-positive bacteria, it was further proposed that plant flavonoids have multiple mechanisms against Gram-negative bacteria, while the cell membrane is also an important action site among them.

Lipophilicity, generally expressed as LogP, is a very important descriptor indicating membrane permeation. LogD, which refers to a pH-dependent mixture of all electrical species at any given pH value, is considered a better descriptor reflecting the actual partitioning and lipophilicity. $LogD_{7.40}$ is the LogD at the pH value of 7.40 which is approximately equal to that in human blood or the media of the MIC test. Both lipophilic parameters are important for drug effects. In our previous study [21], various physicochemical parameters of plant flavonoids were investigated to analyze the correlation between them and the MIC of plant flavonoids against Gram-positive bacteria, and the results indicate that there is a good correlation only between the parameter LogP or $LogD_{7.40}$ and the MIC of plant flavonoids against Gram-positive species. Based on this, both physicochemical parameters were selected for the correlation and regression analyses and to conveniently compare the results from plant flavonoids against Gram-negative and Gram-positive bacteria.

As the structural skeleton of plant flavonoids is similar to that of quinolone antimicrobial agents, 14 flavonoids had been designed and synthesized in a previous study [39]. An evaluation of the DNA gyrase inhibitory and antibacterial activities showed that the antibacterial activities of these flavonoids did not parallel the potency at the enzyme level, and the inhibition of DNA gyrase was only one possible reason for this [39]. Therefore, the study concluded that some mechanisms other than DNA gyrase inhibition may play a role in the antibacterial activity of flavonoids. As inferred in our previous study [20,21], the antibacterial activities of plant flavonoids against Gram-positive bacteria mainly depend on their lipophilicities and not on the inhibition of DNA gyrase as the cell membrane is a major site where plant flavonoids act on these bacteria. Inspired by the multiple action mechanisms of plant flavonoids against Gram-negative bacteria, the LogP values of those designed flavonoids were calculated to explore the correlation between their enzyme inhibitory activities and their LogP values, which ranged from 2.07 to 3.76. Surprisingly, the results (Supplementary Tables S2 and S3) demonstrate a significant correlation between the enzyme inhibitory activities and LogP values of the plant flavonoids, and the character of the obtained regression curve (Figure S3) was very similar to that of the curve (Figure 2a or Figure 2c) with LogP values ranging from 2.07 to 3.76. Furthermore, the antibacterial activities of these flavonoids against Gram-negative bacteria, especially *E. coli*$_{ss}$, completely paralleled the potency at the enzyme level. Although no specific MIC values were provided for those flavonoids against some pathogenic strains of Gram-negative bacteria, their relative antibacterial activities could be roughly obtained from the corresponding MIC values in combination with polymyxin B nonapeptide (PMBN) [35]. As a result, it was further suggested that DNA gyrase is another important target of plant flavonoids against Gram-negative bacteria, which is also supported by other studies [28,40–42].

According to this, the antibacterial activities of plant flavonoids against Gram-positive bacteria should also present a concave feature when the LogP values are less than approximately 3.0 (Figure 3b). Unfortunately, the LogP value of 3.0 is close to the boundary one,

which could possibly cause the curve character to be inconsistent with actual one when the LogP values are less than approximately 3.0 (Figure 3b). This might be similar to the difference in the main target of action of quinolones against Gram-negative (DNA gyrase) and Gram-positive bacteria (Topoisomerase IV). Additionally, their antibacterial activities caused by the inhibition of DNA gyrase were weak overall, according to Figures 2c and 3a.

Along with the increase in the LogP values, the antibacterial activities of the plant flavonoids against both Gram-negative and Gram-positive bacteria increased when the LogP values were higher than approximately 3.6 (Figure 3a,b). However, their antibacterial activities against Gram-positive bacteria increased more quickly than against Gram-negative species. This might be attributed to the difference in the cell envelope structure and the quinone pool composition in the respiratory chain between Gram-negative and Gram-positive bacteria (explained in the following paragraph) [22]. As mentioned in our previous research [22], menaquinones (MKs) are the sole quinones for electron transfer in the respiratory chain of Gram-positive bacteria, while two types of quinones, namely, MKs and ubiquinones, have been discovered in that of Gram-negative bacteria. This may be an important reason why the plant flavonoids showed weaker antimicrobial activities against Gram-negative than against Gram-positive bacteria when the LogP values were more than approximately 3.6 (Figure 3a).

Generally, when the LogP value is approximately between 0 and 3.0, the compound presents good cell membrane permeability to the lipid bilayer. As is well known, the cell envelope of Gram-negative bacteria contains a unique hydrophilic outer membrane and a lipophilic inner membrane which is similar to the cell membrane of Gram-positive bacteria. However, the cell structure of Gram-positive bacteria only contains a cell membrane, without an outer membrane. As shown in Figure 4, when the LogP was less than zero, it was difficult for plant flavonoids to approach the inner membrane of Gram-negative bacteria and the cell membrane of Gram-positive species to reach the target site. This indicates that plant flavonoids exhibit little antibacterial activity against both Gram-negative and Gram-positive bacteria. When the LogP value was between 0 and 3.0, it was easy for the plant flavonoids to cross the inner membrane of Gram-negative bacteria and the cell membrane of Gram-positive species. Thus, plant flavonoids can inhibit the DNA gyrase of Gram-negative bacteria, exhibiting a certain antibacterial activity, while their antibacterial effects on Gram-positive bacteria mainly relies on the membrane action, showing less antibacterial activity. When the LogP value was more than 3.6, it was difficult for the plant flavonoids to cross the inner membrane of Gram-negative bacteria, and their effect gradually changed from the inhibition of DNA gyrase to cell membrane action, including damaging the membrane and inhibiting respiratory chain, thus having similar effects on Gram-positive species. Therefore, their antibacterial activities against both Gram-negative and Gram-positive bacteria show similar trends with the increase in the LogP values between 3.0 and 6.0. However, the antibacterial activity of plant flavonoids against Gram-positive bacteria with the increase in the LogP value increased more rapidly than that against Gram-negative species. This is likely due to the optional electron acceptors such as ubiquinones and MKs in the quinone pool of Gram-negative bacteria, while there are only MKs in that of Gram-positive species. When the logP value was more than 6.7, it was difficult for plant flavonoids to access the inner membrane (action site) due to the obstruction from the hydrophilic outer membrane, and their antibacterial activities against Gram-negative bacteria gradually decreased. Similarly, their antibacterial activities against Gram-positive species also decreased, when the logP value was more than 9.0, even though there is no outer membrane in Gram-positive bacteria. This is likely due to the difficulty that plant flavonoids have in approaching the polarity head of the cell membrane when the logP value is too high. The above statement provides a reasonable interpretation for the characteristics of both regression curves in Figure 3, which, in turn, confirms the antibacterial mechanisms in this study and our previous report [20,21] of plant flavonoids against both Gram-negative and Gram-positive bacteria. Therefore, both the inhibition of DNA gyrase and action on the cell membrane, including membrane damage and the

inhibition of the quinone pool of the respiratory chain, are two important mechanisms of plant flavonoids against Gram-negative bacteria. Additionally, their different antibacterial effects on Gram-negative and Gram-positive bacteria were attributed to these different antibacterial mechanisms and their cell envelope structure.

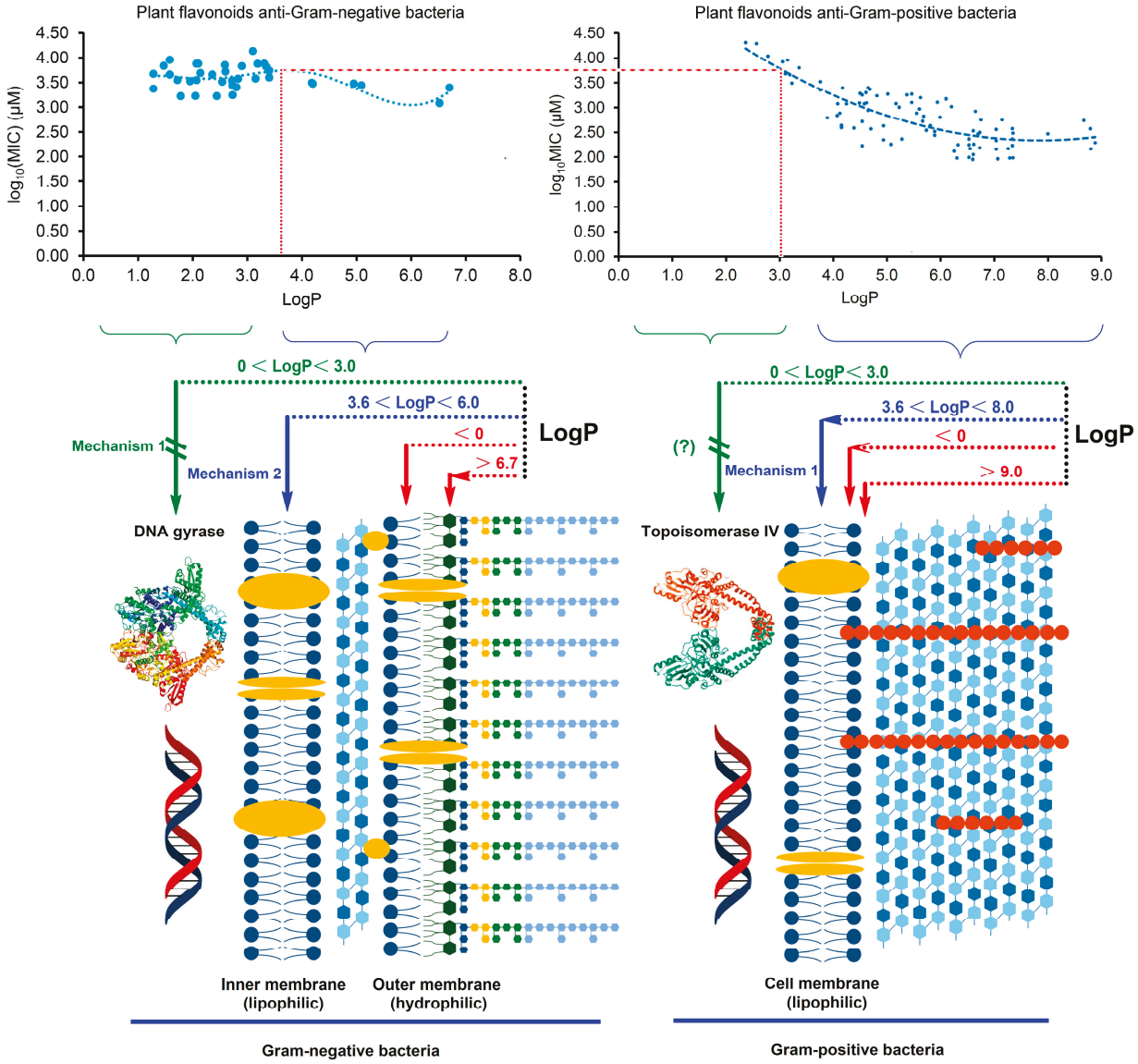

Figure 4. Schematic diagram of the interpretation for the different antibacterial effects and mechanisms of plant flavonoids against both Gram-negative and Gram-positive Bacteria, based on their characteristics of both regression curves shown in Figure 3 and their different cell structures.

Although both regression curves (Figure 2a,b) presented similar characters overall with the change in the LogP values, the MIC values of the tested plant flavonoids were obviously higher than those of the reported plant flavonoids. This was probably due to the different determination conditions, methods, details, and selected pathogenic strains. Among the tested and reported plant flavonoids, nine of them were the same. Thus, their antibacterial activities against *E. coli* ATCC 25922 were reorganized, and they are listed in Table S1, allowing for a comparison of the differences in the tested and reported data [25,28,29,32,34,38]. The results indicate that only the MICs of compound **13** (Licoflavone C) presented more than a 10 times difference between the tested (3026.36 μM) and reported (23.08 μM) values [29]. Therefore, using the broth microdilution method in 96-well plates, the antibacterial activity of this compound against *E. coli* ATCC 25922 was

determined in six replicates, and all the MICs of compound **13** against *E. coli* ATCC 25922 were 3026.36 μM.

As mentioned in Section 2.3, the antibacterial activities of plant flavonoids with logP values less than approximately 3.6 against Gram-negative bacteria were statistically stronger than those against Gram-positive species, and they also increased overall when the LogP value increased to more than approximately 3.6. However, the antibacterial activities of most plant flavonoids against Gram-negative bacteria were weak overall. Additionally, stronger antibacterial activities can be acquired through structural modification based on the antibacterial mechanism of plant flavonoids against Gram-negative bacteria, such as the inhibition of DNA gyrase and the quinone pool of the respiratory chain. However, due to the unique cell envelope structure of Gram-negative bacteria, it is challenging to discover plant flavonoid derivatives with very strong antibacterial activities against Gram-negative species. This is different from the case of Gram-positive bacteria, which does not have a hydrophilic outer membrane and only has the sole electron transfer acceptor menaquinone in the quinone pool [22]. Furthermore, when attempting to discover flavonoids with remarkably inhibitory activity against Gram-negative bacteria, it should also be encouraged to pay an attention to the combinational use of plant flavonoids and clinical antibiotics for combating AMR [7,31,34], as they have a good safety profile and can enhance susceptibility to many antibiotics.

4. Materials and Methods

4.1. Materials, Chemicals and Reagents

Thirty-seven plant flavonoids: icaritin (>98%), isoliquiritigenin (98%), formononetin (98%), isoliquiritigenin (98%), galangin (98%), baicalein (98%), diosmin (95%), hesperetin (97%), puerarin (98%), apigenin (≥95%), diosmetin (98%) and naringenin (97%) were purchased from Shanghai Macklin Biochemical Co., Ltd. (Shanghai, China); α-mangostin (>98.0%), licochalcone A (>98.0%), nobiletin (≥98.5%), tangeritin (≥98.5%), quercitrin (98%), sinensetin (98%), narirutin (98%), orientin (99%) and isoorientin (98%) were purchased from Chengdu Push Bio-technology Co., Ltd. (Chengdu, China); naringin (95%), neohesperidin (≥98%) and hesperidin (95%) were purchased from Shanghai Yuanye Bio-Technology Co., Ltd. (Shanghai, China); eriodictyol (≥98%), eriocitrin (≥98%), rhoifolin (≥98%) and licoflavone C (≥98%) were purchased from Wuhan ChemFaces Biochemical Co., Ltd. (Wuhan, China); glabridin (99.8%) and sophoraflavanone G (>98%) were purchased from Shanghai TopScience Co., Ltd. (Shanghai, China); quercetin (97%) was purchased from Meryer (Shanghai) Biochemical Technology Co., Ltd. (Shanghai, China); methyl-hesperidin (95%) was purchased from Shanghai Acmec Biochemical Co.,Ltd. (Shanghai, China); and didymin (≥98%), 5-demethylnobiletin (≥98%), 4′,5,7-trimethoxyflavone (≥98%), vitexin (≥98%) and isovitexin (≥98%) were purchased from Sichuan Weikeqi Biological Technology Co., Ltd. (Sichuan, China). All the compounds were stored at −20 °C. The stock solutions of the above plant flavonoids were prepared by dissolving them in a certain volume of dimethyl sulfoxide (DMSO) and diluting them with Mueller Hinton broth (MHB) to obtain a concentration of 4096, 8192, or 16,384 μg/mL. The stock solution was mixed well and then diluted to the desired concentration with MHB immediately before use. The concentrations of DMSO in all test systems were kept below 5.0%, and all those in the blank controls were 5.0%.

Casein hydrolysate (Qingdao Hope Bio-Technology Co., Ltd., Qingdao, China), starch soluble, beef extract, and agar powder (Sangon Biotech (Shanghai) Co., Ltd., Shanghai, China) were used to prepare the media. Mueller Hinton Agar (MHA) consisted of casein hydrolysate 17.5 g/L, starch soluble 1.5 g/L, beef extract 3.0 g/L, and agar powder 17.0 g/L, which were dissolved in purified water, and its pH value was maintained at 7.40 ± 0.20. MHB was prepared without agar powder according to the same composition and procedure as MHA. DMSO and 3-(4,5-dimethylthiazol-2-yl)-2,5-diphenyltetrazolium bromide (MTT) were purchased from Sangon Biotech (Shanghai) Co., Ltd. (Shanghai, China), and 96-well plates were purchased from Shanghai Excell Biological Technology Co., Ltd. (Shanghai,

China). All reagents were of analytical or biochemical grade. All TopPette Pipettors (2~20 μL and 20~200 μL) were purchased from DLAB Scientific Co., Ltd., Beijing, China.

4.2. Bacterial Strains and Growth Conditions

E. coli ATCC 25922 and *S. aureus* ATCC 25923 were purchased from American Type Culture Collection, Manassas, VA, USA, and they were stored in Microbank™ microbial storage (PRO-LAB diagnostics, Toronto, Canada) at −20 °C. Prior to use, *E. coli* and *S. aureus* were cultured onto an MHA plate at 37 °C, and then pure colonies from the culture plate were inoculated into MHB at 37 °C for 24 h on a rotary shaker (160 rpm) of a CHA-2 gas bath constant-temperature oscillator (Jintan Yineng Experimental Instrument Factory, Changzhou, China). A 1:100 dilution of the overnight culture was made into fresh MHB, and then incubated at 37 °C until the exponential phase for the following experiments. MHB was used for antimicrobial susceptibility tests.

4.3. Antimicrobial Susceptibility Assay and Prediction

According to the standard procedure recommended by the Clinical and Laboratory Standards Institute (CLSI) [43], the exponential phase culture was diluted with MHB to achieve a bacterial concentration of approximately 1.0×10^6 CFU/mL, and then the susceptibility of the plant flavonoids against *E. coli* ATCC 25922 or *S. aureus* ATCC 25923 was determined using the broth microdilution method on the 96-well plates in triplicate [7]. Based on the preliminary MIC values of the plant flavonoids, the initial concentration of each compound was set as 1024, 2048, or 4096 μg/mL. After the 96-well plate was incubated at 35 °C for 24 h, 20 μL of MTT (4.0 mg/mL) was added to each well, mixed well, and left for 30 min at ambient temperature. The MIC, defined as the lowest concentration of compounds that completely inhibited bacterial growth in the microwells, was assessed by observing no color change in the wells, while the blank wells had sufficient bacterial growth [22].

According to the reported antimicrobial quantitative relationship [20], the MICs of the plant flavonoids against Gram-positive bacteria *S. aureus* were also calculated using the equation $y = -0.1285\,x^6 + 0.7944\,x^5 + 51.785\,x^4 - 947.64\,x^3 + 6638.7\,x^2 - 21{,}273\,x + 26{,}087$. Here, y is the antimicrobial activity (MIC) of the pant flavonoids against *S. aureus*; and x is the LogP value of the corresponding pant flavonoids, calculated using the software ACD/Labs 6.0 (Advanced Chemistry Development, Inc., Toronto, ON, Canada). Generally, the LogP values of the equation range from approximately 2.3 to 9.0. However, an appropriate extension of this range is also workable. It was considered acceptable for the predicted MIC value to fall into the range of 1/4 to 4 of the tested MIC value. Leniently, those MIC values ranging from 1/8× to 8× of the tested MIC value were also considered acceptable events, especially when the LogP value was outside the predicted range while close to both boundary values. This equation was established from 92 data pairs consisting of the LogP values and the MICs of plant flavonoids against Gram-positive bacteria, with an R^2 value of 0.9413.

4.4. Structures and MICs of Reported Plant Flavonoids

As the antimicrobial activities of a certain compound against different pathogenic bacteria and strains vary, data on the chemical structures of plant flavonoids and their MIC against *E. coli* (a representative Gram-negative bacterium) were collected from the literature. Simultaneously, the tested strains of *E. coli* were sourced from American Type Culture Collection (ATCC) where possible. The structures, the MIC values against *E. coli*, and other related information of the plant flavonoids were unsystematically searched for on Google Scholar, and in several databases, such as SciFinder, Medline, Elsevier, ACS, ScienceDirect, Wiley Online Library, and Springer-Link, using the keywords "flavonoid" and "*E. coli*", or and "antimicrobial", or and "antibacterial", and or and "Gram-negative bacteria". Furthermore, the relevant references in the obtained literature were also tracked, and then the structures, the MIC values against *E. coli*, and other related information

regarding the plant flavonoids were collected from the acquired literature. Finally, the structures of the collected compounds were drawn using the software ChemBioDraw Ultra 14.0.

4.5. Correlation and Regression Analyses

The lipophilic physicochemical parameters LogP (Log_{10} of partition coefficient) and $LogD_{7.40}$ (Log_{10} of distribution coefficient at pH 7.40) of the plant flavonoids measured in Section 4.3 or previously reported were automatically calculated from their chemical structures using the software ACD/Labs 6.0 (Advanced Chemistry Development, Inc., Ontario, Canada). Subsequently, the MIC values (μM) and the LogP and $LogD_{7.40}$ values of the plant flavonoids measured or reported were listed in an Excel table. After this, correlation analyses between the calculated LogP or $LogD_{7.40}$ value (x) and the MIC (y) of the plant flavonoids in the table were performed using the software Microsoft Excel 2010 (Microsoft Corporation, Redmond, WA, USA). Simultaneously, corresponding regression equations were established for further verification, and the value of the correlation coefficient (r) was automatically calculated. It is noteworthy that the compounds (Table 2) without accurate MIC values (such as more than the measuring concentration) were not considered for the regression analyses, but their related information was used for the following discussion. Finally, the correlation between the antimicrobial activity MIC of the plant flavonoids against Gram-negative bacteria and their physicochemical parameter LogP or $LogD_{7.40}$ was validated using the r-test. The coefficient of determination (R^2) was also calculated to determine the fitting precisions according to Equation (5) in previous work [20].

4.6. Comparison of the Characteristics of Regression Curves

As referred to from our previous work [20], the MIC was further transformed to the $\log_{10}$(MIC), and then a regression analysis between the $\log_{10}$(MIC) (y) and the LogP or $LogD_{7.40}$ (x) was performed. Then, the characteristics of the regression curves were compared on coordinate maps with the same vertical axis to explore the difference in the antibacterial effects and mechanisms of plant flavonoids against Gram-negative and Gram-positive bacteria, and to determine the possible reasons for the antibacterial effects and mechanisms changing with the lipophilic parameter LogP or $LogD_{7.40}$ value.

5. Conclusions

In summary, the antibacterial activities of plant flavonoids against Gram-negative bacteria are related to their lipophilicities, while their MIC values cannot be effectively predicted from their LogP values like in the case of Gram-positive bacteria. Simultaneously, the antibacterial activities of plant flavonoids against Gram-negative bacteria are generally weak, although most are stronger than those to Gram-positive species when the lipophilic parameter LogP value is less than approximately 3.0. Also, they are weak even when the LogP value is more than approximately 3.6. Unlike mainly acting on the cell membrane of Gram-positive bacteria, plant flavonoids probably have multiple action mechanisms against Gram-negative species, and among them the cell membrane is also an important action site. Moreover, DNA gyrase should also be considered another important target of plant flavonoids against Gram-negative bacteria.

Supplementary Materials: The following supporting information can be downloaded at: https://www.mdpi.com/article/10.3390/ph17030292/s1, Figure S1: Chemical structures of 52 plant flavonoids reported; Figure S2: Another effective regression curve for Equation (6) established from the LogP of the reported plant flavonoids and their $\log_{10}$(MIC) values; Figure S3: Polynomial regression analyses for the LogP (x) of plant flavonoids in Table S2 and the $\log_{10}(IC_{50})$ (y) to DNA gyrase; Table S1: Comparison for the tested and reported MIC values of nine compounds [25,28,29,32,34,38]; **Table S2**: The ACD/LogP values and IC_{50} to DNA gyrase of 14 reported flavonoids, together with their MICs against *E. coli*$_{ss}$ [39]; Table S3: Regression equations established from the LogP (x) values of the reported flavonoids [39] and the IC_{50} or $Log_{10}(IC_{50})$ (μM) values (y) of these flavonoids to DNA gyrase.

Author Contributions: Conceptualization, G.Y.; methodology, G.Y.; software, G.Y.; validation, G.Y., Y.Y. and X.X.; formal analysis, G.Y., Y.Y. and X.X.; investigation, Y.Y., X.X., A.F., L.Z., G.Y., F.L. and Y.W.; resources, G.Y.; data curation, Y.Y., X.X., L.Z., G.Y., F.L. and Y.W.; writing—original draft preparation, G.Y., Y.Y., A.F. and X.X.; writing—review and editing, G.Y., Y.Y., A.F., L.Z. and X.X.; visualization, G.Y. and Y.W.; supervision, G.Y.; project administration, G.Y.; funding acquisition, G.Y. All authors have read and agreed to the published version of the manuscript.

Funding: This research was funded by the National Natural Science Foundation of China, Grant numbers 82360691, 82073745 and 81960636.

Institutional Review Board Statement: Not applicable.

Informed Consent Statement: Not applicable.

Data Availability Statement: Data are contained within the article.

Conflicts of Interest: The authors declare no conflict of interest.

References

1. Murray, C.J.L.; Ikuta, K.S.; Sharara, F.; Swetschinski, L.; Aguilar, G.R.; Gray, A.; Han, C.; Bisignano, C.; Rao, P.; Wool, E.; et al. Global burden of bacterial antimicrobial resistance in 2019: A systematic analysis. *Lancet* **2022**, *399*, 629–655. [CrossRef]
2. Laxminarayan, R.; Sridhar, D.; Blaser, M.; Wang, M.; Woolhouse, M. Achieving global targets for antimicrobial resistance. *Science* **2016**, *353*, 874–875. [CrossRef]
3. Voulgaris, G.L.; Voulgari, M.L.; Falagas, M.E. Developments on antibiotics for multidrug resistant bacterial Gram-negative infections. *Expert Rev. Anti. Infect. Ther.* **2019**, *17*, 387–401. [CrossRef]
4. Jean, S.S.; Gould, I.M.; Lee, W.S.; Hsueh, P.R.; International Society of Antimicrobial Chemotherapy (ISAC). New drugs for multidrug-resistant Gram-negative organisms: Time for stewardship. *Drugs* **2019**, *79*, 705–714. [CrossRef]
5. Kaur, R.; Rani, P.; Atanasov, A.G.; Alzahrani, Q.; Gupta, R.; Kapoor, B.; Gulati, M.; Chawla, P. Discovery and development of antibacterial agents: Fortuitous and designed. *Mini. Rev. Med. Chem.* **2022**, *22*, 984–1029. [CrossRef]
6. Lim, J.S.; Chai, Y.Y.; Ser, W.X.; Haeren, A.V.; Lim, Y.H.; Raja, T.; Foo, J.B.; Hamzah, S.; Sellappans, R.; Yow, H.Y. Novel drug candidates against antibiotic-resistant microorganisms: A review. *Iran J. Basic. Med. Sci.* **2024**, *27*, 134–150. [CrossRef]
7. Xu, X.; Xu, L.; Yuan, G.; Wang, Y.; Qu, Y.; Zhou, M. Synergistic combination of two antimicrobial agents closing each other's mutant selection windows to prevent antimicrobial resistance. *Sci. Rep.* **2018**, *8*, 7237. [CrossRef] [PubMed]
8. Liang, M.; Ge, X.; Xua, H.; Ma, K.; Zhang, W.; Zan, Y.; Efferth, T.; Xue, Z.; Hua, X. Phytochemicals with activity against methicillin-resistant *Staphylococcus aureus*. *Phytomedicine* **2022**, *100*, 154073. [CrossRef]
9. Abdallah, E.M.; Alhatlani, B.Y.; de Paula Menezes, R.; Martins, C.H.G. Back to nature: Medicinal plants as promising sources for antibacterial drugs in the post-antibiotic era. *Plants* **2023**, *12*, 3077. [CrossRef] [PubMed]
10. Thebti, A.; Meddeb, A.; Ben Salem, I.; Bakary, C.; Ayari, S.; Rezgui, F.; Essafi-Benkhadir, K.; Boudabous, A.; Ouzari, H.-I. Antimicrobial activities and mode of flavonoid actions. *Antibiotics* **2023**, *12*, 225. [CrossRef] [PubMed]
11. Dey, J.; Mahapatra, S.R.; Raj, T.K.; Misra, N.; Suar, M. Identification of potential flavonoid compounds as antibacterial therapeutics against *Klebsiella pneumoniae* infection using structure-based virtual screening and molecular dynamics simulation. *Mol. Divers.* **2023**. [CrossRef] [PubMed]
12. Xie, Y.; Yang, W.; Tang, F.; Chen, X.; Ren, L. Antibacterial activities of flavonoids: Structure-activity relationship and mechanism. *Curr. Med. Chem.* **2015**, *22*, 132–149. [CrossRef] [PubMed]
13. Tan, Z.; Deng, J.; Ye, Q.; Zhang, Z. The antibacterial activity of natural-derived flavonoids. *Curr. Top. Med. Chem.* **2022**, *22*, 1009–1019. [CrossRef] [PubMed]
14. Song, L.; Hu, X.; Ren, X.; Liu, J.; Liu, X. Antibacterial modes of herbal flavonoids combat resistant bacteria. *Front. Pharmacol.* **2022**, *13*, 873374. [CrossRef] [PubMed]
15. Zhou, K.; Yang, S.; Li, S.M. Naturally occurring prenylated chalcones from plants: Structural diversity, distribution, activities and biosynthesis. *Nat. Prod. Rep.* **2021**, *38*, 2236–2260. [CrossRef] [PubMed]
16. Górniak, I.; Bartoszewski, R.; Króliczewski, J. Comprehensive review of antimicrobial activities of plant flavonoids. *Phytochem. Rev.* **2019**, *18*, 241–272. [CrossRef]
17. Farhadi, F.; Khameneh, B.; Iranshahi, M.; Iranshahy, M. Antibacterial activity of flavonoids and their structure-activity relationship: An update review. *Phytother. Res.* **2019**, *33*, 13–40. [CrossRef]
18. Panda, L.; Duarte-Sierra, A. Recent advancements in enhancing antimicrobial activity of plant-derived polyphenols by biochemical means. *Horticulturae* **2022**, *8*, 401. [CrossRef]
19. Shamsudin, N.F.; Ahmed, Q.U.; Mahmood, S.; Ali Shah, S.A.; Khatib, A.; Mukhtar, S.; Alsharif, M.A.; Parveen, H.; Zakaria, Z.A. Antibacterial effects of flavonoids and their structure-activity relationship study: A comparative interpretation. *Molecules* **2022**, *27*, 1149. [CrossRef]
20. Yuan, G.; Xia, X.; Guan, Y.; Yi, H.; Lai, S.; Sun, Y.; Cao, S. Antimicrobial quantitative relationship and mechanism of plant flavonoids to gram-positive bacteria. *Pharmaceuticals* **2022**, *15*, 1190. [CrossRef]

21. Yuan, G.; Guan, Y.; Yi, H.; Lai, S.; Sun, Y.; Cao, S. Antibacterial activity and mechanism of plant flavonoids to gram-positive bacteria predicted from their lipophilicities. *Sci. Rep.* **2021**, *11*, 10471. [CrossRef] [PubMed]
22. Zhang, L.; Yan, Y.; Zhu, J.; Xia, X.; Yuan, G.; Li, S.; Deng, B.; Luo, X. Quinone pool, a key target of plant flavonoids inhibiting gram-positive bacteria. *Molecules* **2023**, *28*, 4972. [CrossRef]
23. Mbaveng, A.T.; Sandjo, L.P.; Tankeo, S.B.; Ndifor, A.R.; Pantaleon, A.; Nagdjui, B.T.; Kuete, V. Antibacterial activity of nineteen selected natural products against multi-drug resistant Gram-negative phenotypes. *SpringerPlus* **2015**, *4*, 823. [CrossRef]
24. Chukwujekwu, J.C.; Van Heerden, F.R.; Van Staden, J. Antibacterial activity of flavonoids from the stem bark of *Erythrina caffra* Thunb. *Phytother. Res.* **2011**, *25*, 46–48. [CrossRef] [PubMed]
25. Mandalari, G.; Bennett, R.N.; Bisignano, G.; Trombetta, D.; Saija, A.; Faulds, C.B.; Gasson, M.J.; Narbad, A. Antimicrobial activity of flavonoids extracted from bergamot (*Citrus bergamia* Risso) peel, a byproduct of the essential oil industry. *J. Appl. Microbiol.* **2007**, *103*, 2056–2064. [CrossRef] [PubMed]
26. Martini, N.D.; Katerere, D.R.; Eloff, J.N. Biological activity of five antibacterial flavonoids from *Combretum erythrophyllum* (Combretaceae). *J. Ethnopharmacol.* **2004**, *93*, 207–212. [CrossRef]
27. Bagla, V.P.; McGaw, L.J.; Elgorashi, E.E.; Eloff, J.N. Antimicrobial activity, toxicity and selectivity index of two biflavonoids and a flavone isolated from *Podocarpus henkelii* (Podocarpaceae) leaves. *BMC Complement. Altern. Med.* **2014**, *14*, 383. [CrossRef]
28. Wu, T.; Zang, X.; He, M.; Pan, S.; Xu, X. Structure-activity relationship of flavonoids on their anti-*Escherichia coli* activity and inhibition of DNA gyrase. *J. Agric. Food. Chem.* **2013**, *61*, 8185–8190. [CrossRef]
29. Edziri, H.; Mastouri, M.; Mahjoub, M.A.; Mighri, Z.; Mahjoub, A.; Verschaeve, L. Antibacterial, antifungal and cytotoxic activities of two flavonoids from *Retama raetam* flowers. *Molecules* **2012**, *17*, 7284–7293. [CrossRef]
30. Mohamed, M.S.; Abdelkader, K.; Gomaa, H.A.M.; Batubara, A.S.; Gamal, M.; Sayed, A.M. Mechanistic study of the antibacterial potential of the prenylated flavonoid auriculasin against *Escherichia coli*. *Arch. Pharm. (Weinheim)* **2022**, *355*, e2200360. [CrossRef]
31. Eumkeb, G.; Siriwong, S.; Thumanu, K. Synergistic activity of luteolin and amoxicillin combination against amoxicillin-resistant *Escherichia coli* and mode of action. *J. Photochem. Photobiol. B.* **2012**, *117*, 247–253. [CrossRef]
32. Jaisinghani, R.N. Antibacterial properties of quercetin. *Microbiol. Res.* **2017**, *8*, 6877. [CrossRef]
33. Dzoyem, J.P.; Melong, R.; Tsamo, A.T.; Tchinda, A.T.; Kapche, D.G.; Ngadjui, B.T.; McGaw, L.J.; Eloff, J.N. Cytotoxicity, antimicrobial and antioxidant activity of eight compounds isolated from *Entada abyssinica* (Fabaceae). *BMC Res. Notes* **2017**, *10*, 118. [CrossRef]
34. Eumkeb, G.; Siriwong, S.; Phitaktim, S.; Rojtinnakorn, N.; Sakdarat, S. Synergistic activity and mode of action of flavonoids isolated from smaller galangal and amoxicillin combinations against amoxicillin-resistant *Escherichia coli*. *J. Appl. Microbiol.* **2012**, *112*, 55–64. [CrossRef] [PubMed]
35. Ozçelik, B.; Orhan, I.; Toker, G. Antiviral and antimicrobial assessment of some selected flavonoids. *Z. Naturforsch. C J. Biosci.* **2006**, *61*, 632–638. [CrossRef] [PubMed]
36. Kuete, V.; Simo, I.K.; Ngameni, B.; Bigoga, J.D.; Watchueng, J.; Kapguep, R.N.; Etoa, F.X.; Tchaleu, B.N.; Beng, V.P. Antimicrobial activity of the methanolic extract, fractions and four flavonoids from the twigs of *Dorstenia angusticornis* Engl. (Moraceae). *J. Ethnopharmacol.* **2007**, *112*, 271–277. [CrossRef] [PubMed]
37. Alvarez, M.d.l.A.; Zarelli, V.E.; Pappano, N.B.; Debattista, N.B. Bacteriostatic action of synthetic polyhydroxylated chalcones against *Escherichia coli*. *Biocell.* **2004**, *28*, 31–34. [CrossRef] [PubMed]
38. Song, M.; Liu, Y.; Li, T.; Liu, X.; Hao, Z.; Ding, S.; Panichayupakaranant, P.; Zhu, K.; Shen, J. Plant natural flavonoids against multidrug resistant pathogens. *Adv. Sci.* **2021**, *8*, e2100749. [CrossRef]
39. Ohemeng, K.A.; Schwender, C.F.; Fu, K.P.; Barrett, J.F. DNA gyrase inhibitory and antibacterial activity of some flavones (l). Bioorg. *Med. Chem. Lett.* **1993**, *3*, 225–230. [CrossRef]
40. Fang, Y.; Lu, Y.; Zang, X.; Wu, T.; Qi, X.; Pan, S.; Xu, X. 3D-QSAR and docking studies of flavonoids as potent *Escherichia coli* inhibitors. *Sci. Rep.* **2016**, *6*, 23634. [CrossRef] [PubMed]
41. Verghese, J.; Nguyen, T.; Oppegard, L.M.; Seivert, L.M.; Hiasa, H.; Ellis, K.C. Flavone-based analogues inspired by the natural product simocyclinone D8 as DNA gyrase inhibitors. *Bioorg. Med. Chem. Lett.* **2013**, *23*, 5874–5877. [CrossRef] [PubMed]
42. Lin, H.; Hu, J.; Mei, F.; Zhang, Y.; Ma, Y.; Chen, Q.; Wang, C.; Fu, J.; Yang, M.; Wen, Z.; et al. Anti-microbial efficacy, mechanisms and druggability evaluation of the natural flavonoids. *J. Appl. Microbiol.* **2022**, *133*, 1975–1988. [CrossRef] [PubMed]
43. Clinical and Laboratory and Standards Institute (CLSI). *Methods for Dilution Antimicrobial Susceptibility Tests for Bacteria That Grow Aerobically*, 10th ed.; Approved Standards, CLSI Document M07-A10; Clinical and Laboratory and Standards Institute: Wayne, PA, USA, 2015.

Disclaimer/Publisher's Note: The statements, opinions and data contained in all publications are solely those of the individual author(s) and contributor(s) and not of MDPI and/or the editor(s). MDPI and/or the editor(s) disclaim responsibility for any injury to people or property resulting from any ideas, methods, instructions or products referred to in the content.

MDPI AG
Grosspeteranlage 5
4052 Basel
Switzerland
Tel.: +41 61 683 77 34

Pharmaceuticals Editorial Office
E-mail: pharmaceuticals@mdpi.com
www.mdpi.com/journal/pharmaceuticals



Disclaimer/Publisher's Note: The title and front matter of this reprint are at the discretion of the Guest Editors. The publisher is not responsible for their content or any associated concerns. The statements, opinions and data contained in all individual articles are solely those of the individual Editors and contributors and not of MDPI. MDPI disclaims responsibility for any injury to people or property resulting from any ideas, methods, instructions or products referred to in the content.





Academic Open
Access Publishing

mdpi.com

ISBN 978-3-7258-8192-5